REMOTE SENSING AND DIGITAL IMAGE PROCESSING

Microwave Dielectric Behavior of Wet Soils

by
Jitendra Behari

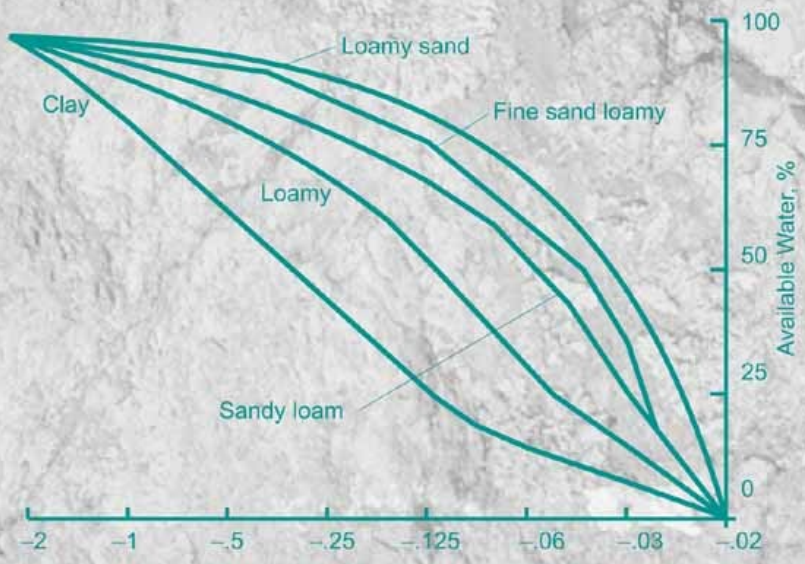

Springer

Microwave Dielectric Behavior of Wet Soils

Remote Sensing and Digital Image Processing

VOLUME 8

The titles published in this series are listed at the end of this volume.

MICROWAVE DIELECTRIC BEHAVIOR OF WET SOILS

by

JITENDRA BEHARI

School of Environmental Sciences,
Jawaharlal Nehru University,
New Delhi, India

Springer

Anamaya

A.C.I.P. catalogue record for the book is available from the Library of Congress

ISBN 1-4020-3271-4 (HB)
ISBN 1-4020-3288-9 (e-book)

Copublished by Springer
233 Spring Street, New York 10013, USA
with Anamaya Publishers, New Delhi, India

Sold and distributed in North, Central and South America by Springer
233 Spring Street, New York, USA

In all the countries, except India, sold and distributed by Springer
P.O. Box 322, 3300 AH Dordrecht, The Netherlands

In India, sold and distributed by Anamaya Publishers
F-230, Lado Sarai, New Delhi-110 030, India

springeronline.com

Printed in India.

PREFACE

Soil moisture plays an important role in the runoff process, and its evaluation can be used as a marker of flood risk or drought occurrence. The data is also required to validate the soil moisture component in a variety of soil types of hydrologic models before a possible flood event, and potentially improves the accuracy of their prediction.

Keeping the above in view, enormous efforts have gone into measurement of soil moisture by *in situ* and remote sensing techniques using microwaves. The subject still remains an important point of investigation for it depends upon a number of parameters, for example, texture, topography and shows space and temporal variability. The advantages of both passive and active remote sensing techniques are discussed in detail.

The book begins with the basics of soil physics and the soil moisture. Soil moisture measurement techniques presented are confined to microwave frequencies. A summary of theoretical models and a mix-up of experimental and theoretical details is included to offer a comparison. A special chapter is added on an upcoming technique of synthetic aperture radar. The book finally concludes with a summary of recent trends and techniques with a possible direction for future work.

The book is primarily aimed to benefit postgraduates and researchers in the area of soil, agriculture physics and microwave remote sensing. The aim is to initiate beginners in the subject. The author will consider his efforts rewarded if it succeeds in such an endeavor.

J. BEHARI

LIST OF SYMBOLS

A_{syn}	Equivalent area of 'synthesized beam'
B	System bandwidth
C	Heat capacity
E	Evaporation from the water surface
e_β	Measured sensitivity of the two layer medium
$e_{surface}$	Emissivity of ground surface
$F(d)$	Visibility function
G_r	Gain of receiving antenna
G_t	Gain of transmission antenna
h	Roughness parameter
K	Boltzman's constant
$k_e d$	Optical thickness
l_ε	Sample length
m_f	Percentage of volumetric field capacity
m_g	Gravimetric moisture content
m_s	Mass of dry soil
m_{st}	Mass of wet soil
m_t	Transition moisture
m_v	Volumetric water content (Soil moisture)
m_{vr}	Relative saturation
m_{vs}	Saturated value
P	Total porosity of the soil
P_a	Pore volume filled with air
P_d	Penetration depth
P_t	Power transmitted by the sensor
$R(\theta)$	Surface roughness
r_β^g	Reflectivity of the ground
r^2	Correlation coefficient
R_p	Polarized surface reflectivity
R_t	Distance between radar and target
T_v	Temperature of the vegetation
T_{atm}	Average temperature of the atmosphere
T_B	Brightness temperature
V_{soil}	Soil reflectivity

W	Day length
W^0	Observed soil moisture
W_p	Wilting coefficient
W_t	Transition point
Y_t	Characteristic admittance of the probe
Z_0	Characteristic impedance of transmission line
ρ_b	Bulk density of soil
ε'	Real part of complex permittivity (dielectric constant)
ε''	Imaginary part of complex permittivity (dielectric constant)
ε''_σ	Conductivity loss
ε''_t	Total dielectric loss
ε	Dielectric constant
Γ_t	Transmissivity of the vegetation layer
β	Empirical constant
ϕ_m	Metric potential
δ_D	Skin depth
ρ_r	Particle density
τ	Relaxation time
ω	Angular frequency ($2\pi f$)
α	Spread in relaxation
ε_0	Permittivity of free space
λ	Wavelength
μ_r	Permeability of the medium
Γ	Reflection coefficient
σ	Ionic conductivity (mos/cm)
σ^0	Backscattering coefficient
σ_dc	Zero frequency electrical conductivity
θ	Soil moisture content
θ_veg	Depth integrated vegetation/water content
φ	Phase constant
$\gamma^{\mathrm{sur}}_{\alpha\beta}$	Surface scattering
$\gamma^{\mathrm{g}}_{\alpha}$	Bistatic scattering coefficient of the ground

CONTENTS

Remote Sensing and Digital Image Processing

1. A. Stein, F. van der Meer and B. Gorte (eds.): *Spatial Statistics for Remote Sensing*. 1999 ISBN: 0-7923-5978-X
2. R.F. Hanssen: *Radar Interferometry.* Data Interpretation and Error Analysis. 2001 ISBN: 0-7923-6945-9
3. A.I. Kozlov, L.P. Ligthart and A.I. Logvin: *Mathematical and Physical Modelling of Microwave Scattering and Polarimetric Remote Sensing*. Monitoring the Earth's Environment Using Polarimetric Radar: Formulation and Potential Applications. 2001 ISBN: 1-4020-0122-3
4. F. van der Meer and S.M. de Jong (eds.): *Imaging Spectrometry.* Basic Principles and Prospective Applications. 2001 ISBN: 1-4020-0194-0
5. S.M. de Jong and F.D. van der Meer (eds.): *Remote Sensing Image Analysis.* Including the Spatial Domain. 2004 ISBN: 1-4020-2559-9
6. G. Gutman, A.C. Janetos, C.O. Justics, E.F. Moran, J.F. Mustard, R.R. Rindfuss, D. Skole, B.L. Turner II, M.A. Cochrane (eds.): *Land Change Science.* Observing, Monitoring and Understanding Trajectories of Change on the Earth's Surface. 2004 ISBN: 1-4020-2561-0
7. R.L. Miller, C.E. Del Castillo and B.A. McKee (eds.): *Remote Sensing of Coastal Aquatic Environments.* Technologies, Techniques and Applications. 2005 ISBN: 1-4020-3090-1
8. J. Behari: *Microwave Dielectric Behavior of Wet Soils*. 2005 ISBN: 1-4020-3271-4

CHAPTER 1

Physical Properties of Soil

Introduction

Soil may be defined as a collection of natural bodies which has been synthesized in profile from a variable mixture of broken and weathered minerals and decaying organic matter. This covers the earth in a thin layer which when mixed with proper amounts of air and water, provides mechanical support and substance for plants. Mineral soils consist of four major components, viz. mineral materials, organic matter, water and air (Fig. 1.1). These exist mostly in a fine state of subdivision and are so intimately mixed that their quantitative separation is rather difficult. Physical properties of soil are of critical importance in relation to growth of plants and to the stability of structures such as roads and buildings. Such properties are commonly considered to be aggregate of size distribution of primary and secondary particles. In addition, continuity of pores; the relative stability of the soil matrix against disruptive forces, both natural and cultural; colour and textural properties are some vital physical soil characteristics. These affect absorption and radiation of energy; and the conductivity of the soil for water, gases and heat and would be usually considered as fixed properties of the soil matrix. But actually some are not fixed because of influence of water content. Properties like water and the air contents are variable in nature. Ordinarily water is an important constituent of soil and despite its transient nature and the degree to which it occupies the pore space, it generally dominates the dynamic properties of soil. Additionally, the properties mentioned above are indicative of soil macroscopic homogeneity which it may not necessarily possess. Broadly speaking soil may consist of layers or horizons of roughly homogeneous soil materials of various types that impart dynamic properties which are highly dependent upon the nature of the layering. Therefore, it is imperative

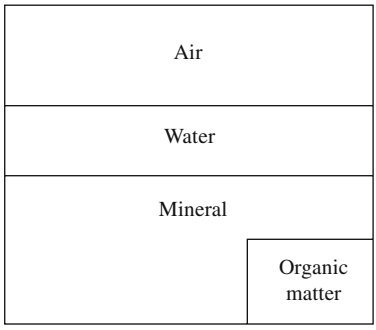

Fig. 1.1 Filling of space in soil (Kirkham and Powers, 1972).

that a discussion of dynamic soil properties include a description of the intrinsic properties of small increments as well as the part properties of the system (Behari, 2001).

From a physical point of view it is primarily the dynamic properties of soil which affect plant growth and the strength of soil beneath roads and buildings. While these depend upon the chemical and mineralogical properties of particles, particle coatings and other factors mentioned above, water content depends upon flow and retention properties. Thus, the relationship between water content and retentive forces associated with the matrix becomes a key physical property of soil.

The soil possesses a large reservoir of water, which has a major impact on many processes. For example, role of soil in the hydrologic cycle is now well understood. North India has been identified as one of four hotspots worldwide where rainfall seems to be directly linked to the amount of moisture in the soil (Narain, 2004). The field water balance is also intimately related with energy balance. A simplified form of the water balance can be represented as an input/output system. Water balance in the soil can be estimated by means of the equation of mass conservation (Franco et al., 2000). If P represents the precipitation as rain or snow, I the irrigation, A the amount lost in the runoff from the surface in underground drainage D and in evaporation from soils and plants (evapotranspiration) ET during the period. A can be negative when water runs on the surface and for D when water comes from the root zone. These are expressed (in mm) (Marshall and Holmes 1988) as

$$P + I = (A + D + ET) \tag{1.1}$$

Equation (1.1) gives the inputs of water to the soil reservoir on left hand side and the outputs (storage) on the right hand side. Runoff occurs when the rainfall exceeds the demands of interception, evaporation and surface storage. It is, thus, clear that most of the water in the hydrologic balance enters the soil for some period of time and is returned to the atmosphere. Another related parameter, the capillary rise, is the amount of water transported upwards from water table to the root zone. The amount of capillary rise would obviously depend on soil type, water table and wetness of the root zone. These processes as well as run off are controlled by soil properties. Thus, the amount of water stored W in a soil horizon of thickness z is given by

$$W = m_v z$$

where m_v is the volumetric water content.

Drainage

Drainage is assumed to take place when soil water is in excess of water capacity of the root zone. This leaves the soil profile as a certain fraction of the moisture surplus (Kerkides et al., 1996). Here, the accumulation of soil water below crop root zone is assumed to be equal to the drainage (Singh et al., 1987). When no drainage takes place, soil moisture depends on daily evapotranspiration (ET) rates and precipitation (Rosenthal et al., 1977). Water loss due to deep percolation and seepage can be considered as a single component parameter (Mishra et al., 1998).

Physical Properties of Mineral Soils

The analytical procedure by which the particles are separated is called *mechanical analysis* and is determination of particle size distribution. Soil structure is the arrangement of soil particles into groups of aggregates. These two properties help to determine not only the nutrient supplying ability of soil solids but also the supply of water and air, which is important to sustain the plant life.

Soil Texture Classes

Soil texture affects the sensing of soil moisture because the dielectric constant changes with the relative amount of sand, silt and clay in the soil though to a lesser extent and can be neglected (Wang and Schmmugge, 1980). Qualitatively, it refers to the feel of the soil material and pertains to the relative proportion of various sizes of particles in a given soil. The traditional method of characterizing particle size in soils is to divide these into three size ranges, viz. sand, silt and clay (Fig. 1.2) as follows:

$$\text{Sand: } > 0.05 \text{ mm}$$

$$\text{Silt: } 0.002 > d < 0.05 \text{ mm}$$

$$\text{Clay: } < 0.002 \text{ mm}$$

Sizes > 2 mm are termed as gravel.

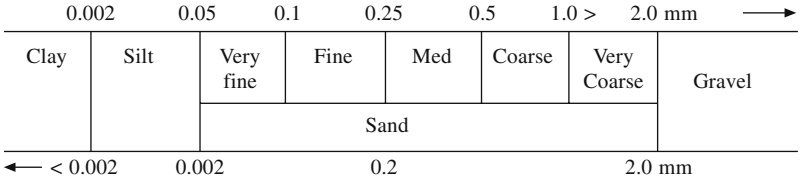

Fig. 1.2 Particle size soil classification.

The overall textural designation class is determined on the basis of mass ratios of these three fractions. Some soils are well graded, i.e. have continuous array of particles of various sizes. Other soils are poorly graded as they contain a dominance of particles of one or several distinct size ranges. The textural classification of a soil provides clue for visual inspection. Such classification is also important for knowing how much water can be held for crop use.

Three broad and fundamental groups of soil recognized are: sands, loams and clays. US Department of Agriculture has devised an accurate and fundamental method for the naming of soils based on mechanical analysis. The relationship between such analysis and class names, shown in Fig. 1.3, essentially represents that a soil is a mixture of different sizes of particles. This shows the relationship between the class name of soil and its particle size distribution. The points corresponding to the percentage of silt and clay present in the soil under consideration are located on the silt and clay lines, respectively. Lines are then projected inward, parallel in the first case to the clay side of the triangle and parallel to the sand side in the second case. The name of the compartment in which the two lines intersect is the class name of the soil in question.

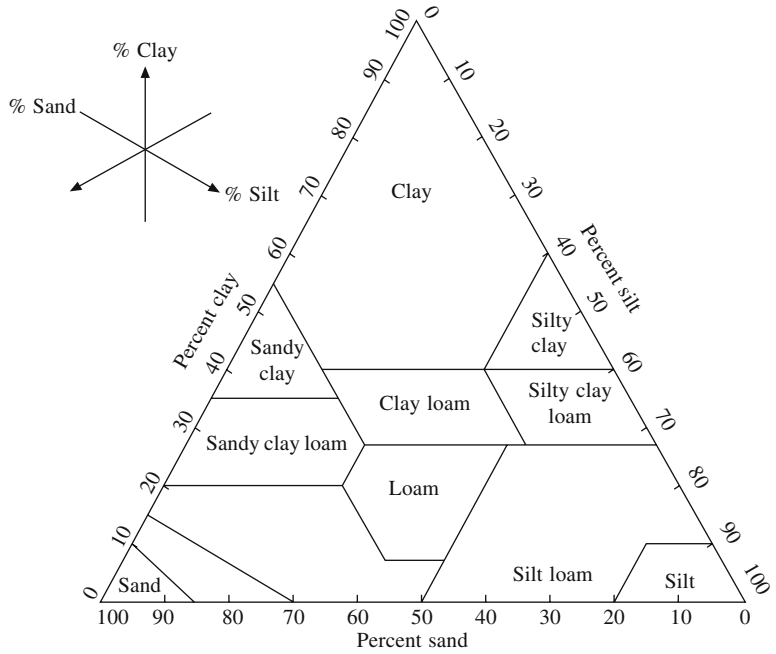

Fig. 1.3 Soil classification triangle (US Department of Agriculture).

Effect of soil texture can be understood by considering the behavior of water as it is added to dry soil. The large dielectric constant of liquid water is due to the water molecules ability to align its dipole moments along an applied field. Thus, anything that would hinder molecular rotation of water molecules, e.g. freezing, very high frequencies or tight binding of water molecules to a soil particle, will reduce dielectric constant of water. Since the first water molecules, which are added to the soil, are tightly bound to the particles' surface, they will contribute only a small increase to the soil dielectric constant. As more water is added above transition point W_t, the additional molecules are farther away from the particles' surface and are more free to rotate and hence, make larger contribution to the soil dielectric constant. The surface area in a soil depends on particle size distribution or texture of the soil. Clay soils, with higher surface area, retain more of the tightly bound water than sandy soils; thus, these transition points occur at higher moisture levels in clay soils (Schmugge, 1983).

In mineral particles, organic materials (both decomposed and undecomposed), numerous living organisms and chemical compounds, such as iron and aluminium oxides are also found in soil. In addition, both water and air, though important components of soil, but being transient in nature, are usually not treated as constituents of the soil matrix. Solid particles of varying sizes make up the 'skeleton' of the soil. Between these particles are interconnected pore spaces that vary considerably in size and shape (Fig. 1.4). In a completely dry soil, all of the pore spaces are filled with air, and in a completely wet soil all of the pore sizes are filled with water. However, in most realistic field situations the pore spaces are filled with water and air. The

physical properties of the soil, including its ability to store water, are very much dependent upon fraction of the bulk soil volume that is filled with water and air. For plant growth and development to be normal, a balance of water and air in the pore space is required to be maintained. If water is limited, plant growth may be inhibited by water stress, and on the other hand, if too much water limits air, then growth may be limited by insufficient aeration.

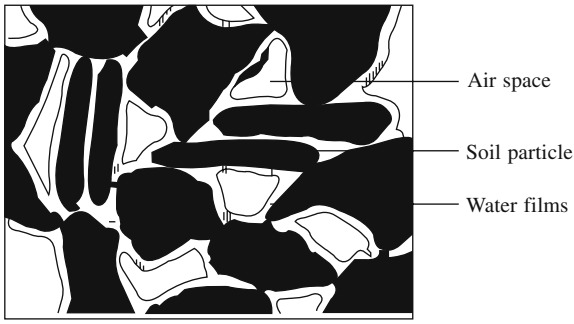

Fig. 1.4 Cross-section of soil.

The approximate volume of composition of a representative silt loam surface soil in optimum condition for a plant growth is as follows:

It contains about 50% pore space (air and water). The soil surface consists of about 45% mineral matter and 5% organic matter. At optimum moisture for plant growth, the 50% of pore space possessed by this representative soil is divided approximately equally, viz. 25% water and another 25% air, which of course depends upon weather conditions (Fig. 1.1). The volume composition of top soil is different from subsoil. They are generally lower in organic matter content, are somewhat more compact and contain a higher percentage of small pores. This is suggestive that they have a higher percentage of minerals and possibly water. Proportion of air and water determines the suitability of plant growth in a particular environment.

Inorganic Constituents in Soils

An examination of a sample of soil illustrates that the inorganic portion is variable in size and composition. It is found to be composed of small rock fragments and minerals of various kinds. The rock fragments are remnants of massive rocks from which the regolith occurs and the soil have been assumed to be formed by weathering. These are usually quite coarse (Table 1.1). On the other hand, the minerals are extremely

Table 1.1 Four major size classes of inorganic particles and their general properties

Size fraction	Common name	Mode of observation	Dominant composition
Very coarse	Stone, gravel	Unassisted eye	Rock fragments
Coarse	Sand	Unassisted eye	Primary minerals
Fine	Silt	Light microscope	Primary and secondary
Very fine minerals	Clay	Electron microscope	Mostly secondary

variable in size. Some are as large as the smaller rock fragments, while others like colloidal clay particles are so small that they can be seen only with an electron microscope. Quartz and some other primary minerals have persisted with little change in composition from the original country rock. The weathering of less resistant minerals has formed other minerals such as the silicate clays and the iron oxides as the regolith developed and soil formation progressed. These minerals are called *secondary minerals*. In general, the primary minerals dominate the coarser fractions of soils, whereas, secondary minerals are most prominent in the fine materials especially in clays. It is, thus, imperative that mineral particle size influences the properties of the soils in the field.

Particle Density of Mineral Soils

One means of expressing soil weight is in terms of the density of the solid particles making up the soil. It is usually defined as the mass of a unit volume of soil solids and is called the *particle density*. In the metric system, particle density is usually expressed in terms of grams per cubic centimeter.

Structure of Mineral Soils

Although the texture is undoubtedly of great importance in determining certain characteristics of a soil, it is evident that the grouping or arrangement of particles also exerts considerable influence. The term *structure*, used to refer to such grouping, is descriptive of the gross, overall aggregation or arrangement of the primary soil components. A profile may be dominated by a single structural pattern. More often, a number of types of aggregation are encountered as one scans various levels. It is apparent that soil conditions and characteristics such as water movement; heat transfer, aeration, bulk density and porosity will be influenced by the structure. In fact, the important physical changes imposed by the farmer in ploughing, cultivating, draining, liming and manuring his land can be termed structural rather than textural. Four primary types of soil structures recognized are: plate like, prism like, block like and spheroidal. The last three are further subdivided into two subtypes each.

Soil Organic Composition

This essentially represents a culmination of incomplete decay and partially synthesized plant and animal residues. The organic matter content of a soil is only about 3 to 5% by weight in a representative mineral top soil. However, its influence on soil properties and consequently on plant growth is far greater than is indicative of the low percentage. Organic matter functions as a 'granulator' of the mineral particles, being largely responsible for the loose, easily managed conditions of productive soils. Also, it is a major source of two important mineral elements, phosphorous and sulphur and essentially the sole source of nitrogen. Through its effect on the physical condition, soil organic matter also increases the amount of water. Soil can hold this water and a portion of this water is available for the plant growth. Finally, organic matter is the main source of energy for soil's micro-organisms. Soil organic matter consists of two general groups: (a) original tissue and its partially decomposed equivalents and (b) the humus.

Bulk Density

An important property, which can be used to characterize the structural state of a soil, is the bulk density defined as

$$\rho_b = \frac{\text{Mass of dry soil}}{\text{Volume of bulk soil}} = \rho_p \frac{cA}{DA} = \rho_p \frac{c}{D} \tag{1.2}$$

where ρ_b is soil bulk density, ρ_p the soil particle density, A is area, c the equivalent depth filled with solid and D the total equivalent of the soil made up of solids, water and air. Bulk density is not a unique value for a soil for it depends upon compaction, swelling, etc. It is, thus, imperative that soil surface ρ_b can change considerably over a season. Below the soil surface ρ_b may be nearly constant in a given climate or may change over a characteristic range during a season. Soils that swell and shrink and have large cracks have special problems that make it necessary to consider large volumes to get reliable values of ρ_b. Soil particle density ρ_p is essentially a constant for a soil with a given texture. It is a measure of the ratio of soil mass to the soil volume actually filled by the solid particles.

Bulk density is a weight measurement by which the entire soil volume is taken into consideration. This is unlike particle density, which is considered with the solids of pore spaces as well. Thus, soils that are loose and porous will have low weights per unit volume (bulk densities) and those that are more compact will have correspondingly higher values. The bulk densities of clay, clay loam and silt loam surface soils may range from 1.0 to as high as 1.60 g/cm^3 depending on their physical conditions. A variation from 1.20 to 1.80 g/cm^3 may be found in sands and sandy loams. Very compact sub-soils, regardless of their texture, may have bulk densities as high as 2.0 g/cm^3 or even higher.

Pore Space

The voids or openings between the particles are collectively known as the pore space. Dry soils have most of their pore spaces filled with air, while for very wet soils, it is the opposite.

Wherever the particle density of soil materials is uniform (taken as 2.65 g/cm^3) it is possible to determine the total pore space fraction of a soil from measurement of the bulk density (mass of dry soil per unit bulk volume) using the formula,

$$\text{Pore space fraction} = 1 - (\rho_b/\rho_p) \tag{1.3}$$

There is considerable variation in the size, shape and arrangement of pores in the soil. The effective size of a pore can be estimated by the amount of force required to withdraw water from the pore. These suction values, expressed in centimetres of water, can be expressed into equivalent pore diameters by using the capillary rise equation

$$r = 2\frac{T}{h_s}dg \tag{1.4}$$

where r is the radius of pore in centimeter, T the surface tension of water, d the

density of water, g the acceleration due to gravity, and h_s is the suction force in centimeters of water.

The ideal soil should have proper assortment of large, medium and small pores. A sufficient number of large or macro-pores (with diameters > 0.06 mm), connecting each other, are needed for the rapid intake and distribution of water in the soil and the disposal of excess water by drainage into the substratum or into artificial drains. When without water, they serve as air ducts. Cracks, old root channels, and animal burrows may serve as large pores. Soils with insufficient functional macro-porosity loose a great deal of rainfall and irrigation water as runoff. They drain slowly and often remain poorly aerated after wetting. One of the first effects of compaction is the reduction of the size and number of the larger pore spaces in the soil.

The primary purpose of the small pores (<0.01 mm in diameter) is to hold water. It is through medium-sized pores (0.06-0.01 mm in diameter) that much of the capillary movement of water takes place. Loose, droughty, coarse, sandy soils have too few small pores. Many tight clay soils may have a greater number of larger pores.

The presence of organic materials having particle densities differing appreciably from those of the mineral particles introduces some error into such computations. Agricultural soils in the plow depth ordinarily have bulk densities ranging from 1.0 to 1.5 g/cm^3 and a pore space fraction from 0.4 to 0.6 g/cm^3, roughly indicating half particle and half pore space.

Soil Temperature

Soil temperature is the most important growth factor of plants. Water movement and availability and the rate of most chemical reactions that release nutrients are also dependent upon soil temperature. Plant environment is controlled by the thermal properties of soils. Temperature of the soil is a function of a number of parameters. Primarily it depends upon absorption of solar radiation and its subsequent, reradiation from the surface, conductive exchange with the air, heat flow within, and the heat capacity of the soil.

Soil colour and surface texture influence both absorption and reradiation. Smooth, light-coloured materials generally reflect light energy and are poor radiators, while rough dark materials absorb and reradiate energy. Thus, rough dark soils tend to warm faster than smooth, light-coloured materials. Organic residues on the soil surface play a major role in determining soil temperature through interception of both incoming and outgoing radiation and bringing about a reduction in the velocity of the air movement at the soil surface. Water content plays a major role in both heat transfer and heat retention, increasing both thermal conductivity and thermal capacity. Change of state of soil water freezing, thawing, and evaporation involves significant quantities of energy as latent heat, which totally controls the thermodynamics of the system.

Thermal Infrared Surface Temperatures

A significant amount of research has been conducted on the diurnal nature of the surface temperature of the soil as observed by a thermal infrared sensor. The temperature of the surface at any given instant of time is dependent on several meteorological and

physical parameters including the soil moisture. Surface temperature is dependent on the thermal inertia of the soil, which in turn depends on thermal conductivity and the heat capacity. If ΔTs is the diurnal temperature difference between the afternoon surface temperature and the early morning surface temperature and T_I the thermal intertia, then $\Delta Ts = f(1/T_I)$, and the diurnal variation D_I is given by

$$D_I = (WP_c k)$$

where W is the day length, P_c the volumetric heat capacity and k the thermal conductivity (Price, 1982). By measuring the amplitude of diurnal temperature change, we can develop a relationship between temperature change and soil moisture. Brightness temperatures at shorter wavelengths are relatively insensitive to soil moisture content.

Soil Water Characteristics

The movement and retention of water in the soil is dependent upon a number of parameters. These include the size, shape, continuity, arrangement of the pores, their moisture content, and the amount of surface area of the soil particles. Movement and retention of water may be characterized by the energy relationship or forces, which control these two phenomena. The hydrology model provides the linkage between near-surface soil moisture and stored water. An important point about soil and water characteristic is that this relationship is nonlinear. Soil water characteristic curves have several uses. One is to determine the maximum specific yields of a soil, which is the maximum amount of water available in an initially saturated soil into a drain at a specific depth. The difference between field capacity and wilting is the available water content and is shown in Table 1.2.

Table 1.2 Field capacity, wilting point, and available water content for various soil types

Soil	Field capacity (FC)	Wilting point (WP)	Available water (FC–WP)
Clay	0.267	0.189	0.078
Silty clay loam	0.229	0.151	0.078
Clay loam	0.207	0.091	0.116
Silty loam	0.191	0.071	0.120
Very fine sandy loam	0.136	0.064	0.072
Coarse sandy loam	0.060	0.036	0.024
Coarse sand	0.013	0.009	0.004

Hanks, 1992, p 41.

Another utility of the soil water characteristic curve is to determine the common matric potential φ_m of two soil volumes that are placed in contact and do not originally have the same φ_m. Figure 1.5 shows a plot of soil-water curves for several soils plotted as a percentage of available water content at a specified φ_m.

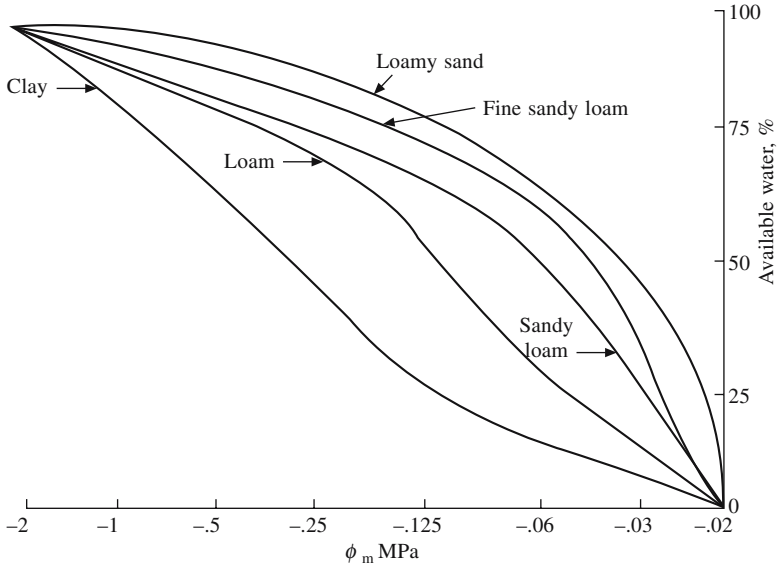

Fig. 1.5 Soil water characteristic curves for five soil types plotted as a percentage of available water at a specified matrix potential (Hanks, 1992).

Water Retention

Water is found in soil in both the liquid and vapour states. The soil air in all the pores, except those in the surface of few centimetres or so of very hot dry soils is saturated with water vapour. Some water is held in the soil pores by the force of adhesion (the attraction of soil surfaces for water molecules) and by the force of cohesion (the attraction among water molecules). Water held by these two forces keeps the smaller pores full of water and also maintains relatively thick films on the walls of many larger pores. When the water in the pores of a layer is filled to the level it can hold, then it moves into the second layer.

Parameters Related to Soil Moisture Retention Under Field Conditions

(i) ***Field Capacity:*** After a soil has been wetted due to rain or irrigation there is a constant rapid downward movement of a portion of the water (internal drainage) due to existence of a hydraulic gradient. After a few days this movement stops. The water content at which such internal drainage ceases is known as the field capacity.

(ii) ***Maximum Retentive Capacity:*** During heavy rain or irrigation the soil might get saturated with water causing instant downward drainage. This saturation point with respect to water is known as the maximum retentive capacity of the soil.

(iii) ***Permanent Wilting Percentage:*** As the soil dries up, plants begin to wilt during daytime in the presence of high temperatures and wind movement. Initially, the plants regain their vigor at night. A time comes when the rate of supply of water is so low that the plants remain wilted night and day. The water content of the soil at this point is called the *permanent wilting percentage*. The amount of soil water held between field capacity and wilting point is called the *available soil moisture*. In

general, approximately half of the total water that a soil can hold at field capacity is available soil moisture.

(iv) *Hygroscopic Coefficient:* If a soil is kept in an atmosphere completely saturated with water vapour (98% relative humidity), it loses the liquid water held even in the smallest of micropores. The remaining water remains associated with soil particle surfaces as absorbed moisture. It is held so tightly that much of it is considered non-liquid and can move only in the vapour phase. The soil moisture content at this point is known as the *hygroscopic coefficient*.

(v) *Tillage:* This is physical manipulation of soil that changes its structure, strength or position in order to improve crop yield and may be required for seed-bed preparation, improving soil-water and soil-air relationship and reduction of impedance to roots and burying of crop residues. Soil moisture strongly controls the behavior of soil in tillage, through several parameters like strength, compactability and adhesion.

(vi) *Evapotranspiration:* One of the important component of water balance in actual field condition is evapotranspiration. Water goes into the air by ever occurring evaporation (E) process from free water surfaces and also simultaneously transpiration (T) from the crops. E and T considered together is evapotranspiration (ET). During idle periods in a field, only E is effective, whereas during crop growth both E and T occur (Tuong et al., 1994). Evaporation from soil surface is a net water loss which does not contribute to crop production and it may constitute 40-70% of the precipitation in arid and semi-arid regions (Wendt et al., 1970). Evaporation from the soil surface can be considered in two stages. First, when the surface soil in moist evaporation proceeds at the constant rate stage. Second, when a critical amount of water is lost, it becomes falling rate stage and is dependent on the hydraulic properties of the soil and the period of initiation of this stage (Ritchie, 1972).

Transpiration rate is dependent on the amount of available soil moisture in the root zone. When soil water is not limiting, T depends on the leaf area index, but when soil moisture is limiting, T is limited by the ratio of available soil moisture to 0.3 of the maximum available moisture content (Kanemasu et al., 1976).

The cumulative evapotranspiration is found to increase at a decreasing rate with time from sowing to harvesting. The cumulative and seasonal evapotranspiration is found to be influenced by depth of irrigation and climatic factors. The seasonal evapotranspiration is found to be more when there are frequent rains (Singh and Kumar, 1993).

(vii) *Soil Tension:* The suction force of tension with which it is held in the soil by adhesion or cohesion may characterize the liquid water. These suction or tension values may be expressed as 'height in centimetres of a unit water column whose weight just equals the force under consideration and the atmosphere's pressure'. Dobson and Ulaby (1981) presented a simple log linear relationship between soil matrix potential or tension T and gravimetric moisture m_g

$$T = A\ 10^{Bm_g} \tag{1.5}$$

where A and B are constants for a given field and depth interval obtained from the desorption measurements. Equation (1.5) allows the estimation of soil tension for the gravimetric moisture associated with each radar data set.

Radar backscattering coefficient σ^0 is given by

$$\sigma^0(\text{dB}) = A \log (T) + B \tag{1.6}$$

Figure 1.6 shows the results of a linear regression for the above model using the multitexture data base. σ^0 (dB) is found to be linearly dependent on log (T) at 4.6 GHz, 10° and horizontal H polarization

$$\sigma^0(\text{dB}) = -2.849 \log (T) + 1.224 \; (\mid r^2 \mid = 0.819) \tag{1.7}$$

where r^2 is the linear correlation coefficient.

Similar results at other combinations of frequency and incidence angles produce similar high correlation for soil depth intervals upto 15 cm.

Computations of Soil Parameters

For gravimetric moisture retention at 0.33 bars, field capacity (FC) can be approximated by the empirical formula on soil composition (Schmugge et al., 1976)

$$\text{FC} = 25.1 - 0.21 \; (\%\ \text{sand}) + 0.22 \; (\%\ \text{clay}) \tag{1.8}$$

Knowledge of soil bulk density permits conversion of FC to a volumetric basis

$$m_v = m_g \times \rho_b \tag{1.9}$$

Wilting coefficient W_p and transition point W_t are calculated by using the Wang and Schmugge model (1980)

$$(W_p) = 0.06774 - 0.00064 \text{ Sand } (\%) + 0.00478 \text{ Clay } (\%) \tag{1.10}$$

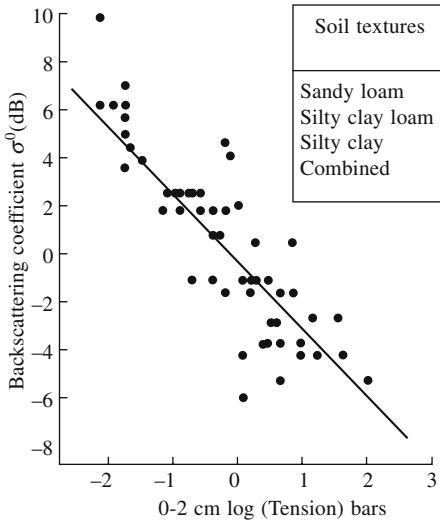

Soil textures	Correlation coefficient	Sample size
Sandy loam	–.908	22
Silty clay loam	–.752	22
Silty clay	–.863	21
Combined	–.819	63

Fig. 1.6 Radar response at 4.6 GHz, 10° and horizontal *H* polarization to 0-2 cm (Dobson and Ulaby, 1981). A log linear model of the moisture tension characteristic is adopted for estimating soil moisture.

$$W_t = 0.49\ W_p + 0.165 \tag{1.11}$$

and

$$r^2 = -0.57\ W_p + 0.48 \tag{1.12}$$

where the correlation coefficient for W_t (= 0.9) and for W_p (= 0.8). This indicates that texture data can be used to estimate the value of W_t for a soil. For the imaginary part of the dielectric constant at low frequencies we would add the term due to conductivity loss ε_σ and the total dielectric loss ε_t'' becomes

$$\varepsilon_t'' = \varepsilon'' + \varepsilon_\sigma'' = \varepsilon'' + 60\ \lambda\sigma = \varepsilon'' + \alpha W c^2 \tag{1.13}$$

where σ is the ionic conductivity (mhos/cm), λ the wavelength (cm), ε_t'' is assumed to be proportional to Wc^2 based on the soil data and α is the parameter chosen to best fit the measured ε_t''.

Soil Thermal Resistivity

Experimental results are obtained by using field thermal probe. The following generalized relationships have been developed for estimating the soil thermal resistivity (Naidu and Singh, 2004).

Dry (Single-phase) Soils

For dry soils (single-phase) the following relationship to estimate soil resistivity is being proposed:

$$\frac{1}{R_T} = 0.01 \times [a \cdot 10^{-3+0.06243\gamma_{dry}}] \tag{1.14}$$

Moist (Single-phase) Soils

Clays and Silts: To obtain resistivity of moist clays and silts (single-phase) the following relationships are proposed:

$$\frac{1}{R_T} = 0.01 \times [b \cdot 10^{-3+0.06243\gamma_{dry}}] \tag{1.15}$$

$$\frac{1}{R_T} = 0.01 \times [1.07 \log (w) + c] \times 10^{-3+0.06243\gamma_{dry}} \tag{1.16}$$

where R_T is the soil thermal resistivity (m.K.W^{-3}), w the moisture content (%) and γ_{dry} is the dry density of the soil (kN.m^{-3}). Parameters a, b and c are dependent on the soil type and its moisture content. Eq. (1.16) can also be used to predict resistivity of silts and sands.

In order to facilitate computation of thermal resistivity of a multiphase soil system, generalized relationships have been developed, assuming that soil consists of six phase system (clays, silts, silty-sand, fine-sand, coarse-sand and gravel). For a naturally occuring soil, the resistivity of different phases can be calculated. These resistivity values are multiplied by certain weights, which can be computed on the basis of their phase fraction.

Soil Air Characteristics

Soil air has several differing features introduced from the atmosphere in several respects. First, the soil air is not continuous but is located in the maze of soil pores separated by soil solids. Second, soil air has generally a higher moisture content than the atmosphere, the relative humidity reaches almost 100% when the soil moisture is optimum. Lastly, the content of the carbon dioxide is usually much higher and that of oxygen lower than found in the atmosphere. Carbon dioxide is often several hundred times more concentrated than ordinarily (0.03%) found in the atmosphere. Oxygen decreases accordingly; and in extreme cases, may be around 10-12%.

As compared to about 20% for normal atmosphere, the content and composition of soil air is determined to a large extent by the soil-water relationships. The air consisting of a mixture of gases moves into those soil pores not occupied by water. Following a rain large pores are first vacated by the soil-water, followed by the medium size pores, as water is removed by evaporation and plant utilization. Thus, the soil air ordinarily occupies the large pores and as the soil dries out, also occupies intermediate in size.

Clay and Humus

The chemical and physical properties of soil are controlled largely by clay and humus. Both these constituents exist in the colloidal state wherein the individual particles are characterized by extremely small size, large surface area per unit weight and the presence of surface charges to which ions and water are attracted. These are centers of activity around which chemical reactions and nutrient exchange occur. Furthermore, by attracting ions to their surfaces, they temporarily protect essential nutrients from leaching and then release them slowly for plant use. Because of their surface charges they also act as a bridge between larger particles, thus, helping to maintain the stable granular structure which is so desirable in a porous, easily worked soil. On a weight basis the humus colloids have greater nutrients and water holding capacities than clay. However, clay is generally present in larger amounts and its total contribution to the chemical and physical properties will usually be equal to that of humus. The best agricultural soils contain a balance of the properties of these two important soil constituents.

Surface Roughness

Surface roughness is an important parameter from agriculture point of view. Measure of surface roughness depends on frequency. A surface can be defined as smooth when the extreme height variation of a surface are smaller than one-fourth of the wavelength, i.e. a surface considered as rough in the X-band (10 GHz, λ = 3.0 cm) will look smooth in the L-band (1.2 GHz, λ = 25 cm). Roughness plays an important part for backscattering from a vegetation canopy, as every crop will be rough above a certain frequency. As soon as this occurs, the dependence of radar backscatter with increasing incidence angle will decrease, as the diffuse component becomes dominant (De Loor, 1993). With increase in microwave frequency, the geometric variation of vegetation

increases more as compared to the effect of dielectric constant (Brisco et al., 1991).

Surface roughness corresponds to the soil surface area interfacing the air and can transmit the upwelling energy. The effect of surface roughness is to increase soil emissivity. Surface roughness $R(\theta)$ effects are modelled using an approach described by Choudhury et al. (1982)

$$R\ (\theta) = 1 - [(1 - e(\theta))\ \exp(-\ h\ \cos^2\ \theta)] \qquad (1.17)$$

where h is roughness parameter, while e and R are the smooth and rough surface emissivities, respectively.

For low frequencies, the effect of roughness can be explained by the single parameter $h = \sigma_s/L$, where σ_s is the surface standard deviation and L is its horizontal correlation length, both expressed in wavelength units. Small values of h (about 0.10 or less) correspond to smooth surfaces. However, right after tillage a value of $h = 0.5$ is possible (Wang et al., 1983). Higher soil surface roughness (microtopography) reduces its microwave reflectivity and hence, increases its emissivity.

Roughness Estimation

Several investigators (Boisvert et al., 1997; Wegmuller et al., 1989; Zribi and Dechambre, 2002) have pointed out that the difference $\Delta\sigma^0$ between signal measurements (in dB) taken at two different incidence angles is essentially linked to soil roughness and depends only weakly on soil moisture. Fig. 1.7 shows simulations of $\Delta\sigma^0$ (with incidence angles, respectively, equal to 20 and 30°) for three different values of soil moisture 10%, 20% and 30%, and three different cases of soil roughness (Zribi et al., 2003). These simulations have been obtained from the Integral Equation Model (IEM), (Fung et al., 1992). From Fig. 1.7, soil moisture effect appears negligible in comparison with roughness effect on $\Delta\sigma^0$. Therefore, we can write

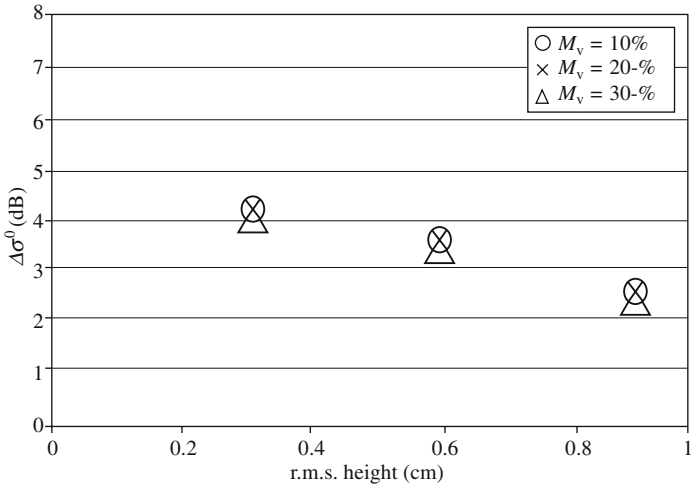

Fig. 1.7 A plot between backscattering coefficient difference $\Delta\sigma^0$ (between 30 and 20°) vs soil moisture and roughness parameters for a bare soil surface (Zribi et al., 2003).

$$\sigma^0(\theta_1) - \sigma^0(\theta_2) \approx h \text{ (roughness)} \tag{1.18}$$

i.e. the simultaneous measurements performed with two different incidence angles present a difference only dependent on soil roughness. In this case, the two different incidence angles correspond to the midbeam and forebeam antennae (Zirbi et al., 2003).

The IEM simulations of the backscattering coefficient were performed for different kinds of surfaces presenting different root mean square (r.m.s.) heights, ranging from 0.3 to 1 cm for a constant water content. It was found that the results were very close for incidence angles around 15°. The soil roughness can be estimated by fitting the σ^0 angular differences to the IEM predictions. In order to obtain a better accuracy, the minimization is performed on a large number of couples of data acquired over a time period during which it can be assumed that the surface roughness at this scale is constant. If n is the number of couples of data, the function to be minimized is

$$F = \sum_{i=1}^{n} [(\sigma_1^i(\theta_1^i) - \sigma_2^i(\theta_2^i)) - (\sigma_{\text{IEM}}^i(\theta_1^i) - \sigma_{\text{IME}}^i(\theta_2^i))]^2 \tag{1.19}$$

where i is the ith measurement, $\sigma_1^i(\theta_1^i)$ and $\sigma_2^i(\theta_2^i)$ are the wind scatterometer backscattering coefficients at incidence angles θ_1^i and θ_2^i, and $\sigma_{\text{IEM}}^i(\theta_1^i)$ and $\sigma_{\text{IME}}^i(\theta_2^i)$ are the IEM simulations at the same incidence angles.

Penetration Depth

One of the basic concepts in electromagnetic remote sensing is the penetration depth which is often referred as the skin depth. These are related but not identical.

An expression for the penetration depth P_{d} can be obtained by considering a wave incident from air upon a soil surface in the z-direction. In general, a part is scattered back into the air and the remaining is penetrated into the medium. If the power at a point beneath the soil surface ($z = 0+$) is P (0+), the power at a depth z is given by the expression (Ulaby et al., 1982)

$$P(z) = P(0+) \exp\left(-\int_0^z ke(z')\,dz'\right) \tag{1.20}$$

Power at a depth d (P_{d}) is the one for which it falls to $1/e$ of its value first beneath the surface

$$\frac{P_{\text{d}}}{P(0+)} = \frac{1}{e} \tag{1.21}$$

Knowing the dielectric properties of the materials involved we can calculate the penetration depth P_{d} by the following relation:

$$P_{\text{d}} = \lambda\,(\varepsilon')^{0.5}/2\pi\varepsilon'' \tag{1.22}$$

For a wavelength λ of 21 cm, ε'' ranges from near zero to a maximum of 5 for very wet soils. The values of ε' will range from about 3 to 30 (dry to wet). For a normally

dry soil ($\varepsilon' = 5$ and $\varepsilon'' = 0.1$) the penetration depth would be about 75 cm and for a wet soil ($\varepsilon' = 30$ and $\varepsilon''' = 5$) would be about 3.7 cm. The penetration depth is a useful concept and indicates the effect of wavelength and soil moisture on the depth of the soil contributing to the measurement. At longer wavelengths for dry soil it is expected that this depth is larger than for short wavelengths and for wet soil. However, the actual values are difficult to compute.

For $|\varepsilon| = (\varepsilon'^2 + \varepsilon''^2)^{0.5}$, and δ the loss angle ($\tan \delta = \varepsilon''/\varepsilon'$)

$$P_d = \frac{\lambda}{4\pi\sqrt{|\varepsilon|} \cdot \sin(\delta/2)} \tag{1.23}$$

Since even for driest materials (e.g. dry sand) $\sqrt{|\varepsilon|} > 1.5$, hence $\sin(\delta/2)$ must be smaller than $\frac{1}{6}\pi = 0.053$ and thus $\tan \delta < 0.106$ to make P_d larger than λ, the wavelength used. This value is reached at a few percent moisture in most materials i.e. in most cases P_d will be smaller than 1 or the penetration depth will usually be smaller than the wavelength used. P_d becomes higher for low frequencies or for dry conditions. It varies from 10 to 30 mm for m_v below 20% and 10 to 15 mm for m_v above it.

Depth of penetration in sandy-loam soil at different moisture content and frequencies is shown in Fig. 1.8 (Troch et al., 1997).

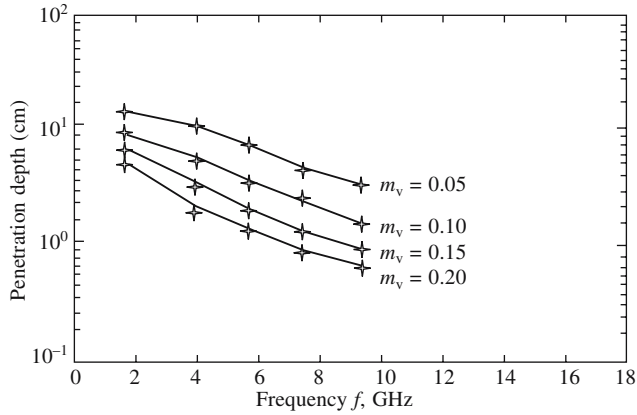

Fig. 1.8 Depth of penetration in a sandy-loam soil at different moisture contents and for different observation frequencies (Troch et al., 1997).

For a given terrain, the depth of penetration of a incident radiation is commonly expressed by the term *skin depth* which is defined as the depth below the surface at which the amplitude of the incident wave will have decreased to about 37% of its value at the surface. This quantity 'skin depth', denoted by δ_D, is related to the wavelength in the medium by the relationship (Ulaby et al., 1978)

$$\delta_D = \left[\frac{\lambda}{\pi g_t \eta}\right]^{1/2} \tag{1.24}$$

where δ_D is the skin depth, g_t the conductivity of the terrain, $\eta = (\mu/\varepsilon)^{1/2}$, in which ε and μ are the permittivity and the permeability of the terrain, respectively.

The above expression indicates that as frequency decreases depth of penetration increases and the vice versa.

The effect of frequency must be considered when interpreting multifrequency radar imagery. The use of multifrequency data may allow distinction between roughness types, as the different wavelengths are sensitive to varying extent, to varying roughness of the investigating surface (Elachi, 1988). Also the attenuation and scattering by vegetation canopy increases with increase in frequency. Therefore, for soil moisture sensing, lower frequencies are preferred than higher frequencies. Moreover, lower frequencies have additional advantages like higher penetration capability in soil profile (Ulaby et al., 1978; Schmullius and Furrer, 1992).

Equivalent Soil Moisture

The equivalent soil moisture (EQSM) is defined as (Newton et al., 1982):

$$\text{EQSM} = \sum_{i=1}^{N} \frac{\text{SM}i\ \text{BT}i}{\text{BT}_{\text{total}}} \tag{1.25}$$

where SMi is the soil moisture content for the ith layer, BTi the contribution to surface brightness temperature from ith layer, BT_{total} is the total brightness temperature at the surface and N the number of layers. It is apparent that the EQSM parameter is a function of both the moisture profile and radiative contribution profile (Newton, 1977). Thus, the EQSM is interpreted as the average soil moisture over the sampling depth. It was determined that the EQSM sampling depth as defined by Newton, (1977) corresponds to the soil depth above which percent of the thermal microwave emission originates. The EQSM parameter does correlate to brightness temperature measurements. The EQSM parameter corresponds most closely to the 0-20 cm soil moisture average.

The thermal sampling depth is defined as (Wilheit, 1978):

$$\delta T = \frac{\sum_{i=1}^{N} X_i\, f_i}{\sum_{i=1}^{N} f_i} \tag{1.26}$$

where f_i is the fraction of radiation incident on the air-soil interface that would be observed in the ith layer and X_i is the depth of the ith layer.

It may be noted that the EQSM and the thermal sampling depths are very similar and much deeper than the reflectivity sampling depth. It can be seen that the brightness temperature just above the soil surface is strongly dependent on soil moisture while the brightness temperature just below the soil surface is only weakly dependent on soil moisture changes. This shows the importance of the air-soil interface transmission coefficient on overall soil emission.

The reflectivity sampling depth obtained by Wilheit (1978) at a depth at which the reflectivity from a soil volume containing linearly varying soil moisture is equivalent

to the reflectivity from a soil volume containing a uniform soil moisture equal to the average of the linearly varying moisture in the depth.

The penetration depth identified by Schmugge et al. (1976), corresponds to approximately a tenth of a wavelength for the reflectivity sampling depth and greater than a wavelength for the thermal sampling depth.

Emissivity of a Soil Layer

There are several approaches leading to the conclusion that the microwave emission from a soil is the result of the integration of the emission from all depths and the importance from each depth decreases with depth. The fraction of this upwelling radiation that is transmitted to the air is called the emissivity and is determined by the dielectric properties of a transmission layer at the surface. Studies indicate this layer to be a few tenths of a wavelength. The rate at which the weighting function decays (the decreasing contribution of each layer) depends upon the wavelength of the sensor and the dielectric profile of the soil. It is, thus, suggestive that for a majority of natural soil surface a longer wavelength sensor provides more information on a thicker soil layer than does at a shorter wavelength. At shorter wavelengths the sensor responds to a very shallow soil layer (< 1 cm at a wavelength of 2.25 cm). As the wavelength increases the depth of the transition layer that the sensor sees through also increases. This layer is about 5 cm at L-band (21 cm). This conclusion also supports a large number of both theoretical and experimental results.

Emissivity of soil e is given by

$$e = 1 - \left| \frac{1 - \sqrt{\varepsilon'}}{1 + \sqrt{\varepsilon'}} \right|^2 \tag{1.27}$$

where ε' is the real part of the dielectric constant.

Percentage volumetric soil moisture is also derived from the relationship with the knowledge of emissivity (Alex and Behari, 1998).

Fresnel's equations relate the complex dielectric constant with the soil emissivity e using the relation

$$e = 1 - r_{\text{soil}} = 1 - | (\cos\theta \sqrt{\varepsilon} - \cos\theta')/(\cos\theta \sqrt{\varepsilon} + \cos\theta') | \tag{1.28}$$

where r_{soil} is the soil reflectivity, θ the angle of incidence (with the normal), ε the complex dielectric of soil and θ' the subsurface incidence angle.

$$\theta' = \cos^{-1} [1 - (\sin^2\theta/\varepsilon)]^{1/2} \tag{1.29}$$

The emissivity of ground surface in terms of soil emissivity and roughness parameter h is given by

$$e_{\text{surface}} = 1 + (e - 1) \exp h \tag{1.30}$$

Since soil emissivity depends to a large extent on the complex dielectric constant, which in turn depends on the volumetric moisture content m_v, we can directly correlate emissivity with m_v. At normal incidence, the emissivity of a soil surface increases

with increasing degree of surface roughness. A typical value of soil surface emissivity is ~0.9 for a dry soil and ~0.6 for a wet soil comprising the 0-5 cm layer (Schmugge et al., 2002).

Microwave Brightness Temperature

The microwave brightness temperature of a soil medium is governed by the dielectric and temperature depth profiles of the soil and by its surface roughness. Due to strong dependence of the soil dielectric constant on moisture content, the brightness temperature T_B also exhibits strong sensitivity to soil moisture content, provided the surface roughness (expressed in wavelength units) is not very large. The mechanisms responsible for microwave emission from land surface and volumes are not well understood. This stems from the fact that land targets have complicated dielectric and complex geometric properties.

For a simple soil emission configuration microwave brightness temperature is given by

$$T_B = t\,(H)\,[rT_{sky} + (1 - r)\,T_{soil}] + T_{atm} \tag{1.31}$$

where $t\,(H)$ is the atmospheric transmissivity for a radiometer at height H above the soil, r is the smooth surface reflectivity, T_{soil} is the kinetic temperature of the soil, T_{atm} is the average temperature of the atmosphere and T_{sky} is the contribution from the reflected sky brightness.

$$T_B(\theta_0, P) = e^{SP}(\theta_0 P)T_s \tag{1.32}$$

where T_B is the soil thermometric temperature, $e^{SP}\,(\theta_0, P)$ is the P-polarized specular emissivity of the soil surface and T_s is the corresponding temperature.

When a vegetation layer is present over the soil surface it introduces attenuation of the radiation emitted by the soil and also contributes thermal emission of its own. It is obvious and confirmed by experimental investigations that vegetation reduces the sensitivity of T_B to soil moisture content and that the reduction in sensitivity depends on the type of vegetation and on the wavelength of observation. There seems to be good correlation between the brightness temperature and the soil temperature for the upper few centimeters of the soils.

For typical remote sensing applications (>>5 cm), the atmospheric transmission will approach 99%, hence Eq. (1.32) can be written as

$$T_B = eT_s \tag{1.33}$$

where e is the emissivity and is dependent upon the dielectric constant of the soil and the surface roughness.

Microwave Emission Model

Microwave brightness temperature is an indication of the energy emitted from the soil. For this knowledge of the dielectric properties and temperature of the soil are needed to calculate the propagation of energy through the soil (Wang, 1987). The brightness temperature T_B (K) measured by the microwave sensor is obtained by (Burke et al., 1998)

$$T_{B_p} = \sum_{i=1}^{n} f_{ip} T_i + R_p T_{sky} \tag{1.34}$$

where p is the indicative of polarization type (horizontal or vertical); f_{ip} is property of the ith layer related to its electromagnetic absorption; T_i the physical temperature of the ith layer and R_p the p-polarized surface reflectivity. The factor f_{ip} are dependent on the soil dielectric properties and the look angle of the sensor. These in turn are dependent upon the fraction of the radiation incident at the surface that is absorbed or emitted by each layer. Most of the energy incident at the soil surface is emitted by the layers nearing it and hence, f_{ip} becomes negligible at greater depths. Also, any atmospheric effects are assumed to be negligible at 1.4 GHz. As the frequency increases the attenuation due to soil and vegetation increases.

The absorption effects of any vegetation present (scattering is assumed to be negligible) are accounted for by expressing the radiometric brightness temperature as a sum of the emission from the soil reduced by the vegetation. The direct emission from the vegetation and that reflected by the soil surface is (Ulaby et al., 1986)

$$T_{B_p veg} = (1 + R_p \Gamma)(1 - \Gamma)(1 - \omega)T_v + (1 - R_s)\Gamma T_{B_p soil} \tag{1.35}$$

where R_s is the net radiation at the soil surface (w/m^2), ω the single scattering albedo and T_v the temperature of the vegetation (K). The transmissivity of the vegetation layer Γ is given as

$$\Gamma = \exp(-T \sec \theta) \tag{1.36}$$

where θ is the look angle measured from nadir and T the optical depth of the vegetation. It is thus obvious that the two parameters required to define the vegetation properties are the optical depth and the single scattering albedo. T is directly proportional to the integrated vegetation water content and also determines the distance seen through the canopy by the sensor. This defines the amount of absorption and emission by the canopy. It can be determined empirically as

$$T = \beta \theta_{veg} \tag{1.37}$$

where β is an empirical constant, defined for a specific vegetation cover type and frequency and θ_{veg} the depth integrated vegetation water content (kg m^{-2}). At 21 cm wavelength (1.4 GHz frequency), β has been shown to vary between 0.08 and 0.15. The single scattering albedo is a parameter that describes the structure of a crop canopy. This parameter is generally very small for most vegetation at L-band frequency (upto approximately 0.04) and has, in this case, been taken to be zero (Jackson and Schmugge, 1991).

The data required to determine the radiometric brightness temperature are the radiometric configuration (wavelength and the look angle from nadir), water content and temperature profiles in the soil, soil texture, and the optical depths. The effective (or significant) depth of soil dielectric properties that influences brightness temperature is much shallower than the depth of the effective soil temperature. The above parameters will be of immense use to agricultural scientists to understand the dielectric behavior of soil.

CHAPTER 2

Dielectric Behavior of Soil

Soil Moisture

From the point of view of the environment, soil moisture is a key parameter. One of the primary resources upon which man depends for his existence is soil moisture. It plays an important role in the interactions between the land surface and the atmosphere, as well as ground water storage. Surface soil is important for its role on the continental watercycle, more specifically on the partition of precipitation between surface runoff and infiltration (Beven and Fisher, 1996) and in partitioning the incoming radiation between latent and sensible heat flux. The energy from the former is radiated into the atmosphere, while the latter (sensible heat) processes the convective heats.

Moisture near the soil surface is a primary factor in determining runoff, infiltration, redistribution, storage and drainage. Soil moisture also plays a vital role in the functioning of ecosystems. Surface soil moisture is a basic component of meteorological cycles and in the determination of agricultural crop yield (Fig. 2.1). It is important in industrial and mining processes. While significant amount of effort have gone into predictive modelling of these processes, few models utilize or even estimate soil moisture. This arises mainly due to the nonavailability of the wide coverage of measurements data, necessary as an input to the dynamic models. Remote sensing techniques offer an alternative means of fulfilling this gap for rapid measurement of the moisture status near the soil surface over extended areas. The technique can also be used to measure soil moisture quantitatively on bare and short vegetated surfaces.

Basic to the soil moisture information is the knowledge of its permittivity (dielectric constant). Therefore, corresponding to a given soil moisture depth profile, a value of permittivity exists which influences the interaction of an electromagnetic wave at the air soil interface as well as the wave propagation properties inside the soil medium. Two techniques have generally been adopted for estimation of soil moisture. One depends directly on experimental measurement while the other on theoretical computations based on measured soil moisture and soil temperature profiles. The soil moisture at any given depth is correlated to the soil moisture at other depths. Therefore, it is difficult to identify experimentally the soil layer to which the radiometer is responding by simply correlating measured brightness temperature to the average soil moisture within different soil layers. A knowledge of the spatial distribution of

soil moisture is critical when assessing crop yields and surface energy balance besides many other related parameters (Schmugge et al., 1980). Information about the variability of soil moisture is essential in designing measurement systems and descriptions of the land-atmosphere surface interactions and related hydrologic phenomena (Cosh and Brutsaert, 1999). As a result, theoretical models have been used to predict the weighting as to how much energy is emitted by individual soil layer. These weighting functions may be applied to soil moisture profiles to determine the depth of penetration and to predict an average soil moisture over this depth.

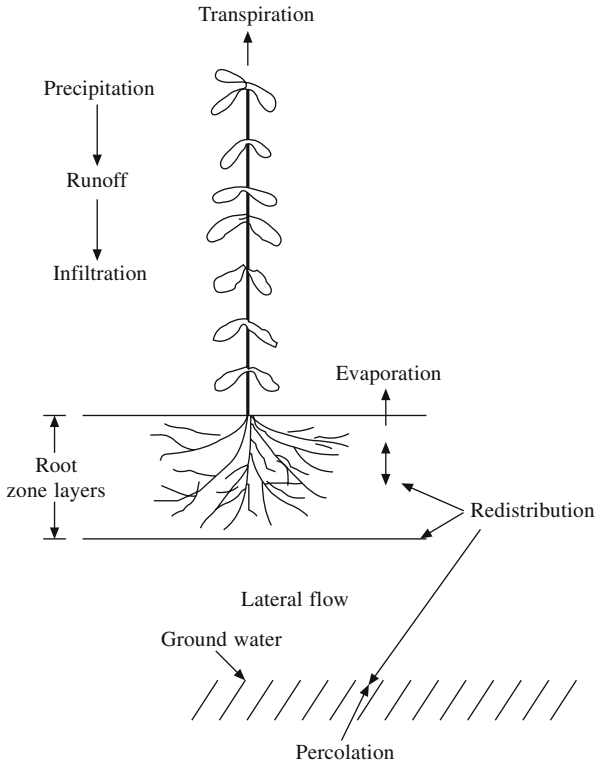

Fig. 2.1 Schematic diagram of soil-plant air flow system.

The soil moisture parameters show variability in depth, i.e. as the soil goes from dry to moist, the depth over which the soil moisture parameters correspond decreases. Variation in slope and curvature, upslope contributing area and relative elevation all affect the distribution of soil moisture near the land surface. In arid environment, soil moisture varies as a result of water flow path, radiative effects and heterogeneity in soil type and vegetation. A parameter called equivalent soil moisture is defined, as a weighted integral of the soil moisture profile times the thermal microwave emission profile. It has been shown that the depths from which energy originates can extend approximately to 20 cm at 1.4 GHz for dry soil. For wet soil at this frequency the depth only extends to a couple of centimeters. However, Newton predicted that the

near surface layers (0-2 cm) had a dominant effect on the emission that could escape from the soil volume.

Several workers have reported experimental measurements of thermal microwave emission that describe the effect of uniform surface roughness and corrugated surface roughness at 1.4 and 10.7 GHz. (Newton et al., 1982). The effect of uniform surface roughness was to decrease the sensitivity of the thermal microwave emission measurement to soil moisture. In addition, the magnitude of this sensitivity reduction for a given surface roughness is frequency dependent. Ulaby et al. (1974) have concluded that at low incident angles (10-15°) and at frequencies near 5 GHz, minimize the effect of surface roughness. It is, thus, suggestive that the frequency and incident angle variation should be investigated with passive microwave remote sensors and the results compared.

Agriculture Applications

In the field of agriculture the requirement of soil water content is highly variable, e.g. one time survey results are needed for finding out the soil moisture storage, available water capacity and moisture retention characteristics, but repeated monitoring of soil moisture is required. This becomes essential to determine levels of soil moisture deficit and extent of soil water depletion by crops, which are dependent upon environmental conditions. A major challenge for measurement, monitoring and modelling of soil water is the extent of variability of soil water in both time and space. The profile of soil water content also varies because of variable conditions such as dry surface with moist lower layer, moist surface with dry lower layer or the soil surface being covered by vegetation/crops or any combination of these.

Radiobrightness is sensitive to soil moisture in agricultural land due to the dominant influence of liquid water upon microwave emissivity. To be of practical use in climatic modeling, crop forecasting or estimating rain water runoff potential, radiobrightness-derived estimates of soil moisture represent the integrated moisture content of the soil from its surface through the root zone. The radiobrightness, an indicative of thermal inertia is an estimate of soil moisture where vegetation is short or sparse.

Soil Moisture Parameters

With the knowledge of soil bulk density ρ_b and soil particle density ρ_p, we can determine other soil water content parameters. For example, mass of water content m_g can be defined as

$$m_g = \frac{\text{Mass of water}}{\text{Mass of dry soil}} = m_w / m_s = \frac{\rho_w b}{\rho_p c} \tag{2.1}$$

where ρ_w is the density of water, b the equivalent depth of water and c the equivalent depth filled with solids. In practice m_g is measured by taking a sample in the field and measuring the mass of the sample before and after drying. The difference in the before m_{s+w} and after m_s measurements give the mass of water. However, knowledge of m_g does not provide sufficient information to tell the equivalent depth of water in the field without knowing the water content on a volume basis. Consequently m_v is defined as

$$m_v = \frac{\text{Volume of water}}{\text{Bulk volume of soil}} = \frac{b}{D} \tag{2.2}$$

and is simply the ratio of the equivalent depth of water to the equivalent depth of the soil made of solid D. Thus, if 360 mm of water is found in 1000 mm of soil, $m_v = 0.36$. This measurement is the most useful expression of soil water content because of the simple and straightforward relation to other parameters of interest. Thus, using Eq. (2.2) the equivalent depth of water is defined as

$$b = m_v D \tag{2.3}$$

These concepts also allow for porosity relations to be expressed in a fairly simple way. The total porosity of the soil is expressed as

$$P = \frac{\text{Total pore volume}}{\text{Bulk volume of soil}} = \frac{(a + b)A}{DA} = \frac{a + b}{D} \tag{2.4}$$

where a is the air space and A the area. The value of P may vary between 0.3 and 0.6 (30 and 60%).

It is thus obvious that for a saturated soil all of the pore volume would be filled with water m_v (saturated) = P. The pore volume filled with air is given as

$$P_a = \frac{\text{Air pore volume}}{\text{Bulk volume of soil}} = \frac{aA}{DA} = \frac{a}{D} \tag{2.5}$$

Another parameter often used is relative saturation m_{vr}, the ratio of m_v to its saturated value m_{vs}, given as

$$m_{vr} = \frac{bA}{(a + b)A} = \frac{b}{a + b} = \frac{m_v}{m_{vs}} \tag{2.6}$$

In practice, measurements of wet mass, dry soil mass, and bulk volume are made from which m_g, m_v and ρ_b are calculated. If ρ_p is known for the soil, the other parameters can be calculated from the above relations. Another fallout from the above equations is

$$m_g = \frac{m_{s+w} - m_s}{m_s} \tag{2.7}$$

where m_{s+w} is the mass of the wet soil and m_s the mass of the dry soil. This equation eliminates the need of finding the mass of the water and depends only on the basic data.

A knowledge of m_v is generally sought as it is convenient to convert it to m_g using the relation

$$m_v = \frac{\rho_b}{\rho_w} m_g \tag{2.8}$$

which requires a knowledge of ρ_b alone. It is common to measure ρ_b once in the

season and to assume that it does not change with time. This assumption is valid for many soils except the top soil.

Soil Moisture Measurements

Relative use of electromagnetic spectrum (frequency dependence) is classified as follows:

Visible and Infrared (0.3-3 μm) Electromagnetic Spectrum

Reflected radiation in the visible region of the electromagnetic spectrum has been demonstrated to have excellent correlation with moisture content, but limited to the top few millimeters of the soil surface. At these wavelengths, the penetration is small and because of cloud cover, the sensitivity rapidly decreases within first few millimeters of the soil surface. In addition, the electromagnetic interaction mode with different dry and wet soil varies widely. Major sources causing uncertainty are surface roughness and surface cover. Therefore, establishing a relationship between the two demands *a priori* knowledge of soil characteristics.

Thermal Infrared Method

Thermal emitted radiation from surface = $e\sigma T^4$, where emissivity $e \sim 0.94$, σ the Stefans constant and T the absolute temperature measurements in the thermal infrared region (10-12 μm) have also been shown to correlate well with the surface moisture content of bare soil where the soil is non-uniform and a fair estimate of soil moisture matrix potential can still be obtained. While this technique appears to offer sensing of moisture at a greater depth than the visible spectrum measurement, it has limitations due to the presence of slightest amounts of vegetation. In addition, both optical reflectance and thermal emission models for estimation of soil moisture requires knowledge of the solar radiation, (irradiance and insolation) which is not always available. In this method, the thermally emitted radiation from the surface is measured and related to soil moisture content.

Diurnal range of surface temperature is dependant upon the following:

Internal factors: Thermal conductivity K and heat capacity C
External factor: Meteorological parameters
Thermal inertia (TI): $(KC)^{1/2}$

Since K and C increase with increase in moisture content and hence thermal inertia increases.

Shih and Jordan (1993) reported that integration of Landsat thermal-IR data with land use under certain conditions might be a useful technique for assessing regional soil moisture conditions. Soil moisture content of the surface (0-2 cm) and seeding zone (0-7.5 cm) and soil surface temperature (sensed by infrared thermometer), are found to be closely (inversely) related with estimated moisture content in both the layers (Rao et al., 1999).

Soil surface temperature and moisture represent the products of energy balance between the land and the atmosphere. They, in turn, also control the infrared and microwave emission.

Microwaves

Microwaves refer to the electromagnetic radiations of frequencies ranging from approximately 300 MHz to 300 GHz. Applications of microwaves have been put to various uses depending on the frequencies range. They have certain distinct advantages over other frequencies, e.g. they propagate through ionosphere with minimum loss, hence most suited for space bound communications as well as for satellite remote sensing. Atmosphere is completely transparent to these radiations. They can also penetrate deep into the soils. Hence, multi-frequency and multipolarization approaches are possible and have been made. The sensitivity of microwave response to soil moisture variation coupled with their relative transparency of the atmosphere (>90%) makes microwave sensors well-suited for soil remote sensing. Also with proper choice of frequency, look angle and polarization, the effect of surface roughness can be minimized.

Lower frequency end of microwave spectrum offers a significant advantage in the measurement of soil moisture. At these frequencies, penetration of vegetative cover is significant and the sampling depth of the measurement may be several centimeters depending on the soil moisture content. Sampling depth is the maximum depth at which the moisture can be measured.

Measurement programs in the microwave region have followed two distinct approaches: (a) employing passive radiometric measurement and (b) using active radar backscattering measurement. Both approaches have demonstrated excellent correlation with soil moisture content. However, there are significant differences between the active and passive techniques which result in differing recommended operating frequencies for the measurement of soil moisture. This difference in frequency would in turn be expected to produce a significant difference in the vegetation penetration capability and the sampling depth.

The volumetric soil moisture can be considered as a monotonically decreasing function of the emissivity of bare soil. If soil roughness conditions do not change during the period of observation, this function can be approximated by a linear relation of the type

$$e = a_0 - a_1 m_v \tag{2.9}$$

where a_0 and a_1 are constants (Wigneron et al., 2003). It has been shown that passive microwave remote sensors can be used to monitor soil moisture over land surfaces (Wang et al., 1990; Van de Griend and Owe, 1994).

Passive Microwave Remote Sensing

Passive microwave studies have consistently shown the lower microwave frequencies (L-band) to be superior for the measurement of soil moisture. The effects of surface roughness are decreased for these longer wavelengths thereby giving higher sensitivity. However, this has limited spatial resolution (5-10 km) and has problem of interference from man-made radiation sources.

Active Microwave Remote Sensing

Active microwave studies have concluded that the optimum sensor configuration is at frequency nearing 5 GHz and at an incidence angle between 7 and 20°. This selection helps to minimize the effects of surface roughness. Even here it has been shown that periodic components of roughness, such as produced by tillage, present some problems.

The commonality in use of both active and passive microwave systems in soil moisture measurement lies in large disparity between the dielectric constant of water (~80) and of dry soil (3-5). This large dielectric constant of liquid water arises due to the alignment of the electric dipole moments of water molecules in response to an applied field. Dielectric constant of soil, therefore, increases with its moisture content.

Both active and passive measurement programs have concluded that the sampling depth of the measurement is dominated by the air-soil and is above a few centimeters depending on the surface moisture content. Programs utilizing both types of sensors have exhibited a pronounced dependence upon soil texture. It has been shown by Schmugge (1983) that the variations in passive measurements due to soil texture may be significantly reduced by expressing the soil moisture as a percentage of field capacity.

Some difference in using multilayer models for prediction of the response have resulted from both coherent and incoherent models. In particular, there are questions regarding the effect of the moisture distribution within the sampling depth.

Nature of soil and its properties like soil depth, texture, organic matter content, precipitation, crop growth, root water extract are some of the important parameters for agriculture and remote sensing studies. Mineralogical composition control the water holding capacity which is of utmost importance for plant life.

Physical Basis of Soil Moisture Measurement Using Microwaves

Dielectric Behavior of Wet Soils

Dielectric constant (ε') of dry soil is essentially independent of temperature and frequency. The imaginary part ε'' is < 0.05. Wet soil behavior is, however, very complex. Over the past two decades, a number of studies have been carried out to determine the dielectric behavior of soil-water mixture (Poe et al., 1971; Hipp, 1974; Hoekstra and Delaney, 1974; Newton and McClellan, 1975; Davis et al., 1976; Wang, 1980; Wang and Schmugge, 1980; Shutko and Reutov, 1982; Dobson et al., 1985; Hallikainen et al., 1985a, b; Jackson and Schmugge, 1989; Rao et al., 1990; Scott and Smith, 1992; Alex and Behari, 1996, Ghosh et al. 1998).

A wet soil medium is a mixture of soil particles, air pockets and liquid water. The water contained in the soil is usually divided into two fractions, viz. bound water and free water. The relative fractions of bound and free water are related to the particle size distribution (or soil texture). These, in turn, are dependent upon the bulk soil density and the shape of the water inclusions.

Bound Water Layer

Bound water refers to water molecules that are contained in the first few molecular layers surrounding the soil influence of meteoric and osmotic forces. Bound water molecules are absorbed on the surface of particles and the dipoles are, therefore, constrained. Surface of particles offers the bonding site. Within a soil volume two physical parameters that describe the surface area are the specific surface area and the bulk density of soil. Figure 2.2 is illustrative of changing these values on the volume of bound water using the formulation of Dobson et al. (1985). The matrix forces acting on a water molecule decrease rapidly with increasing distance from soil particles and, therefore, water molecules that are located several molecular layers away from the soil are able to move within the soil medium with relative ease and hence, are referred to as free water. Dividing the water into bound and free fractions is an approximation of the actual distribution of water molecules in the soil medium. This is based on a somewhat arbitrary criterion for describing the transition betwen bound and free water layers. The amount of water contained in the molecular layer adjoining the soil particles is directly proportional to the total surface area of the soil particles. This in turn, is a function of the size distribution and mineralogy of the soil particles.

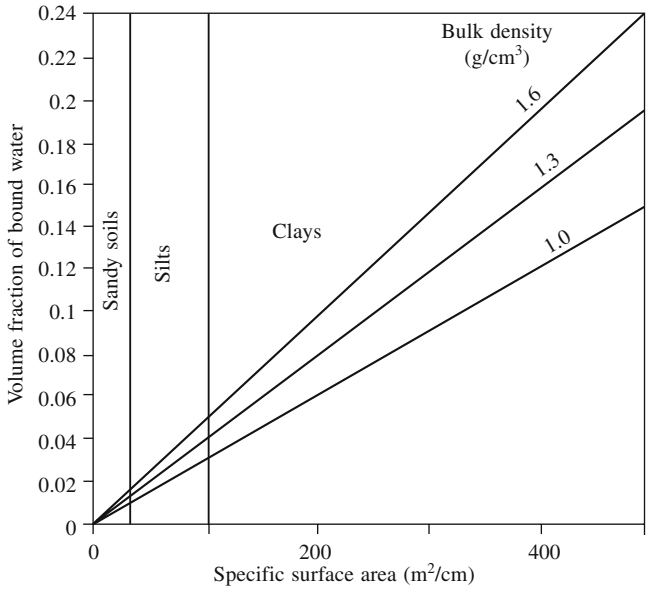

Fig. 2.2 Bound water volume as a function of soil specific surface and bulk density (Jackson and Schmugge, 1989; Dobson et al., 1985).

In a dry soil, absorbed cations are tightly held by negatively charged particle surfaces composed predominantly of clay. When water is slowly introduced into the system, salt precipitates go into the solution, and the adsorbed cations partially diffuse

into the solution adjacent to the particle surfaces. The electrostatic field defined by the particles, however, inhibits this diffusion and results in a charge distribution described by the well known Boltzman and Poisson formulations. Given the large surface charge densities commonly present in soils, cation distribution defined by the double layer model can increase the ion concentration in the bulk solution by an order of magnitude or more relative to the one, measured for a solution extracted from a saturated soil paste. The Stern-Gouy double layer model (Fig. 2.3) accounts for the effects of the surface-charge density, type of cation adsorbed, and salinity of the bulk soil solution upon the distribution of ions as a function of distance from particle surfaces. Assuming that the surface charge σ is uniformly distributed for soil it is related to its cation exchange capacity (CEC) and its specific surface by the relation (Dobson et al., 1985)

$$\sigma = \text{CEC}\, A_v e \times 10^{-9}/A_s, \text{ ESU} \cdot \text{cm}^{-2} \tag{2.10}$$

where e is electronic charge and A_v is the number of charges per equivalent. Since A_s is dominated by the clay fraction, the surface charge density can be treated as being both constant and non-pH dependent.

In general, a soil medium is considered electromagnetically a four component dielectric mixture consisting of air, bulk soil, bound water and free water. Due to the

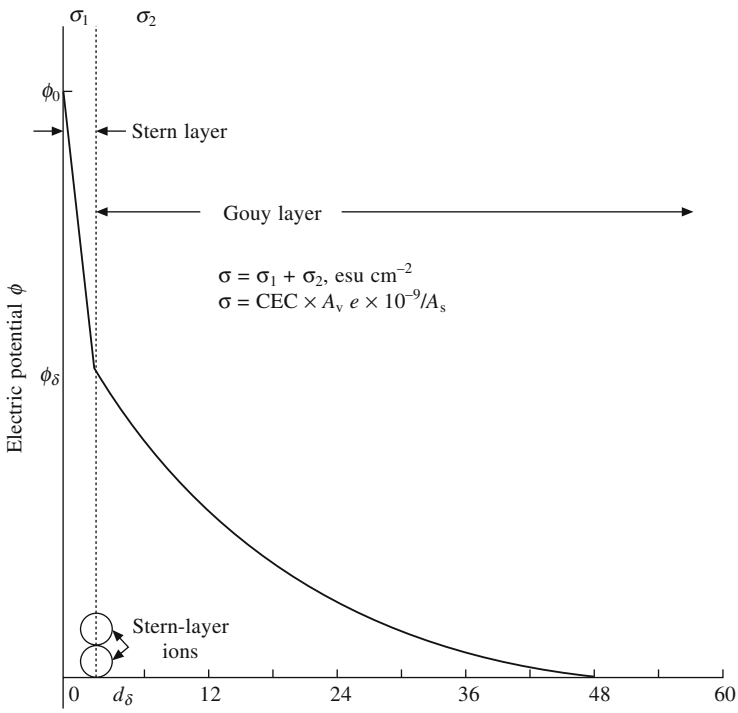

Fig. 2.3 Stern-Gouy double layer model (Dobson et al., 1985).

intensity of the forces acting upon it, a bound water molecule interacts with an incident electromagnetic wave in much the same way that it does when it is in the form of ice, thereby, exhibiting a dielectric dispersion spectrum that is very different from that of free water. The complex dielectric constants of bound and free water are functions of the electromagnetic frequency, physical temperature T and salinity S. Hence, the dielectric constant of the soil mixture is, in general, a function of temperature and salinity and the total volumetric water content.

It is apparent from soil composition that its dielectric constant changes with applied frequency. An alternating electric field of appropriate frequency gives rise to dielectric dispersion. The characteristics orientation motions of the dipoles result in a frequency variation of the dielectric constant, and the consequent appearance of dielectric loss. When the direction of the field changes sufficiently fast, the molecular forces impending the dipole orientation dominate, and the dipoles unable to follow the changes. At these frequencies, the orientations of the permanent dipoles no longer contribute to the dielectric constant. Moreover, in a certain frequency band a phase lag between the field and the dipole orientation develops, and energy is drawn from the electrical source by the material and is dissipated as heat. This phenomenon is described by a complex representation of the dielectric constant,

$$\varepsilon = \varepsilon' - j\varepsilon'' \tag{2.11}$$

where imaginary part ε'' is known as dielectric loss, $\varepsilon''/\varepsilon' = \tan \delta$ is the loss tangent, and δ the loss angle.

Dielectric constant of water is best described by the modified Debye's equation

$$\varepsilon = \varepsilon_\infty + (\varepsilon_s - \varepsilon_\infty)\ (1 + j\omega\tau) \tag{2.12}$$

which in component form reduces to

$$\varepsilon' = \varepsilon_\infty + (\varepsilon_s - \varepsilon_\infty)/(1 + \omega^2\tau^2) \tag{2.13}$$

$$\varepsilon'' = (\varepsilon_s - \varepsilon_\infty)\ \omega\tau/(1 + \omega^2\tau^2) \tag{2.14}$$

where ε_s is the static dielectric constant, ε_∞ is high frequency limit of dielectric constant, ω the applied angular frequency $(2\pi f)$ and τ the relaxation time (time required for the water molecule to align itself with an applied field.

An isolated water molecule possesses a permanent dipole moment. If an electric field is applied, the molecule will orient itself such that its dipole moment is aligned with the field. The orientation response to an infinitely fast step variation of applied electric field is characterized by an exponential function of the form $\exp(-t/\tau)$ with time constant τ. This time constant is called the *relaxation time* and is governed by the interaction of the H_2O molecule with its environment and by the temperature T. If the water molecule is under the influence of nonelectrical forces, such as physical forces, its response to an applied electrical field is impeded by these forces which has the equivalent effect of increasing the relaxation time τ. This accounts for the fact that τ of a bound water molecule is much longer than that of a free water molecule.

Many forms of modified Debye's equations have been proposed to better describe the dielectric behavior of water. Among them Cole-Cole equation is most widely

used and is most accurate

$$\varepsilon = \varepsilon_\infty + (\varepsilon_s - \varepsilon_\infty)/1 + (j\omega\tau)^{1-\alpha} \tag{2.15}$$

Values of ε_s and τ decrease with increase in temperature T. Values of ε_∞ and α are more or less constant for a system. Table 2.1 gives the values of ε_∞, τ and α for water at a given temperature.

Table 2.1

At 20°C	
Values for bound water	Values for free water
$\varepsilon_s = 57.9$	$\varepsilon_s \cong 80.4$
$\varepsilon_\infty = 3.15$	$\varepsilon_\infty = 4.2$
$\tau = 9.3 \times 10^{-6}$ s	$\tau_2 = 4.2 \times 10^{-14}$ s
$\alpha = 0$ (at microwave frequency)	$\alpha = 0.012$

Temperature dependence of relaxation for water as derived from Eq. (2.15) is presented in Table 2.2.

A still more accurate relationship for free water is given as

$$\varepsilon = n^2 + \frac{(\varepsilon_s - \varepsilon_\infty)}{(1 + j\omega\tau_1)^{1-\alpha}} + \frac{(\varepsilon_\infty - n^2)}{1 + j\omega\tau_2} \tag{2.16}$$

$$n^2 = 1.8$$

$$\varepsilon_s = 295.68 - 1.2283 \times T + 2.094 \times 10^{-3}\, T^2 - 1.41 \times 10^{-6}\, T^3$$

$$\tau_1 = 5.62 \times 10^{-15} \exp\,(3.01 \times 10^{-20}/KT).$$

where τ_2 can be determined with the knowledge of initial parameters, T is the temperature in degree Kelvin and K the Boltzman's constant (= 1.3806×10^{-23} J/K), α is known as *spread of relaxation* ε_s and ε_∞, τ, α are unique properties of a particular system.

The dependence on temperature of relaxation parameters for water is given in Table 2.2. Values of ε_∞, τ and α for water at different temperatures using Eq. (2.15) are given in Table 2.2.

Another expression for the static dielectric constant of pure water ε_s is given by (Klein and Swift, 1977)

$$\varepsilon_s(T) = 88.045 - 0.4147\, T + 6.295 \times 10^{-4}\, T^2 + 1.075 \times 10^{-5} T^{-3} \tag{2.17}$$

Table 2.2 H_2O relaxation parameters derived from the Cole-Cole equation

T (°C)	ε_∞	τ (10^{-11} s)	α
0	4.46 ± 0.17	1.79	0.014
10	4.10 ± 0.15	1.26	0.014
20	4.23 ± 0.16	0.93	0.013
30	4.20 ± 0.16	0.72	0.012
40	4.16 ± 0.15	0.58	0.009
50	4.13 ± 0.15	0.48	0.013
60	4.21 ± 0.16	0.29	0.011

while the relaxation time of pure water is given by (Stogryn, 1970)

$$2\pi\tau(T) = 1.1109 \times 10^{-10} - 3.824 \times 10^{-12}T + 6.938 \times 10^{-14}T^2 - 5.096 \times 10^{-16}\ T^3 \quad (2.18)$$

High values of dielectric constant for free water is due to the fact that the water molecular dipoles are free to rotate at microwave frquencies. The dielectric properties of bound water are presumed to lie somewhere between those of ice and liquid water. In several cases, bound water cannot be expelled from a material completely by heat without breaking its structural composition. Hence, in certain cases, we can only determine the total free water and not the total water content.

Relaxation time of bound water τ_{bw} depends on the thickness h (cm) of the film covering soil particles. This dependence has the form

$$\tau_{bw}(+27°C) = (-4.9648 \times 10^{24}h^2 - 3.0867 \times 10^{11} \ln(h) - \frac{7.5092 \times 10^3}{h} + 3.9121 \times 10^{18}h - 5.2036 \times 10^{12})^{-1} \quad (2.19)$$

Here it is assumed that $\tau_{bw} = \tau_w$ at the water film thickness of 10 diameters of water molecule, i.e. h_{10} (water molecule diameter is 2.8×10^{-8} cm) (Boyarskii et al., 2002).

Relaxation time of bound water τ_{bw} molecules differs from relaxation time of free water τ_w and ice τ_c, where $\tau_w < \tau_{bw} < \tau_c$. The τ_{bw} decreases with the number of monomolecular layers of water covering the particles and does not differ τ_w at film thickness of 10 monomolecular layers (Boyarskii et al., 2002).

Bulk Density Effects

It has been demonstrated that for a given soil at a given gravimetric moisture content m_g the measured dielectric constant ε is proportional to the soil packing density ρ (Hillikainen et al., 1985). Assuming the soil to be homogeneous, the randomly dispersed mixture of solids, liquids and air along with all inclusions, is much smaller than the wavelength. The dependence of ε on ρ is explained by the direct dependence of ρ on soil and water volume fractions (Dobson et al., 1985). For swelling clay the specific volume (= $1/\rho$) increases linearly with the gravimetric water content (Sabburg et al., 1997).

Moisture, Texture and Frequency Dependence

At any given moisture content and at all given frequencies, ε' is found to be roughly proportional to the sand content. The effect of soil texture decreases with frequency. As is the characteristics of many dielectric materials, the real part of the dielectric constant decreases with increasing frequency.

Soil Textural Composition

Dependence of soil dielectric constant ε_{soil} on its textural composition for five type of soils is shown in Figs. 2.4 and 2.5 (Hallikainen et al., 1985a).

The variation of ε_{soil} with soil type is reflected in the shape of brightness temperature curves. For oven dried soil ε_{soil} is approximately the same for all soil types and depends

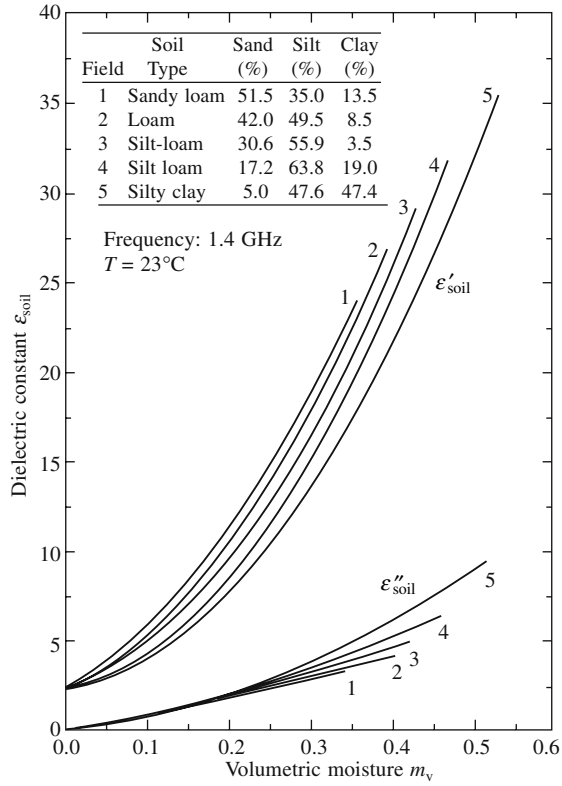

Fig. 2.4 Measured dielectric constant for five soils at 1.4 GHz (Hallikainen et al., 1985a).

on the bulk density only. The variation of ε_{soil} with increasing m_v can be divided into two parts: (i) between $m_v = 0$ and a transition moisture level m_t and (ii) $m_v \geq m_t$. The transition moisture, which is a constant for a given type of soil composition and varies between 0.03 for sands and 0.10 for clays, represents the boundary between the bound water and the free water molecules (Wang and Schmugge, 1980, Schmugge, 1980). Between the transition moisture level, most of the water molecules in the soil water mixture are considered to be at least partially bound to the soil particles by the influence of both matric and osmotic forces. Hence, the effective dielectric constant of these partially bound water molecules is much smaller than that of free water, consequently the dielectric constant of the mixture increases only slowly with increasing m_v. Beyond $m_v = m_t$ the water molecules are considered to be free particles with a dielectric constant much larger than that of soil, thereby exercising a strong influence on the dielectric constant of the mixture. The transition moisture m_t depends on the soil particle surface area per unit volume, and hence a function of soil type.

In the range $m_v \geq m_t$, T_B varies in an approximately linear fashion with m_v, the slope T_B/m_v is approximately the same for the five soil types. The curves are displaced relative to one another because of the fact that five soils have different levels of moisture transition.

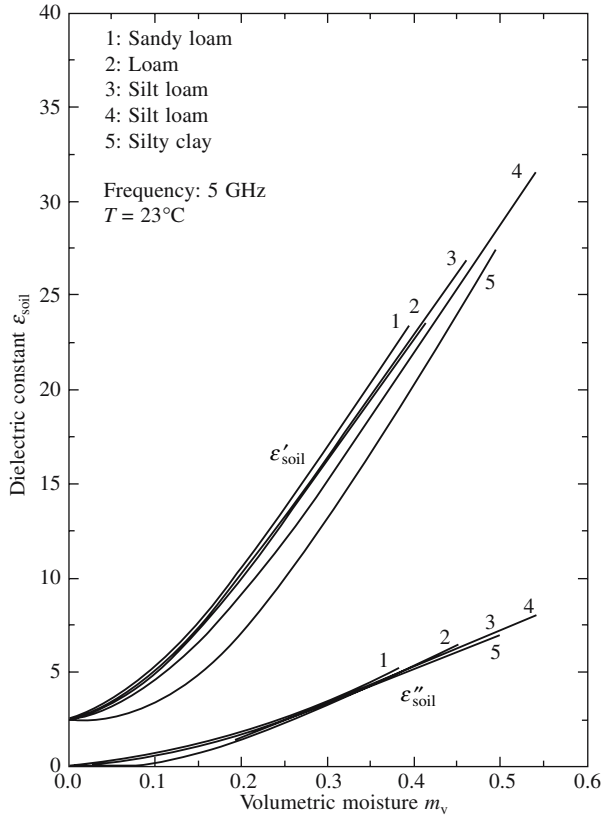

Fig. 2.5 Measured dielectric constant for five soils at 5 GHz.

The effect of texture on the loss factor is more complicated. At 1.4 GHz, ε'' is seen to increase with soil clay content ($m_v \geq 0.2$). At 4.0 to 6.0 GHz, ε'' is nearly independent of soil texture at all moisture conditions. At frequencies of 8.0 GHz and above, ε' is observed to decrease with soil clay fraction. Furthermore, the magnitude of this behavior increases with frequency (Schmugge, 1983; Hallikainen et al., 1985a).

In another study, Alex and Behari (1996) concluded that in case of dry soils the dielectric parameters are not sensitive to the soil texture. However, for wet soils ($m_v > 0.2$) the dielectric parameters are significantly dependent upon the soil texture. In the reported frequency range (0.6-1.2 GHz), they also found that the frequency variation of the dielectric constant is not significant for dry soils but quite prominent for wet soils (Figs. 2.6 and 2.7). This clearly indicates that this is due to the effect of moisture content and the corresponding density variation.

Salinity Dependence

Below 10 GHz the ionic conductivity of saline water may have a marked effect on the loss factor. Consequently, high soil salinity may significantly influence the dielectric properties of wet soil. Minute concentrations of an electrolyte usually impart considerable conductivity to a liquid medium. Apart from its conductivity, the electrolyte

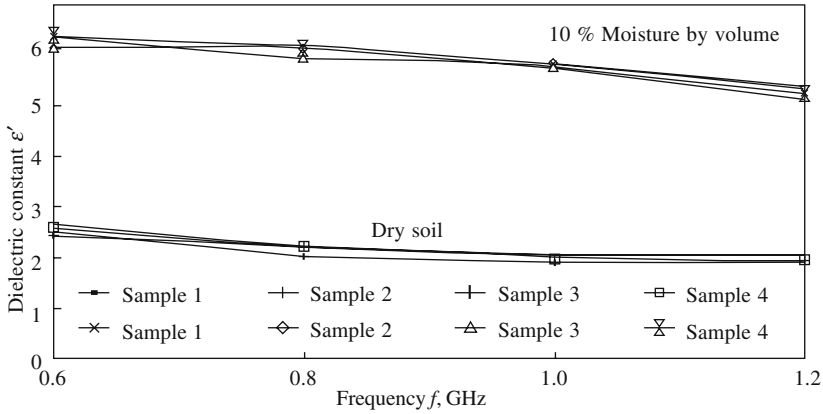

Fig. 2.6 Variation of dielectric constant versus frequency, texture and moisture (10% by volume) (Alex and Behari, 1996).

would be expected to influence the dielectric properties in two ways. First, its ions may associate producing an ion pair or similar solute species of appreciable dipole moment; such solute species will make their own contribution to the dielectric polarization and dispersion. Secondly, the ions or their aggregates in the medium can influence the solvent's molecular interactions due to their strong localized electric fields. In the limit, solvent molecules may be firmly bonded to the ions and hence, give new character of molecules in solution. Some ions markedly change the geometrical pattern of molecular interactions present in water.

The dielectric loss ε'', however, is a parameter which describes the motions of electric charge (conduction phenomena). Conduction can arise from an actual charge transport (i.e. ionic conduction in electrolytes). Thus, observed dielectric loss is made of two terms, viz. the loss due to lag of polarization and the conductive loss

$$\varepsilon'_{\text{obs}} = \varepsilon'_{\text{pol}} + 2\sigma/f \tag{2.20}$$

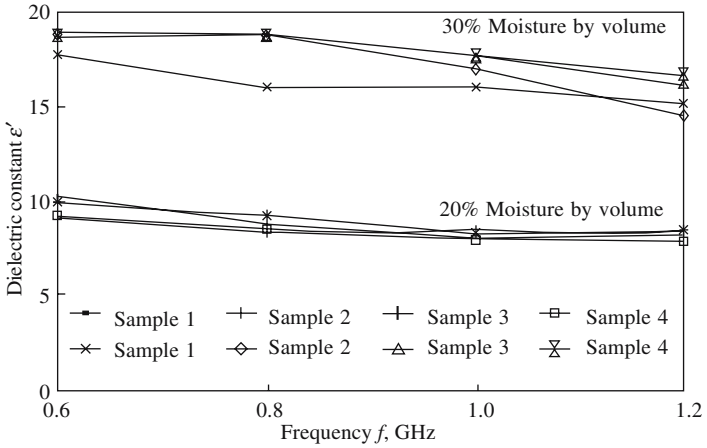

Fig. 2.7 Variation of dielectric constant vs frequency, texture and moisture (20 and 30% by volume) (Alex and Behari, 1996).

The second term is inversely proportional to f. Hence, at microwave region, its contribution to the total dielectric loss can be safely neglected. This relative insensitivity of ε' to ionic content of absorbed water is an important advantage of using microwaves. Also, the loss of dry material is usually small in this region. However, at lower frequencies, this contribution cannot be neglected. Shape and size of granules influence the relaxation frequency of a mixture. Since many shapes and sizes are usually present in complicated systems like wet soil, a large spread in relaxation time is to be expected.

Soil conductivities, even when the soil is waterlogged, are much lower, being in the general range of 10^{-2} S/m as compared to ≈ 5 S/m for sea water. Sandy and gravel soils have conductivities closer to 10^{-5} S/m and granite rocks can have as low as 10^{-4} S/m. Moreover, temperature variation of σ and ε are insignificant above 50°C. The exact form of dielectric dependence of soil on salinity is, however, not well understood.

Temperature Dependence

It is observed that above 0°C, ε'_{soil} and ε''_{soil} exhibit a much weaker dependence on temperature as reported by several workers (Poe et al., 1971; Davis et al., 1976; Hallikainen et al., 1985 a, b). They observed that at temperatures well below freezing point (0°C), ε'_{soil} and ε''_{soil} exhibit a much weaker dependence on frequency compared to their dependence above 0°C.

For bare fields the correlation is high between the brightness temperature and the soil moisture of upto 25%. For those fields with moisture content greater than 25%, the response seems to be more variable. Surface roughness effect is more pronounced for moist fields. In a model developed by Choudhury et al. (1979), the difference in observed brightness temperatures between medium rough (h = 0.3) and rough field is only 6 K for dry fields (soil moisture ~ 0%) but ~ 27 K for wet fields (soil moisture ~ 25%). In general, data for bare fields agree well with theoretical values with an average roughness value of h = 0.5.

For vegetated fields, the sensitivity to soil moisture is still strong. The response at nadir and horizontal polarization are similar. The general trend is that for drier fields there is a slight decrease in brightness response, which is attributed to the vegetation as compared to the bare fields. The general increase in brightness temperature is by the vegetation canopy acting as an additional thermal emitting layer. Typically, for moist fields, the vegetation canopy produces an increase in brightness temperature of about 15 K. The increase is greater for wet fields due to their lower surface emissitivities and consequently higher surface reflectivity.

Using the IR observation and assuming an isothermal layer between the surface and vegetation, emissivity is defined as $e = T_B/T$. The increase in signature due to vegetation is also compensated by the smoother surfaces under the vegetation relative to the furrow irrigated fields which would produce overall lower emissivities. As a result, for drier fields the brightness temperature responses over vegetated fields are similar to, or in some cases, lower than those over bare fields. For vertical polarization,

the vegetation effect is more pronounced such that the response is less sensitive to the background soil moisture content.

Special Class of Soil

Vertisol

The vertisol, an important class of soils, have the characteristic property of changing their bulk density in response to water content. The water management of these soils is particularly important (Sabburg et al., 1997).

The vertisols are known by a variety of names such as black soils, black earths, cracking clays or swelling clays (Sabburg et al., 1997). These have a high cationic exchange capacity (~70 meq/100 g) and have a high specific area (~ 6000 m^2/g). This then permits these to have a high retention capacity of water and makes it important for semiarid regions. When dry, these would shrink and increase in volume when wet. These authors performed the dielectric constants for the following soils: sandy loam (19% clay, 55% sand P_b (1.34-1.76), CEC = 10 meq/100 g); oxisol (62% clay, 19% sand P_b (0.97-1.29), CEC = 10 meq/100 g) and vertisol (70% clay, 14% sand, P_b (0.57-1.09), CEC = 68 meq/100g). The regression for the vertisol at 12 GHz is

$$\varepsilon' = 2.79 + 2.90\ m_v + 36.12\ m_v^2\ (r^2 = 0.932) \tag{2.21}$$

$$\varepsilon'' = 0.020 - 1.46\ m_v + 36.47\ m_v^2\ (r^2 = 0.861) \tag{2.22}$$

where m_v is the volumetric water content.

In a similar manner, Fig. 2.8 (a, b) shows the characteristics of the oxisol and the vertisol. The regression for the vertisol at 4 GHz are

$$\varepsilon' = 3.44 - 12.78\ m_v + 109.65\ m_v^2\ (r^2 = 0.958) \tag{2.23}$$

$$\varepsilon'' = 0.32 - 3.63\ m_v + 34.00\ m_v^2\ (r^2 = 0.96) \tag{2.24}$$

Density Effects

The dry bulk density of soils is not usually of concern of soil moisture measurement. A characteristic of vertisol is that the specific volume (=1/p_b) increases linearly with gravimetric water content m_g and can be expressed as

$$\frac{1}{p_b} = 1.57\ m_g + 0.88\ (r^2 = 0.790) \tag{2.25}$$

Dielectric Behavior of Swelling Clay Soils

Frequency variation of the real part of the permittivity is shown in Fig. 2.9 (a, b) for both sandy loam and vertisol with volumetric water content m_v in the range 0.21-0.29. The sandy loam results are identical to those of Hallikainen et al. (1985a) which are also superimposed. Vertisol results follow the same trend, however, these values are only about half of those for sandy loam at the same frequency and moisture content. The linear regression is

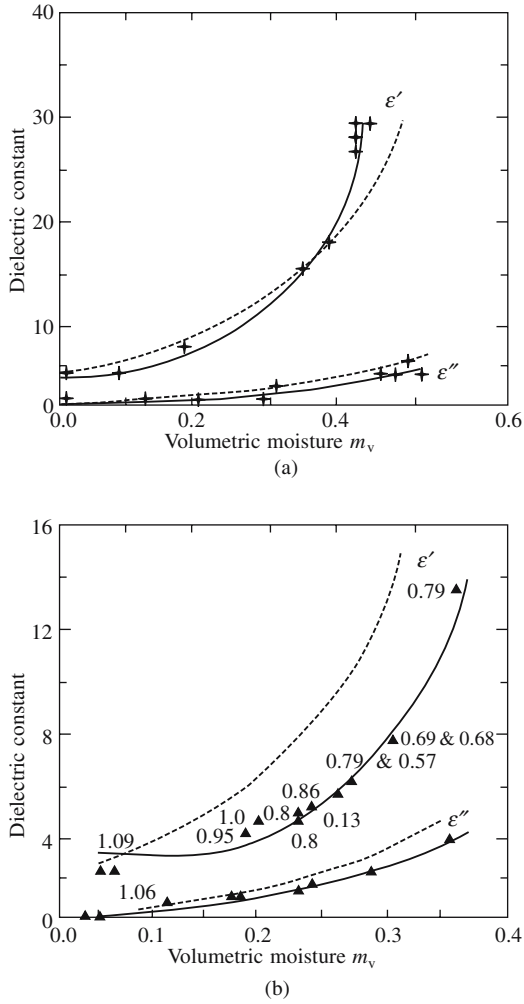

Fig. 2.8 Measured permittivity data versus volumetric moisture content at 4 GHz for (top) oxisol and (bottom) vertisol. Quadratic regressions of these data (solid lines) are shown in comparison with the Hallikainen model (1985 a) (dotted line). Bulk density values (g/cm^3) are indicated for each data value (Sabberg et al., 1997).

$$\varepsilon' = -0.142\, f + 6.93 \quad (r^2 = 0.926) \tag{2.26}$$

where f is the frequency (GHz). This provides excellent agreement with vertisol results.

At higher frequencies, the polarization losses becomes dominant, having maxima at the relaxation frequency, and between these two the loss factor passes through a minimum (Hallikainen et al., 1985 b). The upper two sets of data given in Fig. 2.9 a, b (bottom) show that the sandy loam measured in this study exhibits this typical frequency behavior and that these results are almost exactly the same as those reported by Hallikainen et al. (1985 b) for a very similar soil and moisture content. In contrast

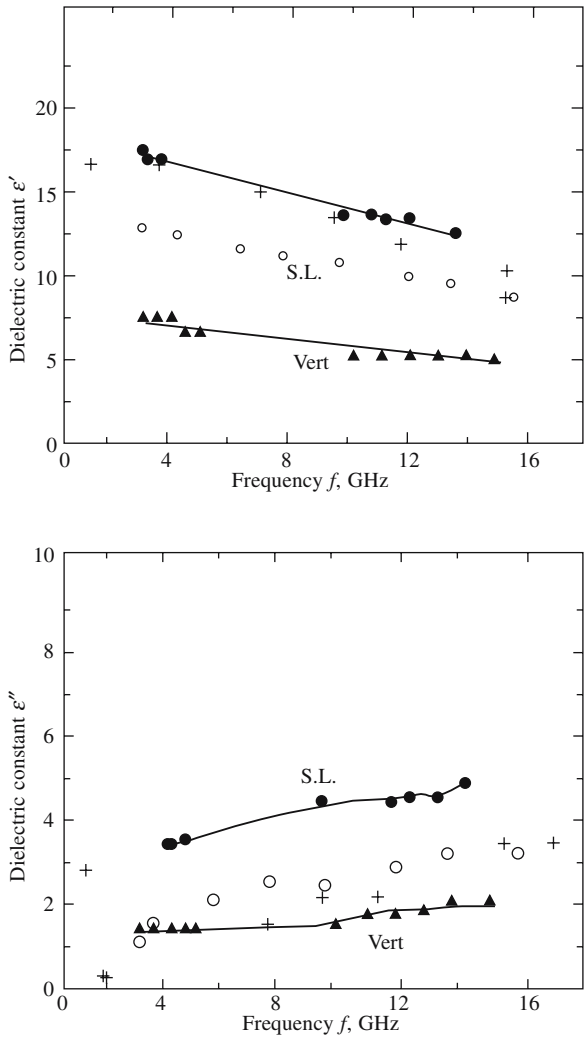

Fig. 2.9 The variation of soil dielectric properties with frequency (top) real part ε', and (bottom) loss factor ε' for both sandy loam (S.L.) and vertisol (Vert). (●●, ▲▲ Experimental; ○○, ++, Hallikainen et al., 1985 a).

the frequency behavior of the vertisol is significantly different. At higher microwave frequencies where dielectric relaxation of free water is the dominant mechanism, the dielectric loss factor is clearly much less for the vertisol in comparison to the sandy loam. This result suggests a significantly lower proportion of free water. Only below 3 GHz does the vertisol loss factor exceed that of the sandy loam and this is attributed to the fact that salt content increases with the clay fraction. Clay soils are expected to possess higher ionic conductivity and hence, be more lossy at lower frequencies.

Frequency behavior of wet vertisol suggest that a substantial fraction of the water exist in the bound rather than in free state. This explains the lower than expected permittivity and the typical behavior of the loss factor.

CHAPTER 3

Measurement of Soil Water Content

Measuring Methods

With the advent of advancing technology several methods have been developed. Data logging capabilities have also greatly contributed to the monitoring capabilities over an extended period of time and in remote areas. A variety of methods for measuring soil water content are summarized in Table 3.1.

Table 3.1 Various soil moisture measurement methods

Classification	Methods
(i) Heating methods	Gravimetric/Volumetric method
(ii) Indirect methods	Tensiometric techniques
(iii) Geophysical methods	Electrical conductivity technique
(iv) Nuclear techniques	(a) Neutron Scattering
	(b) Gamma ray attenuation
	(c) Neutron radiography
	(d) Dual energy gamma sources
	(e) Computer aided tomography (CAT Scan)
	(f) Tritium (^{3}H) tagging
	(g) Use of stable isotopes (^{2}H, ^{18}O)
(v) High frequency electrical techniques	(a) Capacitance measurements well upto radio frequencies
	(b) Time domain reflectometry (TDR) using portable dielectric probes of varying lengths
	(c) Ground penetrating radar (GPR)
(vi) Remote sensing techniques	(a) Visible and near infrared
	(b) Thermal infrared
	(c) Microwave (passive and active) including synthetic aperture radar (SAR)

Microwave Response to Soil Moisture

Soil moisture can be measured by a variety of remote sensing techniques (Jackson et al., 1982; Schmugge, 1983; Stafford, 1988; Baker and Almares, 1990; Engman, 1991). However, only microwaves based remote sensing technology has the ability to

quantitatively measure soil moisture under a variety of topographic and vegetative cover conditions. Thus, potentially it could be extended for routine measurements from a satellite system. A number of experiments using sensors mounted on truck, aircraft and spacecraft have shown that moisture within a thin layer of soil of the order of 5 to 10 cm can be accurately measured for bare and thinly vegetated soil (Theis et al., 1984; Bruckler et al., 1988; Engman, 1991; Ferrazzoli et al., 1992; Mohan et al., 1993; Benallegue et al., 1994).

Importance of Dielectric Constant Measurements: Theoretical background

Dielectric studies of material has been a powerful tool in assessing the structure and behavior of molecular materials (Roberts and Von Hippel, 1946; Von Hippel, 1961). The response of a material to an applied electromagnetic field is determined by the electrical and magnetic properties of the medium under investigation. For a non-magnetic system, the significant property which determines the impedance offered to the incident wave is its dielectric constant. If the medium is lossy, energy is absorbed as the radiation penetrates the material. The amplitude of the wave decreases, i.e. attenuation occurs as energy is absorbed. This is accompanied by a shift in phase. The attenuation and phase shift are dependent on the complex permittivity ε of the medium

$$\varepsilon = \varepsilon' - j\,\varepsilon''$$

where ε' is the relative dielectric constant of an equivalent lossless dielectric and ε'' the relative dielectric loss factor. The complex dielectric constant, thus, has a real and imaginary part, the loss tangent is

$$\tan\,\delta = \varepsilon''/\varepsilon'$$

where δ is the loss angle of the dielectric and its conductivity

$$\sigma = \omega\,\varepsilon_0\varepsilon''$$

where $\omega = 2\pi f$ is the angular frequency of alternating electric field and ε_0 the permittivity of the free space (8.854×10^{-12} F/m). It is, thus, apparent that the two electromagnetic parameters, the attenuation constant and the phase constant are related to the relative dielectric constant ε' and the relative dielectric loss factor ε'' through the values of tan δ and σ which are influenced directly by the moisture content.

Importance of Microwaves in Soil Moisture Content

Soil moisture studies are not suitable in non-microwave regions due to the following:

(a) The reflection co-efficient is not so sensitive to soil moisture variations in the visible region compared to its equivalent parameters like reflectivity and emissivity in other regions of the e.m. spectrum.
(b) Scattering and attenuation due to atmosphere are high.
(c) Reflection coefficient is highly sensitive to soil surface roughness and vegetation cover variation.

Microwave sensors offer the potential for remote sensing of soil moisture because of the large change the addition of water makes to the dielectric constant of dry soil (Alharthi and Lange, 1987).

Microwave Based Experimental Techniques

The microwave technique provides various methods to determine permittivity and dielectric losses (Alex et al., 1994). These can be classified into three groups, viz. the resonator, reflection and transmission methods. The resonator method is mainly suited for measuring thin layers and for determining dielectric losses. In reflection measurements only the upper surface of the sample is investigated, while in contrast, using transmission measurements, the whole layer of material is penetrated by microwaves. Both the methods are accurate and are not influenced by material characteristics like color, emissivity, texture etc.

A variety of experimental procedures for determination of the dielectric parameters of various samples of differing size and shape have been summarised by different authors (Von Hippel, 1961; Montgomery, 1961; Sucher and Fox, 1963; Musil and Zacek, 1986; Suber and Crouch, 1948; Ray Behari, 1987, 1988; Wang et al., 1990; Maizler, 1998; Alex et al., 1994). Keeping these in view, measurement techniques can be broadly classified into two categories, viz. Time domain and Frequency domain techniques. Of the two, the time domain reflectometry (TDR) is of more recent origin. It has been employed by several investigators for the dielectric properties as well as moisture content measurement of soils (Topp et al., 1980; Dalton 1992). In this technique the permittivity of the sample is calculated from the measured resonance frequency and the Q-factor.

The frequency domain technique can further be divided as follows:

(i) Free space technique
(ii) Cavity perturbation technique (Sucher and Fox, 1963; Bayser and Kuerter, 1992; Behari et al., 1982)
(iii) Transmission technique in waveguides/coaxial lines
(iv) Reflection techniques in waveguides/coaxial lines.

Free Space Transmission Technique

The free space transmission system shown in Fig. 3.1 is similar to the waveguide system except that the soil is kept as a dielectric slab between horn antennas. The antenna separation can be altered by altering respective positions and can be handled by two methods, i.e. by varying the sample location between the horn antennas during measurement of the phase shift, and swept frequency loss measurements. Additionally, measurements can be carried out at several sample thicknesses and then averaged. The latter is especially useful for low loss samples such as those represented by dry soils at low frequencies (Hallikainen, 1985a).

Dielectric constant can be computed from

$$\varepsilon' = \left(\frac{\lambda_0}{2\pi}\right)^2 (\beta^2 - \alpha^2) \quad \text{and} \quad \varepsilon'' = \left(\frac{\lambda_0}{2\pi}\right)^2 (2\alpha\beta) \tag{3.1}$$

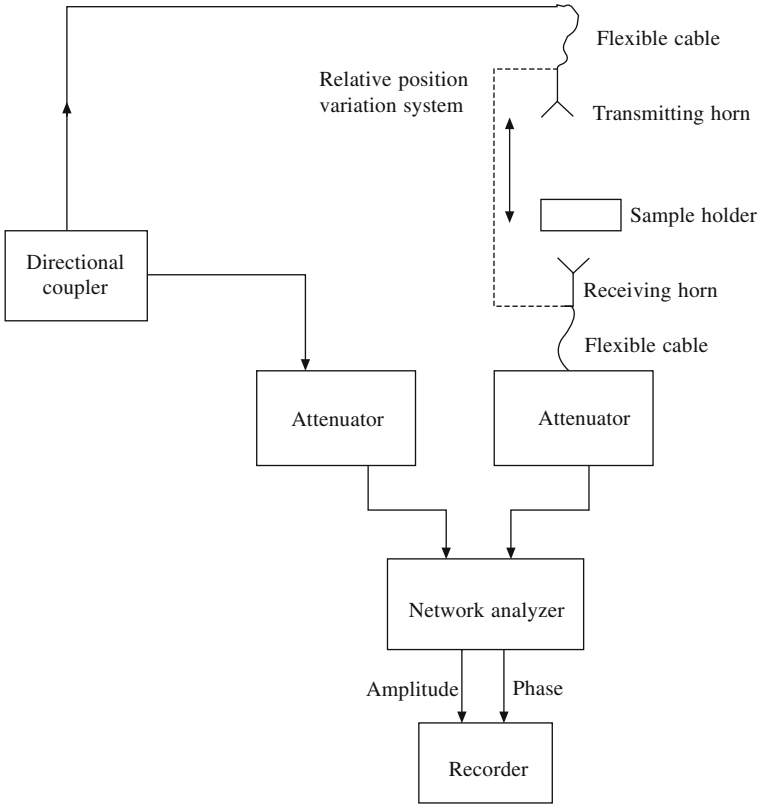

Fig. 3.1 Block diagram for the free space measurement system.

where λ_0 is the free space wavelength, α the attenuation constant and β the phase shift.

The greatest advantage of this method is that it is relatively simple and does not involve solution of a transcendental equation.

Cavity Perturbation Method

The method of measurement involves determination of the change in resonant frequency f and quality factor Q of a cavity when it is loaded with a dielectric (Fig. 3.2). The technique is similar to that adopted by Birnbaum and Franeau (1949), and is characterized by convenience of measurement and simple calculations. The changes in resonant frequency and Q of the cavity are related to real and imaginary parts of the dielectric constant by the expressions given below. Assuming that the sample is located into the cavity where E field is maximum, we get

$$\varepsilon' = \frac{1}{2} + \frac{V_c}{V_s}\frac{(f_1 - f_2)}{f_2}$$

and

$$\varepsilon'' = \frac{1}{4}\frac{V_c}{V_s}\left\{\frac{1}{Q_2} - \frac{1}{Q_1}\right\}$$

The loss is characterized by tan $\delta = \varepsilon''/\varepsilon'$, where V_c is the volume of the cavity, V_s the sample volume and Q_1 and Q_2 are the quality factors without and with the sample, corresponding to the frequencies f_1 and f_2, respectively.

Transmission Technique in Waveguides/Coaxial Lines

This method is particularly suitable for high loss samples. In such cases measurement is based on infinite sample length (Stuchly et al., 1978). Infinite sample is defined as one, when most of the energy entering the sample gets absorbed (Fig. 3.2).

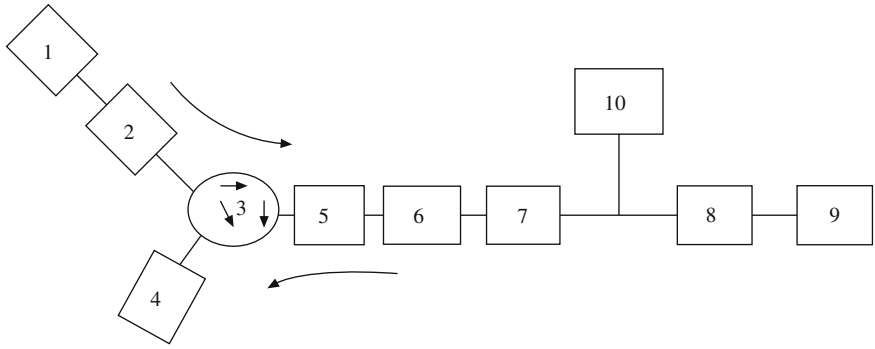

1. Klystron power supply, 2. Klystron with mount, 3. Circulator, 4. Matched load, 5. Variable attenuator, 6. Frequency meter, 7. Slotted section, 8. E.H. tuner, 9. Sample holder cavity/matched load, 10. VSWR meter.

Fig. 3.2 Schematic diagram of infinite sample technique.

The normalized input impedance at the interface of two dielectrics, when the second one is of infinite length, is directly related to the dielectric properties of the two. In a waveguide with (TE_{10}) mode, the relative complex dielectric constant is

$$\varepsilon = \frac{1}{1 + (\lambda_c/\lambda_g)^2} + \frac{1}{1 + (\lambda_c/\lambda_g)^2}\left[\frac{\Gamma_R - j \tan\{k(D - D_R)\}}{1 - j \tan\{k(D - D_R)\}}\right] \qquad (3.2)$$

where λ_g is the guide wavelength, λ_c the cutoff wavelength, Γ_R the VSWR and $(D - D_R)$ is the shift in minima position when an infinite sample is replaced with short circuit. A number of investigators have been successful with this method (Biofot, 1992; Karolkar et al., 1985 etc.).

The Two Point Method

The schematic diagram of this method is shown in Fig. 3.3. Two point method (Sucher and Fox, 1963; Bala Krishna, 1995) is a technique involving measurement of reflection coefficient in a waveguide. This method is suitable for low and medium loss dielectric and can be adopted for measurement of soil complex permittivity at different moisture content. A set-up for measurement has an empty short-circuited waveguide with a probe located at a voltage minimum D_R. The same waveguide, containing a sample length l, has the probe located at a new voltage minimum D.

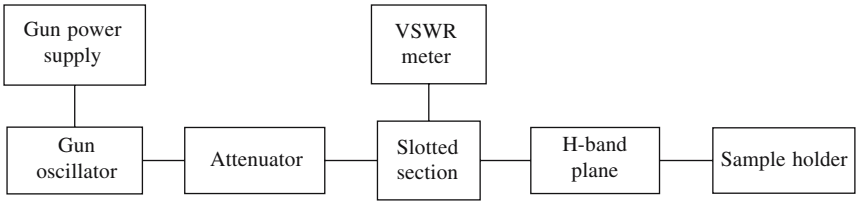

Fig. 3.3 Schematic diagram of the set-up for two point method.

In two point method the complex dielectric constant of soil is given by

$$C \angle -\psi = 1/jkl_\varepsilon - (1 - |\Gamma| e^{j\varphi})/(1 + |\Gamma| e^{j\varphi}) \tag{3.3}$$

where k is the wave number, l_ε the sample length, $|\Gamma|$ the reflection coefficient and φ the phase constant.

The transcendental equation obtained by impedance matching can be written as:

$$\frac{\tan k(D_R - D - l_\varepsilon)}{kl_\varepsilon} = \frac{\tan k_\varepsilon l_\varepsilon}{k_\varepsilon l_\varepsilon} \tag{3.4}$$

The propagation constant $k = 2\pi/\lambda_g$, λ_g being the guide wavelength

$$k_\varepsilon = 2\pi/\lambda\ [\varepsilon_r \mu_r - (\lambda/\lambda_c)^2]^{1/2} \tag{3.5}$$

where μ_r is the permeability of the medium, λ_c the cutoff wavelength and ε the relative permittivity.

$$\varepsilon' = \frac{(x/kl_\varepsilon)^2 \cos\theta' + (\lambda_g/\lambda_c)^2}{1 + (\lambda_g/\lambda_c)^2} \quad (\theta' = 2(\theta - 90)) \tag{3.6}$$

$$\varepsilon'' = \frac{-(x/kl_\varepsilon)^2 \sin\theta'}{1 + (\lambda_9/\lambda_c)^2} \tag{3.7}$$

x and θ values can be calculated using C, ψ graph.

Network Analyzer in Reflection Measurements: Theoretical background

The lumped element approach of Stuchly et al. (1974) is selected for measuring the reflection which is related to the characteristic impedance of the transmission line and that of the sensor probe. The impedance of the sensor is a function of the frequency and relative permittivity of the test sample.

Stabell and Misra (1990) developed a modified procedure for *in vivo* dielectric measurement using an open ended line probe. Any system imperfection is completely bypassed in this method since the calibration is carried out with four materials of known dielectric constants and then the reflection coefficients of these materials are used in the final calculations along with the reflection coefficient of the sample (Fig. 3.4). This method is similar to the monopole antenna technique adopted by (Ray and Behari, 1986, 1987) to measure dielectric constant of biological tissues. The later

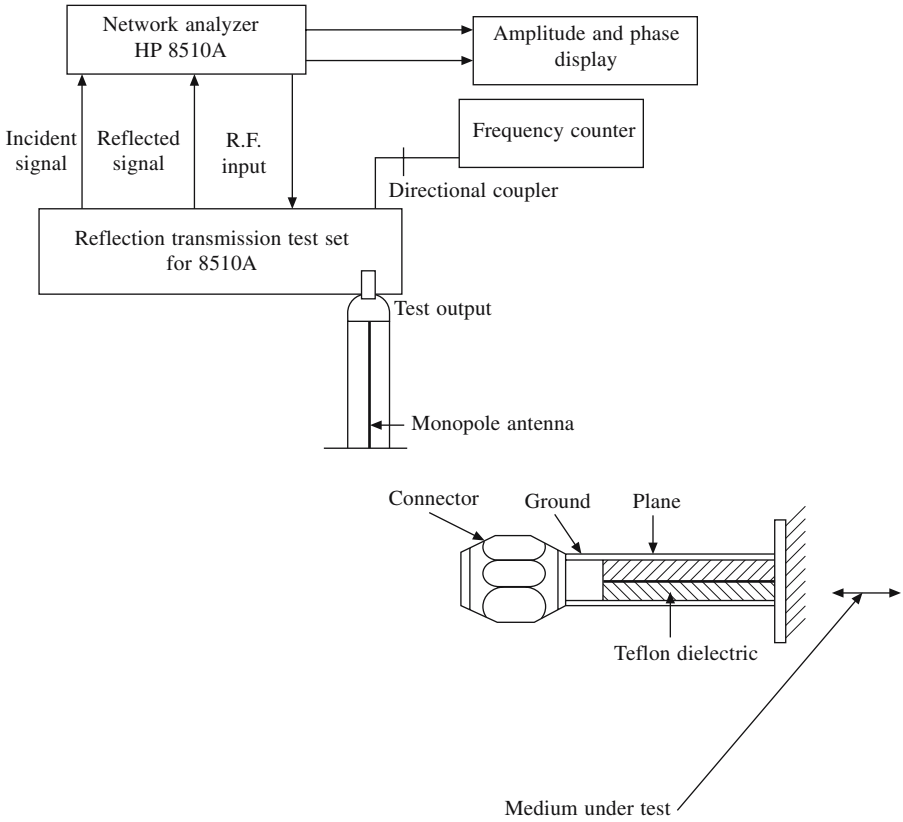

Fig. 3.4 Schematic diagram of instrumentation with network analyzer.

method is beset with uncertainties particularly with the choice of a/l (l being the length of monopole antenna). In the method of Stabell and Misra (1990) a perfect coaxial line is instead adopted.

Under quasi-static approximation, the stationary formula for the aperture admittance of an open ended coaxial line terminated by a semi-infinite medium on the ground plane reduces to (Stabell and Misra, 1990).

$$Y = \frac{-j2\omega I_1}{[\ln(b/a)]^2}\varepsilon - \frac{-j\omega^3\mu_0 I_2}{[\ln(b/a)]^2}\varepsilon^2 + \frac{\pi\omega^4\mu_0^{3/2}}{12}\left[\frac{b^2 - a^2}{\ln(b/a)}\right]^2 \varepsilon^{5/2} \qquad (3.8)$$

where a and b are the inner and outer radii of the coaxial cable, respectively, I_1 and I_2 are two triple integrals dependent on radii but constant otherwise.

The actual admittance of the aperture terminated by a sample is evaluated from the measured reflection coefficient after calibrating the system with three standard materials. If Y_s is the aperture admittance terminated by a sample material, $Y_{1,2,3}$ are aperture admittance in the standard materials, respectively. Then

$$\frac{Y_s - Y_1}{Y_s - Y_2} \times \frac{Y_3 - Y_2}{Y_1 - Y_3} = \frac{d_{s1}d_{32}}{d_{s2}d_{13}} \qquad (3.9)$$

where $d_{ij} = \Gamma_i - \Gamma_j$ and Γ_n represents the measured reflection coefficients for the nth material. Using the fourth standard material and noting the bilinear transformation characteristic of admittance, the coaxial aperture admittance at lower frequency can be written as

$$Y_L = \varepsilon + A_0\varepsilon^2 \tag{3.10}$$

Equations (3.8) and (3.9) are used to determine the complex permittivity of the sample. Assuming the third standard as the short circuit

$$Y_s = (Y_1 + \Delta' Y_2)/(1 + \Delta') \tag{3.11}$$

where $\Delta' = d_{s1}d_{32}/d_{s2}d_{13}$.

The values of Y_{12} are calculated from Eq. (3.10) for a given set of complex permittivities of standards 1 and 2, respectively. The unknown constant A_0 can be calculated using the formula

$$A_0 = \frac{(1 + \Delta)\varepsilon_4 - \varepsilon_1 - \Delta\varepsilon_2}{\varepsilon_1^2 + \varepsilon_2^2 - (1 + \Delta)\varepsilon_4^2} \tag{3.12}$$

where $\Delta = d_{41}d_{43}/d_{42}d_{13}$.

In case of reflection methods in waveguides, the reflection coefficient from a defined reference plane is put to use for permittivity measurements. The reflection coefficient itself may be measured by a slotted line or a network analyzer or by simply forming a resonator terminated by the sample (Stuchly et al., 1978). Both these methods are suitable for either lossless dielectrics or dielectric with medium loss.

Reflection Techniques in Coaxial Lines/Waveguides

The techniques involving measurement of reflection coefficients are:

(a) Single-horn reflectometry method (Arcone and Larson, 1988; Mishra and Behari, 2000).
(b) Coaxial cable reflectometry method (Ghannouchi and Bosisio, 1987; Stuchly et al., 1980).

Reflection methods are usually adopted in a coaxial line sample holder where the reflection coefficient or scattering parameter are determined at a redefined reference plane from the sample holder. The reflection coefficient can be determined very easily with the use of a network analyzer, using swept frequency technique or slotted line apparatus or using a resonator terminated by the sample (Stuchly et al. 1978, 1979, 1980). The resonator method uses an infinite sample where changes in the resonating frequency and Q factor produced by the sample are measured. For the TEM mode, magnitude of the reflection coefficient is $|\Gamma| = \exp[-n(1/Q_\varepsilon - 1/Q_0)]$ and phase angle $\theta = 2\pi n(1 - f_c/f_0)^n$, where f_c is the resonance frequency with sample and f_0 is the resonating frequency of the resonator without the sample. n is dependent on resonator length $= (nc/2l)$, n being an integer. The dielectric parameter is given by

$$\varepsilon = \left[\frac{1 - \Gamma}{1 + \Gamma}\right]^2 \tag{3.13}$$

where $\Gamma = |\Gamma| e^{j\theta}$.

This method can be applied for a lossy material with a high dielectric constant (e.g. a biological tissue) but it is limited to a discrete frequency.

Resonator methods are not suitable for high loss liquids because the resonance peak becomes so broad that it cannot be measured correctly. As an alternative, open cavity methods with high loss liquids filled in a capillary can be applied. A method has been devised by Van loon and Finsey (1975) involving computer analysis of the reflected power profile. The wave propagation constant is determined by fitting an analytical curve to the reflection profile, which then, yields the value of the complex permittivity.

Single-Horn Reflectometry Method: Theory and Description

The single-horn reflectometry method provides a sound technique for *in situ* measurement of dielectric permittivity of lossy materials through direct determination of the surface reflectivity (Arcone and Larson, 1988). In the technique, microwave (of the desired frequency) generated from a suitable source are passed through a waveguide culminating in a standard gain horn antenna (Fig. 3.5) onto the surface of the soil

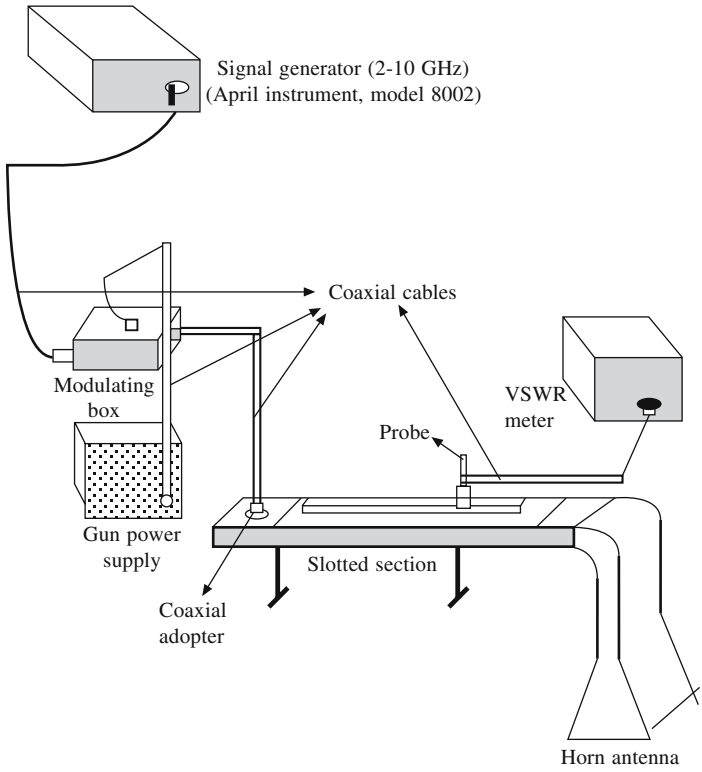

Fig. 3.5 Schematic diagram used in horn antenna method.

sample. A part of the microwaves undergo reflection at the soil surface, and the rest is transmitted into the medium and in due course absorbed after suffering energy loss through attenuation. The reflectivity of the medium is measured with respect to a plane shining metal surface which provides near total reflection. The measurements are carried out with the help of a slotted section provided in the waveguide having a movable probe connected to a VSWR meter.

The apparatus consists of a microwave oscillator acting as the signal source and operating around 2-10 GHz. A standard rectangular waveguide couples the oscillator to the waveguide slotted line through an E-plane aperture standard gain horn. The slotted section is provided with a vernier scale for linear measurement of the minima shift. Besides this a VSWR meter displays the voltage standing wave ratio at the wave minima.

The reflectometer horn aperture is placed at a suitable height which can be varied over the soil surface. This instrument can be used to measure the soil moisture at different depths at different time intervals.

Height Adjusting Setup Description

To meet this requirement a special type of table is developed so that entire setup consisting of slotted line, coaxial adopter and horn antenna can be adjusted at various heights keeping in mind the exposed area by horn antenna (Fig. 3.6). No metallic object should come in the exposed area (Mishra and Behari, 2000).

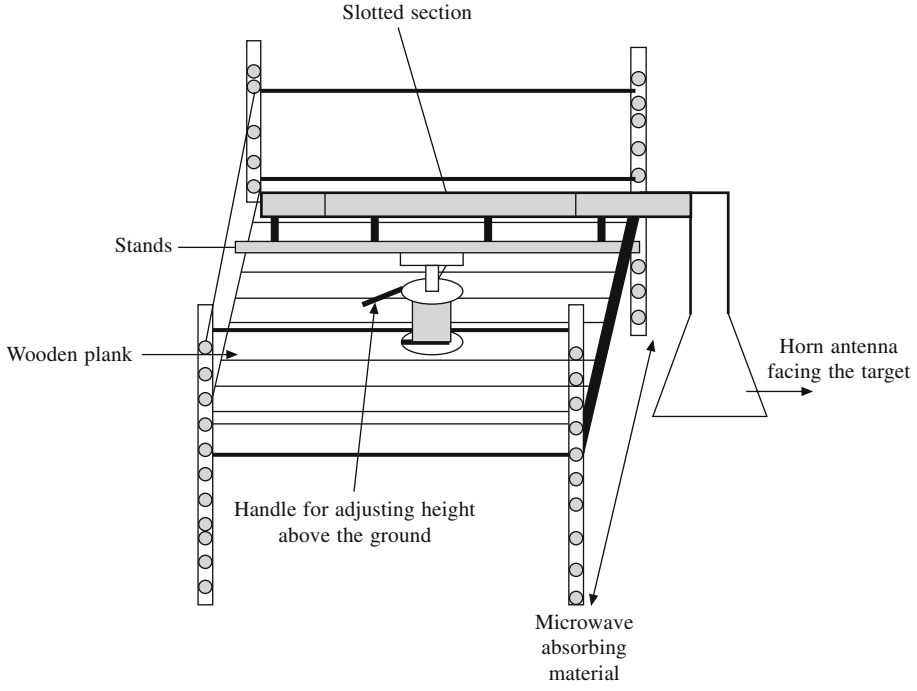

Fig. 3.6 Schematic diagram of height adjustable table using horn antenna technique.

For height variation upto 25-30 cm, a special set-up shown in Fig. 3.6 is desired which is fitted in a wooden plank consisting of a metallic rod on which stands were put that can sustain more than 20 kg weight and are adjusted according to different band slotted section. For higher variation angle, iron rods can be used.

Dielectric constant of field soil can be measured at different heights between $3\lambda_g$ and $4.5\lambda_g$, where VSWR is almost constant. For wavelength greater than X-band it is necessary to have a special setup so that height adjustment may be done frequently keeping the horn antenna perfectly horizontal so that microwaves may normally fall on the exposed surface.

The magnitude of reflectivity | Γ | is given by

$$|\Gamma| = \left|\frac{V_s - 1}{V_s + 1}\right|\left|\frac{V_m + 1}{V_m - 1}\right| \tag{3.14}$$

where *s* indicates horn above soil and *m* the horn above the metal plate.

The phase ϕ of Γ was obtained from

$$\phi = 4\pi\, \Delta x/\lambda_g \tag{3.15}$$

where $\Delta x = D_s - D_m$ (shift in the location of minima with horn above soil and horn above metal plate). λ_g is the guide wavelength (= 2 × Distance between successive minima under short circuit conditions).

For a lossless and electrically thick sample (in this case soil)

$$\varepsilon = \left[\frac{1 + \Gamma}{1 - \Gamma}\right]^2 \tag{3.16}$$

This method is well suited under field conditions.

For normal incidence emissivity directly depends only upon the real part of the dielectric constant.

Limitations

In single-horn reflectometry method the four prerequisite conditions for good results are that:

(a) Exposed surface should be plane.
(b) Microwave should fall normally on the exposed surface.
(c) Horn antenna should be put at a suitable height.
(d) No conducting object should be in the vicinity of the horn antenna.

The method is very efficient if these conditions are met. It also permits measurements to be performed at small grazing angle. There are two possible sources of error in this simple approach that must be carefully looked. The first is surface flatness, which strongly influences the phase measurements. The curvature restriction requires a stiff metal plate to be placed under the entire instrument (rather than just beneath the horn).

The second possible source of error is multiple reflections. These can be serious

when bottom reflectivity is strong, attenuation is low and the upper layer is sufficiently thick to cause a large discrepancy in geometric spreading loss between the surface and bottom reflection.

As mentioned above the simplest approach to soil moisture information would be to use a single frequency sensor to estimate moisture in a 5 cm depth. These values could be used to determine infiltration and/or evaporation and to extrapolate deeper layers. More information about soil moisture are possible if different wavelengths are used adopting this technique.

The Coaxial Cable Method

An open ended coaxial line in contact with semi-infinite medium is analyzed by Gajda (1982) and Misra (1987). The equivalent circuit of this open ended coaxial transmission line with a ground plane consists of a transmission line of characteristic impedance Z_0 terminated by a stray capacitance C_T and conductance G_T. When a test sample is present, the fringing capacitance will partly depend upon the permittivity of the test sample C_2 and partly due to the fringing field inside the transmission line C_1. Conductance of any coaxial line is very small even beyond 1 GHz. The permittivity relations can be written as

$$\varepsilon' = \frac{2|\Gamma| \sin(-\theta)\left(1 + \frac{C_1}{C_2}\right)}{\omega C_T Z_0 (1 + 2|\Gamma| \cos\theta + |\Gamma|^2)} - \frac{C_1}{C_2} \tag{3.17}$$

$$\varepsilon'' = \frac{1 - |\Gamma|^2}{\omega C_T Z_0 (1 + 2|\Gamma| \cos\theta + |\Gamma|^2} \left(1 + \frac{C_1}{C_2}\right) \tag{3.18}$$

where θ is the phase angle.

This dielectric constant and loss factor are both functions of the ratio C_1/C_2 as well as ω, C_T and Z_0. Unfortunately, the ratio of the two capacitances or separately or any component cannot be determined analytically. However, C_1/C_2 can be determined empirically from measurement on known dielectrics. In coaxial cable method the complex permittivity is computed from the reflection coefficient.

Nondestrictive broad band permittivity measurements using open ended coaxial lines as impedance sensors are of great use in a wide variety of fields. However, the impedance measurement sensors are normally done with an automatic network analyzer (ANA).

Figure 3.7 shows the equivalent electrical model of the probe immersed into a test medium with a relative complex permittivity ε. A similar method was adopted by Ray and Behari (1986) to measure dielectric permittivity of biological tissues. An effective transmission line is used to model the fringing electric field in the test medium at the extremity of the probe. For the probe immersed in a dielectric medium (soil in the present case) the terminating admittance at the end of the effective transmission line Y_L is given by

$$Y_L = jY \tan(\beta_d L) \tag{3.19}$$

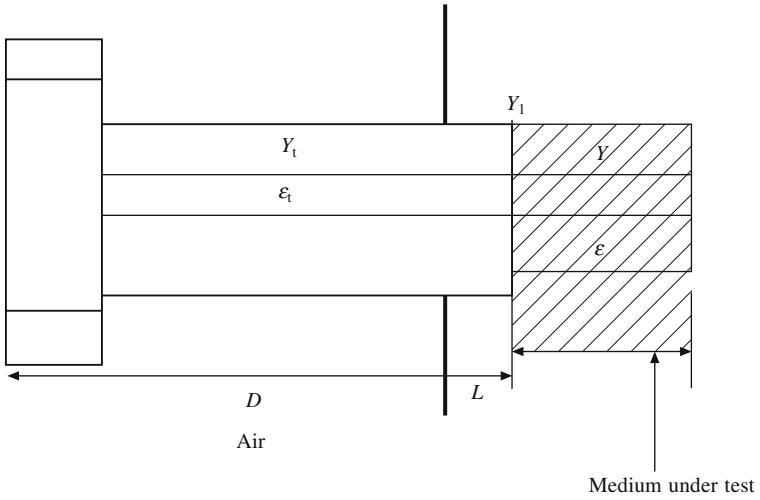

Fig. 3.7 An open ended coaxial line probe radiating in homogeneous medium (Probe model).

where Y is the characteristic admittance of the effective transmission line, β_d the propagation constant in the end of the effective transmission and L the effective transmission line length.

A function of physical parameters of the effective transmission line, Y is expressed as

$$Y = \frac{\sqrt{\varepsilon}}{60 \ln (b/a)} \tag{3.20}$$

where a and b are the inner and outer diameters of the coaxial probe, respectively. Furthermore, the admittance Y_L can be related to the characteristic admittance of the probe Y_t and the measured reflection coefficient reported at the plane Y_1 as

$$Y_L = \left[\frac{1 - \Gamma_m e^{2j\beta_t D}}{1 + \Gamma_m e^{2j\beta_t D}}\right] Y_t \tag{3.21}$$

where $Y_t = \dfrac{\sqrt{\varepsilon_t}}{60 \ln (b/a)}$ is the characteristic admittance of the probe, ε_t the dielectric material inside the coaxial line (subscript t for Teflon, $\varepsilon_t = 2.03 - 0.004j$), D the physical length of the probe, β_t is the propagation constant in coaxial probe, Γ_m is the complex reflection coefficient at the plane L given by the six port reflectometer. Substituting Eq. (3.19) into (3.21) and using the expression for Y as given by (3.20), we get

$$\varepsilon = \frac{-jc\sqrt{\varepsilon_t}}{2\pi f L}\left[\frac{1 - \Gamma_m e^{2j\beta_t D}}{1 + \Gamma_m e^{2j\beta_t D}}\right] \times \cot(x) \tag{3.22}$$

where $x = (2\pi f L\sqrt{\varepsilon})/c$, ε is the complex permittivity of the dielectric under test, c the wave velocity in free space and f the measuring frequency.

The above equation is used to compute the complex permittivity from the knowledge of reflection coefficient.

For accurate measurements of dielectric parameters of soil, a knowledge of probe parameters (D, L) is essential at each measuring frequency. In this case measurement of these parameters is based on the use of two dielectric materials, taken as standards.

Substituting Eq. (3.19) in (3.21), we obtain

$$\Gamma_m e^{2j\beta_t D} = \frac{\rho + \Gamma_m e^{-2j\beta_d D}}{1 + \rho \Gamma_m e^{-2j\beta_d D}} \tag{3.23}$$

where

$$\rho = \frac{\sqrt{\varepsilon_t} - \sqrt{\varepsilon}}{\sqrt{\varepsilon_t} + \sqrt{\varepsilon}}$$

The measurement of D and L is carried out with an iterative computation procedure. The standard dielectric mediums used in the probe calibration procedure are usually air and water. The dielectric constant of pure water are accurately represented by the Cole-Cole Eq. (2.15). This method was previously used by (Ghannouchi and Bosiso, 1987) for measuring the dielectric constant of lossy liquids. For a coaxial probe design it was reported (Li and Chen 1995) that accurate results come from measurement of dielectric constant in the range 1-4 GHz.

Limitations

In the coaxial probe method, the complex dielectric constant is estimated from the measured complex reflection coefficient of the open ended coaxial line pressed against the unknown material. The accuracy of this technique is limited by the small dynamic range of reflection coefficient as a function of ε'. Another problem when applied to soil medium, is the small contact area of the coaxial tip which may be comparable to the soil particles. The soil dielectric constant using coaxial probe is very sensitive to the applied pressure which affects the accuracy of this measurement technique.

With higher frequencies (>8 GHz), the attenuation losses in the cable may be appreciable. With coaxial cable method for lower frequencies (< 1 GHz) some instability problem arises, especially for the low permittivity materials. Therefore, the accuracy of the method is limited.

Precautions

Calibration needs to be checked prior to each cycle of measurement. The tip of the coaxial sensor should be flat and perpendicular to the axis of the coaxial line. Temperature variation may also cause the inner (or outer) conductor to extend beyond the aperture of the coaxial line. The effect is dependent upon the way in which the coaxial cable has been designed. The four parameters which must be considered in the design of the coaxial probe sensing system are: the length of the buried cable, depth, frequency and the type of cable (sensor). The signal frequencies have both upper and lower limits. The lower limit is determined by the requirement $D > \delta_D$ (the skin depth in the soil). The maximum amount of attenuation in the cable that can be

tolerated determines the upper frequency limit. The oscillator is to be chosen to have frequency stability to minimize random phase fluctuations. To minimize the diurnal phase drift due to variations in soil temperature, a phase stabilized cable is used to perform sensing.

The coaxial cable method is preferable for field work in the frequency range 1-7 GHz with different moisture levels and at different depths. In this method correct results are dependent upon the sensor sensitivity. Since the cable method senses the changes in soil permittivity, it can provide an excellent method of monitoring the amount of water available to plants.

Capacitance Probe (CP)

A capacitance probe (CP) consists of an electrode pair separated by a plastic dielectric. The upper and lower electrodes and the plastic separator are in the shape of a cylinder that fits closely inside a plastic access tube. An inductance-capacitance resonant circuit in the probe includes the ensemble of the soil outside the access tube itself, plus the air space between the probe and access tube, as one of the capacitive elements. Changes in the resonant frequency of the circuit depend on changes in the capacitances of the soil-access tube system. Capacitance of a simple two electrode plate capacitor is given by:

$$C = \varepsilon_0 \, \varepsilon_{\text{eff}} \, A/d \tag{3.24}$$

where ε_0 is the permittivity of free space, ε_{eff} is the system effective dielectric constant, A is the overlapping area (m^2) of the plates and d is the distance (m) separating the dielectric plates.

In this procedure probe calibration is an important aspect. Chanzy et al. (1988) showed that the calibrations differ significantly from one probe to another. Once calibrated, the capacitance probe provides accurate soil water measurements, but it is advisable to have at least two replicate probes.

Microstrip Ring Resonator

In order to overcome some of the difficulties encountered in the abovementioned techniques, microwave ring resonator devise is used for measurement of soil dielectric parameters (Sarabandi and Li, 1997). The method is very similar to cavity measurement technique because it also measures the shift in resonance frequency f_0 and quality factor Q due to the loading of the dielectric. In this method the resonator is placed in contact with the soil medium and the shift in resonance frequency and the change in quality factor of the resonator is measured. This similarity arises because the microstrip resonator can be regarded as a partially filled resonator cavity.

It is clear that for partially filled resonator the dielectric changes in f_0 and Q are substantially less affected by the loading of dielectric material. It has been pointed out that with appropriate microstrip resonator design, dielectric constant of soil with moisture content as high as 40% can be measured.

A microstrip ring resonator is a simple transmission line in which resonator is excited at certain frequencies. Depending on the electrical length of the resonance a standing wave pattern forms around the circular path of the resonator. The maximum

voltage of the standing wave occurs at the exciting point. The resonant frequencies correspond to a condition where the parameter of the ring is an integer multiple of the guided wavelength (Fig. 3.8)

$$\lambda_p = \frac{\pi d}{n} \tag{3.25}$$

where d is the diameter of the ring, λ_p the function of the microstrip parameters and n can take integral values 1, 2, 3.... The maximum voltage of the standing wave occurs at the exciting point.

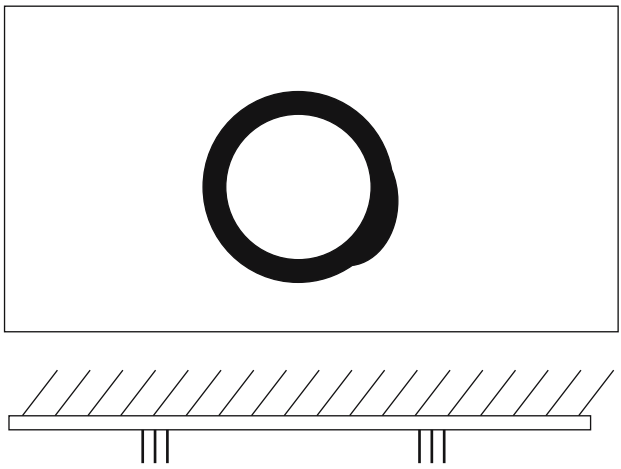

Fig. 3.8 A ring resonator in contact with a dielectric ε.

At resonant frequencies there exist a voltage maximum at $\pi d/2$ away from the excitation point. By placing a transmission line at this voltage maximum point, the field in the resonator can be probed to detect the resonance frequencies. In essence, the transmission coefficient S_{21} of the two port resonator is measured as a function of frequency and the resonant frequencies are identified as frequencies for which S_{21} is maximized. Coupling capacitor is used to lower the resonant frequency. This must be as small as possible for accurate measurement of the resonant frequency. Spectral measurement of S_{21} can also reveal the loss quality factor of the resonator which is a measure of power loss in the resonator. The dissipated power in the resonator includes the dielectric loss, the conductor loss and the radiation loss.

Time Domain Reflectometry (TDR)

TDR operates in the frequency range of 1 MHz to 1 GHz, well below the relaxation frequency of water. Hoekstra and Delaney (1974) and Davis and Annan (1977) reported little frequency dependence of ε' across this range, though the electrical conductivity contributes to dielectric loss if the solution contain ions (De Loor, 1968). ε'' is generally small and insignificant in non-saline homogenous soils.

The use of remote shorting diodes and calibrated reference airlines can, in many cases, considerably improve the accuracy of TDR measurements (Hook et al., 1992; Topp et al., 1996). The signal-to-noise ratio of the reflected signals can be increased by using remotely switched diodes. This combined with a waveform subtraction procedure provides reliable identification of the two reflections that define ε_{air}. The high resolution TDR system has an excellent advantage of detecting very small changes in soil water content. The system can thus be used for quantifying the effects of temperature variations, on the apparent dielectric constant of soils with different water contents (Pepin et al., 1995).

In TDR, the dielectric constant of soil is determined by measuring the propagation time t of a high frequency electromagnetic pulse (e.g. of the orders of 140 ps) launched along a pair of parallel waveguides of known length L buried inside the soil medium. As at the end of waveguide the launched electromagnetic pulse is reflected back to its source, so the path length of the voltage pulse is twice the length of waveguide. Thus, the propagation velocity of pulse V can be written as

$$V = 2\,L/t \tag{3.26}$$

The time delay provides information about the real part of the dielectric constant.

In the electrical transmission line theory the electromagnetic wave propagation velocity in a transmission line is given by (Marshall and Holmes, 1988)

$$V = c\left[\frac{1}{2}\varepsilon\{1 + (1 + \tan^2\delta)^{1/2}\}\right]^{-1/2} \tag{3.27}$$

c is the velocity of an electromagnetic wave in vacuum (3×10^8 m/s) and $\tan\delta = \{\varepsilon'' + (\sigma_{dc}/\omega\varepsilon_0)\}/\varepsilon'$, where σ_{dc} is the zero frequency electrical conductivity.

At very high frequency $\delta \to 0$, so that

$$V = c/(\varepsilon_{eff})^{1/2} \tag{3.28}$$

where ε_{eff} is the effective dielectric constant of the soil being measured.

From (3.26) and (3.27), we get

$$\varepsilon_{eff} = \left(\frac{ct}{2L}\right)^2 \tag{3.29}$$

In Eq. (3.29), putting $L = 3.0.0$ cm, $\varepsilon_{eff} = 25.0$ and $c = 3.0 \times 10^8$ m sec^{-1}, the time of propagation is 5 ns.

The effective dielectric constant ε_{eff} depends on soil moisture content θ, following a linear relationship of the type

$$\sqrt{\varepsilon_{eff}} = C_1\theta + C_2 \tag{3.30}$$

where C_1 and C_2 are constants and depend on the soil type (Topp et al., 1994; Ferre et al., 1996). This signifies the need of only two point calibration.

The advent of diode-shorting techniques in TDR soil water content probes (Hook et al., 1992; Ferre et al., 1996) had led to the design of one piece profile probes. In

a typical design, 6 shorting diodes are placed along a transmission line, spaced 15 or 30 cm apart. The interval between each diode and its neighbor is called a segment. In six-diode probe, there are thus five segments. The diodes are configured to apply a short circuit across the transmission line when activated. Figures 3.9 and 3.10 illustrate the use of multiplexing probe. The probe can be implanted at various locations in the field by choosing a suitable cable length within a radius of 50-100 cm with respect to the body of the apparatus. The system has data logging facility to continuously monitor the soil moisture profile over a period of time.

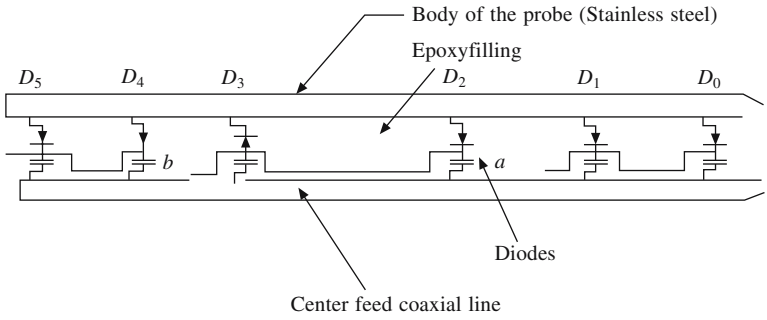

Fig. 3.9 Five segment, six diode profile probe. A high frequency pulse propagated from the D_2 location spreads in both directions towards the ends.

Technically the round trip propagation time for a radio frequency (RF) pulse travelling along a particular segment is obtained by shorting the first diode in a segment, and measuring the time of arrival of the reflection from the discontinuity, introduced by the short circuit. This procedure is repeated for the second diode in the segment, and the two time intervals subtracted. The segment is calibrated by performing time interval measurement in dry sand bulk water having moisture content = 0 and 100%, respectively. The known dielectric constants of water and dry sand are used to calculate the coefficients of a linear equation relating time interval to water content. These coefficients are slightly different for each segment. This procedure amounts to performing a linear interpolation between two known points. There is an implicit assumption that time delay and soil water content are linearily related. The validity of this assumption has been demonstrated by overwhelming statistics obtained from measurements (Hook et al., 1992).

Water content measurements by TDR compare favorably with conventional and neutron scattering technique (Bandyopadhyay, 1995). TDR measurements average soil water content over a depth depending upon the wavelength. Waveguides upto 60 cm length have so far been used (Topp et al., 1994). Using TDR it is possible to infer soil electrical conductivity as well as soil water content (Dalton, 1992, Sundara Sarma et al., 1992). The effective use of TDR water content values for water balance monitoring depends on rapid and reproducible recovery of data from a number of representative locations. These requirements led to the development of automated analyses of the TDR trace (Zegelin et al., 1992) and multiplexing capabilities, which allow measurement of many locations using a single TDR unit.

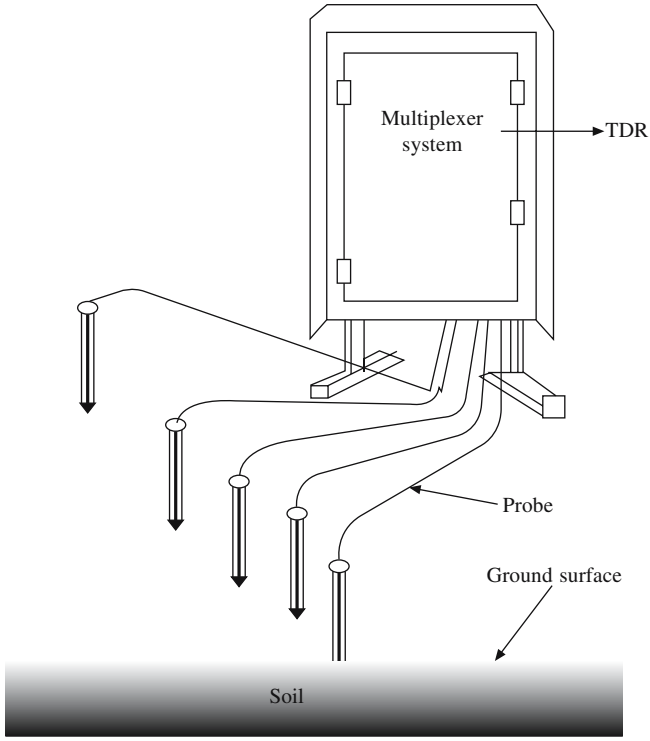

Fig. 3.10 The TDR multiplexing technology to measure soil moisture produces increased signal levels, enabling it to operate in a broader range of soils. These five probes are shown to be simultaneously operative.

It may be mentioned that the accuracy of the TDR method is limited by the resolution of the TDR system itself. Evaluation and improvements are called for in the existing TDR instruments for their effective use for soil water content measurement, particularly in the design of probe type. However, its superiority persists owing to its versatility and easy manoeuverability.

Ground Penetrating Radar (GPR)

GPR has been employed to follow the wetting front movement to monitor changes in soil moisture content (Vellidis et al., 1990). GPR is also a suitable method for monitoring moisture content changes in the vadose zone and permits relatively large measurement scales, appropriate for hydrological models of unsaturated and saturated processes (Binley et al., 2001). GPR is a near-surface geophysical technique that can provide high resolution images of the dielectric properties of the top few tens of meters of the earth (Knight, 2001; van Dam and Schlager, 2000) by using high frequency pulses of electromagnetic (EM) energy.

A major interest in hydrogeology has been flow and transport mechanisms of contaminants within the vadose zone, to understand the soil or rock section between

the surface and ground water table. This technique also has the advantage of providing information between boreholes (XB). In conformation with this XBGPR velocity tomography has been increasingly used to characterize the dynamic change of water content in unsaturated soils. Hence, GPR methods perform best in sites lacking highly electrically conductive materials, such as clay-rich soils (Davis and Annan, 1989). Compared to GPR velocity, GPR attenuation has been less frequently used in hydrogeologic investigations. Attenuation is an intrinsic electromagnetic property and is a function of the conductivity as well as dielectric constant of the soil and the pore fluid. Therefore, it is expected to provide high resolution images from which information can be derived about the spatial heterogeneity of soils, or the distribution of conductive fluids.

GPR measurements can be carried out at several frequencies. Higher frequencies lead to higher spatial resolutions, but correspondingly higher attenuation and, therefore, to a lower depth of penetration. Frequencies commonly used are between 50 MHz and 1 GHz, referring to a wavelength between 6 m and 30 cm in air. The wavelength is shortened due to the higher relative dielectric constant in the soil. In sandy soils the wavelength of the 50 MHz antenna lies between 270 and 110 cm, while the wavelength of the 1 GHz antenna lies between 13 and 5 cm.

Measurements

GPR has been used for measuring soil water contents in various ways. First, antenna separation, which utilizes the method of ground wave propagation. This method is suitable for measuring the water content in the upper layer (10 cm) of the soil. Second, the reflectivity measurements, the velocity of wave in the soil. This method measures the water content between the reflector and the surface of the soil. If the depth of the reflector d is known, the effective dielectric constant ε_{eff} can be calculated by

$$\varepsilon_{\text{eff}} = \left(\frac{ct}{2d} \right)^2 \tag{3.31}$$

where t is the travel time.

The attenuation α is given by

$$\alpha \approx \frac{1}{2} \sqrt{\frac{\mu_0}{\varepsilon_0}} \frac{\sigma}{\sqrt{\varepsilon_{\text{eff}}}} \tag{3.32}$$

where ε_0, μ_0 are the dielectric permittivity (8.85×10^{-12} F/m) and magnetic permeability (417×10^{-7} H/m) in free space, respectively and σ is the electric conductivity of the medium.

Velocity v and attenuation are governed by electrical parameters including the electrical conductivity and the dielectric constant, both depend on water saturation (Daniels, 1996). For common earth materials (Davis and Annan, 1989), the EM wave velocity v is related to the dielectric constant through the simple relation

$$v \approx \frac{c}{\sqrt{\varepsilon_{\text{eff}}}} \tag{3.33}$$

where ε_{eff} is the effective dielectric constant, which can be related to water saturation with a petrophysical model (Roth et al., 1990; Topp et al., 1980). The model used by Roth et al. (1990), gives the effective dielectric as

$$\varepsilon_{\text{eff}} = [(1 - \varphi)\sqrt{\varepsilon_{\text{s}}} + S_{\text{w}}\varphi\sqrt{\varepsilon_{\text{w}}} + (1 - S_{\text{w}})\varphi\sqrt{\varepsilon_{\text{a}}}]^2 \tag{3.34}$$

where ε_{s}, ε_{w} and ε_{a} are the dielectric constants for the solid, water and air components of the soil, respectively, φ is the soil porosity and S_{w} the water saturation.

In crosshole GPR applications, high-frequency EM pulses (commonly with central frequencies of 100 or 250 MHz) are propagated between boreholes in various antenna configurations (Fig. 3.11). A GPR wave attribute that is potentially sensitive to the distribution of water saturation is the arrival time. The combination of Eqs. (3.33) and (3.34) gives the GPR inferred average water saturation at a given depth as

$$S_{\text{w}}, \text{GPR} = \frac{tcL^{-1} - (1 - \varphi)\sqrt{\varepsilon_{\text{s}}} - \varphi\sqrt{\varepsilon_{\text{a}}}}{\varphi(\sqrt{\varepsilon_{\text{w}}} - \sqrt{\varepsilon_{\text{a}}})} \tag{3.35}$$

where t is the recorded travel time and L the separation distance between boreholes (Kowalsky et al., 2004).

Data is acquired by receiver in another depth borehole at some distance away (Fig. 3.11). The angle of the line connecting the transmitting antenna and the receiving antenna, and the horizontal is limited to 45°. This is to avoid influences of wave

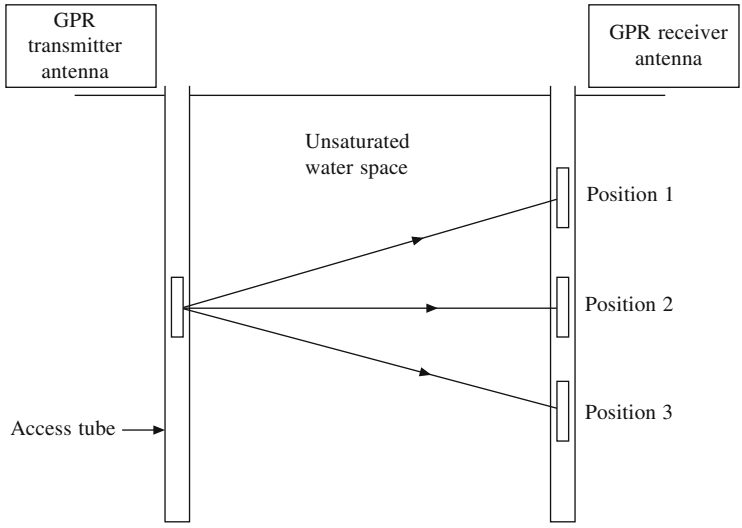

Fig. 3.11 Schematic GPR antenna configuration using the multi-offset gathers in the field investigation. The angle of transmitter and receiver antenna to the horizontal is limited to 45° while the position of transmitter and receiver antenna can vary.

reflections from high angles of antenna, which offset low signal-to-noise ratios and problems with the presence of wires within the ground. For the purpose of measurements the transmitting antenna can be moved to a new position and data can be similarly repeated. Repeating this process creates an array of intersecting ray paths. Each ray path represents the shortest path from the source to the receiver and is perpendicular to the EM wave front. First arrival time (travel time) and the amplitude of the received EM signals give velocity and attenuation.

GPR offers a fast and nondestructive way for estimating the soil dielectric constant. Ground-penetrating radar measurements are based on transmission or reflection of an electromagnetic wave in the studied medium. Wave propagation velocity depends on the dielectric constant of the medium and its spatial variations; wave velocity varies from 30 cm/ns in air to 6 to 15 cm/ns in soils. GPR emits EM microwaves, and measures dielectric constant and uses a free wave that propagates and spreads in the soil, where it will reflect off interfaces with different dielectric constants.

In GPR two modes of operations are possible, viz. the ground mode and the airborne. A strong correlation between the GPR data and the soil water content is observed in both the ground and airborne modes of operation. In the ground mode, soil moisture error is found to be lower than 0.03 m^3/m^3. However, in the airborne mode, soil moisture estimation is less accurate (0.046 m^3/m^3) (Chanzy et al., 1996). This method has a great potential for mapping soil moisture. Its performance is satisfactory on most natural surface as vegetation and surface microtopography.

Weiler et al. (1998) reported that GPR, which uses an unguided EM wave, shows great promise in the future for nondestructive soil water sensing. GPR can measure larger volumes of soil than the TDR and can be utilized without disturbing the soil. This forms a clear advantage over TDR. However, its disadvantage is that automatic measurements are not possible because the instrument is prone to failure in soils with high clay and salinity contents. Since GPR systems are wide band receivers and are, therefore, susceptible to interference from various man made source (e.g. television transmitters, FM radio transmitters etc.). Systematic noise can also be generated in radar profiles, which are multiple reflection events of various origins.

Although GPR antenna direct much of their electromagnetic energy into the sub surface, some is also lost in the air. This happens more often when unshielded antennae are used. Common causes of subsurface reflections are power lines and poles, trees, metallic fences and other similar objects (Neal, 2004).

Lysimeter

Compared to TDR and GPR, where calibration is required, lysimeter measure water changes with great accuracy (Stoffregen et al., 2002). Lysimeters are used in soil hydrology to measure evapotranspiration, capillary rise and ground water recharge. If the lysimeter is weighed, the changes of the total water content in the soil can be calculated with very high accuracy. For most cases in soil hydrology, the change of the water content is an important parameter. The measurements of GPR using a lysimeter offer, therefore, a very good method to calculate the accuracy of GPR for water content changes in the vadose zone. These authors have obtained a calibration curve (for ground water table 2.1 m)

$$\theta = 2.45\ \varepsilon - 3.04$$

where θ is the soil water content and ε the dielectric constant.

Comparison of Various Techniques

Various techniques adopted for soil moisture measurements have relative advantages and disadvantages. The TDR method for soil water content measurement is widely applicable and is mostly used for automated data collection. However, obtaining precision and accuracy is very much dependent on waveform interpretation methods used in software (Evett, 2000). Most of these are based on the relationship between volumetric soil water content and dielectric constant (permittivity) of soils. However, a single equation is not adequate for all soils. Dirksen and Dasberg (1993) reported that this can be valid for the soils with low clay contents (specific surface) and typical bulk densities (ρ_b = 1.35-1.5 g/cm^3). Zegelin et al. (1992) revealed that the use of universal equation gives water balance to within ±10% of soil water content. However, the Maxwell-De Loor's mixing model for the four components (solid phase, tightly bound water, free water and air) can account for both factors with average values of the volume fraction and dielectric constant of the tightly bound water. When using the TDR, it is often of great importance to obtain high depth resolution with minimal disturbance of the soil and to be able to measure close to the soil surface. Reducing the probe size increases the accuracy of TDR in measuring the small measured volume of soil (Nissen et al., 1998; Amato and Ritchie, 1995), though at the expense of soil depth.

Accuracy in measurements, adopting the right calibration equation (within 1 or 2% of volumetric water content) (Roth et al., 1990), excellent spatial and temporal resolution are simple to obtain. Continuous soil water measurement through automation and multiplexing (Baker and Almaras, 1990) favor TDR. However, TDR equipments are expensive, having limited applicability in soils high in swelling clays and organic matter (Zegelin et al., 1992), and under highly saline condition due to signal attenuation (Roth et al., 1992). Moreover, some clays having high surface area and surface charges and high soil moisture content (Zegelin et al., 1992) weakens the TDR signal and limits usefulness of the method.

Frequency domain techniques, as mentioned above, are easy to assemble but cumbersome and not handy. They demand expertise of a type that is not always available. Hilhorst and Dirksen (1995) reported that ionic conductivity can be measured more easily and more accurately with the frequency domain (FD) sensor than with existing time domain sensors. TDR is suited mostly on the studies on stratification detection. Frequency domain reflectometry (FDR) has several advantages over TDR, viz. interpretation of data is direct; it has low power consumption and it is inexpensive. There is no need of an expensive cable tester; its probes can be buried for a long time, because they are designed to withstand harsh environmental conditions and its operation is simple.

All TDR and FDR require special calibration for high clay and organic matter content soils. The propagation of electromagnetic waves is also affected by electrical

conductivity and temperature. High clay content has a similar effect on calibration, but the magnitude is dependent on the clay type. The temperature dependence of the FDR sensor varies with water content, which can be easily corrected (Campbell Scientific, 1998). Since it is of low cost and easy-to-use, FDR techniques are promising for practical use. Because of these properties FDR is being applied on irrigation scheduling. Laboski et al. (2001) and Kukangu et al. (1999) successfully used this technique for irrigation practices. However, the disadvantages of FDR are that accuracy and resolution decrease with decreasing water content, stratification detection is average. Probably for these reasons FDR has yet to find a wide acceptance.

Capacitance sensors are simple means of characterizing the soil dielectric constant. Their design depends on their applications. In particular, the electrode geometry has a critical influence on the extension of the probed region. Moreover, the soil may not always be viewed as a medium of statistically uniform dielectric constant (De Rosny et al., 2001). Mead et al. (1998) showed that the device is also affected by the temperature. For the CP electrodes, the surface area of electrodes is well known but the degree to which the electric force line permeates the soil is uncertain. Thus, it seems that any term equivalent to d (Eq. (3.24)) is not well defined in this soil-access tube since soil, with all its variability in bulk density and water content, becomes the dielectric in the capacitive system. The shape of the field may also be influenced by soil heterogeneity and gaps between the soil and tube wall are induced by tube installation (Bell et al., 1987).

The capacitance probe offers a simple device for monitoring soil moisture automatically. However, its sphere of influence is rather small (a few cubic centimeters only). The results of (Chanzy et al., 1998) showed that the calibrations differ significantly from one probe to another. On the other hand, Evett and Steiner (1995) found poor results with CP gauges and attributed these results to non-uniformity of the soils studied and considerable small measurement volume. They concluded that the CP gauge has limited precision and is unacceptable for routine soil water content measurements.

Tomer and Anderson (1995) compared the results of soil water contents with CP and neutron probe (NP) and data obtained by TDR. They found that the CP gave greater soil water estimates than the NP when the data grouped according to depth. CP measurements were greater than NP measurements at shallow depths. They concluded that CP has several advantages in soil water measurement. Measurement time of the CP is less than for the NP, hazards and expenses incurred with radiation are eliminated, and has good depth resolution. On the other hand, CP has several disadvantages that are related to the small soil volume and the nature of the dielectric response that is measured. Therefore, users of CP should investigate the effects of salts, bulk density, and texture. For dry and coarse textured soils changes in water content are difficult to detect with the CP (i.e. <10 to 12%).

More recently, GPR has also been employed to follow the wetting front movement (Vellidis et al., 1990). GPR is also a suitable method for monitoring moisture content changes in the vadose zone and permits relatively large measurement scales, appropriate for hydrological models of unsaturated processes (Binley et al., 2001). Huisman et al.

(2001) evaluated the GPR performance, TDR and the gravimetric soil water content measurements. The results showed that the calibration equations between GPR and aggregated gravimetrical soil water content were similar to those obtained for TDR, suggesting that available TDR calibrations can be used for GPR.

Conclusions

The restrictive use of neutron probe, the rapid advancement and the decreasing cost of the non-nuclear methods in recent years, brought about to compare these methodologies. This also defines decision-making process for assessing the characteristics of technology in relation to project objectives. Soil water measurements encounter particular problems related to the physics of the method used. Great effort has been devoted in the last decades to the development of new soil water-content sensors based on the capacitance technique or working with TDR or FDR.

Each soil water sensing method has strengths and weaknesses. A strength in one application may be a weakness in another. All of the methods have their own specific field of application. However, they complement each other in some aspects such as sensitivity at low water content. To select the right method, we must have a good understanding of how its qualities fit the requirements of the objective in question. Finally, we conclude whichever sensor we select, it demands rigorous calibration to find their site-specific behavior and plant compatibility.

CHAPTER 4

Microwave Remote Sensing Techniques in Soil Moisture Estimation

Introduction

Remote sensing studies relate to the detection, recording, and analysis of electromagnetic energy, reflected/scattered from the target. This chapter discusses the use of microwaves and its response to soil and the associated moisture content. Remote sensing of soil moisture depends on measurement of electromagnetic energy that has been reflected or emitted from soil surface, with or without the vegetation cover. The presence of moisture also influences effective skin depth. As the moisture content increases, the skin depth decreases and the signal may be scattered from lesser thickness of the soil.

Recent advances in remote sensing technology have demonstrated that soil moisture can be measured by a variety of remote sensing techniques (Jackson et al., 1982; Schmugge, 1983; Staford, 1988; Baker, 1990; Engman, 1991; Jackson, 1993; Engman and Chauhan, 1995; Njoku and O'Neill, 1982). However, only microwave remote sensing technology is credited with the ability to quantitatively measure soil moisture under a variety of topographic and vegetative cover conditions. Thus, potentially it could be extended for routine measurements from a satellite system. A number of experiments using sensors mounted in truck, aircraft and spacecraft have shown that moisture within a thin layer of soil, of the order of 5 to 10 cm can be accurately measured for bare and thinly vegetated soil (Poe, 1971; Theis et al., 1984; Bruckler et al., 1988; Engman, 1991; Ferrazzoli et al., 1992; Mohan et al., 1993; Benallegue et al., 1994).

Detection and recording of electromagnetic energy are made possible because of the series of energy-matter-environment interactions, combining to produce contrast between a target and its background. This is identified by a remote sensing system. Energy is conveyed by means of electromagnetic waves. The energy of these radiations is expressed in units of Quanta ($h\nu$), where h is the Planck's constant and ν the frequency, is the unit of minimum energy known as photon. The underlying principle, on which the whole remote sensing technique is developed, is that all objects on the surface of the earth have their characteristic spectral signatures. Identification of these spectral signatures is the key to the remote sensing techniques. The amount of

energy reflected or emitted from objects varies with frequency (wavelength) throughout the electromagnetic spectrum. The signature of the imaged object is basically governed by the different amount of energy incident upon and reflected from the object, along with the wavelength sensitivity of the sensor at the time of imaging. It is also required for interpretation of all remotely sensed data whether the interpretation is carried out visually or using digital techniques. Further, it helps in specifying requirements for any remote sensing mission, e.g. which optimal wavelength bands to be used or which type of sensor will be best suited for a particular task. While analysing data it may be noted that it may not necessarily be unique or absolute in the real sense. What is more often seen to be of importance is the spectral response pattern.

A unique signature of an object can often be identified if this energy is subdivided into carefully chosen wavelength bands. While systems with broad band response may tend to diminish object-to-background differentiation, selective recording of energy within particular wavelength bands may improve the discrimination of objects and hence the image quality. It is these concepts which form the basis of multiband multispectral remote sensing. Remote sensors, including the human eye and conventional cameras, detect objects because of the way in which electromagnetic radiation in various wavelengths interacts.

Radiant Energy and Flux

For understanding both active and passive remote sensing methods and the inherent problems involved in the optimization of such techniques, a study of radiant energy is necessary. Radiant energy causes a sensor-detecting element to exhibit a physical change, which indicates the evidence of the object in question.

In the context of remote sensing radiation flux is described as the time rate of flow of the quantized energy delivered to a detector. This is called the *photon flux.* The rate of change of visible radiant energy is termed as *luminous flux.* When the radiant flux φ_{rf} is constant, the total radiant energy Q, which passes during time t, is given by

$$Q = \varphi_{rf} t \tag{4.1}$$

Energy delivered to a sensor system by radiant flux causes the detector to operate an image of the scene from which the flux is emanated. However, there is a certain minimum energy threshold for the detector to sense any radiant flux from a given object. Variation in intensity of radiation depends on dielectric properties and/or temperature. Radiant flux is often expressed in the units of watts or joule/sec.

Basis of Microwave Remote Sensing

The term microwave remote sensing encompasses the physics of radiowave propagation and its interaction with material media under investigation. In the recent past, this has resulted into an important tool for monitoring the atmosphere and observation of the earth. It also includes surface and volume scattering emission techniques used for designing microwave sensors and processing of measured data into information about temporal and/of spatial variations of atmospheric, surface and medium characteristics.

A unique advantage of microwave remote sensing at long wavelengths is that

vegetation has an attenuating effect on the background emission unlike the masking effect observed at shorter wavelengths. The primary determinants of this attenuation are the water content of the vegetation and the structure of the canopy. At microwave frequencies, the single scattering albedo term is negligibly small. When this term is set equal to zero and it is assumed that the physical temperature of the vegetation and the soil background are nearly the same, we get

$$e = (TB_c/T_v) = 1 - (1 - e_{sur})\Gamma_t^2 \tag{4.2}$$

where Γ_t is the transmissivity of the vegetation layer, T_v the physical temperature of vegetation, TB_c the Canopy brightness temperature and e_{sur} the emissivity of soil surface. This step in the process requires a measurement of the physical temperature of the vegetation or soil, or both, which can be obtained using thermal infrared satellite instruments. Variation of temperature by 10° introduces a deviation in the soil moisture of less than 3% by volume.

Development of microwave remote sensing technique has made remote estimation of soil moisture over large areas possible over a desired period of time. However, the gap still remains to be filled for improving the accuracy of these estimates for a wide range of natural and agricultural surfaces. Remote sensing systems are ideally suited to the problem of mapping soil moisture over large areas for two reasons. First, by mounting the sensor on an airborne platform, the necessary data can be collected over comparatively large areas in a predetermined manner. Second, the sensor system can be designed to provide spatial resolution such that field specific information can be gathered and distributed to individual farmers. Microwave sensors are useful because the magnitude of the microwave emission from a soil surface is related to the near surface moisture content. Although the depth of measurement of these sensors is generally only a few centimeters, extrapolation of root zone moisture content is possible in some cases. Knowing the strength of the microwave emission, the soil texture and the land surface conditions can be evaluated from microwave data. The basis of all such measurements is the fact that there is a large contrast between the dielectric properties of liquid water and dry soil. Increase in value of the dielectric constant of the soil due to an increase in soil moisture is monitored by microwave sensors. A number of experiments using ground aircaft and space-based sensors operating in the microwave frequency region of electromagnetic spectrum have shown that a surface layer of soil, of the order of 5 cm thickness, can be accurately measured under different atmospheric and vegetation conditions.

Both active and passive sensing systems operate in the microwave portion of electromagnetic spectrum ranging from 1 mm to 1 m. The four advantages of microwave remote sensing over other spectral regions are: (1) atmosphere is effectively transparent, can be penetrated through the clouds, providing all weather clearance in the decimeter range of wavelengths; (2) vegetation can be treated as semi-transparent, allowing the observation of underlying surfaces; (3) microwave measurements are independent of the dielectric properties of the target, which for soil are a function of the amount of water present; and (4) measurement is also independent of solar illumination, permitting continuing day or night observations. However, it also has several disadvantages;

large mass of the source, power and volume requirement and provides low spatial resolution.

The dielectric properties of a medium determine the propagation characteristics for electromagnetic waves in the medium. As a result they affect the emissive and reflective properties at the surface. These two parameters for a soil depend on its moisture content and can be measured in the microwave region of the spectrum by radiometric (passive) and radar (active) techniques (Schmugge et al., 1986; Mohan et al., 1992; Das, 1995; Das et al., 1989, 1994 a, b). The preferential use of microwaves at L-band (21 cm) for the remote sensing techniques is:

(a) maximizes the sensitivity of the observation to the soil moisture
(b) minimizes the effects of vegetation
(c) minimizes the need for additional data for interpretation
(d) maximizes the depth of soil contributing to the measurement
(e) is longest wavelength radio astronomy band with minimal radio frequency interference.

Passive Microwave Remote Sensing

Passive microwave radiometers measure the radiation intensity in accordance with the Planck's law of radiation. It is directly proportional to the physical temperature T, and the emissivity e of the target. Emissivity is a property of the target and varies between zero and unity representing the portion of the blackbody radiation that penetrates the target and is emitted back (Fig. 4.1).

Only a perfect blackbody emits all incoming radiations; therefore the emissivity will in principle be less than one and hence the measured brightness temperature T_B will be less than the physical temperature. A microwave radiometer in space will view a mixture of the atmosphere $T_{B_{atm}}$, the earth's surface TB and reflected cosmic TB_c and sky radiation $T_{B_{sky}}$

$$TB = \tau_{atm} \, (T_{B_{sky}} + TB_c) + T_{B_{atm}} \tag{4.3}$$

where parameter τ_{atm} is the transmissivity of the atmosphere (Fig. 4.2 (a)).

Figure 4.2(b) represents the radiations emitted from the surface reaching the antenna.

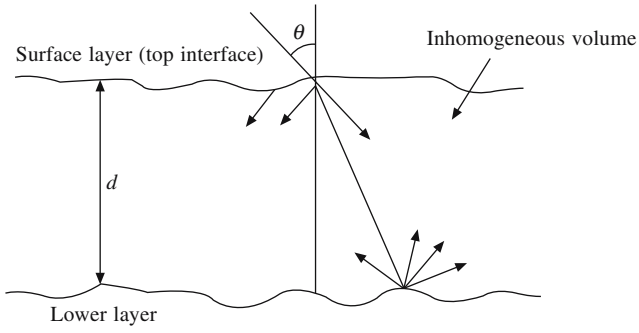

Fig. 4.1 Backscattering concept in a two layer model of the earth surface.

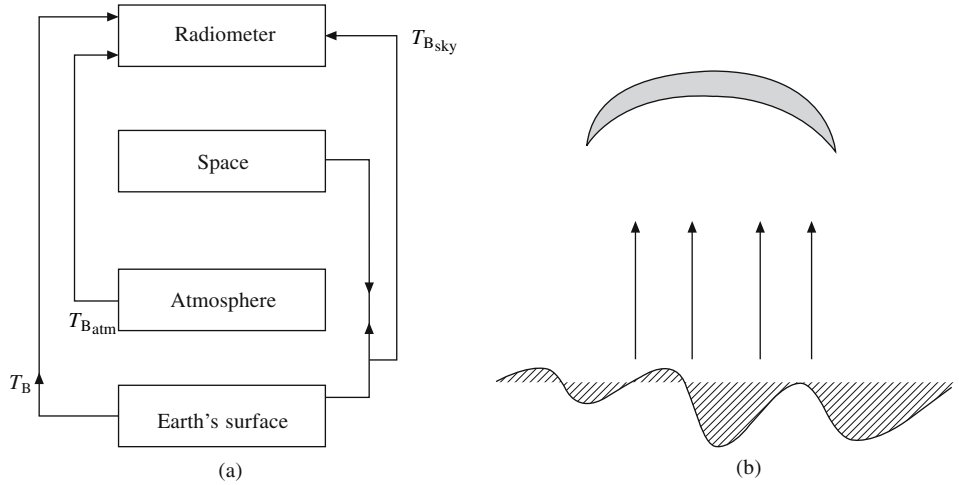

Fig. 4.2 (a) Radiation transfer from various surfaces before reaching the radiometer and (b) radiation emission from the earth.

Passive microwave sensors operating at low frequencies are sensitive to surface soil moisture changes. At microwave wavelengths in the L-band (21 cm wavelength, 1.4 GHz) the transmissivity of the atmosphere is essentially unity, even in the presence of clouds. Sky brightness at the L-band is approximately 5 K and constant for most atmospheric conditions. This rather small value is further reduced by a reflection term that will range from 0 to 0.4 for most land surface conditions. The atmospheric contribution to brightness temperature will also be nearing zero at these wavelengths. The net outcome of these specifications is that the radiometer measured brightness temperature at longer wavelengths is essentially a measurement of the surface brightness temperature, except under extreme atmospheric conditions such as rainfall. This greatly simplifies the interpretation of the data because unlike observations in the visible and infrared, it does not require correction for atmospheric effects.

Passive remote sensing at the long wavelength end of the microwave spectrum has an added advantage of responding to the parameters of the ocean. In addition to soil moisture, sea surface salinity measurements can also be made using airborne radiometers.

Microwave Radiometers

A radiometer is a sensor that is capable of measuring the intensity of a received signal within a specified field of view. Radiometers can be designed to operate at different wavelength intervals, including portions of the infrared and ultraviolet spectra. Radar systems measure the distance to a target by measuring the delay between a transmitted signal and its return to the antenna. Since the speed of the EM waves is known, the distance between the object and the source can be obtained by knowing the time taken to travel.

Microwave energy travels in a straight line from the aircraft to the ground, i.e. a path that defines the shortest distance from the aircraft to a specific point A on the ground (Fig. 4.3). It is apparent that object B is close to the aircraft, than its base B′.

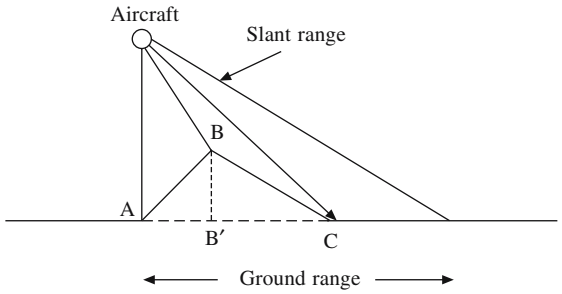

Fig. 4.3 Ground and slant range radar layover.

As a result, echo from the top of the object B reaches the antenna before the echo from the base B′.

It will be closer, if only the short range distance is considered. However, in the ground range domain both, i.e. object B and the base B′ occupy the same geographic position. In the slant range domain they occupy different image positions (Campbell, 2003).

A microwave radiometer consists of a sensitive receiving instrument typically in the form of a horn-or dish-shaped antenna that observes a path directly beneath the satellite. The signal gathered by the antenna is electronically filtered and then displayed. Microwave radiometer have a reference signal from an object of known temperature. The received signal is compared with the reference signal for deriving radiance of the target. Microwave radiometers are designed to receive and record radiations in the range of 0.1 mm to 3.0 cm.

There has been much interest regarding the depth to which the soil moisture can be directly measured using microwave remote sensors (Jackson et al., 1998). Each and every point within a soil emit thermal radiation, and in the microwave region the intensity of this radiation is directly proportional to the thermodynamic temperature. The power P (in watts) received by the radiometer from a target is given by

$$P = kT\Delta f \tag{4.4}$$

where k is the Boltzman's constant, Δf the bandwidth (Hz) and T the apparent source temperature.

The natural thermal microwave emission measured by a microwave radiometer consists of energy arriving at the antenna from any given soil depth and is dependent upon the soil moisture and temperature profile. It then becomes difficult to identify the soil moisture value to which the microwave radiometer value actually corresponds. The observed microwave brightness temperature is the product of the effective emissivity e and the effective temperature $T_B = eT$. Choudhury et al. (1982) divided effective temperative T in terms of surface temperature T_0 and deep soil temperature (T_∞) as $T = T_\infty + C(T_0 - T_\infty)$. These authors used a coherent radiative transfer model and using data base for observed soil moisture and temperature profile obtained C values: 2.8 cm (0.802 ± 0.006) and 21.0 cm (0.246 ± 0.09). The effective emissivity parameter is preferred to brightness temperature for obtaining soil moisture information (Rouse Jr., 1983).

Microwave radiometry can be used to estimate surface soil moisture incorporating correction from vegetation. The nature of this correction term generally involves an evaluation or parameterization of the vegetation canopy's attenuation or transemissivity and single scattering (Burke and Schmugge, 1982; Brunfeldt and Ulaby, 1984). Empirical approaches have been made to determine the functional dependence of the vegetation parameters on microwave wavelength (canopy type and structure) and plant water content using experimental field data. This experimental approach received some success. In principle, it is important not only to characterize the state of the vegetative cover at any given instant but also its evolution. Hence, it is necessary to consider the periodicity of measurements. This depends upon the rate of the vegetative growth. The interval between the two measurements is chosen in such a manner that the growth pattern be considered continuous. Depending upon climatic conditions and the crop phonological stage, the time interval is chosen to vary between 3 and 15 days for annual crops. Since the equation of plant data is time consuming and often unreliable, it may be more effective to stagger individual measurements as a function of time and to interpolate these so that they correspond to the acquisition schedule for remote sensing data. For a better analysis of the population under study the sampling intensity be large. Procedures are adopted for determining the sampling density required to achieve a specified accuracy of estimating a given parameter.

In addition to the above mentioned microwave sensors, other microwave instruments can also be loaded, e.g. thermal infrared radiometer. This produces an estimate of the surface temperature by measuring thermal emission in the 8-14 μm wavelength range. A visible-near infrared radiometer can also be used to measure surface reflectance. Data collection can be done either manually or can also be computer controlled. The former is used in circumstances where the beam is moved from one target to another or the effect of specific changes are to be observed. In the second mode, the system can be used to make observations at specific intervals for desired periods. Due to low data rates, high temporal frequency of observation is possible.

For the purpose of calibration of the radiometers two external reference targets are generally chosen. The targets typically used are sky (~5 K) and absorber (~300 K). These are quite stable references and cover the entire range of instrument response. Water has well known T_B values as functions of temperature and angle. By varying the angle, reference T_B values between 50 and 110 K can be obtained. However, water calibration needs to be done at a location distant from the test site.

Microwave emissivity contains information on the physical conditions of the surface and depends on several parameters, e.g. frequency, observation angle, and polarization. Due to the Brewster angle effect, vertically polarized emission from bare soil at observation angles higher than about 30° is appreciably larger than horizontally polarized emission. The strength of this effect depends on soil moisture and surface roughness, but for a given soil, it is attenuated by vegetation growth. In the lower range of the microwave band, where the radiation is contributed by subsurface layers too, the emission from natural terrain is mainly controlled by soil water content. In the high frequency range the role of vegetation becomes important. Input parameters for computing radiometric properties of soil water system are presented in Table 4.1.

Table 4.1 Input parameters for computing radiometric properties of the soil-water system (Liou and England, 1996)

ρ_s (soil density)	= 2658.9 kg/m^3
ρ_b (bulk density)	= 1382.6 kg/m^3
ε_s (dielectric constant for soil solids)	= $(1.01 + 0.00044\rho_s)^2 - 0.062$
ε_{bw} (dielectric constant of bound water)	= $31 + j\ 15$
d (thickness of bound water layer)	= 3 Å
A (soil specific surface)	= 84000 m^2/kg
α (shape factor)	= 0.65

Raju et al. (1993) used ground based radiometers at frequencies 1.40, 5.05 and 10.65 GHz and data so obtained were simulated by Wilheit model. These authors observed that soil microwave emission was strongly affected by the diurnal variation of soil moisture and temperature profiles. Dobson et al. (1984) have also reported soil texture effects on microwave emission.

The drawback of microwave radiometry has been one of resolution Δx and is given as

$$\Delta x = \frac{k_A \lambda H}{D_A} \tag{4.5}$$

where k_A is the antenna constant (~1.5), λ the wavelength (m), H the altitude (m) and D_A the antenna aperture size (m). Assuming $\lambda = 21$ m and $D_A = 1$ m in Eq. (4.5), we get

$$\Delta x = 0.3H$$

This when applied to truck and aircraft altitudes, provides a poor resolution (Jackson and Schmugge, 1989).

There are alternative methods for obtaining soil moisture from satellite imaging radiometers. Moisture increases the apparent thermal inertia of soil by increasing its thermal conductivity, density and specific heat, and by day time cooling through evapotranspiration. As night time warming content of soil increases, its day-night difference in temperature tends to decrease, and corresponding difference in radiometric brightness also decreases.

The thermal microwave day-night signature will exceed the equivalent thermal infrared signature because soil moisture reduces microwave emissivity, but slightly increases thermal infrared emissivity. While thermal infrared techniques may easily achieve higher spatial resolution, the reduced susceptibility to cloudiness may favor a radiobrightness technique for time varying parameters like soil moisture. Vegetation has the masking effect on the thermal infrared and to a lesser extent on the microwave signatures. The depth of penetration is indicated by the thermal pulse, while the radiometric sensitivity comes from consequent thermal and dielectric changes in the top soil.

A number of microwave radiometric studies in remote sensing has proved this to be a realistic approach for assessing several environmental parameters, particularly

those related to water. Some investigations aimed at evaluating land application capabilities pointed out that even low resolution data can be useful in monitoring gobal changes of surface soil moisture and vegetation cover.

Active Microwave Remote Sensing

Principle

In this method electromagnetic radiations are supplied in the form of radar energy. An elementary consideration shows that a minimum requirement for such a setup would consist of a transmitter, a receiver, an antenna array, and a recorder. Pulses of microwave energy are emitted from an antenna and reflected or scattered at the ground surface. The ranging capability is achieved by measuring the time delay between the time a signal is transmitted toward the terrain and the time its echo is received. Through its ranging capability, an active sensor can measure the distance between antenna and ground. Portion of the energy returned to the antenna is called the *radar return*. This is an important component of the energy and it is this signal, which is used in understanding and interpreting ground properties (Dobson and Ulaby, 1986). Radar return from a ground target depends on its roughness in terms of radar wavelength and is affected by system parameters and terrain properties. Another distinguishing feature of an active sensor is that one can detect frequency and polarization shifts. The system parameters are frequency, depression angle, polarization, look angle and noise. These determine whether incident energy is in the specular or diffusive mode. The commonly used radar wavelength is 8 mm or 3 cm although total radar wave band is 3 mm to 3 m. The terrain parameters are surface geometry, surface roughness and dielectric properties. The slope and aspect of the surface in relation to the sensor has profound effect on returned signal e.g. the relief and shadow effect on SLAR imagery. The complex delectric constant of the surface also plays an important role. The backscattering coefficient from a target (e.g. soil surface) is measured using a scatterometer or space borne sensor and is in turn related to moisture content of soil.

Scatterometers

A scatterometer is essentially a calibrated radar which provides an estimate of backscattering coefficient (σ^0) of extensive targets by comparing it with the power backscattered by the target of known radar cross section. There are two ways of calibrating the radar: (1) internal and (2) external. The former permits the determination of relative scattering coefficient, whereas the latter demands its absolute determination. The scatterometer has its two fold applications: (a) long range and (b) short range. Long range use aircraft/spacecraft while the short range utilizes helicopter or any ground platform. However, some common features pertaining to the two are: (i) large dynamic range, (ii) problem of polarization mixing and (iii) have similar components usage.

The dynamic range required by scatterometers is in the range of 60 dB. This is largely because there is a combination of three kinds of variation in the level of the

backscattered power: (i) variations in the surface dielectric constant ε, (ii) angular variation in σ^0 and (iii) an increase in range with increasing incidence angle θ.

The antenna used in scatterometer system is intended to transmit a signal of a specified polarization and to receive either the same or a different polarization. However, in practice there is always a mix up of various polarizations at the transmitting or at the receiving end or both. From antenna theory it emerges that the polarization purity depends on beam position. The purest polarization is at the center of the beam, while the response to undesired polarization increases towards the edge of the beam.

S- and L-Band Microwave Radiometer (SLMR) System

Some imaging radar systems are side looking. i.e. they scan to one side of the aircraft's flight line. Such systems are generally called side looking airborne radar (SLAR) system. SLAR is used to produce better quality images at resolutions in the 10-20 m range. SLAR forms an image of a strip of land parallel to it and at some distance from, the ground track of the aircraft. This has an all weather capability. SLAR are normally divided into two groups: (i) the real aperture systems that depend on the beam width determined by the actual antenna and is known as real aperture SLAR, and (ii) the synthetic aperture radar (SAR). These systems work by directing a pulsed radar beam at right angle to the direction of the flight of the aircraft. The returning signals reflected by the object on the ground are detected by the receiver aerial and converted to a light signal, which is used to expose a film. The picture taken by SLAR is obtained by scanning the terrain. These systems offer day/night as well as all weather capability to penetrate a cover of vegetation. A schematic view is shown in Fig. 4.4.

To understand its function, let us consider a platform carrying the radar system and move along the linear trajectory (azimuth direction). We investigate now the capability of the system to resolve target in the azimuth direction. Two targets at a given range can be resolved only if they are not within the radar beam at the same time. Accordingly, the azimuth resolution Δx is related to the antenna bandwidth λ/L through the relation

$$\Delta x = r\frac{\lambda}{L} \tag{4.6}$$

where r is the slant range, and L is the (effective) antenna dimensions along the azimuth direction (i.e. the x-direction, Fig. 4.5). For a uniform antenna illumination, L is the same as the physical length.

Equation (4.6) represents the resolution limit of a conventional side-looking real aperture radar (SLAR). To improve the azimuth resolution (in km), it is required to reduce λ, the wavelength of the carrier frequency or to increase L (the antenna dimension) (Mahafza, 1998).

In a typical set-up each linearly polarized microstrip patch antenna is configured as 4×4 phased array having 20° of beam width with a main beam efficiency of 97% and kept in a plate of horizontal polarization. The antenna directs the microwave

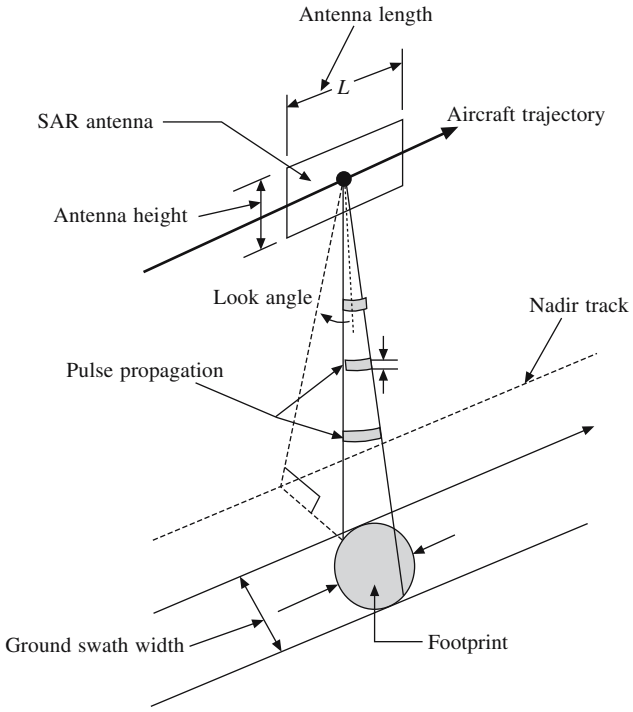

Fig. 4.4 View of a side looking real aperture radar.

energy into a narrow fan-shaped beam. This then defines the narrow path or line across the terrain strip, which is normal to the flight track. The antenna is fed with a pulse of microwave energy, which propagates at a speed of light within the beam and illuminates points along the line. The time delay between the transmitted and received signal gives the distance between the target and the radar ($c\tau/2$), where τ is the time delay and c is the velocity of electromagnetic waves. The antenna and receiver are

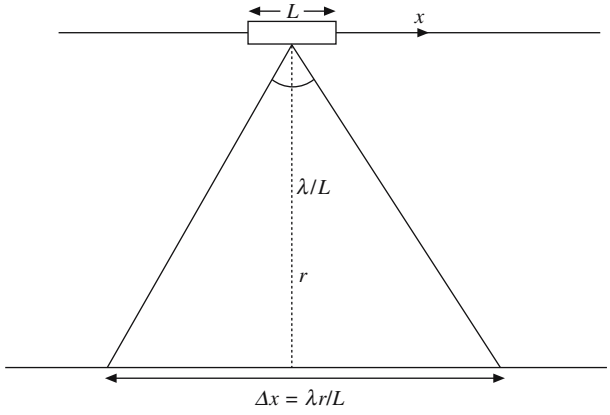

Fig. 4.5 Real aperture radar azimuth resolution.

packed together in a temperature controlled enclosure. Using system software it is possible to monitor the thermal status of the radiometers.

A computer controlled system is loaded on a truck permitting deployment of sensor packages to a height of approximately 10 m above ground with the help of a hydraulic boom. The instrument platform at the end of the boom can be moved at varying angle of incidence from 0° (nadir) to 180° (sky). The azimuthal rotation of the boom is 360°. At the nominal operating height of 5 m with specified field of view of radiometers (20°), the footprint size is chosen as 1.5 m at a viewing angle of 10° of nadir.

The total SLMR system is usually mounted on a hydraulic boom truck. The centers of the S- and L-band radiometers are offset by approximately 1 m in the installation and therefore, the centers of the ground footprints will also be offset. The beams do overlap, but there is the potential for some variation in target properties in the area contributing to the two individual measurements. Target location for the microwave radiometers is often achieved with a color video camera installed on the platform between the two antennas. The look angle of the instrument platform is determined by an inclinometer system (Jackson et al., 1998).

Theoretical Basis

As mentioned above the microwave radiations transmitted by a radar system interact with the ground objects and the reflected or backscattered waves are sensed and stored for further interpretation. The amount of energy arriving at the antenna from any given soil depth is dependent upon the soil moisture and temperature profile and is used for the purpose of calculating backscattered coefficient σ^0.

The power received P_r by the sensor can be expressed by the well known radar equation (Sholink, 1970, Hati, 1996)

$$P_r = K\, \sigma^0\, A$$

$$K = \frac{p_t G_t G_r \lambda^2}{R_t^4 (\pi 4)^3} \tag{4.7}$$

where P_t is the power transmitted by the sensor, G_t the gain of transmission antenna, G_r the gain of receiving antenna, R_t the distance between radar and target (range), λ the wave length of the radar signal, A the effective receiving area of the antenna aperture, and σ^0 the backscattering coefficient, in general, is a function of system parameters like polarization, look angle, frequency and a number of target parameters such as surface roughness, slope, vegetation cover and volume scatter.

The measured value of remote sensing parameter is σ^0. In general, for a terrain, the scattering coefficient, σ^0 depends on the dielectric properties and surface roughness. As σ^0 usually exhibits a wide dynamic range with variation of targets on earth, it is usually expressed in decibel (dB) unit.

If an unknown constant K_t represents the total loss to the system connected to the system connected to the receiver, the output voltage V_r can be represented as

$$V_r = K_t \left[\frac{P_t G_t G_r \lambda^2 \sigma^0 A}{(4\pi)^3 R_t^4} \right]^{1/2} \tag{4.8}$$

The internal calibration of the system is performed by recording the signal through a coaxial delay line of loss L which is connected between transmitter and receiver power line. The voltage received is given by

$$V_{int} = K_t (P_t L)^{1/2} \tag{4.9}$$

Now, the ratio of two voltages is

$$N_1 = \frac{V_r}{V_{int}} = \left[\frac{G_t G_r \lambda^2 \sigma^0 A}{(4\pi)^3 R_t^4 L} \right]^{1/2} \tag{4.10}$$

Any variation in P_t and K_t is removed by this procedure. The external calibration is performed by taking the ratio of output voltage from a target of known cross-section to that of internal delay line. The ratio of two voltages is

$$N_2 = \left[\frac{G_t G_r \lambda^2 \sigma_c^0}{(4\pi)^3 R_c^4 L} \right]^{1/2} \tag{4.11}$$

where σ_c^0 and R_c represent radar cross-section of the calibration target and range of calibration target, respectively. Combining Eqs. (4.10) and (4.11) (N_2/N_1), the following expression of σ^0 (dB) is obtained:

$$\sigma^0(\text{dB}) = -10 \log \sigma^0 + \log \sigma_c^0 - 10 \log A + 40 \log R_t - 40 \log R_c \tag{4.12}$$

Values of N_1 and N_2 are measured by the system while that of A is determined by known beam width.

For bare soil the backscattering coefficient σ^0 is related to soil moisture by the expression (Ulaby et al., 1974)

$$\sigma^0 = A \exp(BM) \tag{4.13}$$

where A and B are constants and M is the soil moisture content. Eq. (4.13) can be rewritten as

$$\sigma^0(\text{dB}) = 10 \log \sigma^0 = 10 \log A + 4.34\, BM = A_1 + SM \tag{4.14}$$

where $A_1 = 10 \log A$ and $S = 4.34\, B$.

The radar sensitivity to soil moisture S is given as

$$S = \frac{\delta \sigma^0}{\delta M} \tag{4.15}$$

The radar response to soil moisture is determined using linear regression analysis in accordance with the above equations.

Description of Scatterometer

The scatterometer operates in 2-8 GHz frequency bands and the system configured as a FM-CW unit to facilitate frequency averaging for getting more independent samples. Two independent dual polarised parabolic reflectors are generally used to transmit/receive signals so that any polarization combinations viz., VV, VH, HV, HH can be selected. The system is housed in a mobile truck having an extendable book to provide a clear height of 20 m above ground. The transmit/receive antennas are mounted on the end of the boom and the look angles can be varied from 0 to 90° in varying steps of 10° each. The technical specifications of a typical scatterometer are given in Table 4.2.

Table 4.2 Technical specifications of a typical scatterometer

Frequency	2-8 GHz
Type	FM-CW
FM Sweep	800 MHz
IF	50 KHz
Polarization	VV, VH, HV, HH
Incident angle	20-50°
Height	20 m
Antenna type	Dual polarized parabolic reflector
Antenna dimension	60 cm
Sensitivity	–97 dB
Dynamic range	50 dB
Calibration	Internal: Using delay lines External: Using corner reflector

Experiments to measure the backscattering coefficient of soil surfaces can be performed indoors using a 60 GHz scatterometer (Fig. 4.6). The characteristics are mentioned in Table 4.3 (Yamasaki et al., 1992). This is a network analyzer based system in which an intermediate frequency signal (2-3 GHz) is mixed with 55 GHz signal to produce frequencies in the range of 57-58 GHz. In a dual polarized two antenna system the transmitting polarization is either horizontal or vertical. Experimental set-up consists of a target soil sample contained over a octagonal styrofoam box, fixed over a turn table. A 2 cm soil sample depth is sufficient because of high attenuation corresponding to this frequency. With this the height and the angle of scatterometer with respect to soil sample can be altered. The time variation of the return power can thus be measured with the network analyzer. The distance between the center of rotation and the center of the illuminated area is maintained around 30 cm. The roughness of the soil surface is measured with a laser profile meter. The scattering coefficients are found to be dependent on angle of incidence (Ulaby et al., 1979).

Applications of Scatterometric Studies

Radar images typically provide crisp, clear representations of topography and drainage. A number of experiments using sensors mounted on trucks, aircrafts and spacecrafts

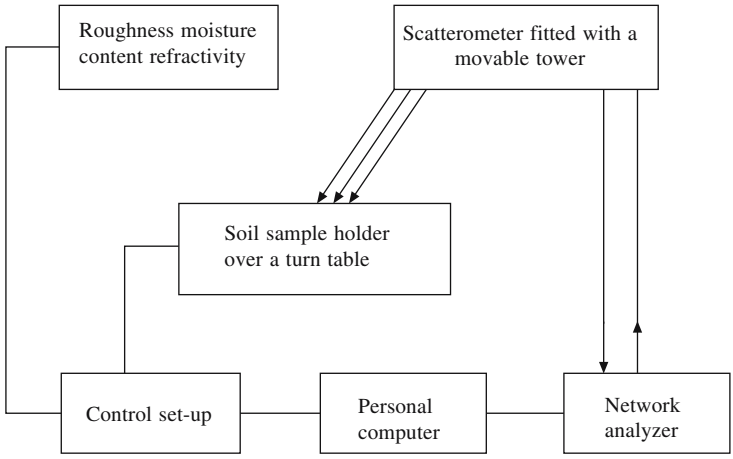

Fig. 4.6 Experimental set-up of a 60 GHz scatterometer.

have shown that the moisture within a thin layer of soil of the order of 5-10 cm can be accurately measured for bare soil and over vegetated surface. As soil moisture increases, the greater dielectric discontinuity between the soil and air causes higher radar backscattering coefficients. At higher moisture values, however, variations reduced due to spatial variability are much lower than at lower soil values.

Table 4.3 The 60 GHz scatterometer characteristics

Frequency	57-58 GHz
Type	Step frequency radar
Transmitter power	0 dBm
Antennas	Scalar lens horn antennas
Gain	31.5 dB
Beam width	4.6°
Polarization	HH, VV, HV, VH
Network analyzer	HP8753A
Minimum detectable power	–100 dBm
Range resolution	15 cm

Backscattering coefficient σ^0 has been determined using a scatterometer fitted on a cherry picker for alluvial sandy loam soil under bare conditions as well as in presence of crops (Das, 2001). The relationship between soil moisture content and backscattering coefficient is determined at 20 and 50° incidence angles and 2.6, 5.0 and 7.4 GHz frequencies at VV, HH, VH and HV polarizations. As anticipated the backscattering coefficient σ^0 is strongly dependent upon the change in soil moisture (0-10 cm depth), at 20° look angle (5.0 GHz and VV). The variation in soil moisture from 5 to 25% results in the increase of σ^0 by about 10 dB. However, at 50° look angle for similar change in soil moisture, the change in σ^0 is around 4 dB. It is inferred that irrespective of frequency and polarization, better significant relationship exists between σ^0 and soil moisture at 20° as compared to 50° look angle, i.e. the lower angle of incidence is suitable for sensing soil moisture.

With the increase in frequency from 2.6 to 7.4 GHz, the values of backscattering coefficient increases, but sensitivity and correlation are better at 2.6 and 5.0 GHz as compared to 7.4 GHz. The correlation between σ^0 and soil moisture (smooth soil cover) were significant for all polarizations at 20° look angle. However, backscattering coefficient σ^0, were found to be more sensitive at like polarizations (VV, HH) compared to cross polarizations (VH, HV) (Bandyopadhyay, 1995).

Crop Covered Soil

Soil having crop cover has been investigated by several methods owing to its agriculture implications (Das, 2001). In wheat, covered soil at 20° look angle (2.6 GHz, VV), σ^0 increased by about 7 dB with the increase in soil moisture from 5 to 30%. However, at 50° look angle, having same frequency and polarization and for similar magnitude of soil moisture variation, σ^0 increased by about 3.5 dB. The correlation between σ^0 and soil moisture at 20° and VV polarization is significant ($r^2 = 0.75$), whereas at 50° look angle the correlation is relatively lower ($r^2 = 0.61$). As in bare soil, σ^0 in wheat covered soil also increases with increase in frequency from 2.6 to 7.4 GHz. However, correlation and sensitivity decreases with increase in frequency, the 2.6 GHz being more sensitive to soil moisture under wheat crop. Like polarizations has better correlation with σ^0 than the cross polarization.

A preferred approach is to have single algorithm relating backscattering coefficient σ^0 with soil moisture for bare and vegetation covered soil. The combined data sets at 20° look angle for bare and wheat covered soil results in better relationship between σ^0 and soil moisture contents over that of wheat covered soil alone. The data also confirms that correlation between soil moisture and σ^0 values decreases with the increase in frequency from 2.6 to 7.4 GHz ($r^2 = 0.78$ to 0.67 at VV polarization). Similar conclusions were drawn for backscattered data available from mustard crop. The correlation between σ^0 and soil moisture contents at 20° look angle and VV polarization is higher ($r^2 = 0.72$) than that at 50° look angle ($r^2 = 0.69$). Here r^2 values also increase with frequency, but no definite trend due to like- or cross-polarization is seen. In case of combined data sets of bare and mustard covered soil, no marked improvement in the correlations between σ^0 and soil moisture is observed over the mustard covered soil alone (Mehta et al., 1995).

System Parameters Affecting Microwave Signature

Frequency

The influence of frequency on radar backscattering is governed by terrain properties, according to the known principles of microwave propagation. The scattering from rough surface is strongly dependent on the frequency. As is evident, a given surface will appear very rough at higher frequency (lower wavelength) compared to lower frequency. In addition, the penetration depth increases with wavelength in microwave region. A L-band signal will penetrate about ten times deeper than a Ku-band signal, thus, providing access to a much larger volume of layer near soil surface (Fung and Ulaby, 1983).

Incident Angle

In a terrain the radar backscattering coefficient is a function of the angle of incidence. The angular dependence of backscattering coefficient is caused due to the surface roughness. For smooth surface, scattering coefficient decreases very sharply with increase in incidence angle. For moderately rough surface, the backscattering return signal decreases. For a very rough surface it decreases slowly with increase in angle of incidence. At small angles radar return provides information about the surface slope distribution at a scale significantly larger than wavelength. At larger angles, the return signal provides information about the small-scale surface structures (Elachi, 1988).

Backscattering coefficient can be described as consisting of two components: a specular part and a diffuse part. The specular part is important around the perpendicular viewing angles, whereas, diffuse component governs the behavior of σ^0 at larger incidence angles i.e. smaller depression or grazing angles. The importance of the latter increases for the rough surface, on the other hand the specular part dominates in the case of smooth surfaces. There is a 'cross-over' point for groups of surfaces with varying roughness (De Loor, 1993).

A series of ground band radar observations have indicated that in the range 10-20° incident angle in the (4-5 GHz) C-band, backscattering coefficient is sensitive to soil moisture (Bernard et al., 1982; Mohan et al., 1990, 1993). Air borne sensors have also confirmed that C-band radar operating at 10°-20° incident angle is sensitive to soil moisture (Bradley and Ulaby, 1981). Ulaby et al. (1979) found that the highest correlation between σ^0 and soil moisture with covering vegetation (corn, soyabeans, sorghum and wheat) is 0.92 at a frequency of 4.25 GHz, 10° incident angle and HH polarization. Ulaby et al. (1986) demonstrated that an optimized instrument for soil moisture estimation possess these characteristics. At such incidence angles the soil backscattered signal does not depend on soil roughness state, but only on soil moisture. But if the incidence angle is greater than 20°, the radar signal scattered from vegetated area can be divided into three components: (i) signal from soil surface volume, which is mainly dependent on the soil moisture content, (ii) signal from the soil surface which is driven by the ground roughness and (iii) signal from vegetation canopy overlying the soil. Presence of vegetation cover includes an additional attenuation to the soil backscattered signal (Quensey et al., 2000).

In case of forest canopy, with increasing incidence angle, surface scattering decreases and becomes less important compared to volume scattering which is the dominant scattering mechanism in dense forest (Moghadam et al., 1994). In nature both surface and volume scattering contributes to the radar backscatter.

Polarization

The amount of backscattering is a function of the polarization of the incident wave. The HH/VV and HV/VH return are different because of the difference between the physical processes involved for these two types of return signals. There are two major physical processes responsible for the like polarized return, these are quasi-specular surface reflection and surface or volume scattering. The cross polarized return is usually weaker than the like polarized return.

The mechanisms responsible for depolarization of microwave signal which produces cross polarized scatterometer return are: (i) quasi-specular reflection as a result of differences between Fresnel coefficients (Fung, 1967) for a homogeneous, two dimensional smoothly undulating surface, (ii) multiple scattering as a result of target surface roughness (Fung and Eom, 1979), (iii) multiple volume scattering due to inhomogenities particularly those embedded within a skin depth, i.e. the depth of penetration of target surface (Leader, 1975) and (iv) anisotropic properties (both physical and geometrical) of the target (Tan and Fung, 1979).

Of the above four possible mechanisms first three are commonly encountered in remote sensing application. The first mechanism is applicable only to smoothly undulating surface, predicts essentially no cross polarized return near the vertical incidence angle and increasingly more return at higher incidence angles except near grazing incidence. However, the level of return remains low as compared with the levels predicted by the second and third mechanisms both of which are applicable to rough terrains with or without vegetation cover. These two mechanisms predict fairly uniform returns over all incidence angles, excepting near grazing incidence angle. In general third mechanism produces higher level returns than the second mechanism. The last of the mechanism can result from either the permittivity or the geometry of the surface (Tan and Fung, 1979).

Combination of System Parameters

An optimal microwave sensors configuration for soil moisture measurement has been suggested by Dobson and Ulaby (1981). It has been shown that for a radar working at 5 GHz, HH polarization at incidence angle between 7 and 17° the σ^0 has high correlation with soil volumetric water content.

Airborne sensors have confirmed that C-band radar operating at 10-20° incidence angle is sensitive to soil moisture (Bradley and Ulaby, 1981). The C-band ERS-1, SAR operating at 23° incidence angle has been reported to be sensitive to soil moisture (Demirrican et al., 1992; Mohan et al., 1993). Under vegetation cover, better soil moisture determination with L-band were reported by Schmullius and Furrer (1992).

Target Parameters Influencing Microwave Signatures

Effect of Roughness and Soil Texture

The ability of the active microwave sensors to measure near surface soil moisture of the order of 5 to 10 cm has been demonstrated through various ground based, airborne and space borne sensors (Ulaby et al., 1982; Mohan et al., 1990, 1992 and 1993). These authors made measurements over the range of roughness scale from smooth (r.m.s. height 1.1 cm) to very rough (r.m.s. height 4.1 cm). It was observed that use of lower frequencies can minimize the variation in scattering coefficient σ^0 related to surface roughness. Following Jackson and O'Neill (1985) it can be summarized as follows:

(a) σ^0 increases with increase of soil moisture, incidence angle θ and frequency.
(b) Maximum correlation between σ^0 and soil moisture occurs at frequencies near 4.5 GHz and incidence angle near 10°, with preference for like polarization.

Surfaces relatively smooth tend to reflect electromagnetic waves in accordance with Fresnel Reflection Coefficient (specular reflection). Therefore, strong backscatter is observed only in nadir direction in case of smooth surfaces. Rough surfaces tend to reradiate uniformly in all directions (diffuse scattering), thereby giving comparatively strong radar returns. For a smooth surface where the surface roughness is much shorter than wavelength, incident energy is reflected off specularly.

For a rough bare soil (Jackson and O'Neill, 1985):

(a) Roughness decreases the sensitivity of σ^0 to soil moisture.
(b) Roughness increases σ^0 ($\theta \sim$ 5-10°)
(c) At incidence angles in the range of 5-10° for a given roughness, all samples produced approximately the same σ^0 at the same soil moisture.
(d) The effect of roughness decreases with increase of soil moisture (4.5 GHz and a 10° incidence angle).

As the roughness scale approaches the same dimension as the wavelength, the scattered energy is dispersed and when the roughness scale exceeds the wavelength of the incident energy scattering is nearly uniform over the hemisphere (Fung, 1967). For minimising the effect of surface roughness on soil moisture determination, Ulaby and Batlivala (1976) suggested the specification of C-band radar, operating at 10-20° look angle.

Backscattering value from a surface increases with increase in dielectric constant of the surface. Since absorbed water has a much smaller permittivity than that of free water hence, microwave backscattering properties of a soil medium depend also on its texture (Ulaby et al., 1974). Bruckler et al. (1988) observed nonlinear relationship between scattering coefficient and volumetric moisture content and obtained significant correlation between them only when the microwave penetration depth in the soil is taken into consideration.

Active microwave remote sensing for the study of soil moisture, Yisok et al. (1992) reveals that vegetation cover and soil surface roughness, (random, periodic or monotonic) should be taken into account as these influence the radar backscattering coefficient σ^0. In theory, a periodic structure, such as the tillage row in an agricultural field, will influence σ^0 value. Fields with row direction perpendicular to the look or azimuth direction will scatter more energy back towards the scatterometer antenna than fields having parallel row direction (Michelson, 1994). In active microwave remote sensing soil texture variation is a source of error. Volumetric soil moisture m_v is more strongly related to σ^0 and then to m_f (Dobson et al., 1983).

Bradley and Ulaby (1981) arrived at the following equation at 1.6 GHz, HH, 15° for 0-5 cm soil moisture

$$\sigma^0 = -18.0 + 0.1 m_f \tag{4.16}$$

where m_f is the percentage of volumetric field capacity.

Effect of Vegetation

Many workers have considered a vegetation canopy as a lossy dielectric layer

characterized by a volume absorption coefficient k_α, bounded by a smooth soil surface on the bottom and by a canopy-air boundary at the top. Since the real part of the relative dielectric constant of a vegetation canopy is only slightly higher than unity, the power reflection coefficient at the canopy-air boundary is of the order of 0.01. Hence, the reflections at that boundary is considered negligible. If the vegetative matter in the canopy is assumed to cause isotropic scattering resulting in a scattering albedo α, where ($\alpha \leq 0.2$), the multiple scattering may be ignored.

The sensitivity of σ^0 to soil moisture is in general decreased by the presence of a vegetation cover. This is due to increased scattering and attenuation of the electromagnetic signal (Tansey and Millington, 2001). When a soil is covered by vegetation the backscattering power from soil suffers a two way attenuation due to its propagation through vegetation layer. It is believed that water and chlorophyl content of the vegetation is mainly responsible for scattering and absorption. The attenuation is in general, a function of the vegetation parameters such as plant height, density, water content and shape of the plant. In addition, the vegetation layer contributes a backscatter component of its own due to volume scattering (Demirican et al., 1992). The sensitivity also decreases with the increase of incidence angle and frequency.

Ulaby et al. (1979) have suggested a simple relationship between the effect of vegetation attenuation on the response of σ^0 to soil moisture variations:

$$\sigma^0 = \sigma_v^0 + \sigma_s^0 e^{-2\alpha} \tag{4.17}$$

where the first term on the right σ_v^0 is the backscatter by the vegetation and second term σ_s^0 is the backscatter by the underlying soil surface; α, in general, is a function of the vegetation parameters (e.g. plant height, water content and shape) and also the radar parameters (f, θ and p).

Experimental data for bare soil indicates (Ulaby et al., 1978) an approximately linear relationship between σ_s^0(dB) and m_x (linear correlation coefficient 0.86). Thus σ_s^0 takes the form

$$\sigma_s^0 = Ae^{Bm_x} \tag{4.18}$$

For vegetation covered case, inserting Eq. (4.18) into (4.17), gives

$$\sigma^0 = \sigma_v^0 + Ae^{(Bm_x - 2\alpha)} \tag{4.19}$$

and

$$\sigma^0\,(\text{dB}) = 10 \log (\sigma_v^0 + Ae^{(Bm_x - 2\alpha)}) \tag{4.20}$$

when $$S_B = \frac{\partial \sigma_s^0}{\partial m_x} \quad \text{and} \quad S_v = \frac{\partial \sigma_v^0}{\partial m_x}$$

S_v can be expressed in terms of S_B as

$$S_v = \frac{S_B}{\left(1 + \dfrac{\sigma_v^0}{\sigma_s^0 e^{-2\alpha}}\right)} \tag{4.21}$$

For $$\sigma_s^0 e^{-2\alpha} << \sigma_v^0, \quad S_v \simeq 0 \tag{4.22a}$$

and $$\sigma_s^0 e^{-2\alpha} >> \sigma_v^0, \quad S_v \simeq S_B \tag{4.22b}$$

Equation (4.22a) represents where vegetation completely masks the soil backscatter contribution while Eq. (4.22b) shows the backscatter is dominated by the soil contribution. These authors have concluded that by comparing S_v values at several frequencies and angles of incidence, radar parameters can be specified such that the dependence of σ^0 and m_x is minimally affected by vegetation cover.

Canopy Attenuation

Most attempts to measure the attenuation coefficient of vegetation canopies have concentrated on the following approaches: (a) measuring the power transmitted through the canopy as detected by a receiver placed beneath the canopy, or (b) measuring of the power reflected from a wide-beam standard target placed beneath the canopy. In both cases, the attenuation is computed by comparing the power measured to the power received by the receiving antenna. As is obvious from electromagnetic theory of wave propagation, transmission approach measures the one way total attenuation of the canopy, whereas the reflection approach measures the two way attenuation.

The major problems with these methods have been: (a) that near field effects resulting from the presence of the vegetation have an influence on the radiation patterns of the receiving antenna and the standard target, and (b) that the inhomogeneity of the vegetation canopy results in large fluctuations among the measurements made for the receiving antenna or the standard target. The measured estimates of attenuation are of limited significance because of the large standard deviations associated with them.

Several workers (Ulaby et al., 1982; van Wesenbuck and Kachanosky, 1988; Mohan et al.,1990, 1992; Engman and Chauhan, 1995) have used wavelength varying from 3 to 30 cm for studying soil moisture under a variety of crops. Wavelengths below 10 cm were found to cause decrease in sensitivity of soil moisture by about 10-20% for grain crops and over that would be expected for bare soil. With broad leaved crops, the sensitivity could be decreased by as much as 80% for wavelength shorter than 10 cm and 40% for 30 cm wavelength. Several investigators (Newton and Rouse, 1980; Schmugge, 1983; Ulaby et al., 1983) have pointed out that microwave emission is sensitive to variation of surface soil moisture and frequencies in the range 1-3 GHz are suitable to monitor soil moisture upto few centimeter depth even under cropped condition.

Working with C-band radar Mohan et al. (1993) have observed the measurements of soil moisture in the presence of wheat cover upto 0-5 cm depth. However, at deeper layer (0-10 cm) there was reduction in correlation value between backscattering coefficients and soil moisture. Jackson et al. (1982) developed a simple soil moisture retrieval model in which the measured biomass of vegetation cover was combined with 1.4 GHz radiometric measurements to obtain the predicted moisture of the underlying soil.

Schmullius and Furrer (1992) examined backscattering from soil under different agricultural crops at various frequencies using scatterometer in L-, C-, X- and Ku-band at cross and like polarizations. These authors have reported that backscattering is better related to soil moisture only at L-band frequency. Benallegue et al. (1994) utilized air borne scatterometer of dual frequencies (C-and X-band) and dual polarizations (HH and VV) for development of soil moisture retrieval algorithm from radar data and found that multiconfiguration radar improves the capacity of imaging radar for soil moisture mapping.

It is apparent that at high frequencies a vegetation may be dense enough and may completely prevent any interaction with the ground. Vegetation itself will contribute atleast part of the return signal. However, interaction with the canopy will also be influenced by the underlying soil moisture, due to the effect it has upon canopy water content (Schumann, 1994). Daughtery et al. (1991) reported that at view zenith angle of 10°, the majority of the returned signal originated at the soil surface with very little backscattering from the corn vegetation. However, soil roughness influences C-band backscatter at small view angles even in the presence of vegetation.

Vegetation Cover and Its Effect on Soil Moisture

When a vegetation layer is present over the soil surface, it attenuates radiation emitted by the soil and contributes thermal emission of its own. Experimental investigations reveal that the presence of vegetation reduces the sensitivity of the brightness temperature T_B to soil temperature, and the sensitivity reduction factor is approximately $Y = 1 - 1/L^2(\theta)$, where $L(\theta)$ is the canopy loss factor. The sensitivity reduction factor Y increases with increasing angle of incidence θ and with increasing microwave frequency (decreasing wavelength). Canopy loss factor can be separated into two parts: an absorption $L_a(\theta)$ and a scattering $L_s(\theta)$ part: $L(\theta) = L_a(\theta) \cdot L_s(\theta)$ (Ulaby et al., 1983).

Canopy losses due to absorption by leaves can be estimated using approximate dielectric mixing formula.

Fresnel Model

Fresnel model can be verified with the help of soil moisture data in different planes of polarization.

A profile of dielectric properties and temperature is found to be uniform. A direct linkage between the soil complex dielectric constant ε and the emissivity e is provided by fresnel reflection equations. For horizontal H polarization and look angle θ, it is written as

$$e(H, \theta) = 1 - (\cos\theta - (\varepsilon_s - \sin^2\theta)^{0.5}/\cos\theta + (\varepsilon_s - \sin^2\theta)^{0.5})^2 \qquad (4.23)$$

The depth from which energy is emitted and sensed by microwave instruments remains unsolved. There is still some ground to be covered relating to the sampling depth. In a realistic situation the depth contributing to the measurements may come from a distribution of depths. The dominant depth depends upon a variety of factors such as

soil type, general climate and system observation variability. To quantitate the above, following methods may be considered:

1. By adopting appropriate interpretation algorithm, operational techniques could be implemented using satellite data.
2. New and potentially more valuable data (i.e. evaporation and infiltration properties of soils) might be obtained using multi-temporal observational systems.

Based on these studies Jackson and O'Neill (1985) concluded that a 4.5 GHz, HH, 10^0 scatterometer system was optimal for estimating soil moisture expressed as a percentage of volumetric field capacity m_f, except for dry soil conditions under dense canopies.

Active and Passive Microwave Remote Sensing: Comparison and a Relation

The soil moisture content can be estimated both by scatterometric and radiometric data. An active microwave device uses energy from the sensors, while the passive sensors detect the energy emitted by the earth's surface (Fig. 4.7). Two quantities describing microwave scattering and emission from natural bodies are the backscattering coefficient σ^0 and the emissivity e, respectively. The backscattering coefficient which is measured for the active sensors, is proportional to the ratio of the intensities of received and transmitted powers. The emissivity of a canopy covered soil is approximated by the normalized temperature T_n (ratio between the brightness temperature measured by the microwave radiometer and the radiance surface temperature monitored with a thermal infrared radiometer). Actually, the latter is not only influenced by the surface temperature, but also by the infrared sensitivity. However, assuming that the infrared sensitivity of vegetation is relatively constant and close to one and that, for low height observations (i.e. from tower and low height aircraft), the effects of atmosphere can be disregarded, the radiance temperature of the observed canopy can be considered a good approximation of the thermometric temperature of the same canopy. Therefore we consider as the normalized temperature T_n as close to the microwave emissivity, although in general, the nonuniformity of temperature profiles affects infrared and microwave radiation in different ways. Both σ^0 and e are dependent on frequency, polarization, and observation angle and are functions of the features of the observed medium. Microwave scattering and emission is mostly influenced by soil parameters at the lower of nadir observation angles θ, especially for lower frequencies, while vegetation effects are dominant at higher observation angles.

The backscattering coefficient σ^0 (dB) of bare and vegetated fields measured at C band ($\theta = 10°$, horizontal H polarization), is found to be correlated to volumetric soil moisture m_v, by the linear relationship (Ferazzoli et al. 1992):

$$\sigma^0 = 0.22 m_v - 8.8 \text{ dB } (r^2 = 0.697) \tag{4.24}$$

The sensitivity obtained is in good agreement with the results of Ulaby et al. (1986). A low value of r^2 is attributed partly to the surface roughness and partly to the

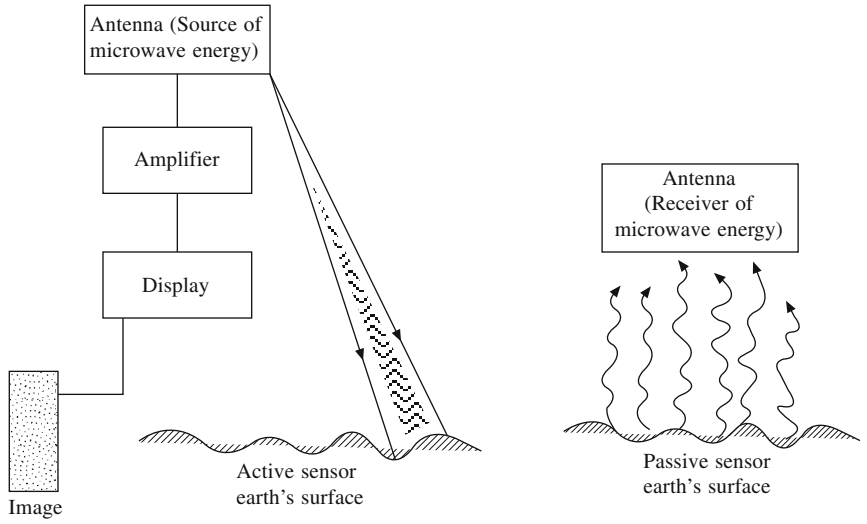

Fig. 4.7

crop covers. At L-band the backscattering has better correlation ($r^2 = 0.84$) to soil moisture content (SMC). A direct comparison of the performane of active and passive L-band sensors in the estimation of SMC can be made. The relation between the radar and radiometric resolutions $\delta\sigma^0$ and δT_B is given by

$$\sigma^0 = -82.3 \frac{\delta T_B}{\delta T_{SM}} \tag{4.25}$$

where T_B is the brightness temperature and T_{SM} the surface temperature. Assuring $T_{SM} = 300$ K and $\delta T_B = 1$ K, we find that the corresponding radar resolution, necessary to obtain the same sensitivity to SMC, is $\sigma^0 = 0.27$ dB. Active and passive microwave remote sensing data are reported on earth terrain and attempts have been made to compare experimental and model generated data.

Because of reciprocity and energy conservation, a relationship exists between the scattering coefficient and emissivity of a medium (Kong et al., 1979). The relationship between active and passive measurements has been derived from the following assumptions (Tsang et al., 1982):

(a) The transmissivity at the top interface is equal to unity and for vegetative layer it is approximately the same (Fig. 4.1).

(b) The surface scattering contribution $\gamma_{\alpha\beta}^{sur}$ can be approximated by the expression

$$\gamma_{\alpha\beta}^{sur}(\Omega_s, \Omega) = \gamma_{\alpha\beta}^{g}(\Omega_s, \Omega) e^{-k_e d(\sec\theta_s + \sec\theta)} \tag{4.26}$$

where $\gamma_{\alpha\beta}^{g}$ is the bistatic scattering coefficient from incident angle $\Omega(\theta, \phi)$ and incident polarization β scattered into direction $\Omega_s(\theta_s, \phi_s)$ and polarization α. This is the value of the ground at $z = -d$ and $k_e d$ is the optical thickness. The exponential

factor above accounts for the extinction within the layer of scatterers and k_e is defined as the extinction coefficient.

(c) The rough surface scattering coefficient $\gamma^{g}_{\alpha\beta}$ is sharply peaked at the specular direction. On the other hand, volume scattering contribution is relatively omni-directional. Tsang et al. (1982) approximated

$$\gamma^{\text{vol}}_{\alpha\beta}(\Omega_s, \Omega) = Y_0 \frac{\cos\theta_s}{\cos\theta + \cos\theta_s}(1 - e^{-k_e d(\sec\theta_s + \sec\theta)}) \tag{4.27}$$

where Y_0 is a constant independent of incident and scattering angles. The factor in the bracket accounts for the finite thickness of the scattering layer and the factor

$$\frac{\cos\theta_s}{\cos\theta + \cos\theta_s} \tag{4.28}$$

accounts for the path lengths of the incident and scattered waves within the layer (Tsang and Kong, 1978).

Tsang et al. (1978) obtained the following approximate relationship between active backscattering coefficient and passive emissivity

$$\sigma_{\beta\beta}(\theta) = \left[1 - e^{(\theta)}_{\beta} - r^{g}_{\beta}(\theta)e^{-2k_e d\sec(\theta)}\right] \times \frac{\cos^2\theta}{F_2(k_e d - \cos\theta)}(1 - e^{-2k_e d\sec\theta}) + \alpha^{g}_{\beta\beta}(\theta)e^{-2k_e d\sec\theta} \tag{4.29}$$

where $\alpha_{\beta\beta}$ is the backscattering coefficient for the like polarization; $e^{(\theta)}_{\beta}$ is the emissivity at an angle θ; r^{g}_{β} is the ground reflectivity at angle θ and polarization β; $\alpha^{g}_{\beta\beta}(\theta)$ is the ground backscattering coefficient and F_2 as described by these authors. Following are the two limits when

1. Observation angle is away from nadir:

$$\alpha^{g}_{\beta\beta} \to 0$$

and

$$\sigma_{\beta\beta}(\theta) = [1 - e_{\beta}(\theta) - r^{g}_{\beta}(\theta)e^{-2k_e d\sec\theta}]\frac{\cos^2\theta}{F_2(k_e d - \cos\theta)}(1 - e^{-2k_e d\sec\theta}) \tag{4.30}$$

In Eq. (4.30) if $\theta = 50°$ and the reflectivity of the ground $r^{g}_{\beta}(\theta)$ to be 0.25 and the optical thickness $k_e d = 0.5$, then the measured sensitivity of the two layer medium $e_{\beta}(\theta)$ is 0.9. Now from Eq. (4.27), the measured backscattering coefficient for the same polarization and observation angle should be around –11.32 dB. In addition to backscattering cross-section $\sigma_{\beta\beta}$ and the emissivity e_{β}, Eq. (4.29), also contains two unknown parameters, viz. the ground reflectivity r^{g}_{β} and the optical thickness $k_e d$.

2. In the limit when the half space $\to \infty$:

$$\sigma_{\beta\beta}(\theta) = \frac{(1 - e_{\beta}(\theta))\cos\theta}{1 - \cos\theta\ln(1 + \sec\theta)} \tag{4.31}$$

This relation gives an estimate of the backscattering of two layer model with the knowledge of the emissivity.

However, the agreement between experiment and theory is not very encouraging (Tsang et al., 1978). This has been attributed to the assumptions involved in the derivation of above equation as: (a) volumetric scattering is relatively isotopic compared with surface scattering and (b) the transmissivity of the top interface is unity.

It is apparent that there are many open-ended aspects to the whole issue of soil moisture measurement using above two techniques (passive and active remote sensing) and needs further exploration for quantification.

CHAPTER 5

Dielectric Constant of Soil

Experimental Results

Hallikainen et al. (1985a) have performed dielectric constant measurements for five different soil types at frequencies between 1.4 and 18 GHz and found that soil texture has a pronounced effect on dielectric behavior, especially at frequencies below 5 GHz. Based on these measurements, they derived separate polynomial expressions, relating the real and imaginary part of ε to the volumetric moisture content m_v, and the percentage of sand and clay. These polynomial expressions are of the form

$$\varepsilon' \text{ (or } \varepsilon'') = (a_0 + a_1 S + a_2 C) + (b_0 + b_1 S + b_2 C)\, m_v + (c_0 + c_1 S + c_2 C)\, m_v^2 \quad (5.1)$$

where S is percentage (by weight) of sand, C percentage of clay, and a_i, b_i, c_i are coefficients which depend on frequency. Knowing the depth of penetration, Hallikainen et al. (1985a) evaluated numerical values for these coefficients at different frequencies. We can now use Eq. (5.1) to estimate the real and imaginary part of the dielectric constant of the soil at the given observation frequency. The depth of penetration as can be calculated at various frequencies using Eqs. (5.1) and (1.22) is shown in Fig. 1.8.

Prediction of e Using Calibration Procedures

If the water content θ is known, the results can be compared to different calibration functions, leading to the following equations. Using Time Domain Reflectometry technique, a broad range of mineral soils can be studied. A single calibration can be applied to calculate soil volumetric water content from its dielectric constant. This relationship is known as the Topp equation (Topp et al. 1980):

$$\theta = -0.053 + 0.0293\varepsilon - 0.00055\varepsilon^2 + 0.0000043\varepsilon^3$$

Although this equation has been described as widely applicable to the mineral soils, calibration for individual soils may be required. In order to account for the fact that organic materials do not follow Topp equation, Roth et al. (1992) suggested a formulation of the type

$$\theta = -0.078 + 0.0448\varepsilon - 0.00195\varepsilon^2 + 0.0000361\varepsilon^3$$

Dielectric constant can be obtained using the above equations (Stoffregen et al. 2002).

In 3-phase model, if ε_i is the relative dielectric constant of the i phase, a is air content (m^3/m^3) and θ the water content (m^3/m^3), then the complex dielectric constant will be

$$\varepsilon = \sqrt{a\varepsilon_{\text{air}}^2 + \theta\varepsilon_{\text{water}}^2 + (1 - a - \theta)\varepsilon_{\text{solid phase}}^2} \tag{5.2}$$

Volumetric Soil Moisture Using Backscattering Data

The volumetric soil moisture m_v upto around 35-40% value is linearly related to the backscattering coefficient σ^0 by the relation (Zribi et al., 2003)

$$m_v = A + B \cdot \sigma^0 \text{ (dB)} \tag{5.3}$$

where A and B are constants to be obtained from m_v vs σ_0 curve. These can be applied to the SAR images, whereby classification can be done by moisture range.

The slope of regression curve is almost the same for all test fields and soil moisture change show linearity of a similar type. In general

$$\Delta m_v = m_{v,2} - m_{v,1} \tag{5.4}$$

The change in volumetric soil moisture is given in terms of change in backscattering coefficient

$$\Delta m_v = A' \, \Delta\sigma^0 \text{ (dB)}$$

where $\Delta\sigma^0$ is the backscatter change, i.e. $\Delta\sigma^0 = \sigma^0$ (dB) $- \sigma_1^0$ (dB) and A' is a constant pertinent to the given set of measurements.

The advantages of this method are: (i) the errors due to the unknown roughness remain relatively small and exact slope of regression is approximated within slope moisture change estimation error of 10%; (ii) calibration error (e.g. local topography etc.) does not affect the quality of the result, as long as the calibration is uniformly maintained for both the measurements and (iii) influence of the incidence angle may also be neglected. Hence it is a useful method for measuring the degree of moisture with a degree of accuracy. However, using this method permits the estimation of only the moisture change (not the absolute soil moisture).

Data Obtained Using Network Analyzer Technique

For elaboration we consider experimental data obtained using network analyzer technique in the range 0.6-1.2 GHz, on dielectric constant of four soils at different moisture contents (Alex and Behari, 1996). The textural contents of four soil types in terms of sand, silt and clay percentages and their corresponding soil parameters are shown in Tables 5.1 and 5.2, respectively. The variations of the dielectric constant with frequency for moisture content varying from 0 to 30% by volume are obtained. The dielectric constant measured for different samples in the frequency range 0.6 to 1.2 GHz varied in the range 2.65 to 2.03 for dry soil, 8.2 to 6.3 for 10% moisture, 10.4 to 8.03 for 20% moisture and 18.2 to 14.89 for 30% moisture. The ε' values, in general, decrease with increasing frequency (Figs. 2.6 and 2.7). The comparison of experimental values with Wang and Schmugge model for real part of complex

Table 5.1 Textural compositions of soil samples

Sample number	Soil texture (%)		
	Clay	Silt	Sand
1	24.9	36.1	39.0
2	21.0	23.1	55.4
3	45.5	31.6	26.4
4	11.9	16.5	71.6

Table 5.2

Field capacity	Wilting point	Transition moisture
22.39	0.163	0.24
18.09	0.133	0.23
20.63	0.240	0.29
12.68	0.079	0.19

permittivity ε' at 1.2 GHz for different moisture conditions is shown in Fig. 5.1. It is apparent that experimental and model values show a reasonably good agreement.

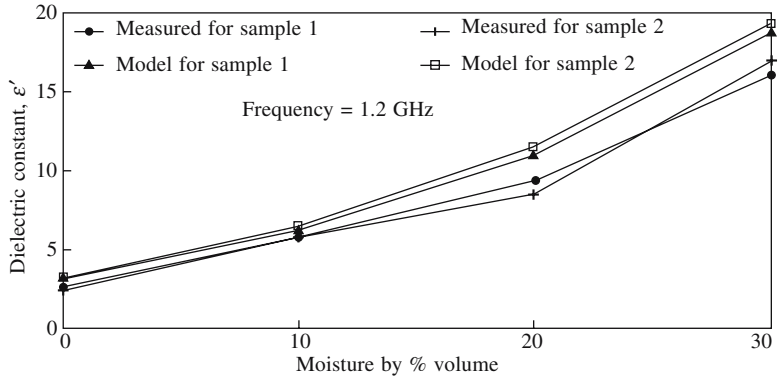

Fig. 5.1 Comparison of Wang and Schmugge model with experimental results.

The variation of ε'' with moisture for all samples (at 1.2 GHz) is shown in Fig. 5.2. This indicates an increase in ε'' with moisture which is attributed to different amount of free and bound water attached because of texture variation.

The relaxation frequency and spread of relaxation for all samples under dry and wet conditions are shown in Table 5.3. It is found that in general the relaxation frequency and spread of relaxation decreases as moisture increases. This trend is dependent upon the soil texture and may be an indication of transition moisture. The texture variation is clearly reflected in the computed value of relaxation frequency.

In case of dry soils the dielectric parameters are not very sensitive to soil texture (p value varied from 0.472 to 0.978). However, for wet soils (moisture content > 20% by volume) the dielectric parameters are significantly dependent upon the soil texture in close agreement with the result of Hallikainen et al. (1985b). In the reported

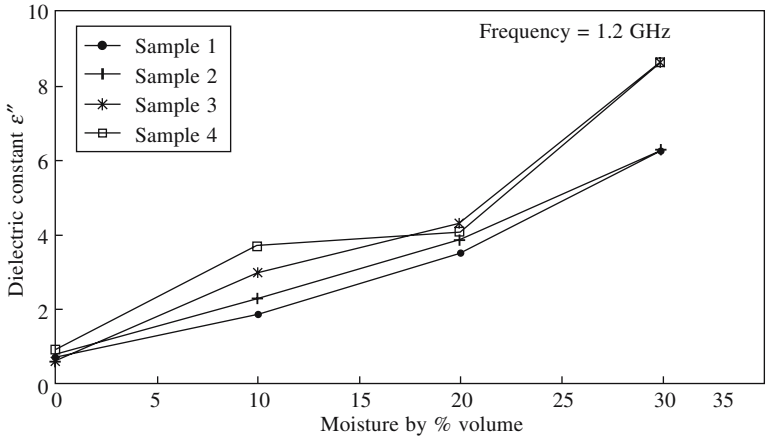

Fig. 5.2 Variation of loss factor with moisture for four samples.

Table 5.3 Relaxation frequency and spread of relaxation for sample under dry and wet condition (0.6-1.2 GHz)

Sample	Transition moisture	Relaxation frequency (MHz) and spread of relaxation for different moisture level			
		Dry	10% by volume	20% by volume	30% by volume
1	0.24	441	319	212	232
		0.09	0.07	0.065	0.047
2	0.23	250	227	163	379
		0.05	0.046	0.033	0.078
3	0.29	434	294	202	211
		0.089	0.05	0.04	0.043
4	0.19	389	306	177	192
		0.08	0.06	0.036	0.039

frequency range, it is found that the frequency variation of the dielectric constant is not significant (p value varied from 0.444 to 0.976) for dry soils but is very significant ($p < 0.0004$) for wet soils. This clearly indicates that this is due to the effect of moisture content and the corresponding density variation. As expected the dielectric constant increases slowly below the transition point and shows an abrupt increase above this (Jackson, 1990; Jackie, 1974). The presence of bound water shifts the relaxation frequency to lower end till it reaches the transition moisture level and above this the relaxation frequency moves to higher values. Since the transition moisture depends on the texture composition, this can also be used for texture characterization. This method can be successfully used for dielectric constant measurement of dry and wet soils over a wide range of frequencies. A properly designed L-band probe can be used for soil moisture estimation at a depth greater then 10-15 cm.

The emissivities of different soils at different moisture levels can be evaluated in

the laboratory for normal incidence from the knowledge of the real part of the dielectric permittivity. It is observed that the emissivity values decreased by an amount approximately equal to the increase of moisture by percent volume. The results indicate that the emissivity values evaluated for normal incidence are: (i) independent of the frequency variation for dry and wet soils, (ii) independent of textural variation in dry and wet stage and (iii) significantly dependent upon the moisture content. The average value of soil emissivity for dry and 10, 20 and 30% volumetric moisture content turns out to be 0.92, 0.83, 0.75 and 0.63 respectively (Fig. 5.3) (Table 5.4). Data available in the literature (Wegmuller et al., 1994; Jackson, 1990) also prove

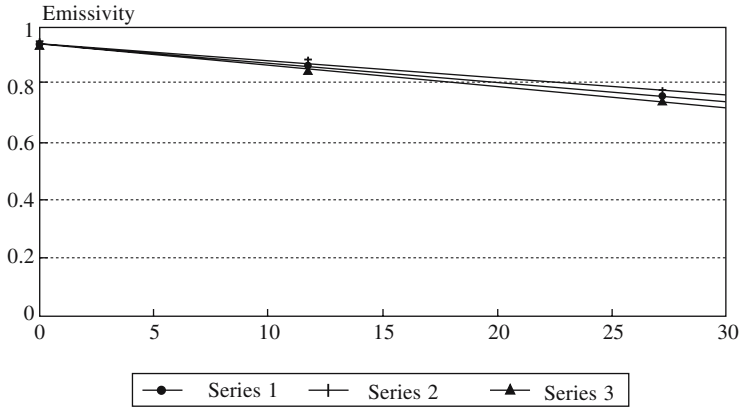

Fig. 5.3 Variation of emissivity *e* with moisture for C-, S- and X-band (Meraman Beach, Goa).

Table 5.4 Emissivity values for normal incidence

Moisture level by volume	Sample number	Emissivity (GHz)			
		0.6	0.8	1.0	1.2
Dry	1	0.93	0.92	0.93	0.93
	2	0.92	0.92	0.91	0.93
	3	0.94	0.95	0.94	0.94
	4	0.91	0.91	0.92	0.91
10%	1	0.81	0.82	0.83	0.85
	2	0.83	0.82	0.83	0.84
	3	0.81	0.83	0.83	0.84
	4	0.82	0.82	0.83	0.83
20%	1	0.73	0.75	0.77	0.77
	2	0.75	0.77	0.76	0.77
	3	0.73	0.75	0.77	0.77
	4	0.75	0.76	0.77	0.78
30%	1	0.64	0.64	0.64	0.64
	2	0.61	0.61	0.63	0.66
	3	0.61	0.61	0.62	0.64
	4	0.64	0.64	0.67	0.67

that emissivity e values for normal incidence are independent of frequency. These results led to formulate following empirical relation to predict the amount of soil moisture from emissivity.

$$\text{Soil moisture content (percent volume)} = -0.8317\ e^{-2} + 2.739\ e^{-1} - 2.04$$

Coefficient of correlation for fitting the equation is 0.91. Validity of this relation was also validated by using the data published by Wegmuller et al. (1994) in the frequency region 2-12 GHz for bare soil. The maximum difference is found to be approximately 9% (Alex and Behari, 1998).

Figure 5.2 shows ε'' variation with moisture for all four samples under investigation. This indicates an increase in ε'' with moisture which is attributed to different amount of free and bound water attached because of texture variation. The bound and free water molecules attached to the soil particle interact with the incident electromagnetic waves differently. If the water content in the soil increases above the transition point, then ε'' increases abruptly. The soil texture determines its bound water capacity. In these experiments the soils used possessed transition point varying between 0.19 and 0.24 and because of this the graphs are inseparable for different textures. This is also suggestive of ε'' dependence on frequency. At the frequencies under investigation the effect is mainly due to the ionic conductivity of soil. The effective conductivity is due to the presence of salts composed primarily of calcium. The concentration of calcium increases with clay content of soil (see Fig. 5.2). Sample 3 has more clay percentage and shows highest value of loss factor for less than about 18% volume moisture. Above this percentage volume samples 3 and 4 almost coalesce. This can be due to the high percentage of sand in the samples. The role of bound and free water is also reflected in the graph. In somewhat linear manner, ε'' increases upto the transition point and above that linearity breaks down. For less than 20% moisture, curve for samples 1 and 2 coincide, while above this, those of samples 1, 2 and 4 show departure. This may be because of texture variations. The data of loss factor for all the samples lie between 0.8 and 8.6 (Fig. 5.2).

General Observations

The general behavior of ε' as a function of moisture content and soil texture can be summarized as follows:

As discussed, ε' increases gradually with increasing moisture content till a certain transition point W_t for all the samples. The transition point W_t is observed to be dependent on the clay content of the samples as has already been pointed out by various investigators (Hallikainen et al., 1985 b; Geiger and Williams, 1972; Hoekstra and Delaney, 1974; Wang et al., 1978; Alex and Behari, 1996; Sabburg et al., 1997). This is due to the large specific surface area of clay particles in comparison to the other basic components of soil, silt and sand. The large specific surface area of clay particles enable them to retain more water in the form of bound water. Now, the dielectric permittivity of bound water is quite lower than that of the bulk free water. When water is added to a clayey soil a greater portion of it is adsorbed as bound water relative to silt and sand. This phenomenon results in wet clayey soils having a

lower net dielectric constant than wet silty and sandy soils at the same moisture level resulting in a higher transition point for the former. In sandy soil the more controlling parameters are bound water factor and the "salinity" factor. Sand having a lower specific surface area has more of free water than bound water at a given moisture content resulting in a higher dielectric constant. Secondly, a low surface area results in a lower cation exchange capacity for sand as compared to clay, i.e. sandy soils are not as open to various physico-chemical processes as clayey soils resulting in a lower salinity of the soil water mixture in the case of sand. The presence of mineral salts decreases the dielectric constant of water and conversely as in this case, their absence keeps it high.

The behavior of the dielectric loss factor ε'' can also be summarized along similar lines but requires an understanding of the phenomenon of dielectric relaxation. It is observed that, like the dielectric constant ε', the loss factor ε'' also increases with increase in moisture content, gradually at first and more steeply beyond the transition point. Clayey soils in general have a lower loss factor at a given moisture level. This phenomena is again explained by the larger specific surface area of clay particles. By virtue of their higher cation exchange capacity, a greater number of physical and chemical processes are facilitated causing large concentration of salts in the soil water solution. An increase in the salt concentration increases the ionic concentration resulting in greater ionic conductivity. The end effect is a lower loss finally reaching a transition point beyond which the increase is very sharp.

Frequency

Figures 2.6 and 2.7 show good agreement between the experimental and computed, results. These display the anticipated feature that ε' and ε'' value decreases with increasing frequency, for a particular value of m_v. The higher value of ε' at lower frequency can be attributed to difference in: (a) relative textural compositions of soils and (b) the frequency dependent dispersion due to the component of free water. Variation of ε' with frequency is generally insignificant upto a moisture content of 10%. It is only above 10% where we find the decreasing nature of ε' with increasing frequency. Even then, the variation of ε' with frequency is much subdued at a lower moisture range (i.e. at 20%) than at higher moisture range (i.e. around 40%).

The data set used by Dobson et al. (1985) are distributed approximately equally among five soil types, whereby dielectric measurements were made at nine frequencies extending between 4.0 and 18 GHz for volumetric moistures between $m_v = 0.01$ and saturation. These authors fitted the data into Eq. (6.10) to determine those values of α and β that yielded minimum r.m.s. difference between the experimental values of ε'_{soil} and ε''_{soil} and those provided by the model. The value $\alpha = 0.65$ was found to be optimum for all soil types; while the magnitude of β was found to vary from about 1.0 for sandy soil to 1.17 for silty clay, and can be related to the sand (S) and clay (C) fractions (by weight) of the soil $\beta = 1.09 - 0.11S + 0.18C$, with a multiple correlation coefficient $r^2 = 0.96$. In a perfect model, a simple linear regression of the calculated values ε against the measured data ε_{meas} would produce a relationship with a zero intercept, a slope of unity and a correlation coefficient r^2 close to unity. The scatter

plot shown in Fig. (5.4) is a typical example of the model performance ε_{soil}. In spite of the wide textural diversity of the soils represented in Fig. 5.4 excellent agreement is obtained between the calculated and measured values of ε'_{soil}. Similar results are obtained for ε''_{soil} Fig. 5.5.

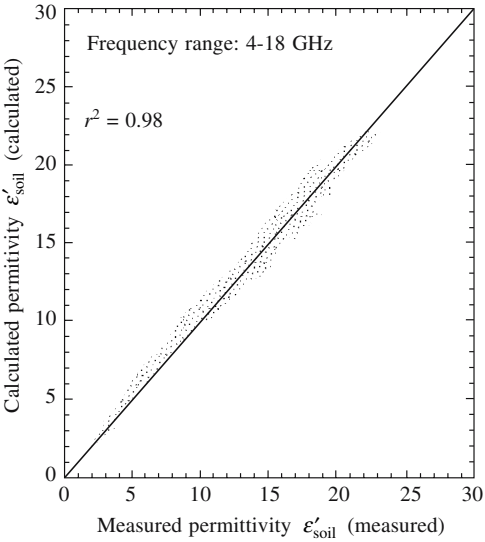

Fig. 5.4 Scatter diagram comparing calculated values to measured values of ε'_{soil}.

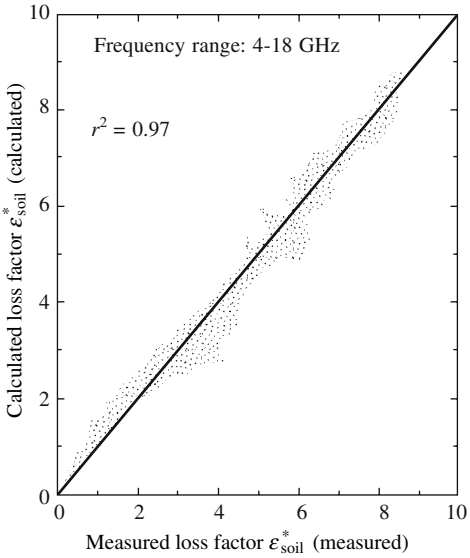

Fig. 5.5 Scatter diagram comparing calculated values to measured values of ε''_{soil}.

Finger Printing of Soil Texture with Moisture

The soils with different texture and a database for a variety of soil type is presented in Table 5.3. The dielectric constant were measured at Ku-band (14.89 GHz) adopting a two point method. The values of ε' and ε'' for each soil sample, were plotted against the volumetric moisture content m_v. The results for selected samples are drawn in Fig. 5.6. The plots are obtained with the help of a curve fitting technique. The general guiding equation for these curves is of the form $Y = a \exp [x/b]$, where the coefficients a and b have different values; in each case x being the volumetric moisture content of the soil. The values of the coefficients a and b and the transition point are also given (Ghosh et al., 1998).

As the volumetric soil moisture increases (>10%), the value of dielectric constant (ε'_{soil}, ε''_{soil}) increases, gradually at first and then shows a steep rise.

The relaxation frequency and spread of relaxation remains constant in case of free water. Here, the above two factors would, in general, be functions of texture and moisture. Relaxation frequency has been calculated from Cole-Cole equation and expressed as a function of texture in the volumetric moisture range of 10-40% (Fig. 5.7). The dip occurs at 75% sand content while the peaks are at 48 and 86%. The dip and the peak values may be attributed to the qualitative change in the mechanism

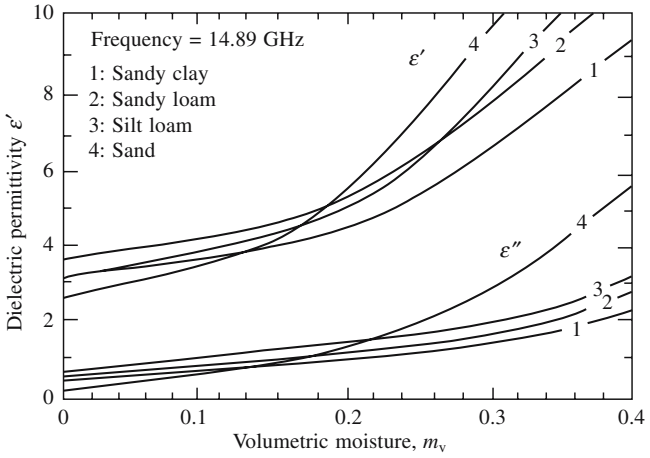

Fig. 5.6 Dependence of dielectric permittivity on soil moisture and texture for four samples.

of soil-water interaction in this textural region. It may be inferred that relaxation frequency value may be identified as a fingerprint for the soil moisture for a given texture composition. Spread of relaxation as calculated from Cole-Cole equation is found to be decreasing with increase in moisture content for all soil samples. This is because at higher moisture dipole relaxation of water is hindered. Due to increasing contribution of free water-soil interaction changes and relaxation spread is lowered.

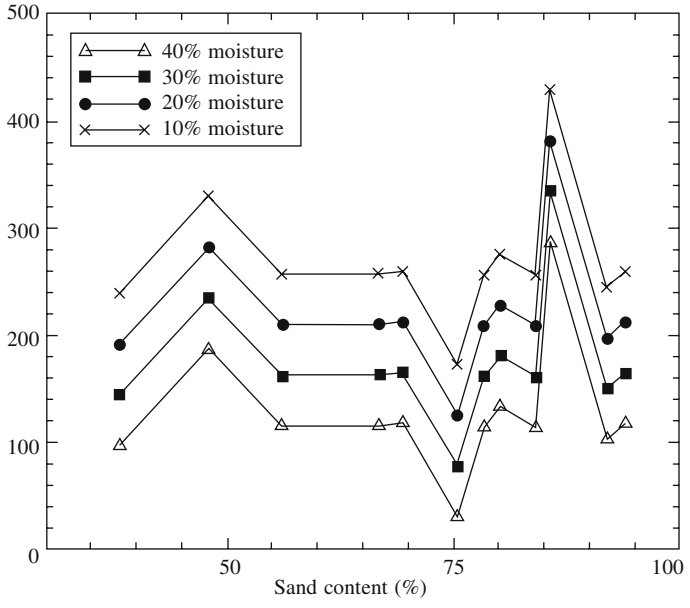

Fig. 5.7 Relaxation frequency vs sand (%) at various soil moisture.

Table 5.5 shows relaxation frequency as a function of soil moisture for different soil samples. It reveals that clay soils have a higher value of relaxation frequency than sandy soils. Also relaxation frequency decreases with an increase in volumetric soil moisture. For a 10% soil moisture a typical value for relaxation frequency comes around 240-330 MHz and spread (α) in the range 0.02-0.07 (Table 5.5). From Fig. 5.8 it is apparent that the relationship between wilting point and transition point

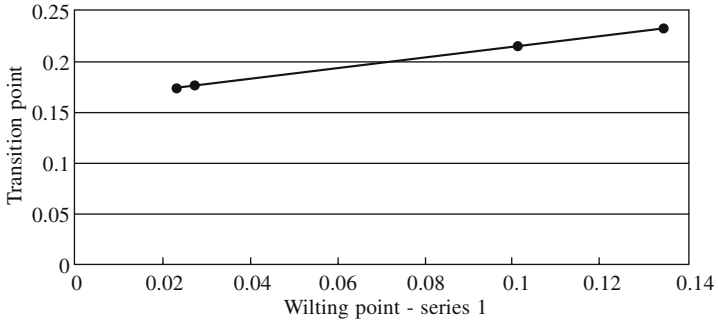

Fig. 5.8 Transition point vs wilting point.

is linear. The relationship is generally valid for all soil types. This suggests that the conclusions drawn for ε' vs transition point are proportionally applicable for wilting point also. For the five samples composition as mentioned in Table 5.6 (Hallikainen et al., 1985a) the brightness vs m_v graph is shown in Fig. 5.9 (Ulaby et al., 1986).

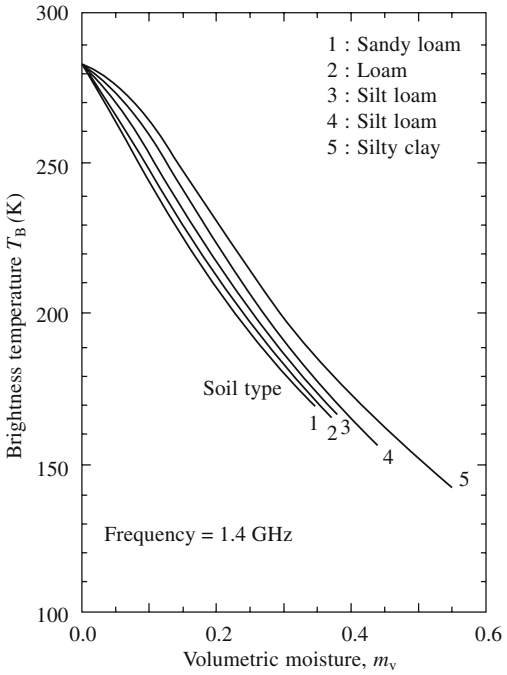

Fig. 5.9 Calculated brightness temperature variation with volumetric moisture content for five soil types.

Table 5.5 Soil texture and quadratic fit coefficients of ε' and ε'' with wilting point W_T relaxation frequency and spread of relaxation

Soil No.	Sand	Silt	Clay	W_T	ε'		ε''		Relaxation frequency and spread of relaxation at various soil moisture			
					a	b	a	b	10%	20%	30%	40%
1	94.10	2.00	3.90	0.17	2.80	0.27	0.25	0.15	258.94	211.64	164.34	117.04
									0.05	0.04	0.03	0.02
2	56.10	6.00	37.90	0.17	3.22	0.37	0.56	0.22	256.68	209.38	162.08	114.78
									0.05	0.04	0.03	0.02
3	75.50	10.00	14.50	0.18	2.95	0.33	0.33	0.21	172.57	125.27	77.97	30.67
									0.02	0.01	0.00	0.00
4	38.10	52.00	9.90	0.18	3.20	0.31	0.56	0.23	239.53	192.23	144.93	97.63
									0.04	0.03	0.02	0.01
5	66.81	13.73	19.46	0.19	2.98	0.36	0.35	0.17	257.43	210.13	162.83	115.53
									0.05	0.04	0.03	0.02
6	69.50	10.00	14.50	0.17	2.33	0.18	0.34	0.11	259.63	212.33	165.03	117.73
									0.05	0.04	0.03	0.02
7	78.50	9.00	12.50	0.17	3.49	0.36	0.45	0.22	256.07	208.77	161.47	114.17
									0.05	0.04	0.03	0.02
8	85.90	5.20	8.90	0.18	3.00	0.33	0.43	0.21	429.25	381.95	334.65	287.35
									0.11	0.10	0.09	0.08
9	94.10	2.10	3.80	0.19	2.60	0.26	0.30	0.14	259.61	212.31	165.01	117.71
									0.05	0.04	0.03	0.02
10	84.20	5.90	9.90	0.17	2.90	0.28	0.30	0.17	255.72	208.42	161.12	113.82
									0.05	0.04	0.03	0.02
11	48.00	32.90	19.10	0.17	3.07	0.21	0.33	0.20	329.91	282.61	235.31	188.01
									0.07	0.06	0.06	0.05
12	80.30	10.60	9.10	0.17	3.10	0.30	0.34	0.14	275.80	228.50	181.20	133.90
									0.05	0.04	0.03	0.03
13	92.05	0.74	7.21	0.19	2.85	0.24	0.27	0.13	244.32	197.02	149.72	102.42
									0.04	0.03	0.02	0.01

Table 5.6 Soil texture (Hallikainen et al., 1985a)

Soil sample under investigation	Soil number	Soil type	Soil texture (%)		
			Sand	Silt	Clay
	1	Sandy loam	51.5	36.1	13.4
	2	Loam	42.0	49.5	8.5
	3	Silt loam	17.2	63.8	19.0
	4	Silty clay	5.0	47.6	47.4
	5	Clay	13.0	6.5	80.5

It may be seen from Eq. (1.27) that the emissivity is dependent only on the real part of the dielectric constant. A plot of soil texture vs ε' (sand % vs ε') for C-, S- and X-band of frequencies yields a dip/hump, which in the present investigations may correspond to the relaxation frequency for a given texture and moisture (Fig. 5.10 a, b, c). We find that there is a hump in the vicinity of 80% sand. A similar relationship is also observed for ε''. As anticipated there is found to be a decrease in relaxation frequency with the increase in volumetric soil moisture and correspondingly the spread in relaxation time.

In Situ Methods

A simple method of soil moisture measurement in field with the suggested set-up (see Chapter 3) is possible with a fair degree of accuracy. To verify the efficacy of the method measurements have been carried out over C-, S- and X-band frequency range at various moisture levels. A comparison of the data obtained *in situ* conditions and by two point method (14.89 GHz) reveals that real part of the permittivity offers an excellent agreement. The imaginary part, which is dependent on the sample treatment is hence indicative of a departure in ε'' values. Results indicate that Horn antenna method can serve as a standard experimental method for soil moisture measurements in field situations (Table 5.7).

The coaxial cable method should be tried in field within the frequency range 1-7 GHz with different moisture level and at different depths. For ε'' the correct results can be obtained by using *in situ* methods only.

Bound Water Problem in Relation to Experimental Data

Figures 5.11 and 5.12 show model calculations (Boyarskii et al., 2002) and experimental dependencies (Hallikainen et al., 1984) of real components of dielectric constant of wet soil on frequency for sandy loam at a soil temperature of +10°C (volumetric wetness of soil $m_v = 4.3\%$ (Fig. 5.11) and $m_v = 24.3\%$ (Fig. 5.12), density of dry soil

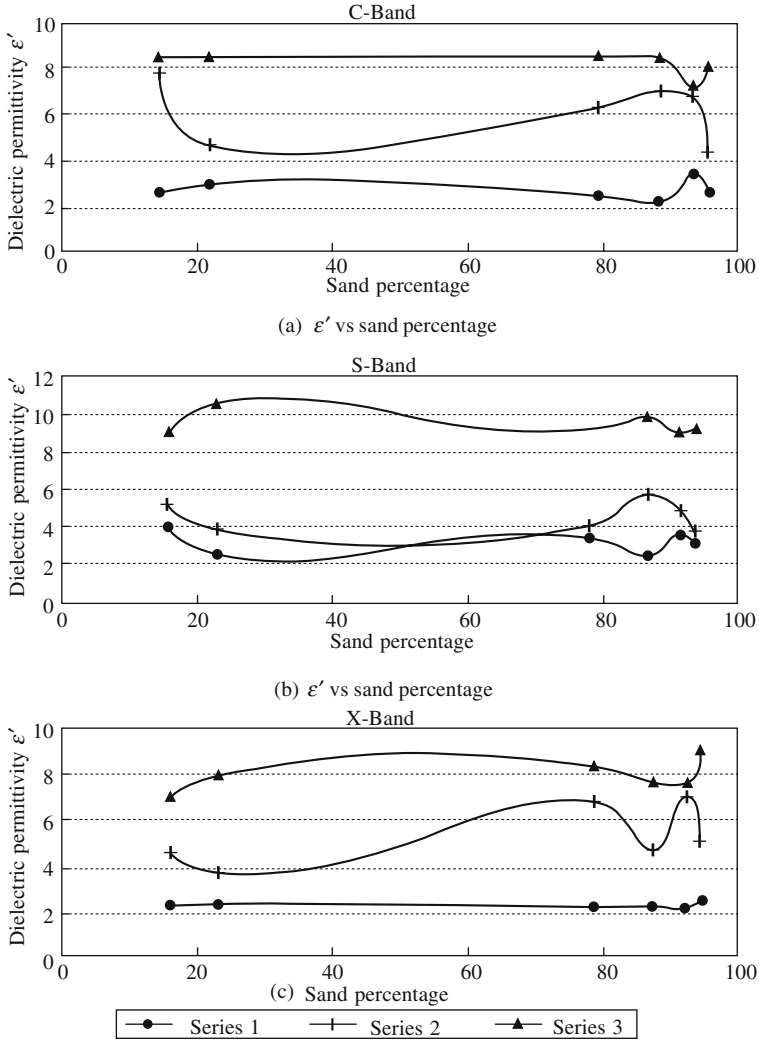

Fig. 5.10 ε' vs sand percentage.

of 1.54 g/cm^3 and weight fraction composition of soil: sand M_{sa} = 51.51%, silt M_{si} = 35.06%, clay M_{cl} = 13.43%). In compliance with the fraction composition of the soil as well as in line with the suggested model, at low wetness (4.3%), where all water in the soil is bound, while at high wetness (24.3%), it is free.

Experimental values in Figs. 5.11 and 5.12 are given with corresponding measurement errors which for the real component of dielectric constant constituted not more than 5% for the whole range of frequencies, wetnesses and soil temperatures. Analysis of dependencies presented in Figs. 5.11 and 5.12 bring us to the conclusions that at low soil moisture level model should take bound water into account. This is shown in the difference of dielectric constant values calculated at low (4.3%) and high soil

Table 5.7 Dielectric permittivity by the reflectometry method and comparison with two point method

Sample	Values at various heights above ground		Average		Value by two-point method	
	ε'	ε''	ε'	ε''	ε'	ε''
1	3.82	0.29				
	2.88	0.18				
	2.80	0.26	3.14	0.25	3.14	0.29
	3.08	0.20				
	3.14	0.32				
2	2.77	0.13				
	3.19	0.20				
	2.92	0.28	2.99	0.23	3.04	0.29
	3.07	0.32				
	3.01	0.24				
3	2.85	0.30				
	2.55	0.22				
	2.83	0.08	2.74	0.16	2.74	0.20
	2.69	0.09				
	2.79	0.11				

moisture (24.3%) which confirms that with growing wetness, dielectric properties of bound water approaches those of free water.

It is necessary to underline that in this model ε_{eff} assumes the presence of bound water in a soil only when there is a clay fraction in that soil. In real soils, bound water

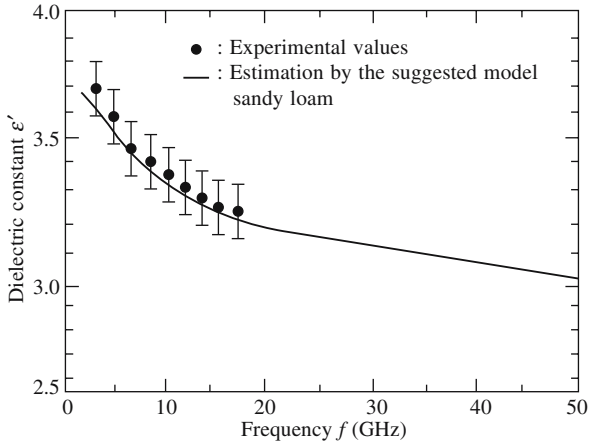

Fig. 5.11 Frequency dependencies of real components of dielectric constant of sandy loam at soil volumetric wetness of 4.3%.

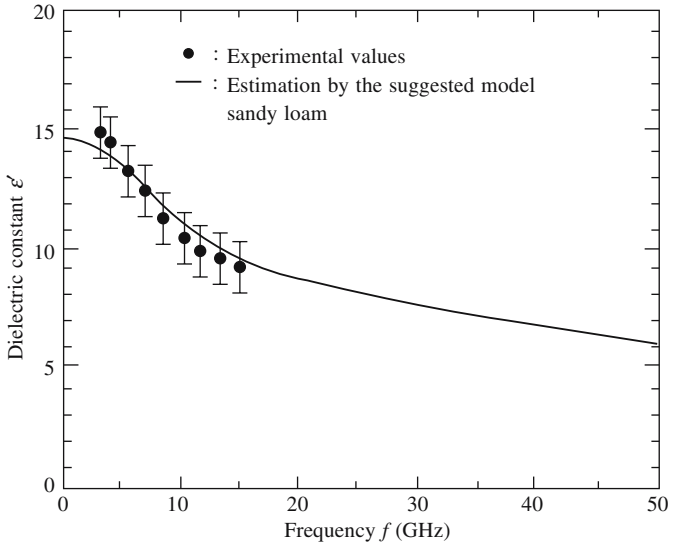

Fig. 5.12 Frequency dependencies of real components of dielectric constant of sandy loam at soil volumetric wetness of 24.3%.

films cover other particles as well (sand and silt). However, the maximum thickness of bound water is 10 monomolecular layers (2.8×10^{-7} cm). According to (Boyarskii et al., 2002) the amount of bound water on sand and silt particles is less than 0.1%.

CHAPTER 6

Soil Moisture Models

Mixing rules relating the macroscopic dielectric properties of heterogeneous media to those of their constituent phases and the internal structure of the mixture have been a subject of continuing research for a long time. The ability of treating a random medium with an effective permittivity that contains the information on how the inhomogeneties of the material affect the electric field behavior is essential to researchers in several fields like remote sensing, industrial and medical applications of microwaves, and material science.

Attempts have been underway to model the microwave dielectric behavior of soil water mixtures. Oldest have been the two component model to more elaborate four component physical soil models. A simple two component model (soil plus water) can at best, exhibit the correct trend for ε_{soil} vs m_v but cannot account for the difference on soil type. Later models have taken explicit consideration of bound water in the overall dielectric behavior of mixture. Other successfully adopted approaches include introducing adjustable soil specific or frequency specific parameters.

Wang and Schmugge Model

Wang and Schmugge (1980) have offered an empirical mixing formula at 1.4 and 5 GHz that explicitly treats a bound water layer and an air volume fraction in addition to the dry soil bulk water components. In their treatment, the complex dielectric constant components are linearly combined over two separate regions, i.e. water components W_c is less than or greater than the maximum bound water (transition moisture m_t) fraction. The expression for the complex dielectric constant (of a soil-water mixture) in this model is

$$\varepsilon = W_c\, \varepsilon_x + (P - W_c)\, \varepsilon_a + (1 - P)\, \varepsilon_r;\ W_c < m_t \tag{6.1}$$

with

$$\varepsilon_x = \varepsilon_i + (\varepsilon_w - \varepsilon_i)(W_c/m_t)Y \tag{6.2}$$

and

$$\varepsilon = m_t\varepsilon_x + (W_c - m_t)\, \varepsilon_w + (P - W_c)\, \varepsilon_a + (1 - P)\, \varepsilon_r;\ W_c > m_t \tag{6.3}$$

with

$$\varepsilon_x = \varepsilon_i + (\varepsilon_w - \varepsilon_i)\, Y \tag{6.4}$$

$$Y = -0.57\, W_T + 0.481$$

Here P is the porosity of dry soil (= $1 - P_s/P_r$), where P_s is the density of dry soil and P_r the density of the associated solid rock, ε_a, ε_w, ε_r and ε_i are the dielectric constants of air, water, rock and ice, respectively and ε_x the dielectric constant of the initially absorbed water. Y is a parameter which can be chosen to best fit Eqs. (6.1) and (6.3) and to the experimental data. For the soil samples used in the dielectric measurements at 1.4 and 5 GHz, P_s lies in the range of 2.2-1.7 g/cm^3, while P_r varies between 2.6 and 2.75 g/cm^3. Entering the average value of P_s for the soil samples gives $P = 0.5$. It can be shown that with either $P = 0.4$ or $P = 0.6$, the calculated dielectric constants of soil-water mixture differ only slightly from those with $P = 0.5$. The dielectric constants of ice (real and imaginary) are assumed to be approximately 3.2 and 0.1, respectively (Evans, 1965). The dielectric constants (real and imaginary) of a solid rock vary (Campbell and Ulrichs, 1969) but the respective values of 5.5 and 0.2 fit well with the experimental value of dry soils. With the Wang and Schmugge (1980) model, the values of field capacity (FC), transition moisture m_t, and wilting point W_T are determined from the set of expressions mentioned earlier (Eqs. (1.10)-(1.12)).

The imaginary part of the total dielectric constant at low frequencies ε'' is given as

$$\varepsilon_t'' = \varepsilon'' + \alpha\ W_c^2 \tag{6.5}$$

where ε'' is the imaginary part of the mixed dielectric constant and α is chosen to best fit the measured ε_t''. The second term in ε_t'' represents the conductivity.

Wang and Schmugge (1980) carried out laboratory experiments on three soils ranging from sand to heavy clay at wavelength 21 cm and demonstrated that the moisture content at transition region was higher in soils having higher clay content than in sandy soils. The water content at the transition level W_t on a volumetric basis ranged from 17% for the sand to 33% for heavy clay. Based on analysis of this type of measurement for a wide variety of soils, it has been demonstrated that the transition level moisture was linearly correlated to an estimated wilting point moisture content for the soils at both 1.4 and 5 GHz.

In most of the reports found in literature, dielectric data are plotted as a function of either m_v or m_g or both. It is apparent from Fig. 6.1 that there is a greater degree of scattering about the regression curve for m_g as compared to m_v. This is shown for two different bulk densities. Hence, it is often preferred to plot dielectric data (ε', ε'') against m_v (Ulaby et al., 1986).

Dielectric Mixing Models of Soil

Many mixing formulae have been reported in the literature since the early work of Rayleigh. Table 6.1 gives a list of the mixing formulae considered to be adequate for a comparison with the experimental data acquired in recent years. The majority of these formulae dealt only with a mixture of two constituents (Wang and Schmugge, 1980). These basically implied a direct dependence of the mixture dielectric constant ε on the dielectric constants (ε_1 and ε_2) and the volume fractions (f_1 and f_2) of the constituents. Fig. 6.2 shows a set of curves generated by the eight formulae without

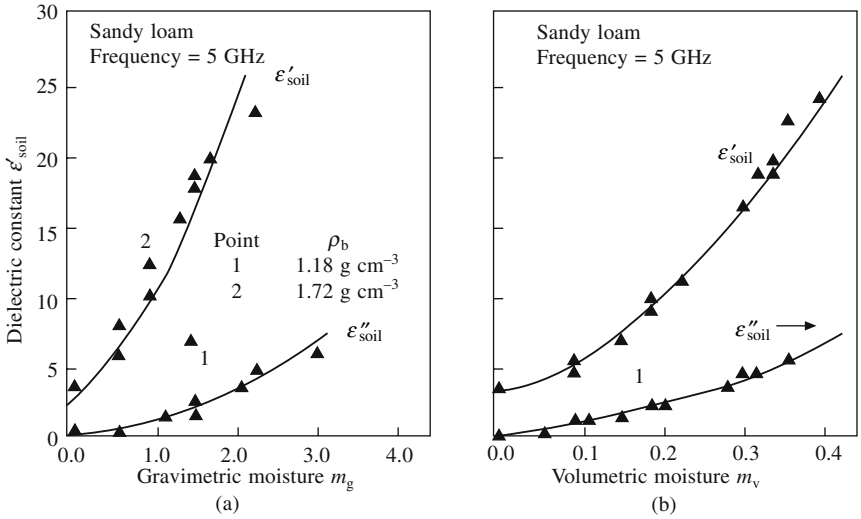

Fig. 6.1 Comparison of measured soil dielectric constant data plotted as a function of gravimetric and volumetric moisture content (Hallikainen et al., 1985a).

free adjustable parameters. The measured dielectric constants at 1.4 GHz as a function of the volumetric water content for Yuma sand, Vernon clay and Miller clay are also included in the figure for comparison. It is concluded from Fig. 6.2 that the value of ε' computed from the eight formulae is not in good agreement with the experimental results. Some of the curves present a good but partial agreement with the experimental data but not over the entire moisture range under study. Only the real parts ε of the measured and computed dielectric constants appear in Fig. 6.2. The imaginary part is quite variable and its exclusion does not alter the main conclusions.

Semi-Empirical Model

Physical aspects of soil have also been used to develop a relatively simple semi-empirical model (Dobson et al., 1985). A four component mixture model for soil is written as (Ulaby et al., 1986)

$$\varepsilon_{soil}^{\alpha} = v_{ss}\,\varepsilon_{ss}^{\alpha} + v_a\,\varepsilon_a^{\alpha} + v_{fw}\,\varepsilon_{fw}^{\alpha} + v_{bw}\,\varepsilon_{bw}^{\alpha} \tag{6.6}$$

where the subscripts ss, a, fw and bw denote soil solids, air, free water and bound water, respectively.

Now
$$\varepsilon_{ss} \cong 4.7 - j0 \tag{6.7}$$

and
$$v_{ss} = 1 - \rho_\phi$$

$$v_a = \rho_\phi - m_v$$

$$m_v = v_{fw} + v_{bw}$$

$$\rho_\phi = (\rho_{ss} - \rho_b)/\rho_{ss} \cong 1 - 0.38\ \rho_b$$

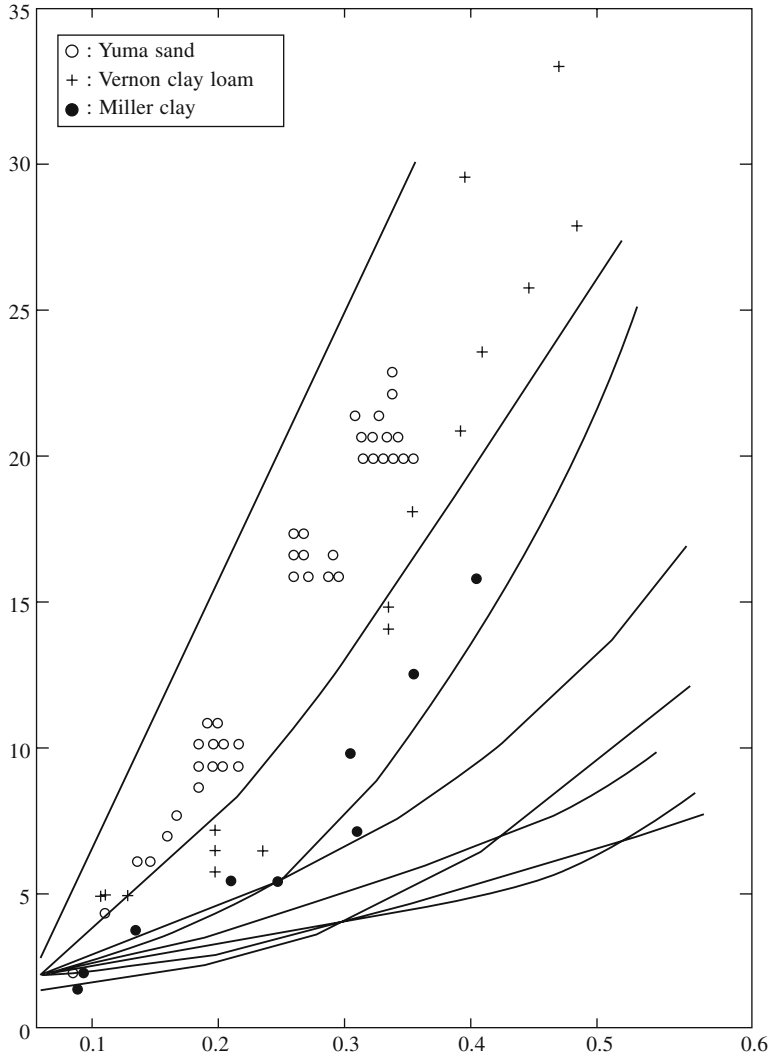

Fig. 6.2 A comparison of measured dielectric constant of three soils using mixing models.

where ρ_ϕ is the soil porosity, $\rho_{ss} \cong 2.65$ g cm^{-3} is the density of the solid soil material, and m_v is the total volumetric moisture content. With these simplifications, Eq. (6.6) reduces to

$$v_{fw}\,\varepsilon_{fw}^{\alpha} + v_{bw}\,\varepsilon_{bw}^{\alpha} \cong m_v^{\beta}\,\varepsilon_{fw}^{\alpha} \tag{6.8}$$

where β is an adjustable parameter to be determined empirically. With these relations Eq. (6.6) becomes

$$\varepsilon_{soil}^{\alpha} = (1 - \rho_\phi)\,\varepsilon_{ss}^{\alpha} + \rho_\phi - m_v + m_v^{\beta}\,\varepsilon_{fw}^{\alpha} \tag{6.9}$$

$$\cong 1 + \frac{\rho_b}{\rho_{ss}}\,(\varepsilon_{ss}^{\alpha} - 1) + m_v^{\beta}\,(\varepsilon_{fw}^{\alpha} - 1) \tag{6.10}$$

β varies between approximately 1.0 and 1.16 for the five soil types, viz. sandy loam, loam, silt loam (two types) and silty clay (Fig. 6.3). If the model is limited to frequencies higher than 4 GHz, the effects of soil salinity are considered unimportant.

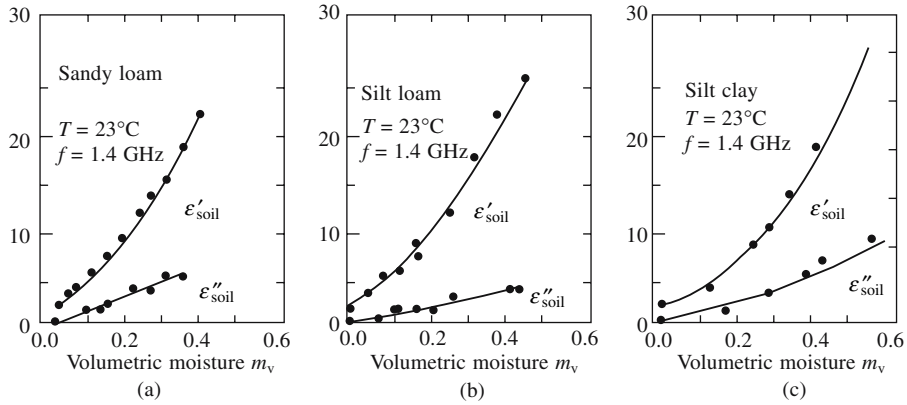

Fig. 6.3 Comparison of the dielectric constant predicted by the physical soil dielectric mixing model with measured values at 1.4 GHz for: (a) sandy loam, (b) silt loam and (c) silty clay. —: Measured; •: Calculated (Ulaby et al., 1986).

Other Models

It is clear from Fig. 6.2 that the calculated variations of ε with moisture content W_c from any one of the eight formulae do not give a good description to the measured results. The calculated ε from the Bottecher's (1952) formula matches the measured ε of Miller clay quite well, but there is no free parameter to adjust for the other soil types. The Brown's (1956) formulation gives a ε vs. moisture curve with a steep slope over the entire moisture range of interest. The steepness of the slope, with some offset constant, fits nicely with the observed rapid increase of ε with W_c over the region $W_c > m_t$. However, the difficulty arises regarding the portion $W_c \leq m_t$. The Birchak et al. (1974) formula gives a ε-moisture curve generally close to the measured data points but does not produce good fit over the entire moisture range for a given soil. The remaining formulae of Rayleigh (1892); Brugeman (1935); Kharadly and Jackson (1935); Nerpin and Chudnovskii (1970) and Wagner (1914) are not applicable in the soil water mixture where $W_c \geq 0.5$ cm^3/cm^3. The formulae of Weiner (1910) and Pearce (1955) contain a free parameter which can be adjusted to fit the experimental data. However, it has not been possible to obtain a good fit over the entire moisture range 0-0.5 cm^3/cm^3.

There have been several attempts to model the microwave dielectric behavior of soil water mixtures. More than two component models have been proposed (Hoekstra and Delaney, 1974; Wang, 1980) which explicitly recognize the importance of the bound water in the overall dielectric behavior of the mixture. Using these models, it is possible to obtain better agreement with the measured data. This is partly because the more elaborate formula includes adjustable soil specific or frequency specific parameters.

In addition, following formula describes the dielectric behavior of mixture (Bruggeman, Bottcher and Odelevsky (Statistical):

$$\varepsilon_m = A + \sqrt{A^2 + \frac{\varepsilon_1 \varepsilon_2}{2}} \tag{6.11}$$

where $A = \frac{1}{4}[(3W_1 - 1)\,\varepsilon_1 + (3W_2 - 1)\,\varepsilon_2]$, ε_m, ε_1, ε_2 is the dielectric permittivity of mixture and its components, respectively, and W_1, W_2 are components of the volumetric fraction of water.

Another expression called 'refractive' formula which describes the dielectric behavior of mixture is

$$\sqrt{\varepsilon_m} = W_1 \sqrt{\varepsilon_1} + W_2 \sqrt{\varepsilon_2} \tag{6.12}$$

This was derived to enable calculation of complex dielectric permittivity with the assumption that the size of the dispersed particle is much less than the wavelength (i.e. $d << \lambda$).

Equation (6.12) may be generalized for the multicomponent mixtures

$$\sqrt{\varepsilon_m} = \sum_i W_i \sqrt{\varepsilon_i} \tag{6.13}$$

An inadequacy of above models of soil matrix is that these are neither comprehensive nor universally applicable. These involve a number of rigid assumptions which more often do not exactly conform to the realistic field situations. Hence, the domain of theoretical modelling of soil matrix still demands a fresh look.

Analysis of theoretical assumptions involved and its interaction with microwave radiations in deriving the original formulae and results of comparisons between calculated values and experimental data permit the following conclusions:

In 3-30 cm range the 'refractive' formula may be used as a good working model. Some differences between experimental data and calculations for the imaginary part of the dielectric constant may be explained by the presence of salt in the soil samples.

Bruggeman-Hanai formulation may be considered as models of dielectric constant of soil in the moisture range from 0.05 to 0.10 g/cm^3.

Alex and Behari (1996) in their study put forward an empirical model for calculation of the volumetric soil moisture from the real part of complex dielectric permittivity of the soil sample. Their proposed approach consists of two steps. In the first step, the emissivity e of the soil sample is calculated by a known formula using just the real part of the complex dielectric constant

$$e = 1 - \left[\frac{1 - \sqrt{\varepsilon'}}{1 + \sqrt{\varepsilon'}}\right]^2 \tag{6.14}$$

In the second step, the volumetric soil moisture is calculated using a relationship involving e, viz.

$$m_v\,(\%) = -08317\, e^{-2} + 2.793\, e^{-1} - 2.04 \tag{6.15}$$

This provides a method of calculating the soil moisture content directly by the knowledge of the microwave dielectric permittivity and has potential to transform into a useful tool in *in situ* soil moisture measurement.

Status of the Available Mixing Models

Many sincere efforts have gone into the measurement of the relative permittivity of soil water mixtures at microwave frequencies. However, relatively few attempts have been made to model the observed behavior in terms consistent with a physical soil model. An important missing ingredient has been an explicit consideration of bound water fraction. Bound water is held in soil by electromolecular and molecular surface forces. It can be imagined that the closer the water layer is to the particle, more of it is distorted with respect to the free water and to the ice. This state brings about difference in various physical properties (Boyarskii et al., 2001). An ideal model formulation would provide for the observed effects of various soil components on the complex dielectric behavior of the soil-water-air system as a function of frequency. Such factors include soil bulk density (compaction), soil composition (particle size distribution and mineralogy), volume fraction of soil-water components, salinity of soil solution, and possibly temperature. An examination of several classical mixing formulae shows that these inadequately describe at least one of the observed effects at frequencies of 1.4 and 5 GHz. Since these formulae consider the mixing of a two-component system only (soil with free water), these are unable to account for the complex behavior of a soil medium consisting of soil particles with variable packing densities. This is covered by a film of adsorbed water and has large pore spaces filled with either bulk solution or air (depending upon the matric potential of the system). The dielectric models serve the following purposes: (1) provide convenient means for predicting soil dielectric behavior for use in microwave emission and scattering calculations, and (2) present a physically based theoretical mixing model that is dependent upon measurable soil parameters only, i.e. requiring no adjustable parameters. The first purpose is fulfilled by an empirical model using a dielectric mixing approach and is dependent upon readily measured soil characteristics such as soil gravimetric moisture m_g, soil bulk density ρ_b and weight percent of the sand and clay fractions. Secondly, one assumes a four-component dielectric mixing of soil solids, air, bulk water in the Gouy layer and bound water in the stern layer, wherein the quantities and characteristics of the bulk and bound water fractions are determined by a soil physical model. Mixing formulation is achieved by adopting an approach that is useful in describing heterogeneous aqueous mixtures.

In order to fully account for the frequency and soil dependence of ε, it is necessary to treat bound water as a distinct component of soil water system having dielectric constant in the range 20 to 40. The mixing approach which uses disc like inclusions of air, bulk water and bound water, is found to be an appropriate formulation for describing the curvature of ε (m_v), the soil texture and bulk density dependence of ε, and the frequency dependence of ε from 1.4 to 18 GHz. The soil physical model provides estimates of both the volume fraction of bound water and the effective conductive loss of the bulk soil solution. The diffusion of cations into the soil solution keeps the effective conductive loss of the bulk solution high.

Dielectric mixing models that are proposed relate the effective dielectric permittivity of a heterogeneous medium with the properties of the constituent materials. The restriction for this approach is that the sizes of the inclusions in the mixture have to be considerably smaller than the wavelength in order to avoid the scattering effects.

The multiplicity of mixing formulae presented in the literature is a reflection of the randomness in the structure of these heterogenous materials of interest. An exact solution for the electromagnetic problem with random parameters and boundaries is not available as yet. This has led to the existence of several mixing theories, demanding an experimental confirmation. Common to all of the mixing theories is the basic requirement for the validity of their use—the spatial variation of the electric field has to be lesser than the variation in the structure of the medium. This implies that the sizes of the inclusions contents of the mixture or the correlation distance (in case the medium is describable by a continuous permittivity function) have to be considerably smaller than the wavelength of the electric field λ. The requirement is that the maximum chord of an inclusion is about $\lambda/2\pi$. The effective permittivity, thus, be a complex number and include loss parameters. These are essentially absorption losses which arise due to constituent components.

The Effective Permittivity ($\boldsymbol{\varepsilon_{\text{eff}}}$)

Consider a mixture with dielectric background material of permittivity ε_0 containing n scatterers in unit volume, each of polarizability α. The background permittivity ε_0 need not be that of free space and, in fact, it can have any value including the complex ones. In mixing formula that results from the analysis, only the relative permittivities of the component permittivities with respect to ε_0 are considered important.

It is customary to define the effective permittivity or the macroscopic permittivity ε_{eff} of a random medium as ratio between the average displacement D and the average field E as

$$D = \varepsilon_{\text{eff}}\, E \tag{6.16}$$

The displacement depends upon the polarization P in the material

$$D = \varepsilon_0\, E + P \tag{6.17}$$

The polarization can be calculated from the dipole moments p of the scatterers; it is the dipole moment density in this polarizable material

$$P = np \tag{6.18}$$

This treatment assumes that the dipole moments are the same for all scatterers; if there are different polarizabilities, they have to be summed up by weighting each dipole moment with its number density, and the polarization consists of a sum, or an integral.

The dipole moment depends on the polarizability and the exciting field E_{e}

$$p = \alpha\, E_{\text{e}} \tag{6.19}$$

For spherical scatterers, the exciting field is

$$E_e = E + \frac{P}{3\varepsilon_0} \tag{6.20}$$

Therefore, the effective permittivity is

$$\frac{(\varepsilon_{eff} - \varepsilon_0)}{(\varepsilon_{eff} + 2\varepsilon_0)} = \frac{n\alpha}{3\varepsilon_0} \tag{6.21}$$

The problem is how to calculate the dipole moment induced in the scatterers. This entails solving the internal field of a scatterer in a quasi-static field, i.e. finding the solution of the Laplace equation.

It is worth noting that the scatterers in the mixture need not be of the same size. As long as each of the scatterers satisfies the quasi-static requirement, their relative polarizabilities are the same and have to be multiplied with the volume fraction to sum up to the average polarization, the last equation being perfectly valid. On the other hand, if the mixture contains scatterers with different polarizabilities such as in the simplest case, spheres of N different permittivities, they have to be multiplied by their individual volume fractions, and Eq. (6.21) gets modified into

$$(\varepsilon_{eff} - \varepsilon_0)/(\varepsilon_{eff} + 2\varepsilon_0) = \sum n_i\alpha_i/3\varepsilon_0 \tag{6.22}$$

The use of this formula requires that the different types of scatterers be distributed homogeneously in the mixture in the scales of the order of wavelength.

Rayleigh Mixing Formula

The simplest mixture consists of a background medium and spherical scatterers. Let the permittivity of the former be ε_0, that of the latter ε_1 and the volume fraction of the scatterer f_1. The polarizability of this kind of scatterer depends on the field ratio between the inside and outside fields when the scatterer is in a static field. The polarizability of a scatterer with radius a_1 is

$$\alpha = 4\pi\varepsilon_0 \; a_1^3(\varepsilon_1 - \varepsilon_0)/(\varepsilon_1 + 2\varepsilon_0) \tag{6.23}$$

Hence, according to Eq. (6.17), the effective permittivity of this mixture is

$$(\varepsilon_{eff} - \varepsilon_0)/(\varepsilon_{eff} + 2\varepsilon_0) = f_1(\varepsilon_1 - \varepsilon_0)/(\varepsilon_1 + 2\varepsilon_0) \tag{6.24}$$

This formula is known as the *Rayleigh mixing formula.*

A modification of general mixing model may contain many arbitrarily shaped scatterers. The model contains two free parameters u and v, and with different choices for these parameters, many mixing formulae presented earlier can be obtained. v can be seen as an indicator of how the polarization of neighboring inclusions is taken into account in calculating the dipole moment of a single scatterer v for one-dimensional scatterer and in three dimensions, the situation might be different. Experimental results might give the solution for finding the correct v. The value of v may depend on the filling factor and it could be different for sparse and dense mixtures. For sparse

mixtures the effect of v is small and u is considered as the shape factor for the inclusions. This may be to have any arbitrary shape (not necessarily spherical) for the inclusions. The value of u will vary depending upon the shape and is equal to 2 for spherical inclusions. Like v, here also, experimental results might give the solution for finding the correct u; and the value of u might also depend on the filling factor.

If the scatterers are not spherical, but of any arbitrary shape, then in Eq. (6.24) 2 is replaced by u, where u is a shape factor that is often determined empirically. Hence, Eq. (6.24) becomes

$$(\varepsilon_{\text{eff}} - \varepsilon_0)/(\varepsilon_{\text{eff}} + u\varepsilon_0) = f_i(\varepsilon_i - \varepsilon_0)/(\varepsilon_i + u\varepsilon_0) \tag{6.25}$$

As the limiting cases, it can be seen to give the component permittivities

$$\varepsilon_{\text{eff}} = \varepsilon_0 \text{ for } f_1 = 0 \text{ and } \varepsilon_{\text{eff}} = \varepsilon_1 \text{ for } f_1 = 1 \tag{6.26}$$

These are two basic requirements for a good mixing formula.

Equations (6.20) and (6.23) apply when a scatterer is situated in an unbounded homogeneous material of permittivity ε_0, which is not the case as mixtures are considered. However, for sparse mixtures where the distance between scatterers is large, the derivation and the result are probably justified because the perturbation field of a scatterer possesses a $1/r^3$-like distance dependence, and its effect is small even at regions of the nearest neighboring scatterers. For dense mixtures the question arises about the apparent permittivity that the scatterer 'sees' beyond its surface. If the permittivty outside the scatterer is ε_{eff}, the polarizability of the scatterers would increase the average polarization in the mixture in a nonself-consistent manner leading to a still bigger value for ε_{eff}. Therefore, for denser mixtures the Rayleigh mixing formula needs modification. In addition to possessing the properties of giving the component permittivities in the limit as $f_1 = 0$ and $f_1 = 1$, the modified formula should simplify to the Rayleigh formula for sparse mixtures, i.e. for cases $f_1 << 1$. A quasi-heuristic consideration gives the following result for the effective permittivity:

$$(\varepsilon_{\text{eff}} - \varepsilon_0)/\{(\varepsilon_{\text{eff}} + u\varepsilon_0) + v(\varepsilon_{\text{eff}} - \varepsilon_0)\} = \sum f_i(\varepsilon_i - \varepsilon_0)/\{(\varepsilon_i + u\varepsilon_0) + v(\varepsilon_{\text{eff}} - \varepsilon_0)\} \tag{6.27}$$

where the coefficient v is an arbitrary positive number, and the value $v = 0$ can be seen to give the classical Rayleigh mixing formula.

It also approaches the Rayleigh formula for small volume fractions f_i, where ε_{eff} is close to the background permittivity value and $v\ (\varepsilon_{\text{eff}} - \varepsilon_0)$ is small.

Equation (6.27) is implicit for the effective permittivity. An iterative solution of Eq. (6.27) converges well.

The Effect of v

Equation (6.27) is valid for complex permittivity also. If components are lossy, then so is the mixture. From the complex Eq. (6.22), the real and imaginary parts of ε_{eff} can be solved. If the losses of the inclusion phases are small and the background material is lossless, then as v increases, both real and imaginary parts of the effective permittivity

become higher. Putting $v = 0$, Eq. (6.27) reduces to (6.25) which is the standard equation for mixtures with one-dimensional scatters. However, $v \neq 0$ in case of three-dimensional scatterers as influence of the neighboring scatterers cannot be neglected.

Comparison with Other Mixing Models

The mixing theory presented above is compared with formulae presented in the literature that have been derived to explain the dielectric behavior of heterogeneous mixtures. For simplicity, the comparison is made between formulae that apply to spherical scatterers and spherical inhomogeneity geometries, although many of the formulae presented apply also to ellipsoidal inclusions. This is because the essence of a mixing formula can be seen already from the spherical case, and the generalization to ellipsoids is unnecessary as far as the comparison with rivalling models is concerned. Also for the same reason, the review is limited to mixtures that contain one type of scatterers in the background medium of permittivity ε_0. The extension to more types of inclusions can be easily carried out. With these considerations, proposed mixture formula becomes

$$(\varepsilon_{\text{eff}} - \varepsilon_0)/\{(\varepsilon_{\text{eff}} + 2\varepsilon_0) + v(\varepsilon_{\text{eff}} - \varepsilon_0)\} = f_1(\varepsilon_1 - \varepsilon_0)/\{(\varepsilon_1 + 2\varepsilon_0) + v(\varepsilon_{\text{eff}} - \varepsilon_0)\} \quad (6.28)$$

Nearly all the authors use a different notation in reporting their mixing formulae. In the following review, everyone's notation is translated to the one followed in our analysis, i.e. for two phase mixtures, the inclusion material has a permittivity ε_1 and volume fraction f_1. Most of the formulae in the literature deal with homogeneous scatterers, but there are also some that apply for two layer spheres.

The formula containing the polarizability but with no consideration of v is named the Lorentz-Lorentz formula or the Clausius-Mossotti relationship and is given as (Sihvola and Kong, 1988)

$$\varepsilon_{\text{eff}} = \varepsilon_0 + 3\varepsilon_0 f_1 \frac{\dfrac{\varepsilon_1 - \varepsilon_0}{\varepsilon_1 + 2\varepsilon_0}}{1 - f_1 \dfrac{\varepsilon_1 - \varepsilon_0}{\varepsilon_1 + 2\varepsilon_0}} \quad (6.29)$$

In solid state physics, the relation referred to as the average T-matrix approximation (ATA) is given in the form

$$\varepsilon_{\text{eff}} = \frac{\langle \varepsilon(r) \rangle - f_1 \varepsilon_1 \dfrac{\varepsilon_1 - \varepsilon_0}{\varepsilon_1 + 2\varepsilon_0}}{1 - f_1 \dfrac{\varepsilon_1 - \varepsilon_0}{\varepsilon_1 + 2\varepsilon_0}} \quad (6.30)$$

where the notation $\langle \varepsilon(r) \rangle$ implies the spatial average of the inhomogeous permittivity function $\varepsilon(r)$

$$\langle \varepsilon(r) \rangle = f_1 \varepsilon_1 + (1 - f_1)\, \varepsilon_0 \quad (6.31)$$

Bohren and Battan (1982) have analysed radar backscattering and have presented a two phase mixing formula for precipitation in the atmosphere. The formula applies for ellipsoidal scatterers. Given for spheres, it is

$$\varepsilon_{\text{eff}} = \varepsilon_0 + f_1(\varepsilon_1 - \varepsilon_0)\frac{b}{1 - f_1(1 - b)} \tag{6.32}$$

where $b = \dfrac{3\varepsilon_0}{\varepsilon_1 + 2\varepsilon_0}$.

This is easily seen to be equal to Eq. (6.31).

Formulae with $v = 2$

Formulae are also known that can be derived for Eq. (6.31) with the value 2 for the parameter v. In this case the mixing formula becomes

$$(\varepsilon_{\text{eff}} - \varepsilon_0)/3\varepsilon_{\text{eff}} = f_1((\varepsilon_1 - \varepsilon_0)/(\varepsilon_1 + 2\varepsilon_{\text{eff}}) \tag{6.33}$$

This is widely known as the Bottcher mixing formula. It can be represented in several forms. For example, the unknown ε_{eff} can be solved from the second order equation and given as a function on f_1, ε_0 and ε_1.

Another implicit form is

$$\varepsilon_{\text{eff}} = \varepsilon_0 + f_1(\varepsilon_1 - \varepsilon_0) \cdot \frac{3\varepsilon_{\text{eff}}}{\varepsilon_1 + 2\varepsilon_{\text{eff}}} \tag{6.34}$$

This is known as the Polder-van Santen (1946) formula and is much used in remote sensing applications to predict and explain the dielectric behavior of snow.

Similar representation of Eq. (6.32) due to Taylor (1946) is

$$\frac{\varepsilon_{\text{eff}}}{\varepsilon_0} = 1 - 3f_1\frac{\varepsilon_{\text{eff}}}{\varepsilon_0}\frac{1 - (\varepsilon_1/\varepsilon_0)}{2\varepsilon_{\text{eff}}/\varepsilon_0 + \varepsilon_1/\varepsilon_0} \tag{6.35}$$

In the strong influence theory of solving the electromagnetic fields in a random medium, the dyadic Green's function is decomposed, and for the propagator, field, and scatterer, new interpretations are given. In the bilocal approximation, the spatial average of the scatterer term is zero, which in this low-frequency case will be

$$\varepsilon(r) - \varepsilon_{\text{eff}}/\varepsilon(r) + 2\varepsilon_{\text{eff}} = 0 \tag{6.36}$$

De Loor (1968) has studied dielectric mixtures containing water. His result for the effective permittivity is

$$\varepsilon_{\text{eff}} = \varepsilon_0 + f_1(\varepsilon_1 - \varepsilon_0)\frac{3\varepsilon^*}{\varepsilon_1 + 2\varepsilon^*} \tag{6.37}$$

This formula contains a new permittivity value ε^*. According to De Loor, ε^* is the "effective internal dielectric constant" (a different concept than the mixture effective permittivity ε_{eff}) in which all interactions and spatial irregularities of the other inclusions are accounted for. De Loor's studies on a variety of materials have shown that the

value of ε^* lies between ε_0 and ε_{eff}. However, de Loor's formula is not consistent in the sense that it does not give the scatterer permittivity ($\varepsilon_{\text{eff}} = \varepsilon_1$) for complete filling ($f_1 = 1$) unless the choice $\varepsilon^* = \varepsilon_{\text{eff}}$ is made, in which case it reduces to the Polder-van Santen formula (1946)

$$\varepsilon_{\text{eff}} = \varepsilon_0 + f_1 (\varepsilon_1 - \varepsilon_0) \frac{3\varepsilon_{\text{eff}}}{\varepsilon_1 + 2\varepsilon_{\text{eff}}} \tag{6.38}$$

The above model with this background can be customised to a wet soil medium. Wet soil has essentially, drysoil (with dielectric constant $\varepsilon_{\text{drysoil}}$) as the background medium and three other components dispersed in it are: (i) bound water, (ii) free water and (iii) air. Let their volume fractions be f_{bw}, f_{fw} and f_{a}, respectively. Also, let their dielectric constants be ε_{bw}, ε_{fw} and ε_{a}. If the effective dielectric constant of the wet soil medium (which is a four component mixture) is taken as ε_{eff}, then the following mixture formula results from Eq. (6.27)

$$\frac{(\varepsilon_{\text{eff}} - \varepsilon_{\text{dry soil}})}{(\varepsilon_{\text{eff}} + u\varepsilon_{\text{dry soil}}) + v(\varepsilon_{\text{eff}} - \varepsilon_{\text{dry soil}})} = f_{\text{fw}} \frac{(\varepsilon_{\text{fw}} - \varepsilon_{\text{dry soil}})}{(\varepsilon_{\text{fw}} + u\varepsilon_{\text{dry soil}}) + v(\varepsilon_{\text{eff}} - \varepsilon_{\text{dry soil}})}$$

$$+ f_{\text{bw}} \frac{(\varepsilon_{\text{bw}} - \varepsilon_{\text{dry soil}})}{(\varepsilon_{\text{bw}} + u\varepsilon_{\text{dry soil}}) + v(\varepsilon_{\text{eff}} - \varepsilon_{\text{dry}})} + f_{\text{a}} \frac{(\varepsilon_{\text{a}} - \varepsilon_{\text{dry soil}})}{(\varepsilon_{\text{a}} + u\varepsilon_{\text{dry soil}}) + v(\varepsilon_{\text{eff}} - \varepsilon_{\text{dry soil}})} \tag{6.39}$$

where u, v have their usual meanings defined earlier. This can be used to predict the dielectric constant of wet soil (Sahu, 1998; Behari et al., 2001).

Calculations

The various parameters of the dielectric mixing model proposed above and the formula used to describe are discussed as follows:

Dielectric constant of free water ε_{fw} calculated from Eq. (2.15) and that of bound water ε_{bw} calculated from the Cole-Cole Eq. (2.14) (Table 2.1) are as follows:

Dielectric constant of air ε_{a} is taken as $1 - j0$.

Dielectric constant of dry soil $\varepsilon_{\text{dry soil}}$ is taken as $4.7 - j\ 0.05$. (6.40)

Porosity $= 1 - (p_{\text{s}}/p_{\text{r}}) = 1 - (p_{\text{s}}/2.66)$

where p_{s} is the bulk density and p_{r} the density of the rock ($\cong 2.66$).

Volume fraction of air f_{a} is calculated as f_{a} = porosity – volumetric moisture content, volume fraction of bound water f_{bw} = volumetric moisture content multiplied by X where X is the fraction of bound water in the total water content of the wet soil. It is a free parameter and lies in the range of 0.05-0.10. Volume fraction of free water f_{fw} = volumetric moisture content multiplied by $(1 - X)$. In Eq. (6.39), u, v are taken as free parameters, where u is the shape factor (= 2 for spherical inclusions) and v the interaction factor (= 0 if neighboring inclusions have no influence on each other). Emissivity of the soil e can be obtained using Eq. (1.21) and emissivity of the soil surface e_{surface} by Eq. (1.30). In this model, u, v and x are free parameters which are adjusted to achieve a best fit of theoretical data with the experimental ones.

The dielectric constant are measured of a particular soil type at a particular moisture content and frequency and then the values of u, v and X of the theoretical model are optimized through the method of iteration to predict the above experimental values. These values of u, v and X are then taken as standard for the whole range of moisture and frequency. The abovementioned procedure leads to the following results.

The values can be computed with the help of the following four experimental values:

ε_{soil} at 1.4 GHz and 20% soil moisture
ε_{soil} at 1.4 GHz and 30% soil moisture
ε_{soil} at 18 GHz and 20% soil moisture
ε_{soil} at 18 GHz and 30% soil moisture

This is to explain the results between 0 and 40% soil moisture levels. This ensures that estimates do not have any upper or lower frequency bias. Also, 20% and 30% soil moisture can be selected as these are the typical values for soil moistures in a typical agricultural field. The expressions for u, v and X are as follows:

$$u = -0.0167 * \text{Sand} - 0.05062 * \text{Silt} - 0.01112 * \text{Clay} - 0.0335 * \text{Moisture\_Content} + 0.085467 * \text{Frequency} + 7.956237$$

$$v = -0.00525 * \text{Sand} + 0.021627 * \text{Silt} - 0.02642 * \text{Clay} + 0.1095 * \text{Moisture\_Content} + 0.007001 * \text{Frequency} + 3.976294$$

$$X = 0.001677 * \text{Sand} + 0.001649 * \text{Silt} + 0.001267 * \text{Clay} + 0.001515 * \text{Moisture\_Content} + 0.002417 * \text{Frequency} - 0.09101 \quad (6.41)$$

It must, here, be emphasized that these values are not constant; but be dependent on soil type. Fraction of bound water in the total moisture content X can also be correlated with the soil texture parameters. The general comparison of the theoretical and experimental curves for different soils, as a function of frequency and texture along with moisture content can be summarized as follows:

Moisture Content

Figure 6.4 shows the dielectric constant as a function of m_v at various frequencies, obtained using the texture data (Table 5.5) for loamy soil (Hallikainen et al., 1985 a). There curves follow the usual feature of first a gradual increase upto a certain point, beyond which the increase is much rapid. A similar behavior is shown by ε'' vs m_v plot. As m_v increases, the specific ionic concentration falls leading to an increase in the loss factor finally reaching a transition point beyond which the increase is very sharp. Fig. 6.5 shows emissivity versus volumetric soil moisture at various angles of incidence, and confirms a good agreement.

Conclusion

A simple modified empirical model has been found to better describe the observed dielectric constants of soil-water mixtures. In this model, the dielectric constants of a soil-water mixture are computed from the known dielectric constants of air, dry

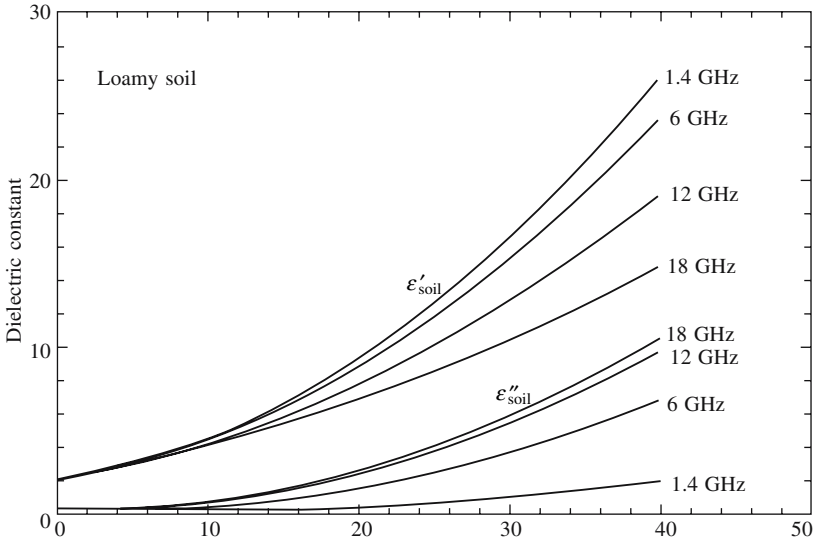

Fig. 6.4 Theoretical dielectric constant as a function of m_v.

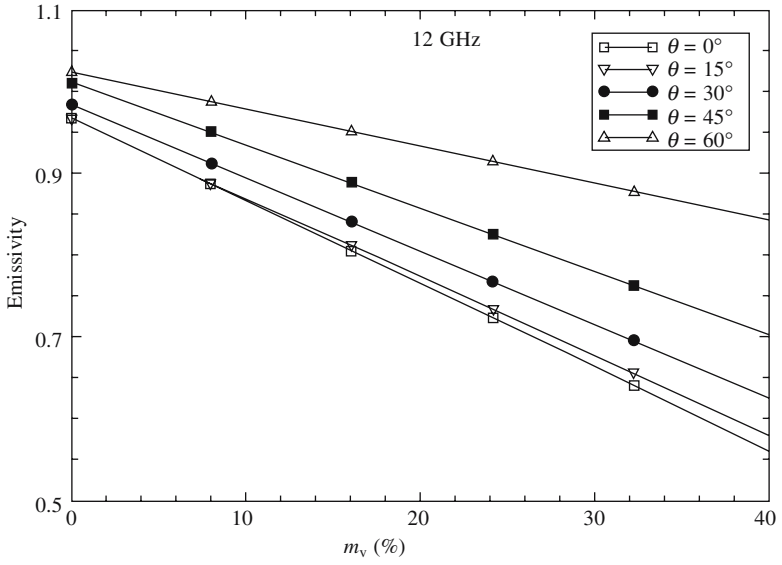

Fig. 6.5 Emissivity as a function of soil moisture at different angles of incidence.

soil, free and bound water at a given frequency, and the volume fraction of each constituent in the mixture. In the proposed heterogeneous dielectric mixing model, homogeneous scatterers of any shape are immersed in a homogeneous background material. The result is a general mixing formula for the effective macroscopic permittivity of the mixture. The treatment is self-consistent: if any component in the mixture occupies all the space, i.e. its volume fractions become unity, the effective permittivity also equals the permittivity of this component.

The empirical model gives a better description of the dielectric behavior of various soil-water mixtures than the previously existing mixing formulae. The main reason for the success of the model is that it takes into account shape factor and interaction factor of the constituents. These two free parameters are denoted as u and v, respectively and it appears that for certain positive values of u and integral values of v, many previously known mixing formulas result from the formula proposed here. For one-dimensional scatterers, interaction factor can be taken as negligible (i.e. $v = 0$). However, this is, in general, not true in case of three-dimensional scatterers. Similarly, $u = 2$ for spherical scatterers, but, not so for arbitrarily shaped scatterers. An exact solution for a random problem in three dimensions can be found by the method of iteration if experimental value of effective permittivity is given at any frequency and volume fraction.

The parameters u, v contained in the mixing formula are introduced quasi-heuristically. At low volume fractions of the scatterer phase, v has little effect, but for a high dielectric constant, e.g. mixtures containing water and high-volume filling ratios especially, mixing formulae with different values for v predict considerably different results, a larger value for v giving a larger effective permittivity. Therefore, the physical significance of the quantity v from the point of view of a single inclusion is to represent different ways of taking into account the effect of neighboring scatterers. Using the value $v = 2$, for example, replaces the background permittivity ε_0 in the denominator by the effective permittivity ε_{eff} itself, and the resulting quotient can be interpreted as being the ratio between the inside and outside fields of a sphere, as it is immersed in a background material of ε_{eff} instead of ε_0.

The parameter v appears in the form $v\ (\varepsilon_{\text{eff}} - \varepsilon_0)$. However, this is not the only possibility. It can also be shown that the mixing formula passes the tests required if $v\ (\varepsilon_{\text{eff}} - \varepsilon_0)$ is replaced by $F\ (\varepsilon_{\text{eff}} - \varepsilon_0)$, where $F(X)$ is any function with the property

$$\lim_{X \to 0} F(X) = 0 \tag{6.42}$$

The difference between the results of mixing of formulae with different degrees of self-consistency manifests itself at high volume filling ratios where the interaction between the adjacent scatterers plays a major role. Because of the many degrees of freedom of the distribution of small scatterers in the mixture, a plain volume-fraction description of the mixture is not exhaustive and like F function is needed to account for the different possible microstructures in the mixtures. This model gives a method for estimating the dielectric properties of soil over a wide range of frequencies with soil texture information and the dielectric constant of water as the input parameters.

Boyarskii et al. (2002) Model

A wet soil medium is modeled as an aerial medium with spherical inclusions of particles divided into three fractions, viz. sand, silt and clay with dielectric constants ε_{sa}, ε_{si} and ε_{d}, respectively. It is assumed that volumetric wetness V_{w} grows from 0% to max (V_{bw}), at which bound water dielectric properties become similar to those of free water, water being present only in the shape of films around clay particles and

Table 6.1 Mixed formulas used for comparison with the measured dielectric constants of soil-water mixtures

Source	Formula	Remarks
Rayleigh (1892)	$\frac{\varepsilon-1}{\varepsilon+2}=f_0\frac{\varepsilon_0-1}{\varepsilon_0+2}+f_1\frac{\varepsilon_1-1}{\varepsilon_1+2}$	$f_0+f_1=1$
Bottcher (1952)	$\frac{\varepsilon-\varepsilon_1}{3\varepsilon}=f_0\frac{\varepsilon_0-\varepsilon_1}{\varepsilon_0+2\varepsilon}$	
Brown (1956)	$\varepsilon=f_0\varepsilon_0+f_1\varepsilon_1$	$f_0+f_1=1$
Birchak et al. (1974)	$\sqrt{\varepsilon}=f_0\sqrt{\varepsilon_0}+f_1\sqrt{\varepsilon_1}$	$f_0+f_1=1$
Bruggeman (1935)	$\left(\frac{\varepsilon}{\varepsilon_1}(1-f_0)^3=\frac{\varepsilon_0-\varepsilon}{\varepsilon_0-\varepsilon_1}\right)^3$	
Wanger (1914)	$\frac{\varepsilon-\varepsilon_1}{3\varepsilon_1}=f_0\frac{\varepsilon_0-\varepsilon_1}{\varepsilon_0+2\varepsilon_1}$	
Kharadly and Jackson (1953)	$\frac{\varepsilon-\varepsilon_1}{\varepsilon+2\varepsilon_1}=f_0\frac{\varepsilon_0-\varepsilon_1}{\varepsilon_0+2\varepsilon_1}$	
Wiener (1910)	$\varepsilon=\frac{f_0\varepsilon_0 u+\varepsilon_1 f_1}{f_0 u+f_1}$,	F is an adjustable parameter
	$u=\frac{\varepsilon_1+F}{\varepsilon_0+F}$	$f_0+f_1=1$,
Pearce (1955)	$\varepsilon=\varepsilon_0\frac{f_1(1-F)}{1+f_1F}(\varepsilon_1-\varepsilon_0)$	$-1<F<1$
		f_0, f_1 = fractional volume of each constituent

is bound. At wetnesses $V_w \geq \max(V_{bw})$, water in films covers particles of all fractions and is supposed to be free. Permittivity of wet soil ε_{eff} $(=\varepsilon'_{eff}+i\varepsilon''_{eff})$ can be found from the equation

$$\varepsilon_{eff}^{-1}=1-\frac{4\pi n_{cl}(\varepsilon_{cl}^{bw}+2)\frac{\{f_w\}_{cl}}{K^2}}{2\varepsilon_{eff}+\varepsilon_{cl}^{bw}}-\frac{4\pi n_{sa}(\varepsilon_{sa}^{w}+2)\frac{\{f_w\}_{sa}}{K^2}}{2\varepsilon_{eff}+\varepsilon_{sa}^{w}}$$

$$-\frac{4\pi n_{si}(\varepsilon_{si}^{w}+2)\frac{\{f_w\}_{si}}{K^2}}{2\varepsilon_{eff}+\varepsilon_{si}^{w}}-\frac{4\pi n_{w}(\varepsilon_{w}+2)\frac{\{f_w\}_{w}}{K^2}}{2\varepsilon_{eff}+\varepsilon_{w}} \tag{6.43}$$

where n_d, n_{sa}, n_{si} and n_w are concentrations of clay, sand, silt particles and water drops; ε_{cl}^{bw}, ε_{sa}^{w} and ε_{si}^{w}, respectively, are permittivities of clay, sand and silt particles covered by bound water film; while ε_w is dielectric onstant of free water; $\{f_w\}_{cl}$ is

averaged over particle sizes amplitude of forward scatter of clay particle covered by bound water film; $\{f_w\}_{sa}$, $\{f_w\}_{si}$ and $\{f_w\}_w$ are averaged over particle sizes amplitudes of forward scatter of sand and silt particles covered by free water film and a spherical drop of water, respectively, and k is a constant. Scatter amplitudes are calculated according to the Mie theory (Bohren and Huffman, 1983). These authors have pointed that effective dielectric constants of soil particles covered by water film, ε_{cl}^{bw}, ε_{sa}^{w}, ε_{si}^{w} are defined by the Braggeman formula (Bohren and Huffman, 1983). Thus the model of ε_{eff} of wet soil considered here takes into account the structure of soil as well as free and bound water present in it.

CHAPTER 7

Synthetic Aperture Radiometer

Introduction

Passive microwave sensors have been widely used in radiometer systems (e.g. Jackson et al., 1999). These are suitable for retrieving surface soil moisture in no or low vegetation areas. In the presence of vegetation and to penetrate into deeper soil, there is a need of a radar to achieve required resolutions at lower frequencies with reduced antenna size. To address these questions synthetic aperture radar (SAR) (single or multi-frequencies) are often used. SAR is based upon principles, differing significantly from those of real aperture radars and is capable of overcoming the shortcomings of the latter. The term, synthetic aperture denotes the artificial length of the antenna, in contrast to the real aperture based upon the actual physical length of the antenna, used with the real aperture systems.

Every object on the earth is emitting radiations corresponding to its absolute temperature. A portion of these radiations falls in the microwave region. Properties of the atmosphere, which directly affect the microwave detection, is atmosphere itself (which is a source of microwave energy and this illuminates ground objects). There are several atmospheric windows in the microwave region. By using a sensor with a detector designed to receive wavelengths in one of these windows, it is possible to image ground objects. In addition to temperature of the object, other important physical properties that determine the characteristics of these radiations are emittance, transmittance and reflectance. The character of natural radiation sources that contribute to the reflected and transmitted radiations is also important. Selection of the wavelengths for operation and the aperture size would be determined primarily by the resolution needed to map particular sources. Thus, if one assumes the use of the maximum aperture attainable at each wavelength, the wavelength to be used is determined by the resolution requirements, which dictate operation at the shortest possible wavelength.

The potential of SAR interferometric techniques for the retrieval of vegetation parameters was investigated using ERS-1 data over agricultural and forested test sites. An interferometrically derived forest map can also be generated (Wegmuller and Werner, 1995). SAR can also be used to detect surface changes resulting from earthquakes, volcanoes and other related phenomena. It is established that return

signals from synthetic aperture radar (SAR) are affected by surface characteristics such as the roughness, correlation length and dielectric constant of the soil.

Synthetic Aperture

Antennas in a Linear Array

From the geometry, it is clear that an outgoing wave at the nth element leads in phase at the $(n + 1)$th elements by $kd \sin \beta$, where $k = 2\pi/\lambda$, d is the spacing between two elements and λ is the electromagnetic wavelength. Assuming that the elements in the array are isotropic, the electric field at a far field point with direction sine equal to $\sin \beta$ is (Fig. 7.1)

$$E(\sin \beta) = \sum_{i=1}^{N} e^{(j(i-1)(kd \sin \beta))} \tag{7.1}$$

Expanding the summation in this equation yields

$$E(\sin \beta) = 1 + e^{(jkd \sin \beta)} + \ldots + e^{j(N-1)\, kd \sin \beta} \tag{7.2}$$

This is a geometric series, which can be reduced to

$$E(\sin \beta) = \frac{1 - e^{jNkd \sin \beta}}{1 - e^{jkd \sin \beta}} \tag{7.3}$$

$$|E(\sin \beta)| = \left| \frac{\sin\left(Nkd \sin \frac{\beta}{2} \right)}{\sin\left(kd \sin \frac{\beta}{2} \right)} \right| \tag{7.4}$$

which is a periodic function of $kd \sin \beta$, and its period is equal to 2π.

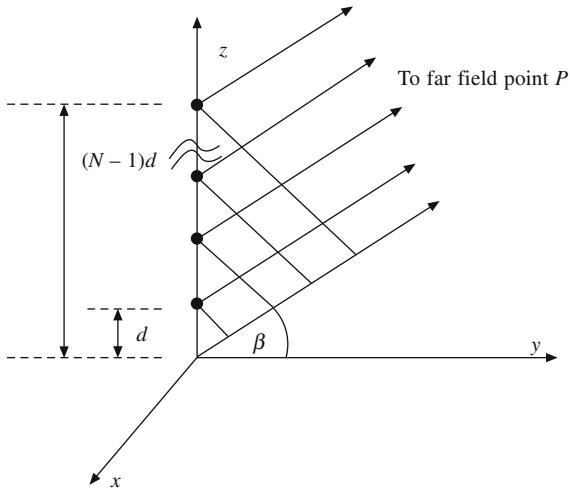

Fig. 7.1 Geometry of real or synthetic array.

The normalized two-way array pattern is given by

$$G(\sin\beta) = |E_n(\sin\beta)|^2 = \frac{1}{N^2}\left(\frac{\sin\left(Nkd\sin\frac{\beta}{2}\right)}{\sin\left(kd\sin\frac{\beta}{2}\right)}\right)^2 \tag{7.5}$$

A synthetic array is formed by the linear motion of a single element, transmitting and receiving from distinct positions that correspond to the element locations in a real array. The synthetic array geometry differs from that of a real array in that the array exists only at a single element position at a time.

Since a synthetic array exists only at a single location at a time, therefore, the returns received by the successive array positions differ in phase by

$$\delta = k\Delta r \tag{7.6}$$

where $k = 2\pi/\lambda$ and $\Delta r = 2d\sin\beta$ in the round trip path difference between consecutive element positions. The two way array pattern for a synthetic array is the coherent sum of the returns at all the array positions.

Thus, the overall two way electric fields for the synthetic array is

$$E(\sin\beta) = 1 + \exp(-j2\delta) + \exp(-j4\delta) + \ldots + \exp(-j2(N-1)\delta)$$

$$= \sum_{n=1}^{N} \exp(-j2(n-1)kd\sin\beta) \tag{7.7}$$

The two way radiation pattern is then

$$G(\sin\beta) = |E(\sin\beta)| = \left|\frac{\sin(Nkd\sin\beta)}{\sin(kd\sin\beta)}\right| \tag{7.8}$$

Equations (7.5) and (7.8) indicate the two-way radiation for a real array of the form $(\sin\theta/\theta)^2$ while it is $(\sin 2\theta/2\theta)$ for the synthetic array, i.e. the resolution of a synthetic array of length L (aperture size) is equal to that of a real array with twice the aperture size ($2L$), as illustrated in Fig. 7.2.

Doppler Effect

An issue connected with the synthetic antenna concept is the one based on the Doppler frequency shift. This arises because of the systematic changes in the frequency experienced by the radar signals as it is scattered by the landscape. Objects within the landscape experience different frequency shifts in relation to the distance from the aircraft track. At a given instant, objects at the leading edge of the beam reflect a pulse with an increase in frequency due to their position ahead of an aircraft and those at the trailing edge of the antenna experience a decrease in frequency. Knowledge of frequency shift permits the system to assign reflections to their connect positions on the image and to synthesize the effect of a long antenna (Fig. 7.3).

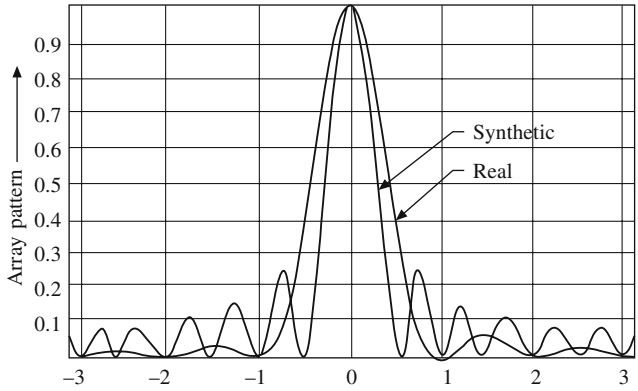

Fig. 7.2 A comparison between real and synthetic arrays (Mahafza, 1998).

The total Doppler frequency excursion between $-v/L$ to v/L is the Doppler's band width

$$\Delta f_D = 2v/L \tag{7.9}$$

This is the bandwidth appropriate to the signal. The Doppler bandwidth is totally independent from range location of the target, which accounts for the range independence of the azimuth resolution.

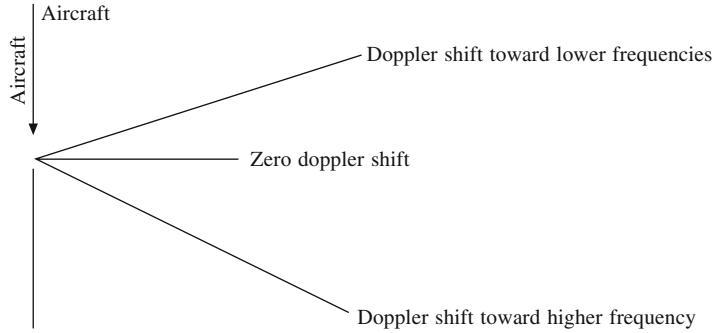

Fig. 7.3

Synthetic Array Approach

It can be understood that an array of antennas is equivalent to a single antenna moving along the array line as long as the received signals are coherently recorded and then added. Assuming that the radar sensor is moving at a velocity v, the length L' of the antenna main beam footpoint on the surface in the azimuth direction is equal to

$$L' = 2\lambda \frac{h}{L} \tag{7.10}$$

As the sensor moves, successive echoes are recorded at points X_1, X_2, ... X_n ... along the flight line. An onboard stable oscillator is used as a reference and the echoes are

recorded coherently as a function of time. These echoes are then combined to synthesize a linear array. From Fig. 7.4(a) and (b) it can be seen that the maximum array length that could be achieved is equal to L', the real antenna footpoint. The synthesized array will have a beam width θ_s as

$$\theta_s = \frac{\lambda}{L'} = \frac{L}{2h} \tag{7.11}$$

and the resulting footpoint on the ground is

$$X_a = h\theta_s = \frac{L}{2} \tag{7.12}$$

This result is indicative of the finest resolution achievable using a synthetic array.

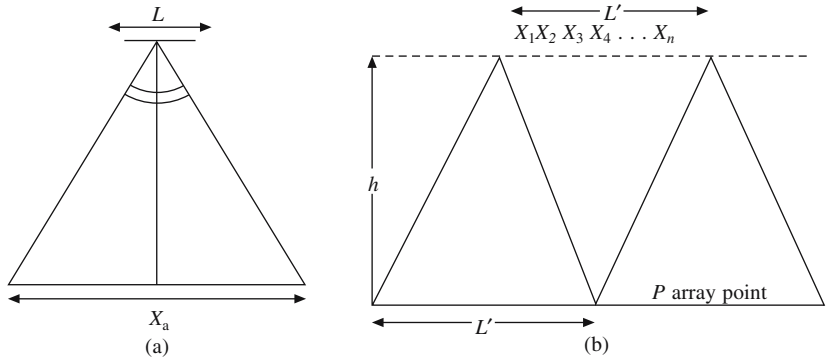

Fig. 7.4 (a) The radar sensor moving with a velocity and (b) as the sensor moves the position of successive echoes is given as $X_1 \ldots X_n$.

Equations (7.11) and (7.12) have two notable features:

(1) Ultimate resolution is independent of the range, wavelength and the area being imaged. This stems from the fact that farther is the sensor, the larger the footpoint on the ground, hence, longer the synthetic array.
(2) Finer resolution can be achieved with a smaller antenna. Thus, smaller the antenna, larger is the footpoint and synthetic array. This leads to a finer synthetic beam, and therefore, a finer resolution (Elachi, 1987).

Synthetic Aperture Radiometer

Theoretical Background

The concept of aperture synthesis was earlier used in radio astronomy to obtain higher resolving power with an antenna array using small number of individual elements. In this, a very long antenna is synthesized by moving a small one along a convenient path. The advantage of aperture synthesis is that it can achieve spatial resolutions equivalent to total power radiometers with large effective collecting area

(= A_{sys}) using small antennas A_e. This causes a reduction in sensitivity, which is compensated, since the synthetic aperture system does not need to scan and collect energy from many independent antenna paths.

The main limitation of these sensors, referred to as real aperture radars (RARS) is the poor resolution available with the operating wavelength. This is referred to as sensor-to-surface distance times the sensor angular resolution; the latter is proportional to the ratio between the radiation wavelength and the sensor antenna dimension. Fig. 7.5 (a) gives the position of the aircraft so that it traverses specific region of the landscape. The position (1) falls in the area illuminated by the radar beam. A SAR system utilizes the fact that the objects within the scene are illuminated by the radar over an interval of time, as the aircraft moves along the flight path. A SAR system receives the signal scattered from the landscape during its flight path. Fig. 7.5 (b) shows the block diagram of the instrumental set-up for SAR syntheses.

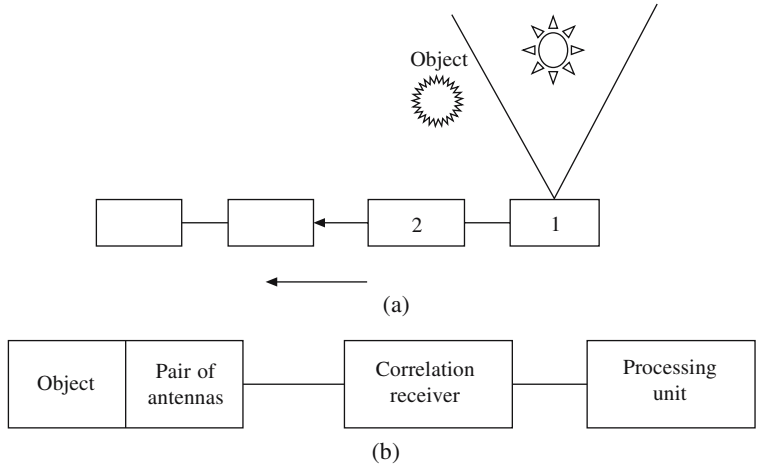

Fig. 7.5 (a) Synthetic aperture system receives backscattering signals as the antenna moves along the object. 1: Object falls within the radar illumination; 2: Object falls outside and (b) block diagram of synthetic aperture radar.

The measurement of soil moisture and sea surface salinity is important for exploring the earth environment. These parameters are measured at L-band (1.413 GHz) and are important for understanding the global hydrologic cycle, energy exchange with the atmosphere and, therefore, are important for improving understanding of weather and climate change (Le Vine et al., 1989). However, the scientific requirements for the measurement of these parameters globally from space demand a resolution on the order of 10 km. To obtain resolution of 10 km at 1.4 GHz would require an aperture of more than 15 m in a low earth orbit at an altitude of 800 km. The technical problems encountered in placing large scanning antennas of this size in an orbit are prohibitive, thereby discouraging the use of passive microwave sensors. A typical value of an aircraft antenna diameter is 1 m. A possible means to overcome the size limitation is to adopt aperture synthesis. In this method correlation receivers are used to coherently measure the product of the signal from pairs of antennas with differing

antenna spacings. A schematic diagram of aperture synthesis and the pictorial view is shown in Fig. 7.6. It is a coherent imaging sensor used in this technique, is an all weather device having high resolution and possesses night imaging capabilities.

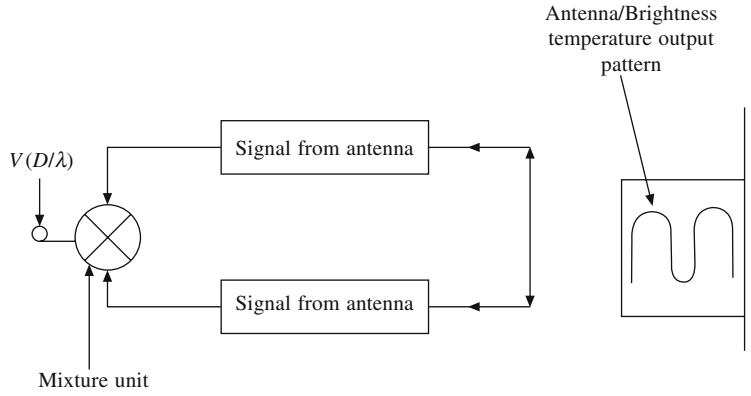

Fig. 7.6 The two-dimensional synthetic aperture radiometer.

The S- and L-microwave radiometer (SLMR) is a dual frequency passive sensor system operating at S-band (2.65 GHz or 11.3 cm) and L-band (1.413 GHz or 21.2 cm). The radiometric sensitivity of each radiometer is 0.1 K for a one second integration time. The SAR interferometric phase is essentially a measure of the path length difference between the target and the two sensor positions. It can be used to derive the three-dimensional (3-D) of the image resolution element, allowing the derivation of the height maps and the capability or recording minute variations overtime (Rosen et al., 2000). The signal obtained by the antenna is processed to obtain higher resolution.

Experimental Description

The concept of applying aperture synthesis to remote sensing from space is to evolve a configuration that permits substantial thinning of the array and at the same time maintaining radiometric sensitivity to meet the demand of the situation. The use of technique in two-dimension for earth observation is shown in Fig. 7.7. In aperture synthesis, the coherent product (correlation) is proportional to the spatial Fourier transform of the intensity of the source at a frequency which depends on the spacing between the antennas. By this method, it is possible to determine the Fourier spectrum of the source and then a map of the source itself. The resolution obtained in this manner depends on how well is the spectrum sampled. The size of the antenna is not important. The signal from pairs of antennas is measured at different antenna-pair spacing.

If the outputs of the two isotopic antenna elements are multiplied, the equivalent output is described by the relationship (Swift et al., 1991)

$$F(d) = \int_{-\pi/2}^{\pi/2} T_{\mathrm{B}}(\theta) \exp\left[-j\left(\frac{2\pi d}{\lambda}\right)\theta\right] d\theta \tag{7.13}$$

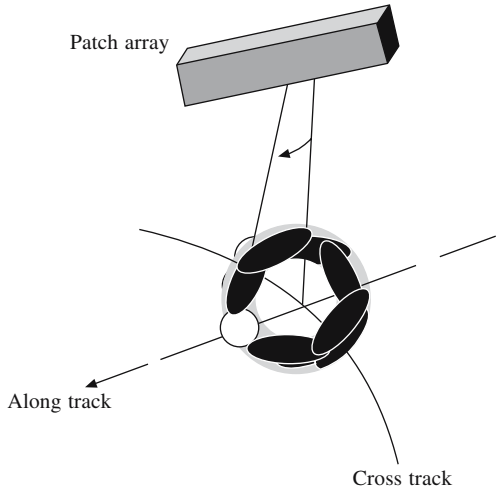

Fig. 7.7 The mixing of signals from a pair of antenna and then fed to processing unit in a synthetic aperture radiometer. On the screen is the output pattern.

where θ is the incidence angle and $F(d)$ the visibility function. For the space ($0 < d < D$), F is the Fourier transform of the thermal emission (Fig. 7.7).

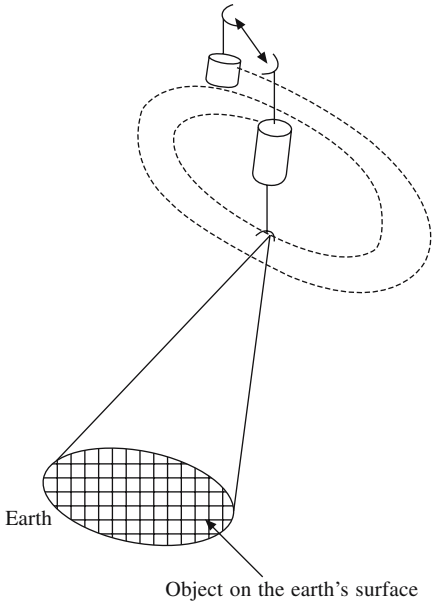

Fig. 7.8 Illustration of the use of aperture synthesis for remote sensing of the earth (adopted from Le Vine, 1999).

Figure 7.8 illustrates the application of this technique to remote sensing from space. Consider two antennas in orbit, one spiralling around the other, and interrogating the same target on the surface of the earth. At intervals (indicated by the dashes), the signals from the two antennas (thermal radiations received from the surface) are multiplied and then averaged. It can be shown that this product is proportional to the Fourier transform of the brightness temperature of the scene evaluated at a frequency that depends on the spacing between antennas. Hence, every dash in Fig. 7.8 represents the measurements of a sample point of the Fourier transform of the scene at a different frequency (Le Vine, 1999). When the spiral is complete, sampled transform can be inverted to obtain an image of the object. The reconstructed image so obtained, includes all the pixels in the entire field of view of the antennas. In the synthetic aperture radar interferometry two small antennas means a decrease in signal-to-noise ratio for each measurement compared to a filled aperture. This results in a decline of

radiometric sensitivity in the image. In practice, remote sensing from space, time limitations are dictated by the motion of the spacecraft (about 7 km/s) in low earth orbit and consequently, the time constant of the object.

In this case the sensitivity obtained with aperture synthesis is proportional to that obtained with a local power radiometer of the same temperature bandwidth and integration. The figure of merit of a single total power radiometer is indicated by ΔT as (Swift et al., 1991)

$$\Delta T = \frac{T_{sys}}{\sqrt{BT}} \tag{7.14}$$

where T_{sys} is the system noise temperature, B the system bandwidth, and T is the post detection integration. In addition ΔT of the thinned array depends upon the size of the array and the degree of thinning.

Signal-to-Noise Ratio (SNR)

Signal-to-noise ratio is defined as the change in mean output as a result of the presence of the signal divided by the standard deviation of the output when the signal is zero.

Following Le Vine et al. (1990), we can write an input voltage X_i in the form

$$X_i = X_i^0 + \chi_i \tag{7.15}$$

where X_i^0 is the antenna's output from a constant background (ambient signal) over which voltage changes are imposed and χ_i is the voltage change against this background, which contains the relevant information, and is to be detected.

Redundancy Array

Consider an array of n antennas and assume that measurements are made on all $n(n+1)/2$ antenna pairs. If n is large and no pairs have the same baseline and are having uniform space (zero redundancy), ΔT becomes

$$\Delta T = \frac{T_{sys}}{\sqrt{BT}} \frac{A_{syn}}{nA_e} \tag{7.16}$$

where A_{syn} is the equivalent area for the synthesized beam.

ESTAR

The application of aperture synthesis for remote sensing has been demonstrated successfully using an aircraft instrument called electronically scanned thinned array radiometer (ESTAR) (Fig. 7.9). To make measurements from space, in ESTAR a balance is obtained between the achievable sensitivity and the reductions in the antenna size (i.e. nA_e) (Murphy et al., 1987; Le Vine et al., 1989).

The concept is to obtain an increase in sensitivity by doing aperture synthesis in one direction only. In this setup, spatial resolution is achieved in the long track dimension by employing long stick antennas aligned parallel to the motion of the spacecraft. The resolution in the other dimension is achieved by means of aperture synthesis using pair of stick antennas (Le Vine et al., 1989; Swift et al., 1986). As mentioned, aperture synthesis reduces the required number of stick antennas. In a typical set-up (Le Vine et al., 1990) the centre frequency is chosen as 1.413-5 MHz. The signal from each antenna is split and mixed to 113.5 MHz in one path and 143.5 MHz in the other. The system, thus, produces output around 30 MHz. In this configuration, the number of sticks chosen is such that in a minimum redundancy array, spacing is an integer multiple of $\lambda/2$. The stick antennas produce a narrow 'fan-like' beam providing resolution in the direction of motion and with little resolution in the cross track dimension. ESTAR has five sticks and each stick antenna consists of a row of eight dipoles. The stick antennas are spaced at integer multiples of $\lambda/2$ (10.5 cm L-band). With the configuration employed in ESTAR it is possible to obtain synthesized beam with a width of about ± 3° at nadir in the cross track dimension. The synthesized beam is scanned in the cross track dimension using ESTAR, whereby synthetic aperture images can be calibrated for the measurement of soil moisture. The sensitivity in this SAR configuration is obtained from the relationship

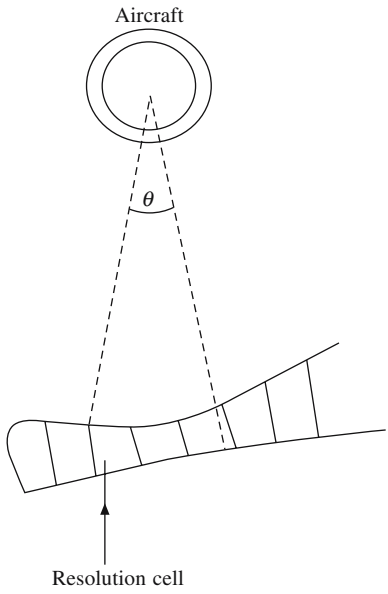

Fig. 7.9 ESTAR radiometer for remote sensing from an aircraft.

$$\Delta T = \frac{T_{sys}}{\sqrt{BT}} \frac{L}{nW} \tag{7.17}$$

where L and W is the length and width of the stick, respectively, and A_e (= WL) is the area. This is the sensitivity of each pixel in the image formed by the hybrid sensor. The ratio (L/nW) is the total available area, which is occupied with receiving antenna. By reducing L/nW (fill factor), one can reduce the weight but at the same time it reduces the sensitivity. Hence, for the applications to remote sensing from space, an adjustment be made between thinning of array and the required sensitivity. In the application to soil moisture the required measurement can be carried out keeping empty space to the extent of 80% (Le Vine et al., 1989).

ESTAR is essentially an L-band radiometer in the hybrid configuration. It is practical for application in space and requires simple processing. An algorithm based

on the regression analysis of the simulated surface backscattering coefficients by the single scattering model (Integral Equation Method, IEM) is developed. This provides an estimation of soil moisture and surface roughness parameter from L-band SAR co-polarized measurements over bare and short vegetated fields. The single scattering (IEM) is quite complex and its simplification is sought for practical applications. This simplification procedure takes the form of a regression between the calculated backscattering coefficients and surface parameters (i.e. soil moisture, r.m.s. surface height, surface correlation length). The general features of the ESTAR image correspond to the major feature of the landsat image.

Aircraft ESTAR

Swift et al. (1991) have described an airborne (prototype) system that uses five stick antennas consisting of a linear array of eight dipoles. The stick antennas are spaced at integer multiples of a half wavelength (~10.5 cm). The result is a synthesized beam at nadir in the cross track dimension.

Hydrostar

Hydrostar is a synthetic aperture radiometer designed to (i) obtain global maps of soil moisture and (ii) sea surface salinity from space. This measurement employs aperture synthesis in the cross track dimension, operating at L-band with horizontal polarization. By using aperture syntheses in the cross track dimension, the aperture needed in space is reduced to less than 20% of that needed for a filled aperture of the same resolution and does not require need for mechanical motion. Hydrostar has sixteen antennnas arranged in a minimum redundancy configuration. Typical features of hydrostar are shown in Table 7.1.

Table 7.1 Typical specifications of a hydrostar (Le Vine, 1999)

Frequency	1.413 GHz
Polarization	Horizontal
Field of view	± 450 km
Pointing	Nadir
Dimensions	5.8 × 9.5 meters
Antennas	16 Waveguide sticks
Resolution	30 km (minimum)
Sensitivity	1 K
Accuracy	3 K and more

The instrument consists of three major components: (i) antenna system, including the stick antennas and the deployment structure, (ii) RF system and (iii) signal-processing unit. In its normal operating mode, the integration time per image is set at 0.55. Following are the features of hydrostar mission:

(1) Sunsynchronous orbit.
(2) Employs 675 km orbit and revisit time of approximately three days.
(3) Processing in the cross track dimension to ± 35°.

Meteorological Observations

From present point of interest the critical *in situ* observation is the soil moisture. For gravimetric soil moisture sampling, the method adopted is to extract mass of soil from a known depth and then obtaining a wet and oven dried weight. A practical problem associated with long term intensive studies is that if one attempts to take all the samples within the footprint of a sensor, the intrusion of surface over time may alter its surface conditions. To overcome this problem a large and homogeneous area is chosen to permit sampling outside the SLMR footprint. However, some variability within the chosen area is still possible over a period of time. This is based on visual observation. Soil moisture sample can be collected at 0-1, 0-3, 0-5 and 0-15 cm depth from soil layers over an area adjacent to the sensor footprint. Each time microwave data can be collected from desired layer.

Sensitivity to soil moisture for bare soil remains about the same down to a wavelength of 5 cm. As is obvious that in the presence of vegetation the use of longer wavelengths for soil moisture estimation provides greater sensitivity. When shorter wavelengths (< 5 cm) are used, sensitivity declines. This corresponds to the fact that as the wavelength decreases, attenuation increases, suggesting an increase in sensitivity to vegetation water content. The general trend is indicative of that the rate of change is rather small down to 10 cm and then shows a rapid increase. Due to an increase in sensitivity to vegetation structure at short wavelength, the wavelength decreases while scattering increases. Accounting for scattering at these shorter wavelengths necessitates the use of more sophisticated models and consequently a lot more information about the canopy, which may not be available for soil moisture by remote sensing measurements. For soil moisture determination an accuracy of such information is not reliable. To fill this gap, ground truth data may be obtained on a miniature scale by frequency domain or time domain techniques, over a described depth and duration.

An extremely shallow depth of the soil (<1 cm) contributes to the measured brightness temperature at X- and *ka*-band of wavelengths. At the L-band, the effects are apparent upto a depth of 5-10 cm. This is the same depth that some workers have adopted based on experimental evidence (Jackson and Schmugge, 1989).

Analysis of SAR Data

The ERS scatterometer is a radar operating at 5.3 GHz and has been flown over European Remote Sensing satellites ERS-1 and ERS-2. The ERS scatterometer illuminates the earth surface in three different directions using three antennas. Multiple weaving capabilities of this instrument permits to separate seasonable vegetation and soil moisture effects on the signal. The instrument has a spatial resolution of 50 km. SAR has flown from ERS-1 and ERS-2.

Moghaddam et al. (2000) developed the concept of a SAR system operating simultaneously at UHF (435 MHz) and VHF (118 MHz) to enable vegetation and deep soil penetration. These authors have concluded that in a tall boreal forest stand at least two frequencies and multiple polarizations are needed to solve the inverse problem of computing soil moisture by separating the canopy and soil contributions and have claimed their results within 4% (volumetric) of the general measurements.

With the availability of ERS-1 data over different geographical areas, various investigators have examined ERS-1 SAR response to soil moisture. Demirican et al. (1992) and Mohan et al. (1992) have obtained high values of correlation coefficients between radar backscatter and soil moisture in presence of corn and mustard, respectively. Mohan et al. (1993) subsequently prepared soil moisture map demonstrating the possibility of using ERS-1 SAR for soil moisture mapping over large areas. ERS-1 SAR sensor suitability for soil moisture determination has also been demonstrated by various other investigators (Venkataratnam, 1993; Rambatch et al., 1982).

The sensitivity of SAR to differences in soil water has been shown in previous studies (Dobson and Ulaby, 1986; Dobson et al., 1992; Wooding et al., 1993). In fact, Dobson et al. (1992) conclude that ERS-1 SAR is sensitive to the level of near surface soil water for bare and grass covered soils and that soil water is predictable from SAR measurements in those conditions.

Mathieu et al. (2003) established relationship between radar set SAR data and surface moisture content of agricultural soils. They found that the average radar backscatterer is well correlated to the seasonal change of the average moisture content ($r^2 = 0.75$), although the data with a strong vegetation growth affected the relationship. They further pointed out that organic soils exhibit a lower backscatter, especially at lower moisture content levels, suggesting that soil type is important for monitoring soil moisture changes. At the field level the relationship is much lower ($r^2 = 0.44$). The quality of the relationship was proportional to the vegetation cover and is crop dependent.

Sahebi et al. (2003) made an estimation of the moisture content of bare soil from RARARSAT-1, SAR adopting simple models. Previous results have described the relationship between σ^0 (dB) and volumetric soil moisture m_v as linear

$$\sigma^0 = C + Dm_v \tag{7.18}$$

where C is the backscattering coefficient of a dry soil and $D = d\sigma/dm_v$ is the radar sensitivity to soil moisture that is dependent upon the radar configuration (Attema and Ulaby, 1978).

The backscattering coefficient varies with the sensor parameters (frequency, polarization and incidence angle) and the target parameters (roughness and moisture for a bare soil). In Eq. (7.18), for a given frequency and polarization, soil moisture is related to D, in which case C can be expressed as a function of roughness and incidence angle. Sahebi et al. (2003) used two models based on Eq. (7.18). The first model (Ji et al., 1995) expresses as

$$\sigma^0 = C^1 + A^1 S + Dm_v \tag{7.19}$$

where A^1 and C^1 are the constants for a given radar configuration and S the r.m.s. height of surface roughness (cm).

The second model (Champion, 1996) is

$$\sigma^0 = C_1 + C_2 \cos(\theta)\, C_3 + Dm_v \tag{7.20}$$

where θ is the incidence angle and C_1, C_2 and C_3 are constant coefficents.

According to Eqs. (7.19) and (7.20), it would appear that neither of these models

could represent all the variables that have an influence on the radar response. Ji's model (1995) depends on the roughness, though not sensitive to the incidence angle. Sahebi et al. (2003) proposed a model using the r.m.s. height roughness and incidence angle as

$$\sigma^0 \text{ (dB)} = A_1 + A_2\, C \cos(\theta) + A_3 + A_4 \ln(S) + Dm_v \tag{7.21}$$

The constants A_1, A_2, A_3, A_4 and D were calculated for a configuration of C-band, horizontal H polarization, using the nonlinear least square method. The model describes the soil moisture content for all soil moisture content for all radar configurations, even for incidence angles near 50° and over rough surfaces.

Oldak (2003) carried out mapping of near-surface soil moisture on regional scale using ERS-2 SAR-data. For multi-temporal backscatter, they reported relation between soil moisture V_{SM} and the backscattering coefficient in the form

$$V_{SM} = a(\sigma_{f_1}/\sigma_{f_2}) + b \tag{7.22}$$

V_{SM} is related to normalized radar backscatter soil moisture index (NBMI).

NBMI is defined as

$$\text{NBMI} = \frac{\sigma_{f_1} + \sigma_{f_2}}{\sigma_{f_1} - \sigma_{f_2}} \tag{7.23}$$

where σ_{f_1} and σ_{f_2} are backscatter values at different times t_1 and t_2, respectively, and a and b are constants. SAR images available from the ERS-2 satellite platform can be used to monitor soil moisture changes over extended periods at the regional scale.

It is hoped that further investigations in this area will quantitate the soil moisture data.

CHAPTER 8

Conclusion and Future Challenges in Remote Sensing

Despite the fact that enormous efforts have gone into the modeling and experimentation regarding soil moisture, it still remains an attractive subject of investigation, for its dependence on a variety of parameters. Use of soil moisture as an input produces slightly better results compared to those using brightness temperature. The physical linkages between soil moisture and soil texture is much stronger than those between brightness temperature and soil texture. At a particular point in time and place soil moisture content is influenced by (1) precipitation history, (2) texture and heterogeneity of the soil, which is key to the water-holding capacity, (3) topography, the slope and variation of the land surface, which affects runoff and infiltration and (4) the vegetation and land cover, which influences evapotranspiration and deep percolation.

A significant knowledge base exists in the soil physics and groundwater literature that focuses on development and refinement of methods to estimate soil physical and hydraulic properties (Van Genuchten and Nielsen, 1985; Feddes et al., 1988; Jury et al., 1991; Ahuja et al., 1993). Most of these studies, however, have used laboratory scale or *in situ* measurements to describe and predict soil properties.

Microwaves contribute very insignificantly to the energy budget of the earth-atmosphere system. However, its mode of travel and interaction with the atmospheric environment and at the earth surface in this remote frequency range renders it a valuable tool to obtain information about soil moisture and important parameters for the earth-atmosphere energy budget and its hydrological cycle. Clouds contribute to the microwave radiations to an extent, which in the lower frequency end is closely related to the integrated cloud liquid water content (Simmer, 1999).

The use of various active and passive microwave remote sensors (Georgakakos, 1996) has enhanced the capability to monitor soil moisture across a range of scales (i.e. hundreds of square meters to thousands of square kilometers) (Dubayah et al., 1997; Oldak et al., 2002) with varying resolution encompassing various soil types (e.g. texture) topographic features (e.g. slope), vegetation and climatic conditions. This is primarily due to the availability of better analogue components and circuits and on the other hand due to the impressive progress in the field of digital signal processors (Ottl et al., 2000). A comparative projection of these two techniques is shown in Fig. 8.1.

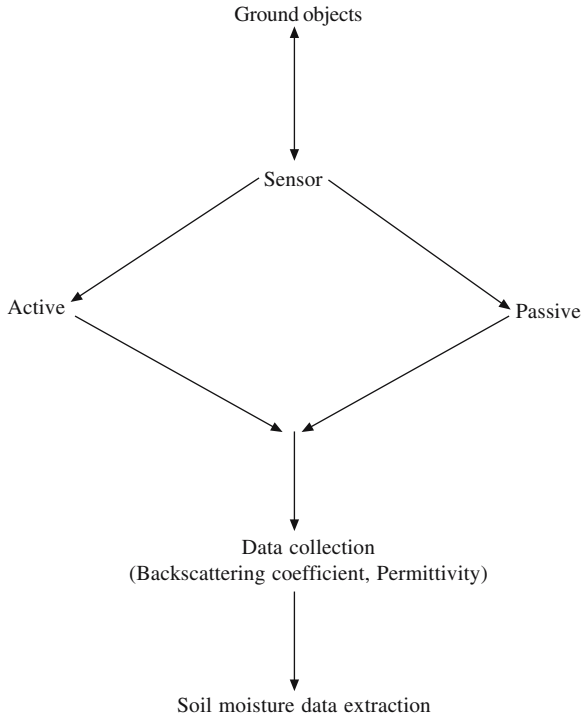

Fig. 8.1 Soil moisture extraction by microwave remote sensing.

Ground based experiments and some aerial borne observations have initiated recent airborne systems. The main factors which affect the accuracy of this determination include vegetation cover, soil properties and surface roughness. Vegetation is the most important because a thick enough layer can totally obscure the soil surface from observation. However, surface roughness will reduce the range of the microwave response by as much as half in extreme situations, more probably the effect is perhaps a 10-20% reduction in sensitivity. Physical principles and experimental verification suggest that a 21 cm radiometer of suitable size (20 m) can provide repetitive information about surface soil moisture variations on a global scale with a spatial resolution useful to hydrometeorology and hydroclimatology (Schmugge et al., 2002).

Georeferencing and co-registration of multitemporal data are essential to enable ground sets to be traced over time and satellite data to be compared with ancillary data. These results also demand the need of ground truth data to validate. These include radiometric field measurements, surface features, description and mapping, as well as soil sampling for laboratory analysis.

Passive Remote Sensing

Passive microwave remote sensing is becoming an increasingly large source of information for several aspects relating to the atmospheric sciences. Passive microwave measurement also contributes to our understanding of the energy and water cycle of

the earth-atmosphere system. An accurate knowledge of basic atmospheric parameter like the temperature and water vapor profile, cloud properties and precipitation will have an overhaul bearing on remote sensing parameters.

Using remote sensing techniques it is possible to determine the moisture content of the surface layer of the soil by about one-fourth of a wavelength thickness, i.e. about 0-5 cm layer using a 21 cm wavelength. In general, it has been found that the longer wavelengths are better for increased sampling depth and also help in reduction of noise factors such as vegetation and surface roughness (Schmugge and Jackson, 1994; Wigneron et al., 1998).

With remote sensing we not only observe the surface but can also obtain the spatial variability. If the observations are made repeatedly, we can as well obtain the temporal variability. A major focus of remote sensing research in hydrology has been to develop approaches for estimating hydrometeorological states and fluxes. The primary set of variables include land surface temperature, near surface soil moisture, snow cover/water equivalent, water quality, landscape roughness, land use and vegetation cover. Methods have been used to quantify the components of the water and energy balance equation using remote sensing methods.

Energy and water balance at the land surface are closely linked to the energy balance equation as (Schmugge et al., 2002)

$$R_N - G = H + LE$$

where R_N is the net radiation, G the soil heat flux, H the sensible heat flux and LE the latent heat flux. The quantity $R_N - G$ is the available energy and LE represents the water vapor exchange rate across the surface atmosphere interface.

Measurements of soil physical hydraulic properties are time consuming and expensive. In addition, a large number of measurements are necessary to quantify their space time variability. Reliable measurement of these properties is confounded by the extreme spatial heterogeneity and inherent nonlinearity of soil characteristics. Therefore, it is desirable to develop simplified methods to characterize soil media properties over large areas. Future goals are therefore restricted to obtain soil media properties over large remote and inaccessible areas where conventional *in situ* techniques may not be easily available or will be too expensive and time consuming.

Future Trends

Smooth surface such as water layer or ground-ice beneath an eolian surface may be detectable down to ~4.4 to ~6.5 m with P-band (441 MHz, 68 cm) (Daniels et al., 2003). Airborne and spaceborne radar instruments through the range 100 MHz (3 m) to 10 GHz (3 cm) along with the use of theoretical models have great potential for subsurface environmental exploration in 15% of the world's surface falling under arid and hyperarid zone. Interference and scattering experiments with buried reflectors of finite size (Fig. 8.2) have been deployed to quantify and evaluate through modeling the subsurface detection depth across the microwave wave band into the VHF band (10 GHz to 150 MHz). Results can also be compared with the optical modeling approach (Blumberg et al., 2002). These scattering models together with optical

modeling scenarios will allow us to predict and understand the detection of subsurface specular surfaces as a function of polarization, frequency, angle of incidence, radar sensitivity, soil composition and moisture. The prediction is of immense use in the design and selection of airborne and spaceborne radar instrumentation. If this technique is successful, experiments can be performed with buried rough surfaced objects in sand and other soils types.

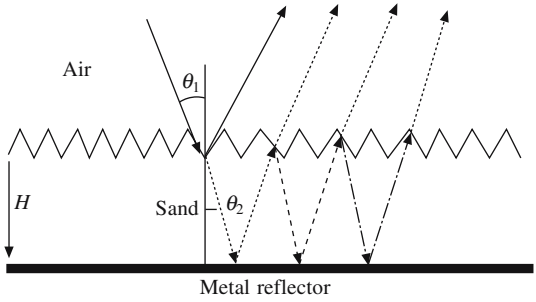

Fig. 8.2 Microwave propagation in the air-soil-reflector interfaces and sand layer. Total microwave power reflected is the sum total of that reflected from the successive interfaces.

Passive microwave measurement remains the major source of information to determine instantaneous precipitation and its occurrence over a period of time, on a global scale. The retrieval quality of precipitation over ocean areas is currently in the range of surface based radar measurement (uncertainty about a factor of two); over land areas error margin may be more. For the redistribution of the net radiation energy absorbed at the surface, vegetation and soil moisture are the most important parameters by way of controlling the turbulent fluxes of sensible and latent heat between land surface and atmosphere. Thus, sensors in the solar spectral range are mostly sufficient to monitor vegetation changes, which partly control evapotranspiration via the canopy resistance. But passive microwave signatures may provide different set of valuable information (Bennartz and Gutman, 1998). Soil moisture controls evapotranspiration most effectively when the soil becomes dry. Since soil moisture determines the land surface temperature via the separation into sensible and latent heat, therefore, soil moisture is an important input parameter for atmospheric modeling. Bennartz and Gutman (1998) first showed theoretically that the downwelling microwave radiation at the bottom of the atmosphere is related to the difference of the vertically and horizontally radiation measured at the top of the atmosphere. They also proved with model calculations that the downwelling microwave radiation is related to the downwelling broadband thermal infrared radiation. Measurements over the oceans like cloud liquid water, total water vapor content and wind speed can significantly contribute to better weather forecasting due to the advanced assimilation techniques that can handle many complex set of informations, like satellite measured radiances, without being constrained to the model variables.

The value of operational monitoring of soil moisture by *in situ* methods is rather limited for regional and global scale problems. Currently remote sensing techniques

provide the most feasible capability to bridge this gap and monitor soil moisture variations over a desired range of space and time (Schmugge et al. 1980, Jackson and Schmugge, 1989; Islam and Engman, 1996; Engman, 1997).

However, the remote sensing technique has to go a long way to find comparison with ground based observations. The shallow moisture sensing depth (<10 cm) imposes a serious limitation on the use of passive microwave measurement of soil moisture for land atmosphere interaction studies. Kostov and Jackson (1993) concluded that proper integration and sequential assimilation of remote sensing of soil moisture combined with physical modeling appeared to be the most promising approach to solve the demand of profile of soil moisture estimation. An illustration, using model generated data, of such an approach was provided by Entekhabi et al. (1994). They used hourly brightness temperature from their model generated profiles and showed that the estimated profile closely approximates the model generated profile during a one week period of drying soil moisture conditions. To assess the efficacy of this approach, an experimental verification is required. A single daily assimilation of surface soil moisture is guided by the consideration that traditional passive microwave radiometer experiments provide one observation of surface at a given wavelength (Jackson et al., 1997). A comparison of predicted and observed soil moisture profile would provide a comparison of precipitation measurements and surface soil moisture measurements. Once the soil moisture profiles are predicted these can be compared with *in situ* measurements, which are always taken as the correct data. For a specific layer, there are three time series W^0, W^p and W^m, denoting observed soil moisture, predicted soil moisture with precipitation measurements, and predicted soil moisture with atmospheric forcing as well as sequential assimilation of daily microwave measurements, respectively. Absolute error E is defined as follows (Li and Islam, 1999):

$$E_i^p = |W_i^p - W_i^0|; \quad i = 1, 2, 3, 4$$

$$E_i^m = |W_i^m - W_i^0|; \quad i = 1, 2, 3, 4$$

The state of soil moisture at the surface and in the profile plays an important role in the partitioning of sensible and latent heat fluxes and infiltration and surface runoff.

Daily assimilation of surface soil moisture predicts the soil moisture profile and partitioning of surface fluxes better than the model prediction alone. The profile prediction is less accurate for deeper layers. This is because the model has only four prognostic layers, and the distance between the two consecutive layers, increases geometrically as we go into the deeper layers. In reality, microwave provides instantaneous measurements of soil moisture. Thus, additional experiments are needed with actual measurements of surface soil moisture from remote sensing to confirm and extend the findings of this research. Experimental results from Li and Islam (1999) provide an understanding of relative merits of precipitation measurements and microwave measurements of surface soil moisture for the estimation of soil moisture profile. To characterize the space-time structure of soil moisture profile and

surface fluxes partitioning, we need to extend the methodology over large areas. This will require a distributed land surface model which incorporates spatially variable atmospheric forcing and surface parameters into the model formulations. Radiometric measurements are strongly sensitive to the hydrological characteristics of the soil and of the vegetation canopy. The 1.4 GHz measurements are mainly sensitive to surface soil moisture m_v whereas 5 GHz measurements are sensitive to both m_v and to the vegetation water content W_v.

An inherent difficulty of remotely sensed soil moisture measurement is in relating soil moisture variability at the scale of the footprint to large or small scale soil moisture variability (Stewart et al., 1996). The resulting emissivity for soil changes from about 0.95 for dry soil to about 0.6 for wet soils at a rate of approximately 0.01% volumetric moisture content. Kim and Stricker (1996) showed that from the perspective of annual water budget a homogenous equivalent soil exists for the sandy soil but not for the loam soil. Charpentier and Groffman (1992) studied the effects of topography and moisture content on the variability of soil moisture within remote sensing pixels. They reported that remote sensing reflected soil moisture conditions less accurately on pixels with increased topographic variability and less precisely when soil is dry. Mohanty et al. (2000) have shown that location on the slope is very important in determining soil moisture variation, suggesting that a simple averaging of soil moisture values over the slope may lead to errors at different time scales. Western et al. ((1999) have suggested that the presence of vegetation tends to diminish the soil moisture variations caused by topography.

Remote sensing, however, cannot replace ground based methods for providing high quality profile data at a point. Its advantage is in mapping conditions at regional, continental and even global scales and on a repetitive basis. It has been shown that repetitive measurements of microwave brightness temperatures can yield subsurface soil hydraulic properties (Burke et al., 1998).

For most satellite systems the periodicity of revisit can be a critical problem in studies involving rapidly changing conditions such as surface soil water content. With very wide swaths it is possible to obtain twice daily coverage with a polar orbiting satellite. Currently, all passive microwave sensors on satellite platforms operate at high frequencies (>7 GHz). A more recent option is the multiple frequency advanced microwave scaning radiometer (AMSR) satellite system that will include a 6.9 GHz channel. AMSR holds great promise for estimating soil water content in regions of low levels of vegetation. To pursue the use of space observations a space based system with a 1.4 GHz channel would provide improved global soil moisture information (Kerr et al., 2001). With these data it is possible to obtain not only soil moisture but also vegetation water content at a 50 km resolution (Wigneron et al., 2000). Soil moisture alone, with good temporal repetition on a daily basis at a resolution (410 km) on a regional scale, can be obtained (Wigneron et al., 2003).

However, a major link to be established is that there is no distinction made between soil and vegetation canopy components. Hence, vegetation water use or stress cannot be assessed. With some additional formulations for estimating canopy transpiration, and the dual requirement of energy and radiative balance of the soil and vegetation components, a better closure in agreement can be achieved.

With the advent of space borne synthetic aperture radar (SAR) system, much research has been conducted on detecting, assessing and mapping agriculture, forest, wet land, rangeland and urban features (Metternicht, 1999). Active sensors, particularly the synthetic aperture radar onboard the European Remote Sensing satellite has obtained a spatial resolution better than 50 m (Zribi et al., 2003). However, more efforts are required to investigate the possibility of using air and space borne microwave data for mapping areas degraded by salinization (Metternicht and Zinck, 2003; Singh et al., 1990; Taylor et al., 1996). While the real part of the permittivity is independent of soil salinity and alkalinity, the imaginary part is highly sensitive to variations in soil electrical conductivity, but with no significant effect variations in alkalinity. This aspect can be exploited for characterization of the land under investigation.

Water Quality Assessment

Assessment of water quality has remained an attractive subject of research for its importance needs no emphasis. Water quality is a general descriptor of water properties in terms of physical, chemical, thermal, and/or biological characteristics. Ultrasound has been used for water quality assessment by measurement of attenuation and velocity. However, this technique cannot be used over very large volume.

Remote sensing techniques for monitoring water quality depend on the ability to measure these changes in the spectral signature backscattered from water and relate these variations by empirical or analytical models to water quality parameters. Substances in surface water can significantly change backscattering characteristics. The optimal wavelength used to measure a water quality parameter is dependent on the substance being measured, its concentration and the sensor characteristics. Major pollutants present and affecting water quality in water bodies across the landscape are suspended sediments (turbidity), algae, dissolved organic matter (DOM), thermal releases, aquatic vascular plants, pathogens, oils and may be many more. Several of these parameters are capable of changing the energy spectra of reflected solar and/or emitting thermal radiation from surface waters which can be measured by remote sensing techniques. Empirical or analytical relationships between spectral properties and water quality parameters are established. The general forms of these empirical equations are (Schmugge et al., 2002)

$$Y = A + BX \quad \text{or} \quad Y = AB^{X}$$

where Y is the remote sensing measurement (i.e. radiance, reflectance, energy) and X the water quality parameter of interest (i.e. suspended sediment, chlorophyll etc.). A and B are empirically derived factors. In empirical approaches statistical relationships are determined between measured spectral/thermal properties and measured water quality parameters. Often information about the spectral/opticals characteristic of the water quality parameter is used to aid in the selection of best wavelength(s) or best model in this empirical approach. The empirical characteristics of these relationships make it pertinent in their use to a given condition.

Suspended sediments are the most common pollutant both in weight and volume in surface waters of fresh water systems (Lal, 1994; Robinson, 1971). Suspended

sediments increase the radiance emergent from surface waters in the visible to near infrared (VNIR) portion of the electromagnetic spectrum (Ritchie et al., 1976). While most researchers and managers agree that suspended sediments can be mapped with remotely sensed data, the technique with the current spatial resolution of satellite data (Ritchie, 2000; Ritchie and Schiebe, 2000) does not allow the detailed mapping of water bodies or measurements in or from streams needed over desired area. Spectral data obtained using currently available satellites (i.e. landsat) do not permit discrimination of chlorophyll in waters with high suspended sediments (Dekker and Peters, 1993; Ritchie et al., 1994a, b). Gitelson et al. (1994) have shown a linear relationship between chlorophyll and the difference between the emergent energy in the primarily chlorophyll scattering range (700-705 nm) and the primarily chlorophyll absorption range (675-680 nm). The relationship exists even in the presence of high suspended sediment. These findings suggest new approaches for application of airborne and spaceborne sensors to exploit these phenomena to estimate chlorophyll in surface waters under all conditions as hyperspectral sensors are launched and data become available. Hyperspectral data from space platforms will allow to discriminate between water quality parameters and to develop a better understanding of light/water/substance interactions. Such information are required for developing algorithms that will allow the use of full resolution electromagnetic spectrum to monitor water quality parameters.

One area is in developing a framework for combining multifrequency remote sensing information, from the visible to microwave wavelengths for more reliable estimation of vegetation and soil properties and states. There is empirical and theoretical evidence that SAR backscatter in combination with optical data may provide useful information about crop water stress (Moran et al., 1997, 1998). At high frequencies (~13 GHz), field experiments have shown that the radar signal is particularly sensitive to such plant parameters as leaf area index, plant biomass and percentage of vegetation cover. At low frequencies (~5 GHz), many studies have shown that the radar signal is very sensitive to soil moisture, though this sensitivity decreased with increasing vegetation cover.

The different regions of the electromagnetic spectrum have complementary capabilities for spectral separability of the salinity-alkalinity classes. This calls for data reason to increase the efficiency of the remote sensing data. It has been shown that the merging of visible and infrared with microwave data achieved a better discrimination of the alkaline and nonaffected areas than landsat TM band alone, with 35-40% increase in accuracy (Metternicht, 1996).

The best monitoring results are obtained when remote sensing data are combined with field and laboratory data. In this regard, geographic information system offer the advantage of integrating data of diverse nature in terms of scale, time, source and structure.

Accurate topographic maps are still not available over huge areas of our globe. One reason is the cloud coverage over tropical regions and the other is the intensive work involved in photogrammetric evaluations. Remote sensing applications either alone or in combination with modeling are, therefore, enormous, possibly providing many hidden informations.

References

1. Ahuja, L.B., Wendroth, O. and Nielson, D.R, (1993). Relationship between initial drainage of surface soil and average profile saturated conductivity. *Soil Sci. Soc. Am. J.* **57:** 19–25.
2. Alex, Z.C. and Behari, J. (1996). Complex dielectric permittivity of soil as function of frequency, moisture and texture. Inds. *J. Pure Appl. Phys*. **34:** 319–323.
3. Alex, Z.C. and Behari, J. (1998). Laboratory revaluation of emissivity of soils. *Intl. J. Remote Sens.* **19 (7)**: 1335–1340.
4. Alex, Z.C., Behari, J. and Zaidi, Z.H. (1994). Biological tissue characterization at microwave frequencies: A Review: technical Review, IETE, Vol. II, No. 1.
5. Alharthi, A. and J. Lange. (1987). Soil water saturation: Dielectric determination. *Water Res.* **23:** 591–595.
6. Amato, M. and Ritchie, J.T. (1995). Small spatial scale soil water content measurement with time-domain reflectometry. *Soil Sci. Soc. Am. J*. **59:** 325–329.
7. An Liou, Y. and England, A.W. (1996). Annual temperature and radio brightness signatures of bare soils. *IEEE Trans. Geo. & Remote Sens.* **34:** 90–99.
8. Arcone, S.A. and Larson, R.W. (1988). Single horn reflectometry for *in situ* dielectric measurements at microwave frequencies. *IEEE Trans. Geo. & Remote Sens.* **26:** 89–92.
9. Baker, J.M. (1990). Measurement of soil water content. *Remote Sens. Review* **5:** 263–279.
10. Baker, J.M. and Almaras, R.R. (1990). System for automating and multiplexing soil moisture measurement by time-domain reflectometry. *Soil Sci. Soc. Am. J.* **54:** 1–6.
11. Bala Krishna (1995). M. Phil. Dissertation "Soil Texture Characterization at Microwave Frequencies", Jawaharlal Nehru University, New Delhi.
12. Bandyopadhyay, S. (1995). Soil moisture and wheat growth assessment by microwave and optical remote sensing. Ph.D. Thesis, P.G. School, IARI, New Delhi, pp. 125.
13. Bayser, A. and Kuerter, J.Z. (1992). Dielectric property measurements of materials using the cavity technique. *IEEE Trans. Micro. Theo. Tech. MTT*. **40:** 2108–2110.
14. Behari, J. (Ed) (2001). Physical methods of soil characterization. Narosa Publishing House, New Delhi, India.
15. Behari, J., Haresh Kumar and Aruna, R. (1982). Effect of ultraviolet light on the dielectric behaviour of bone at microwave frequencies. *Annals of Biomedical Engineering* **10:** 139–144.
16. Behari, J., Sahu, S.K. and Mishra, S.K. (2001). Microwave Dielectric Constants of Soil: Theory and Experiment. In: Physical Methods of Soil Characterisation (J. Behari, Ed). Narosa Publishing House, New Delhi.
17. Bell, J.P., Dean, T.J. and Hodnett, M.G. (1987). Soil moisture measurement by an

improved calibration resistance technique, part 2: Field techniques, evaluation, and calibration. *J. Hydrol*. **93:** 79–90.
18. Benallegue, M., Normand, M., Galle, S., Decambre, M., Taconet, O., Vidal-Madjar, D. and Prevot, L. (1994). Soil moisture assessment at a basin scale using active microwave remote sensing: the Agriscatt-88 airborne campaign on the Orgeval water shed. *Intl. J. Remote Sens.* **15:** 645–656.
19. Bennartz, R. and Tutman, G.G. (1998). Global land surface properties infra red from clmbined passive microwave and visible/near infra red satellite data. In preprints of the 9th Conference on Satellite Meteorology and Oceanography, pp 301–303, AMS (1998).
20. Bernard, R., Matin, P.H., Thony, J.L., Vauclin, M. and Vidal-Madzar, D. (1982). C-band radar for determining surface soil moisture. *Remote Sens. Environ*. **12:** 189–200.
21. Beven, K.J. and Fisher, J.I. (1996). Remote sensing and scaling in hydrology. In: Scaling Issues in Hydrology, J.B. Stewart et al. (Eds), Wiley, Chichester.
22. Binley, A., Winship, P., Middleton, R., Pokar, M. and West, J. (2001). High-resolution characterization of vadose zone dynamics using cross-borehole radar. *Water Res.* **37:** 2639–2652.
23. Biofot, A.M. (1992). Broadband method for measuring dielectric constant of liquids using an automatic network analyzer. *IEEE Proc*. **136:** 492–498.
24. Birchak, J.R., Gardner, C.G., Hipp, J.E. and Victor, J.M. (1974). High dielectgric constants microwave probes of sensing soil moisture. *Proc. IEEE* **62:** 93–98.
25. Birnbaum, G. and Franeau, J. (1949). Measurement of the dielectric constant and loss of solids and liquids by a cavity perturbation method. *J. Appl. Phys.* **20:** 817–818.
26. Blumberg, D.G., Freilinkher, V., Fuks, I., Kaganovskii, Y., Maradudin, A.A. and Rosenbluh, M. (2002). Effects of roughness on the retroreflection from dielectric layers. *Waves in Random Media* **12:** 279–292.
27. Bohren, C.F. and Battan, L.J. (1982). Radar backscattering of microwaves by spongy ice spheres. *J. Atmos. Sci.* **39:** 2623–2628.
28. Bohren, C.F. and Huffman, D.R. (1983). Absorption and scattering of light by small particles. John Wiley & Sons, Inc.
29. Boisvert, J.B., Gwyn, Q.H.J., Chanzy, A., Major, D.J., Brisco, B. and Brown, R.J. (1997). Effect of surface soil moisture gradients on modeling radar backscattering from bare fields. *Intl. J. of Remote Sens.* **18(1):** 153–170.
30. Botteher, C.J.F. (1952). Theory of electric polarization, Elsevier, Amesterdam.
31. Boyaraskii, D.A., Tikhonov, V.V. and Komarova, N. Yu. (2002). Model of dielectric constant of bound water in soil for applications of microwave remote sensing. *Progress in Electromagnetics Res.* (PIER) **35:** 251–269.
32. Bradley, G.A. and Ulaby, F.T. (1981). Aircraft radar response to soil moisture. *Remote Sens. Environ*. **11:** 419–438.
33. Brisco, B., Brown, R.J., Snider, B., Sofko, G.J., Kochler, J.A. and Wacker, A.G. (1991). Tillage effect on the radar backscattering of green stubble fields. *Intl. J. Remote Sens.* **12:** 2283–2298.
34. Brown, W.F. (1956). Dielectrics. In: Encyclopedia of Physics, vol. 17, Springer, Berlin.
35. Bruckler, L., Witono, H. and Stengel, P. (1988). Near surface soil moisture estimation from microwave measurements. *Remote Sens. Environ*. **26:** 101–121.
36. Bruggeman, D.A.G. (1935). Berechnung verschiedner physikallischer konstanten von heterogenen substanzen. *Ann. Phys.* (Leipzig), **24:** 636–664.
37. Brunfeldt, D.R. and Ulaby, F.T.C. (1984). Measured microwave emission and scattering in vegetation canopies. *IEEE Trans. Geo. & Remote Sens*. **GE-22:** 520–524.

38. Burke, E.J., Gurney, R.J., Simmonds, L.P. and O'Neill, P.E. (1998). Using a modeling approach to predict soil hydraulic properties from passive microwave measurements. *IEEE Trans. Geo. & Remote Sens.* **36(2):** 454–462.
39. Burke, K.H. and Schmugge, T.J. (1982). Effects of varying soil moisture contents and vegetation canopies on microwave emissions. *IEEE Trans. Geo. & Remote Sens.* **GE-20:** 268–274.
40. Campbell, J.B. (2003). In: Introduction to remote sensing (Third Edition). Taylor and Francis, London and New York, 205–224.
41. Campbell, M.J. and Ulrichs, J. (1969). Electrical properties of rocks and their significance for lunar radar observations. *J. Geophys. Res.* **74:** 5867–5881.
42. Campbell Scientific, (1998). CS615 water content reflectometer user guide. Campbell Scientific, INC., Logan, UT.
43. Champion, I. and Faivre, R. (1997). Sensitivity of the radar signal to soil moisture: Variation with incidence angle, frequency and polarization. *IEEE Trans. Geo. & Remote Sens.* **35(3)**: 781–783.
44. Chanzy A., Chadoeuf, J., Gaudu, J.C., Mohrath, D., Richard, G. and Bruckler, L. (1998). Soil moisture monitoring at the field scale using automatic capacitance probes. *European J. of Soil Sci.* **49:** 637–648.
45. Chanzy, A., Tarussov, A., Judge, A. and Bonn, F. (1996). Soil water content determination using ground-penetrating radar. *Soil Sci. Soc. Am. J.* **60:** 1318–1326.
46. Charpentier, M.A. and Groffman, P.M. (1992). Soil moisture variability within remote sensing pixels. *J. Geophys. Res.* **97:** 18987–18995.
47. Choudhury B.J., Schmugge T.J., Chang A. and Newton, R.J., (1979). Effect of surface roughness on the microwave emission from soils. *J. Geophys. Res.* **84:** 5699.
48. Choudhury, B.J., Schmugge, T.J. and Mo, T. (1982). A parameterization of effective soil temperature for microwave emission. *J. Geophys. Res.* **87:** 1301–1304.
49. Cosh, M.H. and Brutsaert, W. (1999). Aspects of Soil Moisture Variability in the Washita '92 Study Region. *J. of Geophys. Res*. pp. 104, No. D16, **19:** 751–757.
50. Dalton, F.N. (1992). Development of time domain reflectometry in measuring soil water content and bulk soil electrical conductivity, pp. 143–167 in G.C. Topp et al., (Eds.) Advances in measurement of soil physical properties: Bringing theory into practice. *Soil Sci. Soc. of America*, Spec. Publ. 30.
51. Daniels, D.J. (1996). Surface penetrating radar. London: Institute of Electrical Engineers.
52. Daniels, J., Blumberg, D.G., Vulfson, D.A., Kotlyar, A.L., Freiliker, V., Ronen, G. and Ben-Asher, J. (2003). Microwave remote sensing of physically buried objects in the Negev Desert: Implications for environmental research. *Remote Sens. of Environ.* **86:** 243–256.
53. Das, D.K. (2001). Soil water content measurement using modern techniques. In: Physical methods of soil characterization (J. Behari, Ed). Narosa Publishing House, New Delhi, pp. 25–28.
54. Das, D.K. (1995). Advances and future thrusts in the application of remote sensing techniques for sustainable crop production. Platinum Jubilee Lecture delivered at the 82nd Session of Indian Science Congress (Section of Agricultural Sciences), Jadavpur University, Calcutta, Jan. 3–8, 1995.
55. Das, D.K., Sundara Sarma, K.S. and Kalra, N. (1994a). Role of remote sensing in management of natural resources for sustainable agriculture and environment. In: Natural Resources Management for Sustainable Agriculture Environement (Ed. D.L. Deb), Angkor Publishers (P) Ltd., New Delhi, pp. 353–366.

56. Das, D.K., Sundara Sarma, K.S. and Mohan, S. (1994b). Research approach in agricultural applications of microwave remote sensing. Proc. Nat. Symp. on 'Microwave Remote Sensing and Users Meet'. Jan. 10–11, 1994; Space application Centre, Ahmedabad; pp. 140–150.
57. Das, D.K., Tomar, K.P. and Singh, G. (1989). Remote sensing technique as an aid to integrated water management for improving productivity in rainfed and irrigated areas. In: Maximising Crop Production in Rainfed and Problem Areas. Eds. D.K. Das and K.R. Sarkar, ISAS, pp. 423–427.
58. Daughtery, C.S.T., Ranson, K.J. and Beihl, L.L. (1991). C-band backscattering from corn canopies. *Intl. J. Remote Sens.* **12:** 1097–1109.
59. Davis, J.L. and Annan, A.P. (1977). Electromagnetic detection of soil moisture: Progress report I. *Can. J. Remote Sens.* **3:** 67–73.
60. Davis, J.L. and Annan, A.P. (1989). Ground penetrating radar for high resolution mapping of soil and rock stratigraphy. *Geophys. Prospect* **37:** 531–551.
61. Davis, J.L., Topp, G.C. and Annan, A.D. (1976). Electromagnetic detection of soil water content. Progress Report II. Workshop Proc. Remote Sensing of Soil Moisture and Groundwater, Royal York Hotel, Toronto, Canada.
62. De Loor, G.P. (1968). Dielectric properties of heterogeneous mixtures containing water. *J. Microwave Power* **3:** 67–73.
63. De Loor, G.P. (1993). Radar backscatter of crops. In: Current Topics in remote sensing Vol. 3 Land observation by remote sensing-Theory and Applications (Ed. H.J. Buiten and J.G.P.W. Clevers) Gordon and Breach Science Publishers, 1993.
64. De Rosny, G., Chanzy, A., Parde, M., Gaudu, J.C., Frangi, J.P. and Laurent, J.P. (2001). Numerical modeling of a capacitance probe response. *Soil Sci. Soc. Am. J.* **65(1):** 13–18.
65. Dekker, A.G. and Peters, S.W.M. (1993). The use of Thematic Mapper for the analysis of eutrophic lakes: a case study in the Netherlands. *Intl. J. Remote Sens.* **14** (5): 799–821.
66. Demirican, A., Ramach, H. and Mauser, W. (1992). Extraction of plant and soil parameters from multi-tempral ERS-1 SAR data of the Freiburg test site. Proc. First ERS-1 Symp., 4–6 Nov. 1992, Cannes, France, pp. 631–639.
67. Dirksen, C. and Dasberg, S. (1993). Improved calibration of time domain reflectomtry soil water content measurements. *Soil Sci. Soc. Am. J.* **57:** 660–667.
68. Dobson, M. and Ulaby, F. (1986). Active microwave soil moisture research. *IEEE Trans. Geo. & Remote Sens.* **24:** 23–36.
69. Dobson, M.C. and Ulaby, F.T. (1981). Microwave backscatter dependence on surface roughness, soil moisture and soil texture. Part-III: Soil Tension. *IEEE Trans. Geo. & Remote Sens.* **GE-19:** 51–61.
70. Dobson, M.C., Kouyate, F and Ulaby, F.T. (1984). A reexamination of soil textural effects on microwave emission and backscattering. *IEEE Trans. Geo. & Remote Sens.* **GE-22:** 530–536.
71. Dobson, M.C., Kouyate, F. and Ulaby, F.T. (1983). A re-examination of the soil texture effects on microwave emission and backscattering. Proceedings of the IEEE International Geoscience and Remote Sensing Symposium, San Francisco, California.
72. Dobson, M.C., Ulaby, F.T., Hillikaines, M.T. and El-Rayes, M.A. (1985). Microwave dielectric behavior of wet soil-Part II: Dielectric Mixing Models. *IEEE Trans. Geo. & Remote Sens.* **GE-23:** 35–46.
73. Dubayah, R., Wood, E.F. and Lavallee, D. (1997). Multiscaling analysis in distributed modeling and remote sensing: An application using soil moisture. In: Quatrocchi,

D.A., Goodchild, M. (Eds.). Scale in Remote Sensing and GIS. Lewis Publishers, New York, pp. 93–112.
74. Elachi, C. (1988). Spaceborne radar remote sensing application and techniques. IEEE Press, New York.
75. Engman, E.T. (1991). Application of microwave remote sensing of soil moisture for water resources and agriculture. *Remote Sens. Environ.* **35:** 213–216.
76. Engman, E.T. (1997). Soil moisture, the hydrologic interface between surface and ground water. Remote Sensing and Geophysical Information Systems for Design and Operation of Water Resources Systems (Proceedings of Rabat Symposium S3, April IAHS Publ. No. 242 1997) pp. 129–140.
77. Engman, E.T. and Chauhan, N. (1995). Status of microwave soil moisture measurement with remote sensing. *Remote Sens. Environ.* **51:** 189–198.
78. Entekhabi, D., Nakamura, H. and Njoku, E.G. (1994). Solving the inverse problem for soil moisture and temperature profiles by sequential assimilation of multifrequency remotely sensed observations. *IEEE Trans. Geo. & Remote Sens.* **32:** 438–448.
79. Evans, S. (1965). Dielectric properties of Ice and Snow. A Review, *J. Glaciol.* **5:** 773–792.
80. Evett, S.R. (2000). Some aspects of time domain reflectometry, neutron scattering and capacitance methods for soil water content measurement. IAEA-TECDOC-1137, 5–51.
81. Evett, S.R. and Steiner, J.L. (1995). Precision of neutron scattering and capacitance type moisture gauges based on field calibration. *Soil Sci. Soc. Am. J.* **59:** 961–968.
82. Feddes, R.A., Menenti, M., Kabat, P. and Bastiaanssen, W.G.M. (1988). Is large scale inverse modeling of unsaturated flow with areal average evaporation and surface soil moisture as estimated from remote sensing feasible? *J. Hydrol.* **100:** 69–111.
83. Ferrazzoli, P., Paloscia, S., Pampaloni, P., Schiavon, G., Solimini, D. and Coppo, P. (1992). Sensitivity of Microwave Measurement to vegetation biomass and soil moisture content-A case study. *IEEE. Trans. Geo. & Remote Sens.* **30:** 750–756.
84. Ferre, P.A., Rudilph, D.L. and Kachanoski, R.G. (1996). Spatial averaging of water content by time domain reflectometry: Implications for twin rod probes with and without dielectric coatings. *Water Res.* **32:** 271–279.
85. Franco, J., Abresqueta, J.M., Hernansaez, A. and Moreno, F. (2000). Water balance in a young almond orchard under drip irrigation with water of low quality. *Agriculture Water Management* **43:** 75–98.
86. Fung, A.K., Lee, Z., and Chen, K.S. (1992). Backscatter from a randomly rough dielectric surface. *IEEE Trans. Geo. & Remote Sens.* **30(2)**: 356–369.
87. Fung, A.K. (1967). Theory of cross-polarized power return from a random surface. *Appl. Sci. Res*. **18:** 56–60.
88. Fung, A.K. and Eom, H.J. (1979). Multiple scattering and depolarization by a randomly rough krichhoff surface remote sensing. Technical report, Univ. Kansas, Lawrence, Kansas, pp. 369–374.
89. Fung, A.K. and Ulaby, F.T. (1983). Matter energy interaction in the microwave region. In: Manual of remote sensing. Vol. I (2nd ed) (Ed. Moore R.K.) *Am. Soc. Photogramm*, pp. 115–164.
90. Gajda, G.B. (1982). A method for the measurement of permittivity at radio and microwave frequencies. IEEE Sym. MIT Society, p. 112–118.
91. Geiger, F.E. and Williams, D. (1972). Dielectric constants of soils at microwave frequencies. NASA TMS-65987, Washington, D.C.

92. Georgakakos, K.P. (Ed) (1996). Soil moisture theories and observations. *J. Hydrol*. **184:** 1–152.
93. Ghannouchi, Fadhel, M. and Bosiso Renato, G. (1987). A new six-port calibration method using four standards and avoiding singularities. *IEEE Trans. on Instr. and Meas.* **IM-36 (4)**: 1022–1027.
94. Ghosh, A., Pyne, S. and Behari, J. (1998). Dielectric parameters of dry and wet soils at 14.89 HGz. *Ind. J. Radio Space. Phys.* **27:** 130–134.
95. Gitelson, A., Mayo, M., Yacobi, Y.Z., Paroarov, A. and Berman, T. (1994). The use of high spectral resolution radiometer data for detection of low chlorophyll concentrations in Lake Kinneret. *J. Plankton Res.* **16:** 993–1002.
96. Hallikainen, M., Ulaby, F.T., Dobson, M.C. and E1 Rayes, M. (1984). Dielectric measurement of soils in the 3 to 37 GHz band between –50°C and 23°C 1984. IEEE Intl. Geosci. Remote Sensing Symp. (IGA RSS' 84) Digest, StraSBOURG, France, 27–30 August, pp. 163–168.
97. Hallikainen, M.T., Ulaby, F.T., Dobson, M.C., E1-Rayes, M.A. and Wu, L.K. (1985a). Microwave dielectric behaviour of wet soil Part -I, Empirical models and experimental observations. *IEEE Treans. Geo. & Remote Sens*. **GE-23:** 25–33.
98. Hallikainen M.T., Ulaby, F.T., Dobson, M.C. and E1-Rayes, M.A. (1985b). Microwave dielectric behaviour of wet soil-Part II: Dielectric-mixing models. *IEEE Trans. Geo. & Remote Sens.* **GE-23:** 35–46.
99. Hanks, R.J. (1992). Applied soil physics: Soil water and temperature applications (Second Edition) Narosa Publishing House, New Delhi, p. 1–21.
100. Hati, K.M. (1996). Studies on *in situ* dielectric properties of representative soils of India and microwave response of Maize crop. Ph. D. thesis, Indian Agriculture Research Institute, New Delhi.
101. Hilhorst, M.A. and Dirksen, C. (1995). Dielectric water content sensors: Time domain reflectometry versus frequency domain. In: College on Soil Physics; Dielectric soil water content and electric conductivity Measurements. Intl. Center for Theoretical Physics, Trieste, Italy.
102. Hipp, J.E. (1974). Soil electromagnetic parameters as a function of frequency, soil density and soil moisture. *Proc. IEEE* **62:** pp. 98–103.
103. Hoekstra, P. and Delaney, A. (1974). Dielectric properties of soils at UHF and microwave frequencies. *J. Geophys. Res.* **79:** 1699–1708.
104. Hook, W.R., Livingston, N.J., Sun, Z.R. and Hook, P.B. (1992). Remote diode shorting improves measurement of soil water by time domain reflectometry. *Soil Sci. Soc. Am. J.* **56:** 1384–1391.
105. Huisman, J.A., Sperl, C., Bouten, W. and Verstraten, J.M. (2001). Soil water content measurements at different scales: Accuracy of time domain reflectometry and ground-penetrating radar. *J. Hydrol.* **245:** 48–58.
106. Islam, S.I., Engman, E.T. (1996). Why bother for 0.0001% of Earth's Water? Challenges for Soil Moisture Research. *Eos. Trans. Am. Geophys. Union* **77:** 420.
107. Jackie E. Hipp (1974). *Proc. IEEE* **62:** 98–103.
108. Jackson, T.J. (1990). Laboratory evaluation of a field portable dielectric soil moisture probe. *IEEE Trans. Geo. & Remote Sens.* **28:** 241–245.
109. Jackson, T.J. (1993). Measuring surface soil moisture using passive microwave remote sensing. *Hydrological Processes* **7:** 139–152.
110. Jackson, T.J., Le Vine, D.M., Hsu, A.Y., Oldak, A., Starks, P.J., Swift, C.T., Isham, J. and Haken, M. (1999). Soil moisture mapping at regional scales using microwave

radiometry: the Southern Great Plains hydrology experiment. *IEEE Trans. Geo. & Remote Sens*. **37:** 2136–2151.
111. Jackson T.J. and O'Niell, P. (1985). Aircraft scatterometer observations of soil moisture on range land watershek. *Intl. J. Remote Sens.* **15:** 1585–1593.
112. Jackson, T.J., O'Neil, P.E., Swift, C.T. (1997). Passive microwave observation of diurnal surface soil moisture. *IEEE Trans. Geo. & Remote Sens.* **35:** 1210–1221.
113. Jackson, T.J. and Schmugge, T.J. (1989). Passive microwave remote sensing system for soil moisture: Some supporting research. *IEEE Trans. Geo. & Remote Sens.* **27:** 225–235.
114. Jackson, T.J. and Schmugge, T.J. (1991). Vegetation effects on the microwave emission of soils. *Remote Sens. Environ.* **36:** 203–212.
115. Jackson, T.J., Schmugge, T.J. (1989). Passive microwave remote sensing system for soil moisture: Some supporting research. *IEEE Trans. Geo & Remote Sens.* **27:** 225–235.
116. Jackson, T.J., Schmugge, T.J. and Wang, J.R. (1982). Passive microwave sensing of soil moisture under vegetation canopies. *Water Res.* **18:** 1137–1142.
117. Jackson, T.J., Schmugge, T.J., O'Neill, P.E. and Parlange, M.B. (1998). Soil water infilteration observation with microwave radiometers. *IEEE Trans. Geo. & Remote Sens.* **36(5):** 1376–1383.
118. Jury, W.A., Gardner, W.R. and Garder, W.H. (1991). Soil Physics, 5th ed., Wiley, New York.
119. Kanemasu, E.T., Stone, L.R. and Powers, W.L. (1976). Evapotranspiration model tested for soybean and sorghum. *Agron. J.* **68:** 569–572.
120. Karolkar, B., Behari, J. and Prim, A. (1985). Biological tissue characterization at microwave frequencies. *IEEE Trans. Micro. Theo. Tech.* **MTT-33**: 64–66.
121. Kerkides, P., Michalopoulou, H., Papaioannou, G. and Pallatou, R. (1996). Water balance estimates over Greece. *Agricultural Water Management* **32:** 85–104.
122. Kerr, Y., Waldteufel, P., Wigneron, J.P., Martinuzzi, J.M., Font, J. and Berger, M. (2001). Soil moisture retrieval from space: The soil moisture and ocean salinity (SMOS) Mission. *IEEE Trans. Geo. & Remote Sens.* **GE-39:** 1729–1735.
123. Khardly, M.M.Z. and Jackson, W. (1953). Properties of artificial dielectrics comprising arrays of conducting elements. *Proc. Inst. Elec. Eng*. **100:** 199–212.
124. Kim, C.P. and Stricker, J.N.M. (1996). Influence of variable soil hydraulic properties and rainfall intensity on the water budget. *Water Res*. **32:** 1699–1712.
125. Kirkham, D. and Powers, W.L. (1972). In: Advanced, Soil Physics, Wiley Interscience New York, London, Sydney, Toronto, P.1.
126. Knight, R. (2001). Ground penetrating radar for environmental applications. *Annual Review of Earth and Planetary Sci.* **29:** 229–255.
127. Kong, J.A., Tsang, L., Zungia, M., Shin, R., Shine, J.C. and Chang, A.C. (1979). Theoretical modeling and experimental data matching for active and passive microwave remote sensing of earth terrain. Int. Symposium Terrain profile contours EM wave propogation (AGARD: NATO meeting Norway).
128. Kostov, K.G. and Jackson, T.J. (1993). Estimating profile soil moisture from surface layer measurements: A review *Ground Sensing*, 125–136.
129. Kowalsky, M.B., Finsterle, S. and Rubin, Y. (2004). Estimating flow parameter distributions using ground-penetrating radar and hydrological measurements during transient flow in the vadose zone. *Adv. in Water Resour.* **27:** 583–599.
130. Kukangu, G., Savage, M.J. and Johnston, M.A. (1999). Use of sub-hourly soil water

content measured with a frequency-domain reflectometer to schedule irrigation of cabbages. *Irrigation Sci.* **19:** 7–13.

131. Laboski, C.A.M., Lamb, J.A., Dowdy, R.H., Baker, J.M. and Wright, J. (2001). Irrigation scheduling for a sandy soil using mobile frequency domain reflectometry with a checkbook method. *J. of Soil and Water Conservation* **56(2)**: 97–100.
132. Lal, R. (1994). Soil erosion. Soil and Water Conservation Society, Ankeny, Iowa.
133. Le Vine, D.M. (1999). Synthetic aperture radiometer systems. *IEEE Trans. MIT* **47(12):** 2228–2236.
134. Le Vine, D.M., Kao, M., Tanner, A.B., Swift, C.T. and Graffis, A. (1990). Initial results in the development of a synthetic aperture microwave radiometer. *IEEE Trans. Geo. & Remote Sens.* **28:** 614–619.
135. Le Vine, D.M., Wilheit, T.T., Murphy, R. and Swift, C. (1989). A multifrequency microwave radiometer of the future. *IEEE Trans. Geo. & Remote Sens.* **27(2):** 193–199.
136. Leader, J.C. (1975). Polarization dependence in FM scattering from Rayleigh scatterer's embedded in dielectric slab. *J. Appl. Phys.* **46:** 4371–4391.
137. Li, J. and Islam, S. (1999). On the estimation of soil moisture profile and surface fluxes partitioning from sequential assimilation of surface layer soil moisture. *J. Hydrol.* **220:** 86–103.
138. Li-ching-Lieh and Chen, Kun-Mu (1995). Determination of electromagnetic properties of materials using flanged open-ended coaxial probe full wave analysis. *IEEE. Trans. Instr. and Meas.* **44(1):** 10–26.
139. Maizler (1998). Microwave permitivity of dry sand. *IEEE. Trans. Geo. & Remote Sens.* **36(1):** 317–319.
140. Marshall, T.J. and Holmes, J.W. (1988). Soil Physics. Cambridge University Press, Cambridge, New York, p. 64.
141. Mead, R.M., Soppe, R. and Ayars, J.E. (1998). Capacitance probe observations of daily soil moisture fluctuations. Tektan, USDA-ARS.
142. Mehta, N.S., Mohan, S., Das, D.K., Sundara Sarma, K.S., Bandyopadhyay, S. and Burman, D. (1995). Microwave studies of soil/crop using ground based scatterometer data scientific report. SAC/RSA/RSAG/ARDSR/01/95.
143. Metternicht, G. (1999). Current status and future prospectives of radar remote sensing for cartographic applications. *Cartography* **28:** 1–16.
144. Metternicht, G.I. (1996). Detecting and monitoring land degradation features and processes in the Cochabama valleys, Bolivia: A synergistic approach. ITC Publication, vol. 36. Enschede, The Netherlands. International Institute of Aerospace Survey and Earth Sciencies, pp. 390.
145. Metternicht, G.I. and Zinck, J.A. (2003). Remote sensing of soil salinity: Potentials and constraints. *Remote Sens. of Environ.* **85:** 1–20.
146. Michelson, D.B. (1994). ERS-I SAR backscattering coefficients from bare fields with different row direction. *Intl. J. Remote Sens.* **15:** 2679–2685.
147. Mishra, A., Ghorai, A.K. and Singh, S.R. (1998). Rainwater, soil and nutrient conservation in rice lands in eastern India. *Agricultural Water Management* **38:** 45–57.
148. Mishra, D.K. (1987). A study on coaxial line excited monopole probes for *in situ* permittivity measurements. *IEEE Trans. Instr. Meas*. **IM-36(4):** 1015–1019.
149. Mishra, U.S. and Behari, J. (2000). Measurement of *in situ* soil moisture at microwave frequencies. *Ind. J. Remote Sens.* **28:** 1–5.
150. Moghadam, M., Durden, S. and Zebker, H. (1994). Radar measurement of forested areas during OTTER. *Remote Sens. Environ*. **47:** 154–166.

151. Moghaddam, M., Saatchi, S. and Cuenca, R.H. (2000). Estimating subcanopy soil moisture with radar. *J. Geophys. Res*. **105(D11):** 14899–14911.
152. Mohan, S., Mehra, N.S., Mehta, R.L., Patel, P., Rajak, D.R., Srivastava, H.S., Das, D.K., Sundara Sarma, K.S., Saxena, C.M. and Sutradhar, A.K. (1990). Assessment of ERS-1 SAR data for soil moisture estimation. Proc. 1st ERS-1 Workshop on Space at the Service of Our Environment, Cannes, pp. 635–639.
153. Mohan, S., Mehta, N.S., Mehta, R.L., Patel, P., Patel, I.D., Patel, M.R. and Patel R.B. (1992). Monitoring of paddy crop at 5.0 GHz. SAC/RSA/RSG/SIR-C/SN/01/92.
154. Mohan, S., Mehta, N.S., Mehta, R.L., Patel, P., Patel, I.D., Patel, H.R. and Patel, R.B. (1993). C-band radar response to soil moisture: Bare soil and wheat covered soil. SAC/RSA/RSAG/ERS-I/SM/04/93.
155. Mohanty, B.P., Skaggs, T.H. and Famiglietti, J.S. (2000). Analysis and mapping of field scale soil moisture variability using high resolution ground based data during the Southern Great Plains 1997 (SGP97) hydrology experiment. *Water Res.* **36:** 1023–1032.
156. Montgomery, C.G. (Ed.) (1961). Dielectric materials and application. The Technical Press, MIT and John Wiley & Sons, New York.
157. Moran, M.S., Vidal, A., Troufleau, D., Ioue, Y. and Mitchell, T.A. (1998). Ku- and C-band SAR for discriminating agricultural crop and soil conditions. *IEEE Geo. & Remote Sens.* **36:** 265–272.
158. Moran, M.S., Vidal, A., Troufleau, D., Qi, J., Clarke, T.R. and Pinter Jr., P.J. et al. (1997). Combining multifrequency microwave and optical data for crop management. *Remote Sens. Environ.* **61:** 96–109.
159. Murphy, R. et al. (1987). High-resolution multi-frequency microwave radiometer, NASA technical report of the high resolution multi-frequency microwave radiometer instrument (HMMR) panel, Washington, D.C.
160. Musil, J. and Zacek, F. (Ed.) (1986). Microwave measurements of complex permittivity by free space method and their application. Elsevier Publishers, Amsterdam.
161. Naidu, A.D. and Singh, D.N. (2004). A generalized procedure for determining thermal resistivity of soils. *Intl. J. Thermal Sci*. **43:** 43–51.
162. Narain, S. (2004). In: Down to Earth (2004) A relation not be ignored September 15, Centre for Science and Environment, New Delhi, P-22.
163. Neal, A. (2004). Ground-penetrating radar and its use in sedimentology: Principles, problems and progress. *Earth-Science Reviews* **66:** 261–330.
164. Newton, R.E. and McClellan, W.R. (1975). Permittivity measurements of soils at L-band. Tech. Rep. RSC-58, Texas A&M, University College Station, TX.
165. Newton, R.W. (1977). Microwave remote sensing and its applications for soil moisture detection. Remote Sensing Center, Texas.
166. Newton, R.W. and Rouse, J.W. (1980). Microwave radiometer measurement of soil moisture content. *IEEE Trans. Antennas Propag*. **AP-28:** 680–686.
167. Newton, R.W., Black, Q.R., Makanvand, S., Balachard, A.J. and Jean, B.R. (1982). Soil moisture information and thermal microwave emission. *IEEE Trans. Geo. & Remote Sens.* **GEW-20:** 275–281.
168. Nissen H.H., Moldrup, P. and Henriksen, K. (1998). High-resolution time domain reflectometry coil probe for measuring soil water content. *Soil Sci. Soc. Am. J*. **62:** 1203–1211.
169. Njoku, E.G. and O'Neill, P.E. (1982). Multifrequency microwave radiometer measurements of soil moisture. *IEEE. Trans. Geo. & Remote Sens.* **GE-20:** 468–474.

170. Odelovsky, V.I. (1951). Raschct oboschennoi, provodimosti geterogennih system. *GTF* **21(6):** 667–685.
171. Oldak, A., Pachepsky, Y., Jackson, T.J. and Rawals, W.J. (2002). Statistical properties of soil moisture images revisited. *J. Hydrol.* **255:** 12–24.
172. Oldak, A., Jackson, T.J., Starks, P. and Elliott, R. (2003). Mapping near-surface soil moisture on regional scale using ERS-2 SAR data. *Intl. J. of Remote Sens.* **24(22):** 4579–4598.
173. Or, D. and Wraith, J.M. (2000). In Handbook of Soil Science. Editor-in-chief M.E. Sumner. pp. A53-A63. CRC press, New York.
174. Ottl, H., Moreira, A. and Suss, H. (2000). Some results of new microwave remote sensing experiments. *Acta Astronautica* **47(2-9):** 355–363.
175. Pearce, C.A.R. (1955). The permittivity of two-phase mixtures. *Brit. J. Appl. Phys.* **6:** 358–361.
176. Pepin S., Livingston, N.J. and Hook, W.R. (1995). Temperature-dependent measurement errors in time domain reflectometry determinations of soil water. *Soil Sci. Soc. Am. J.* **59(1):** 38–43.
177. Poe, G.A. (1971). Remote sensing of the near surface moisture profile of specular soils with multi-frequency microwave radiometry. Proc. SPIE Seminar on Remote Sensing of Earth Resources and the Environment. Palo Alto. CA. 135–145.
178. Poe, G.A., Stagryn. and Edgerton, A.T. (1971). Determination of soil moisture content using microwve radiometry. Final Tech. Rep. 1684-1. Aerojet General Corp. E1. Monte. CA.
179. Polder, D. and Van Santen, J.H. (1946). The effective permeability of mixtures of solids. *Physica*. **12:** 257.
180. Price, C.J. (1982). Estimation of regional scale evapotranspiration through analysis of satellite thermal infrared data. *IEEE Trans. Geo. & Remote Sens.* **GE-20(3):** 286–292.
181. Quesney, A., Mascle, S.L.H., Taconet, O., Madjar, D.V., Wigneron, J.P., Loumagne, C. and Normand, M. (2000). Estimation of watershed soil moisture index from ERS/SAR data. *Remote Sens. Environ.* **72:** 290–303.
182. Raju, S., Rao, K.S. and Wang, J.R. (1993). Estimation of soil moisture and surface roughness parameters from back-scattering coefficient. *IETE Trans. Geo. & Remote Sens*. **GE-31:** 1094–1099.
183. Rambatch, M., Demirican, A. and Mauser, W. (1982). Correlation between soil moisture and back scatting coefficient of ERS-1 Symp. Cannes, France, November 4–6.
184. Rao, B.B., Rao, G.S., Savani, M.B. and Shekh, A.M. (1999). Estimating surface and seedling zone soil moisture using remotely sensed data. *Annals. Agri. Bio. Res.* **4(1):** 7–9.
185. Rao, P.V.N., Raju, C.S. and Rao, K.S. (1990). Microwave Remote Sensing of soil moisture: Elimination of texture effect. *IEEE Trans. Geo. & Remote Sens*. **GE-28:** 148–151.
186. Ray, S. and Behari, J. (1986). Microwave absorption in lossy liquids. *Phys. Med. Biol.* **31(9):** 1031–1040.
187. Ray, S. and Behari, J. (1987). *In vivo* dielectric measurement of biological tissues in the frequency ranges 0.4–1.3 GHz. *J. Bioelectricity* **6(1):** 71–91.
188. Ray, S. and Behari, J. (1988). *In vitro* impedance of biological tissues in the frequency range 0.4–1.3 GHz. *J. Electromagnetic Wave Appl.* **2(56):** 459–471.
189. Rayleigh, R. (1892). On the influences of obstacles arranged in rectangular order on the properties of a medium. *Phil. Mag*. **34:** 481–502.

190. Ritchie, J.C. (2000). Soil erosion. In: Schultz, G.A., Engman, E.T., (ed), Remote sensing in hydrology and water management. Springer-Verlag, Berlin, p. 271–286.
191. Ritchie, J.C., Grissinger, E.H., Murphey, J.B. and Garbrecht, J.D. (1994a). Measuring channel and gully cross-sections with an airborne lidar altimeter. *Hydrol. Process J.* **7:** 237–244.
192. Ritchie, J.C., Schiebe, F.R., Cooper, C.M. and Harrington Jr., J.A. (1994b). Chlorophyll measurements in the presence of suspended sediment using broad band spectral sensors aboard satellites. *J. Freshwater Ecol.* **9(2):** 197–206.
193. Ritchie, J.C., Schiebe, F.R. and McHenry, J.R. (1976). Remote sensing of suspended sediment in surface water. *Photogram Eng. Remote Sens.* **42:** 1539–1545.
194. Ritchie, J.T. (1972). Model for predicting evaporation from a row crop with incomplete cover. *Water Resour. Res*. **8:** 1204–1213.
195. Ritchie, J.C. and Schiebe, F.R. (2000). Water quality. In: Schultz G.A., Engman E.T., editors. Remote sensing in hydrology and water management. Germany: Springer-Verlag, Berlin, p. 287–303, 351–402.
196. Roberts, S. and Von Hippel, A.R. (1946). A new method for measuring dielectric constant and loss tangent in the range of EM Waves. *J. Appl. Phys.* **17:** 610–645.
197. Robinson, A.R. (1971). Sediment: Our greatest pollutant. *J. Soil Water Conservat.* **53(8):** 406–408.
198. Rosen, P.A., Hensley, S., Joughin, I.R., Li, F.K., Madsen, S.N., Rodriguez, G. and Goldstein, R.M. (2000). Synthetic aperture radar interferometry. *Proc. IEEE* **88(3):** 331–382.
199. Rosenthal, W.D., Kanemasu, E.T., Raney, R.J. and Stone, L.R. (1977). Evaluation of an evapotranspiration model for corn. *Agron. J*. **69:** 461–464.
200. Roth, C.H., Malicki, M.A. and Plagge, R. (1992). Empirical evaluation of the relationship between soil dielectric constant and volumetric water content as the basis for calibrating soil moisture measurements by TDR. *J. of Soil Sci.* **43:** 1–3.
201. Roth, K., Schulin, R., Flühler, H. and Attinger, W. (1990). Calibration of time domain reflectometry for water content measurement using a composite dielectric approach. *Water Resour. Res.* **26:** 2267–2273.
202. Rouse Jr., J.W. (1983). Comments on the effects of texture on microwave emission from soils. *IEEE Trans. Geo. & Remote Sens.* **GE-21(4):** 508–511.
203. Sabburg, J., Ball, A.R. and Hancock, N.H. (1997). Dielectric behavior of moist swelling clay soils at microwave frequencies. *IEEE Trans. Geo. & Remote Sens.* **35(3):** 784–787.
204. Sahebi, M.R., Bonn, F. and Gwyn, Q.H.J. (2003). Estimation of the moisture content of bare soil from RADARSAT-1SAR using simple empirical model. *Intl. J. Remote Sens.* **24(12):** 2575–2582.
205. Sahu, S.K. (1998). Estimation of soil moisture as a function of dielectric constant and texture. M. Phil thesis, Jawaharlal Nehru University, New Delhi.
206. Sarabandi, K. and Li, E.S. (1997). Microwave ring resonator for soil moisture measurements. *IEEE Trans. Geo. & Remote Sens*. **35:** 1223–1231.
207. Schmugge, T., Wilheit, T., Webster, W. and Gloersen, P. (1976). Remote sensing of soil moisture with microwave radiometer-II, NASA, Tech. Note IN-D-8321, GSFC, Green belt, MD.
208. Schmugge, T.J. (1980). Effect of texture on microwave emission from soils. *IEEE Trans. Geo. & Remote Sens.* **GE-18:** 353–361.
209. Schmugge, T.J. (1983). Remote sensing of soil moisture: Recent advances. *IEEE Trans. Geo. & Remote Sens.* **GE-21:** 336–344.

210. Schmugge, T.J. and Jackson, T.J. (1994). Mapping surface soil moisture with microwave radiometers. *Meteorol. Atmos. Phys.* **54:** 213–223.
211. Schmugge, T.J., Jackson, T.J. and Mckim, H.L. (1980). Survey of methods for soil moisture determination. *Water Resour. Res.* **16:** 961–979.
212. Schmugge, T.J., Kustas, W.P., Ritchie, J.C., Jackson, T.J. and Rango, A. (2002). *Adv. in Water Resour.* **25:** 1367–1385.
213. Schmugge, T.J., O'Neill, P.E. and Wang, J.R. (1986). Passive microwave soil moisture research. *IEEE Trans. Geo. & Remote Sens.* **24:** 12–22.
214. Schumann, R. (1994). Microwave remote sensing: Introduction and applications in agriculture, forest and soil moisture. Presented at ERS-1 workshop in Karachi, Pakistan and Hyderabad, India, p. 1–8.
215. Schumullius, C. and Furrer, R. (1992). Frequency dependence of radar backscattering under different moisture conditions of vegetation covered soil. *Intl. J. Remote Sens.* **13:** 2233–2245.
216. Scott, W.R. and Smith, G.S. (1992). Measured electrical constitutive parameters of soil functions of frequency and moisture content. *IEEE Trans. Geo. & Remote Sens.* **GE-30:** 621–623.
217. Shih, S.F. and Jordan, J.D. (1993). Use of Land sat Thermal-IR data and GIS in soil moisture assessment. *J. Irrigation and Drainage Engineering* **119(5):** 868–879.
218. Sholink, M.I. (1970). Radar Handbook. McGraw-Hill Book Co. pp. 27–36.
219. Shutko, A.M. and Reutov, E.M. (1982). Mixture formulae applied in estimation of dielectric and radiative characteristics of soils and grounds at microwave frequencies. *IEEE Trans. Geo. & Remote Sens.* **GE-20:** 29–32.
220. Sihvola, A.H. and Kong, J.A. (1988). Effective permittivity of dielectric mixtures. *IEEE Trans. Geo. & Remote Sens.* **26(4):** 420–429.
221. Simmer, C. (1999). Contribution of microwave remote sensing from satellites to studies on the earth energy budget and the hydrological cycle. *Adv. Space Res.* **24(7):** 897–905.
222. Singh, P. and Kumar, R. (1993). Evapotranspiration from wheat under a semiarid climate and a shallow water table. *Agricultural Water Management* **23:** 91–108.
223. Singh, P., Wolkewitz, H. and Kumar, R. (1987). Comparative performance of different crop production functions for wheat (*Triticum aestivum L.*). *Irrig. Sci.* **8:** 273–290.
224. Singh, R., Kumar, V. and Srivastav, S. (1990). Use of microwave remote sensing in salinity estimation. *Intl. J. of Remote Sens.* **11:** 321–330.
225. Stabell, K.F. and Misra, D.K. (1990). An experimental technique for *in vivo* permittivity measurement of materials at microwave frequencies. *IEEE Trans.* **MTT-38:** 337–339.
226. Staford, J.V. (1988). Remote, noncontact and in site measurement of soil moisture content: A review. *J. Agri. Engine. Res.* **41:** 151–172.
227. Stewart, J.B., Engman, E.T., Feddes, R.A., Kerr, Y., editors (1996). Scaling up in hydrology using remote sensing. Wiley, Chichester, p. 255.
228. Stoffregen, H., Yaramanci, U., Zenker, T. and Wessolek, G. (2002). Accuracy of soil water content measurements using ground penetrating radar: Comparison of ground penetrating radar and lysimeter data. *J. Hydrol.* **267:** 201–206.
229. Stuchly, M.A. et al. (1980). Coaxial line reflection methods for measuring dielectric properties of biological tissues at radio and microwave frequencies: A Review. *IEEE Trans. Instr. and Meas.* **IM-29(3):** 176–183.
230. Stuchly, S.S. et al. (1979). A method for measurement of the permittivity of thin samples. *J. Microwave Power* **14:** 7–11.

231. Stuchly, S.S., Stuchly, M.A. and Carraro, B. (1978). Permittivity measurements in a resonator terminated by an infinite sample. *IEEE Trans. Instr. Meas*. **IM-27:** 436–439.
232. Stuchuly, S.S., Pzepecka, M.A. and Kander, M.F. (1974). Permittivity measurements at microwave frequencies using leemped elements. *IEEE Trans. Meas.* **23:** 56–62.
233. Suber, W.H. and Crouch, G.E. (1948). Dielectric measurement method for solids at microwave frequencies. *J. Appl. Phys.* **19:** 1130–1135.
234. Sucher, M. and Fox, J. (1963). Handbook of microwave measurements. Vol. II, Polytechnic Press of the Polytechnic Institute of Brooklyn, pp. 503–506.
235. Sundara Sarma, K.S., Burman, D., Sharma, R.K. and Das, D.K. (1992). Soil moisture estimation by time domain reflectometry in saline and alkali soils. Proc. 57th Annual Convention of ISSS. Nat. Sem. Development in Soil Science, CRIDA, Hyderabad, November 26–29: pp. 3–5.
236. Swift, C.T., Le Vine, D.M. and Ruf, C.S. (1991). Aperture synthesis concepts in microwave remote sensing of the earth. *IEEE Trans.* **MTT-39(12):** 1931–1935.
237. Swift, C.T., Ruf, C., Tanner, A. and LeVine, D. (1986). The electronically steered thinned array radiometer ESTAR, In: Proceedings of the international Geoscience and Remote Sensing Symposium, pp. 591–593, Zurich, Switzerland.
238. Tan, H.S. and Fung, A.K. (1979). A first order theory of wave depolarization by a geometrically an isotopic random medium. *Radio Sci*. **14:** 377–386.
239. Tansly, K.J. and Millington, A.C. (2001). Investigating the potential for soil moisture and surface roughness monitoring in dry lands using ERS SAR data. *Intl. J. Remote Sens.* **22(11):** 2129–2149.
240. Taylor, L. (1965). Dielectric properties of mixtures. *IEEE Trans. Antennas Propagat.* **AP-13(6):** 943–947.
241. Taylor, G.R., Mah, A.H., Kruse, F.A., Kierein-Young, K.S., Hewson, R.D. and Bennett, B.A. (1996). Characterization of saline soils using airborne radar imagery. *Remote Sens. of Environ.* **57:** 127–142.
242. Theis, S.W., Balnchard, B.J. and Newton, R.W. (1984). Utilization of vegetation indices to improve microwave soil moisture estimates over agricultural lands. *IEEE Trans. Geo. & Remote Sens.* **GE-22:** 490–495.
243. Tomer, M.D. and Anderson, J.L. (1995) Field evaluation of a soil water-capacitance probe in a fine sand. *Soil Sci.* **159:** 90–98.
244. Topp, G.C. Davis, J.L. and Aunnan, A.P. (1980). Electromagnetic determination of soil water content: Measurement in coaxial transmission lines. *Water Res.* **16:** 574–582.
245. Topp, G.C., Zegelin, S.J. and White, I. (1994). Monitoring soil water content using TDR. An overview of progress. In: K.M. O' Connor et al. Eds. Symposium on time domain reflectometry in environmental applications. North Western University, Evanston, IL Spec. Publ. pp. 67–89.
246. Topp, G.C., Watt, M. and Hayhoe, H.N. (1996). Point specific measurement and monitoring of soil water content with an emphasis on TDR. *Can. J. Soil. Sci.* **76:** 307–316.
247. Troch, P.A., Vandersteene, F., Sh, Z., Hoeben, R. and Wüthrich, M. (1997). Estimating microwave observation depth in bare soil through multi-frequency scatterometry, In: 1st EMSL User Workshop Proceedings, Ispra, Italy, April 23–24, 1996.
248. Tsang, L. and Kong, J.A. (1978). Radiactive transfer theory for active remote sensing of half space random media. *Radio. Sci.* **13:** 763–773.
249. Tsang, L., Blanchard, J., Newton, R.W. and Kong, J.A. (1982). A simple relation

between active and passive microwave remote sensing measurements on earth terrain. *IEEE Trans, Geo. & Remote Sens.* **20(4):** 482–485.

250. Tuong, T.P., Wopereis, M.C.S., Marquez, J.A. and Kropff, M.J. (1994). Mechanism and control of percolation losses in irrigated puddle rice fields. *Soil Sci. Soc. Am. J.* **58:** 1794–1803.
251. Ulaby, F.T., Bradley, G. and Dobson, M.C. (1979). Microwave backscatter dependence on surface roughness, soil moisture and soil texture; part II, vegetation covered soil. *IEEE Trans. Geo. Electron.* **GE-17(2):** 33–40.
252. Ulaby, F.T. (1974). Radar measurement of soil moistrure content. *IEEE Trans. & Antenna Propagat*. **AP-22:** 257–265.
253. Ulaby, F.T. and Batlivala, P.P. (1976). Optimum radar parameters for mapping soil moisture. *IEEE Trans. Geo. Electron.* **GE-14:** 81–93.
254. Ulaby, F.T., Allen, C.T. Eger III, G. and Kanemasu, E. (1984). Relating the microwave backscattering coefficient to leaf area index. *Remote Sens. Environ.* **14:** 113–133.
255. Ulaby, F.T., Aslam, A. and Dobson, M.C. (1982). Effect of vegetation cover on the radar sensitivity to soil moisture. *IEEE Trans. Geo. & Remote Sens.* **GE-20:** 476–481.
256. Ulaby, F.T., Cihlar, J. and Moore, R.K. (1974). Active microwave measurements of soil water content. *Remote Sens. of Environ.* **3:** 185–203.
257. Ulaby, F.T., Dobson, M.C. and Batlivala, P.P. (1978). Microwave backscatter dependance on surface roughness, soil moisture and soil texture, Part I, Bare soil. *IEEE Trans. Geo. Electron*. **GE-16:** 286–295.
258. Ulaby, F.T., Moore, R.K. and Fung, A.K. (1986). Microwave remote sensing active and passive Vol. III. Artech. Horse Inc. pp. 1550–2102.
259. Ulaby, F.T., Razani, M. and Dobson, M.C. (1983). Effects of vegetation cover on the microwave radiometric sensitivity to soil moisture. *IEEE Trans. Geo. & Remote Sens.* **GE-21:** 51–61.
260. Van Dam, R.L. and Schlager, W. (2000). Identifying causes of ground-penetrating radar reflections using time-domain reflectometry and sedimentological analyses. *Sedimentology* **47:** 435–449.
261. Van de Griend, A.A. and Owe, M. (1994). Microwave vegetation optical depth and inverse modeling of soil emissivity using Nimbus/SMMR satellite observations. *Meteor. and Atmos. Physics* **54:** 225–239.
262. Van Genuchten, M. Th. and Nielsen, M.T. (1985). On describing and predicting the hydraulic properties of unsaturated soils. *Ann. Geophys.* **3(5):** 615–628.
263. Van Loon, R. and Finsey, J. (1975). The precise microwave permittivity measurements of liquids using a multipoint technique and curve fitting procedures. *J. Phy. D.* **8:** 1232–1243.
264. Van Wesenbuck, I.J. and Kachanosky, R.G. (1988). Spatial and temporal distribution of soil water in the filled layer under a corn crop. *Soil Sci. Soc. Am. J.* **52:** 363–368.
265. Vellidis, G., Smith, M.C., Thomas, D.L. and Asmussen, L.E. (1990). Detecting wetting front movement in a sandy soil with ground penetrating radar. *Trans. ASAE* **33:** 1867–1874.
266. Venkataratnam, L. (1993). Estimation of soil moisture using ERS-1 SAR data. Proc. Second ERS-1 Symp Hambeing, 9–14 October.
267. Von Hippel, A.R. (1961). Dielectric materials and applications. The Tech. Press of MIT and John Wiley & Sons Inc., New York.
268. Wagner, K.W. (1914). Arch. Elektrochem., Vol. 3, 100.
269. Wang, J.R. (1980). The dielectric properties of soil water mixtures at microwave frequencies. *Radio Sci.* **15M:** 977–985.

270. Wang, J.R. (1987). Microwave emission from smooth bare fields and soil moisture sampling depth. *IEEE Trans. Geo. & Remote Sens.* **GE-25:** 616–621.
271. Wang, J.R. and Schmugge, T.J. (1980). An empirical model for the complex dielectric permittivity of soils as a function of water content. *IEEE Trans. Geo. & Remote Sens.* **GE-18:** 288–295.
272. Wang, J.R., O'Neill, P.E., Jackson, T.J. and Engman, E.T. (1983). Multifrequency measurements of the effects on soil moisture, soil texture and surface roughness. *IEEE Trans. Geo. & Remote Sens.* **GE-21:** 44–50.
273. Wang, J.R., Schmugge, T. and Willimas, D. (1978). Dielectric constants of soils at microwave frequencies-II. NASA Tech. Paper 1238, Godlard Space Flight Center. Greenbelt, MD.
274. Wang, J.R., Schmugge, T.J., McMurtrey, J.E., Gould, W.I., W.S. and Fuchs, J.E. (1982). A multi-frequency radiometric measurement of soil moisture content over bare and vegetated fields. *J. Geophys Res.* **9:** 416–419.
275. Wang, J.R., Shiue, J.C., Schmugge, T.J. and Engman, E.T. (1990). The L-band PBMR measurements of surface soil moisture in FIFE. *IEEE Trans. Geo. & Remote Sens.* **33(5):** 1153–1161.
276. Wang, J.R., Shiue, J.C., Schmugge, T.J. and Engman, E.T. (1990). The L-band PBMR measurements of surface soil moisture in FIFE. *IEEE Trans. Geo. & Remote Sens.* **28:** 906–913.
277. Wegmuller, U., Matzler, C. and Schanda, E. (1989). Microwave signature of bare soil. *Adv. in Space Res.* **9(1):** 307–316.
278. Wegmuller, U., Mitzler, C., Huppi R. and Schanda, E. (1994). Active and passive microwave signature catalog on bare soil (2–12 GHz). *IEEE Trans. Geo. & Remote Sens.* **32:** 698–702.
279. Wegmuller, U.R.S. and Werner, C.L. (1995). SAR interferometric signatures of forest. *IEEE Trans. Geo. & Remote Sens.* **33:** 1153.
280. Weiler, K.W., Steenhuis, B.T.S., Boll, J. and Samuel Kung, K.J. (1998). Comparison of ground penetrating radar and time domain reflectometry as soil water sensors. *Soil Sci. Soc. Am. J.* **62:** 1237–1239.
281. Wendt, C.W., Olsen, T.L., Haus, H.J. and Willis, W.O. (1970). Soil water evaporation. In: 'Evapotranspiration in Great Plains'. Res. Comm. Great Plains Agric. Council Publ. No. 50, Kansas State Univ. Mappotan, Kansas.
282. Western, A.W., Grayson, R.B., Bloschl, G., Willgoose, G.R. and McMahon, T.A. (1999). Observed spatial organization of soil moisture and its relation to terrain indices. *Water Res*. **35:** 797–810.
283. Wiener, O. (1910). Leipziger Berichte, **62:** p. 256.
284. Wigneron, J.P., Calvet, J.C., Pellarin, T., Vande Griend, A.A., Berger, M. and Ferrazzoli, P. (2003). Retrieving near surface soil moisture from microwave radiometric observations: Current status and future plans. *Remote Sens. Environ*. **85:** 489–506.
285. Wigneron, J.P., Schmugge, T., Chanzy, A., Calvet, J.C. and Kerr, Y. (1998). Use of passive microwave remote sensing to monitor soil moisture. *Agronomie* **18:** 27–43.
287. Wilheit, T. (1978). Radiactive transfer in a plane stratified dielectric. *IEEE Trans. Geo. Electron.* **GE-16:** 138–143.
288. Wobschall, D. (1977). A theory of the complex dielectric permittivity of soil containing water: The semidisperse model. *IEEE Trans. Geo. Electron.* **GE-15(1):** 49–58.
289. Wigneron, J-P., Waldteufel, P., Chanzy, A., Calvet, J-C. and Kerr, Y. (2000). Two-D microwave interferometer retrieval capabilities of over land surfaces (SMOS Mission). *Remote Sens. Environ.* **73(3):** 270–282.

290. Yamasaki, H., Awaka, J., Takahashi, A., Okamoto, K. and Ihara, T. (1992). Measurement of soil backscattering with a 60 GHz scatterometer. *IEEE Trans. Geo. & Remote Sens.* **30(4):** 761–766.
291. Yisok, O.H., Sarabandi, K. and Ulaby, F.T. (1992). An empirical model and an inversion technique for radar scattering from bare soil surfaces. *IEEE Trans. Geo. & Remote Sens.* **GE-23:** 370–381.
292. Zegelin, S.J., White, I. and Russell, G.F. (1992). A critique of time domain reflectometry technique for determining soil water content. In: G.C. Topp et al., Eds. Advances in measurement of soil physical properties. Bringing theory into practice. Soil Sci. Soc. America, Madison, W1. *Spec. Publ.* **30:** 187–208.
293. Zribi, M. and Dechambre, M. (2002). A new empirical model to retrieve soil moisture and roughness from C-band radar data. *Remote Sens. of Environ.* **84:** 42–52.
294. Zribi, M., Le Hégarat-Mascle, S., Ottlé, C., Kammoun, B. and Guerin, C. (2003). Surface soil moisture estimation from the synergistic use of the (multi-incidence and multi-resolution) active microwave ERS Wind Scatterometer and SAR data. *Remote Sens. Environ.* **86:** 30–41.

Index